

# Folding polymer chains via orthogonal non-covalent interactions : function through structure

**Citation for published version (APA):**

Artar, M. (2016). *Folding polymer chains via orthogonal non-covalent interactions : function through structure*. [Phd Thesis 1 (Research TU/e / Graduation TU/e), Chemical Engineering and Chemistry]. Technische Universiteit Eindhoven.

**Document status and date:**

Published: 28/04/2016

**Document Version:**

Publisher's PDF, also known as Version of Record (includes final page, issue and volume numbers)

**Please check the document version of this publication:**

- A submitted manuscript is the version of the article upon submission and before peer-review. There can be important differences between the submitted version and the official published version of record. People interested in the research are advised to contact the author for the final version of the publication, or visit the DOI to the publisher's website.
- The final author version and the galley proof are versions of the publication after peer review.
- The final published version features the final layout of the paper including the volume, issue and page numbers.

[Link to publication](#)

**General rights**

Copyright and moral rights for the publications made accessible in the public portal are retained by the authors and/or other copyright owners and it is a condition of accessing publications that users recognise and abide by the legal requirements associated with these rights.

- Users may download and print one copy of any publication from the public portal for the purpose of private study or research.
- You may not further distribute the material or use it for any profit-making activity or commercial gain
- You may freely distribute the URL identifying the publication in the public portal.

If the publication is distributed under the terms of Article 25fa of the Dutch Copyright Act, indicated by the "Taverne" license above, please follow below link for the End User Agreement:

[www.tue.nl/taverne](http://www.tue.nl/taverne)

**Take down policy**

If you believe that this document breaches copyright please contact us at:

[openaccess@tue.nl](mailto:openaccess@tue.nl)

providing details and we will investigate your claim.

# Folding Polymer Chains *via* Orthogonal Non-covalent Interactions

Function Through Structure

PROEFSCHRIFT

ter verkrijging van de graad van doctor aan de Technische Universiteit Eindhoven, op gezag van de rector magnificus prof.dr.ir. F.P.T. Baaijens, voor een commissie aangewezen door het College voor Promoties, in het openbaar te verdedigen op donderdag 28 April 2016 om 16:00 uur

door

Müge Artar

geboren te Ulus, Bartın, Turkije

Dit proefschrift is goedgekeurd door de promotoren en de samenstelling van de promotiecommissie is als volgt:

voorzitter:	prof.dr.ir. J.C. Schouten
promotor:	prof.dr. E.W. Meijer
copromotor:	dr.ir. A.R.A. Palmans
leden:	prof.dr. S. Perrier (University of Warwick) prof.dr.ir. J.C.M. van Hest (Radboud Universiteit) prof. dr. R.P. Sijbesma
adviseur(s):	dr. T. Terashima (Kyoto University) dr.ir. J.P.A. Heuts

*Het onderzoek of ontwerp dat in dit proefschrift wordt beschreven is uitgevoerd in overeenstemming met de TU/e Gedragscode Wetenschapsbeoefening.*

*To dad,  
Babama,*

*“I am a survivor of a concentration camp. My eyes saw what no person should witness: gas chambers built by learned engineers. Children poisoned by educated physicians. Infants killed by trained nurses. Women and babies shot by high school and college graduates. So, I am suspicious of education.*

*My request is:*

*Help your children become human. Your efforts must never produce learned monsters, skilled psychopaths or educated Eichmanns. Reading, writing, and arithmetic are important only if they serve to make our children more human.”*

– An excerpt of a letter written by a Holocaust survivor to educators, published in “Teacher and Child” by Dr. Haim Ginott.

*Cover design:* Müge Artar & ICMS Animation Studio

*Printed by:* Gildeprint, Enschede

A catalogue record is available from the Eindhoven University of Technology Library

*ISBN:* 978-90-386-4054-9

This work has financially been supported by the Council of Chemical Sciences of the Netherlands Organization for Scientific Research (NWO) (ECHO-CW-713011001).

# Table of contents

## Chapter 1

<i>Introduction</i> .....	5
1.1 Function through structure in Nature .....	6
1.2 Controlled radical polymerization techniques .....	6
1.3 Function through structure in synthetic macromolecular systems .....	8
1.4. Single chain polymeric nanoparticles .....	9
1.4.1 Non-dynamic single chain polymeric nanoparticles .....	10
1.4.2 Dynamic single chain polymeric nanoparticles .....	10
1.4.3 Characterization of dynamic SCPNs .....	14
1.5. Catalysis in confined spaces .....	17
1.5.1 Dynamic single chain polymeric nanoparticles as compartmentalized catalysts .....	17
1.6 Aim and outline .....	21
1.7 References.....	22

## Chapter 2

<i>Exploring the self-assembly of polymer pendant benzene-1,3,5 tricarboxamides</i> .....	29
2.1 Introduction.....	30
2.2 Effect of molar mass dispersity on folding of poly(EHMA-co-BTAMA) .....	32
2.2.1. Synthesis of poly(EHMA-co-BTAMA) with a narrow molar mass dispersity .....	33
2.2.2. Synthesis of poly(EHMA-co-BTAMA) with broad molar mass dispersity .....	34
2.2.3. Circular dichroism studies .....	35
2.3 Investigating the effect of distribution over the polymer chain on the self-assembly of pendant BTAs.....	36
2.3.1. Synthesis of random copolymers .....	36
2.3.2. Synthesis of diblock copolymers .....	36
2.3.3. Synthesis of gradient copolymers .....	37
2.3.4. Circular dichroism studies .....	39
2.3.5. Dynamic light scattering .....	40
2.3.6. Atomic force microscopy .....	42
2.4 Discussion and conclusion .....	42
2.5 Experimental .....	43
2.5.1. Instrumentation, materials, and methods .....	43
2.5.2. Synthesis .....	44
2.6 References.....	47

## Chapter 3

<i>Triblock copolymers for creating complex secondary structures by orthogonal self-assembly</i> .....	51
3.1 Introduction.....	52
3.2 Design and synthesis of ABC triblock copolymers carrying pendant supramolecular motifs in the side chains.....	53
3.3 Folding of the triblock copolymers <i>via</i> multiple hydrogen bonds .....	59
3.4 Conclusions.....	68
3.5 Experimental.....	69

3.5.1. Materials .....	69
3.5.2 Instrumentation .....	69
3.5.3. Synthesis .....	70
3.6 References.....	73
<b>Chapter 4</b>	
<i>Exploring orthogonal self-assembly in water soluble triblock copolymers</i> .....	77
4.1 Introduction.....	78
4.2 Design of amphiphilic triblock (UBU) and random (U) copolymers .....	81
4.3 Synthesis and post-functionalization of amphiphilic block copolymers.....	83
4.4 Monitoring BTA helical self-assembly with CD spectroscopy .....	89
4.5 Monitoring UPy dimerization <i>via</i> <sup>1</sup> H-NMR .....	90
4.6 Monitoring the size of the functionalized polymers <i>via</i> DLS.....	93
4.7 Probing hydrophobicity <i>via</i> Nile Red experiments.....	93
4.8 Conclusions.....	95
4.9 Experimental .....	96
4.9.1. Materials .....	96
4.9.2. Methods .....	96
4.9.3. Synthesis .....	97
4.10 References.....	101
<b>Chapter 5</b>	
<i>Understanding the catalytic activity of single chain polymeric nanoparticles in water</i> .....	105
5.1 Introduction.....	106
5.2 Design and synthesis of catalytically active SCPNs.....	107
5.3 CD, DLS and fluorescence characterization of P1-P5 in solution.....	112
5.4 Transfer hydrogenation of cyclohexanone in water.....	114
5.5 Conclusions.....	117
5.6 Experimental.....	118
5.6.1. Materials .....	118
5.6.2. Characterization .....	118
5.6.3. Synthesis .....	119
5.6.3.1. General procedure for polymerizations .....	119
5.6.3.2. General procedure for ruthenium catalyst loading .....	120
5.6.3.3. General procedure for transfer hydrogenation in water .....	121
5.7 References.....	121
<b>Chapter 6</b>	
<i>Single chain polymeric nanoparticles as selective hydrophobic reaction spaces in water</i> .....	125
6.1 Introduction.....	126
6.2 SCPN catalyzed oxidations.....	127
6.2.1. Polymer design and synthesis .....	127
6.2.1. Oxidation reactions.....	129
6.3 Competition experiments.....	131
6.3.1. Oxidation reactions.....	131
6.3.2. Transfer hydrogenation reactions .....	134

---

6.3.3. The origin of the selectivity .....	134
6.4 Towards SCPN catalyzed cascade reactions in water.....	135
6.5 Conclusions.....	139
6.6 Experimental.....	139
6.6.1. Materials .....	139
6.6.2. Instrumentation.....	140
6.6.3. Synthesis.....	141
6.6.4. Catalysis procedures .....	141
6.7 References.....	142
<b><i>Summary</i></b> .....	147
<b><i>Summary in Turkish</i></b> .....	149
<b><i>Summary in Dutch</i></b> .....	151
<b><i>Curriculum Vitae</i></b> .....	153
<b><i>List of Publications</i></b> .....	155
<b><i>Acknowledgements</i></b> .....	157





# Chapter 1

## *Introduction*

*Part of this work has been published:*

\*M. Artar, E. Huerta, E. W. Meijer, A. R. A. Palmans, In: *Sequence-Controlled Polymers: Synthesis, Self-Assembly, and Properties* (Eds.: J.-F. Lutz, T. Y. Meyer, M. Ouchi, M. Sawamoto), American Chemical Society, Washington, D.C., **2014**, Vol. 1170, p 313.

\*M. Artar, A. R. A. Palmans, In: *Catalysis within nanoconfined spaces* (Ed: R. Poli), Springer, Berlin, accepted for publication.

### 1.1 Function through structure in Nature

Biomacromolecules consist of an exact number of monomers that are positioned in a highly specific way along their backbone. Although the number of monomers that Nature uses is limited, biomacromolecules possess a high degree of complexity and functionality: secondary interactions confer a precisely defined three-dimensional structure in solution to biomacromolecules, from which specific properties arise (Figure 1.1).<sup>1</sup> For example, the compartmentalization present in enzymes is key for creating active sites in which substrates are readily and selectively activated and converted into products.<sup>2</sup>

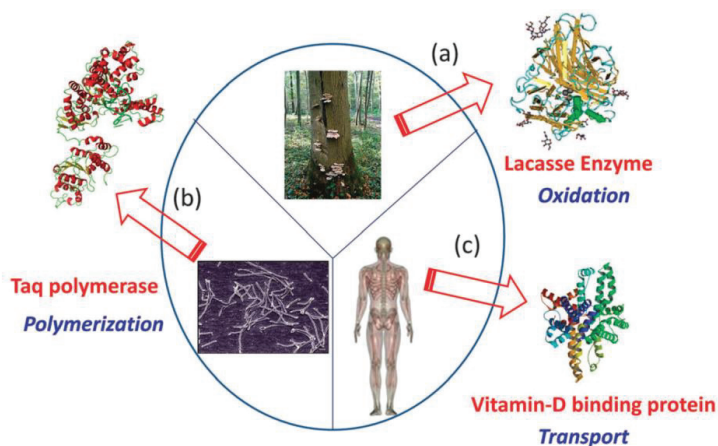


**Figure 1.1** Several proteins with specific biological functions have been taken as inspiration source for the construction of functional biomimetic single chain nanoparticles (SCNPs): Lacase enzyme from *Pleurotus ostreatus* (a), Taq polymerase from *Thermus aquaticus* (b), and vitamin-D binding protein (DBP) from human serum. (c) Reproduced with permission from reference 3.

The ability to achieve the perfection of Nature in forming ordered structures in three dimensions has greatly inspired synthetic polymer chemists but at the same time is a formidable challenge. To achieve function through controlling the three-dimensional structure, precise control over the length of polymer chains and location of specific monomers along the polymer backbone is required. However, it is important to keep the synthetic efforts low, while achieving the control of synthetic systems with high molecular mass.

### 1.2 Controlled radical polymerization techniques

In the past decades, the field of polymer chemistry has made noteworthy steps in making polymers with a defined length and control over the nature of the end-groups. Metal-catalyzed olefin polymerizations,<sup>4</sup> cationic,<sup>5</sup> and anionic<sup>6</sup> polymerizations, ring-opening metathesis polymerizations (ROMP),<sup>7</sup> and controlled radical polymerizations (CRP), such as reversible addition fragmentation chain transfer polymerizations (RAFT),<sup>8-10</sup> nitroxide-mediated polymerizations (NMP),<sup>11,12</sup> atom transfer radical polymerizations (ATRP),<sup>13-15</sup> and single electron transfer polymerizations (SET-LRP),<sup>12</sup> have been developed and are widely employed in both academic and industrial fields. Especially controlled radical polymerization procedures

nowadays permit to control the polymer's molecular weight, the molar mass dispersities and the end-groups. More recently, advances in understanding reactivity profiles of monomers, in combination with automated polymerization procedures, afforded a remarkable degree of controlling the sequence of the monomers.<sup>16-19</sup> Moreover, the topology of the polymers can be controlled by the careful selection of initiators and monomers, thus achieving a highly selective polymerization process (Figure 1.2),<sup>20,21</sup> while at the same time also highly functionalized monomers are accepted during the polymerization procedure.<sup>22,23</sup>

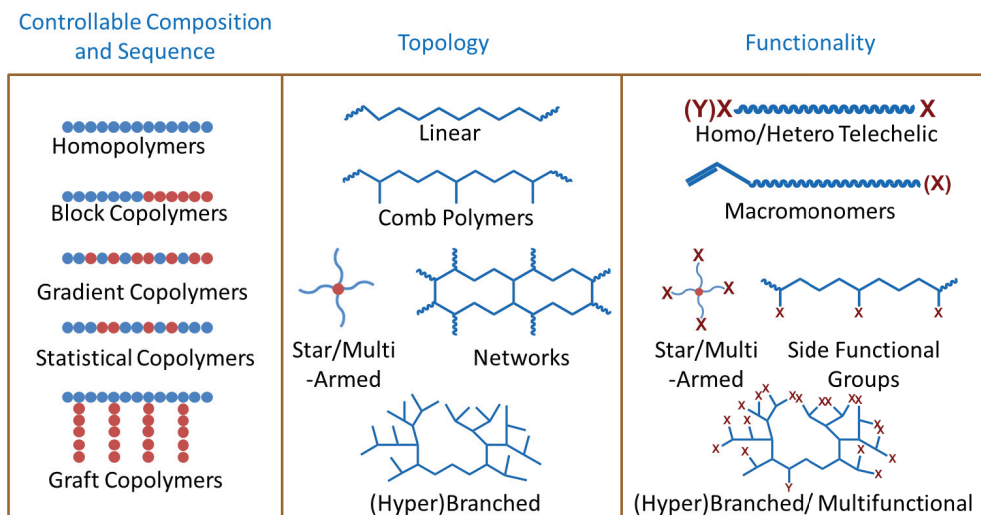


**Figure 1.2** Possible polymeric architectures offered by CRP techniques.

Emerging in the mid-90s, NMP has been employed in the polymerization of vinyl(amide), vinyl(esters) and styrenes *via* reversible termination events that are governed by the nitroxide radicals.<sup>24</sup> Especially the new generation NMP systems are well-known for their *simplicity* among other CRP techniques, since a thermal initiation mechanism is applied and no external radical source is required.<sup>25</sup> However, commercially available NMP agents can only be applied to a limited monomer library *e.g.* styrenes and acrylates.<sup>8,11,12</sup>

Discovered by Rizzardo *et al.*<sup>26</sup> in 1998, RAFT polymerization can be applied to various types of monomers, including (meth)acrylates, (meth)acrylamides, acrylonitrile, styrenes, dienes and vinyl monomers. A reversible equilibrium is created by a variety of sulfur-based chain transfer agents (CTAs) and thus a metal-free, living system is achieved. Nevertheless, the CTA moieties result in inherently colorful RAFT products, which is undesirable for applications such as coatings. Moreover, decomposition of the CTA groups may present toxicity issues for biological applications and an unpleasant odor, due to the release of thiocarbonyl thio compounds.<sup>27</sup> However, many approaches have been developed for the removal of the CTA units such as aminolysis and radical treatment.<sup>28</sup>

Lastly, independently reported by Sawamoto *et al.*<sup>29</sup> and by Matyjaszewski *et al.*<sup>30</sup> in 1995, the ATRP technique can be applied to a large library of monomers, such as

(meth)acrylates, (meth)acrylamides, acrylonitrile and styrenes.<sup>14</sup> The living character of the technique is based on the equilibrium created by a reversible single electron oxidation and reduction of the transition metal.<sup>31</sup> A clear disadvantage of ATRP are the heavy metals applied in the polymerization, which is undesirable for commercial applications. Recent developments, however, allow efficient polymerizations with a decreased transition metal catalyst content, by use of modified techniques like activators regenerated by electron transfer (ARGET)<sup>32</sup> and initiators for continuous activator regeneration (ICAR)<sup>33,34</sup> Moreover, ATRP enables the easy access to large variety of polymeric architectures, including linear, star, brush and gradient architectures (Figure 1.2).<sup>14,35,36</sup>

### 1.3 Function through controlling structure in synthetic macromolecular systems

The merger of advanced CRP techniques with either covalent or supramolecular chemistry results in the preparation of tailor-made polymers that show programmed self-assembly. The formed structures are restrained in conformational mobility and adopt a defined size and shape.<sup>37,38</sup> As a result, particles of tunable sizes and dimensions in which the inside and outside properties can be independently controlled, have become accessible. Such *compartmentalized* structures are foreseen to have a wide application potential, especially if they were compatibilized with water as the solvent (*vide infra*).

Several approaches have been followed to attain such compartmentalized structures in synthetic macromolecules, and with those, many functions have become accessible.<sup>39,40</sup> For example, cyclic and amphiphilic block copolymers,<sup>41</sup> nanogels,<sup>42</sup> and dendritic structures<sup>43</sup> have been actively explored for *i.a.* drug delivery applications.<sup>44</sup> Star-polymers,<sup>45,46</sup> dendrimers<sup>47-49</sup> and polymersomes (Figure 1.3)<sup>50</sup> afford containers of nanometer-sized dimensions in which embedded, site-isolated catalysts, perform a variety of catalytic and cascade catalytic reactions. Alternatively, amphiphilic block copolymers self-assemble in water into compartmentalized structures and when catalysts are attached to the hydrophobic interior, catalysis in water becomes accessible for catalysts that are normally inactive in pure water.<sup>51</sup>

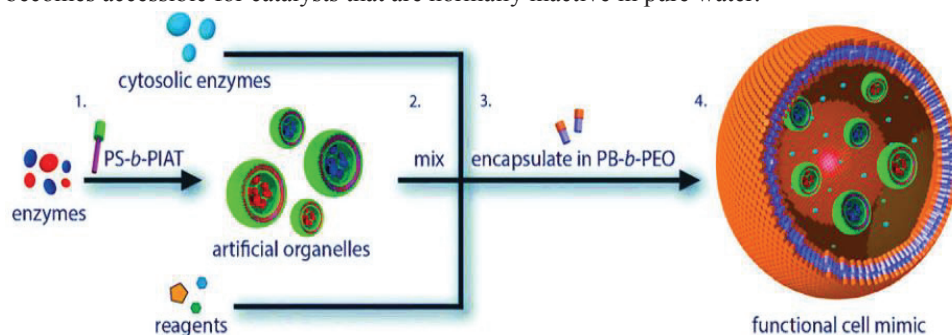


**Figure 1.3** The concept of the cell mimic reported by Lecommandoux *et al.*, which shows the initial encapsulation of different enzymes in polystyrene-*b*-poly(3-(isocyano-*l*-alanyl-amino-ethyl)-thiophene) (PS-*b*-PIAT) nanoreactors (1), followed by mixing of the organelle mimics, cytosolic enzymes, and reagents (2), before encapsulation of the reaction mixture in polybutadiene-*b*-poly(ethylene oxide) (PB-*b*-PEO) vesicles (3) to create the functional cell mimic (4), inside which enzymatic multicompartement catalysis takes place. Reproduced with permission from reference 50.

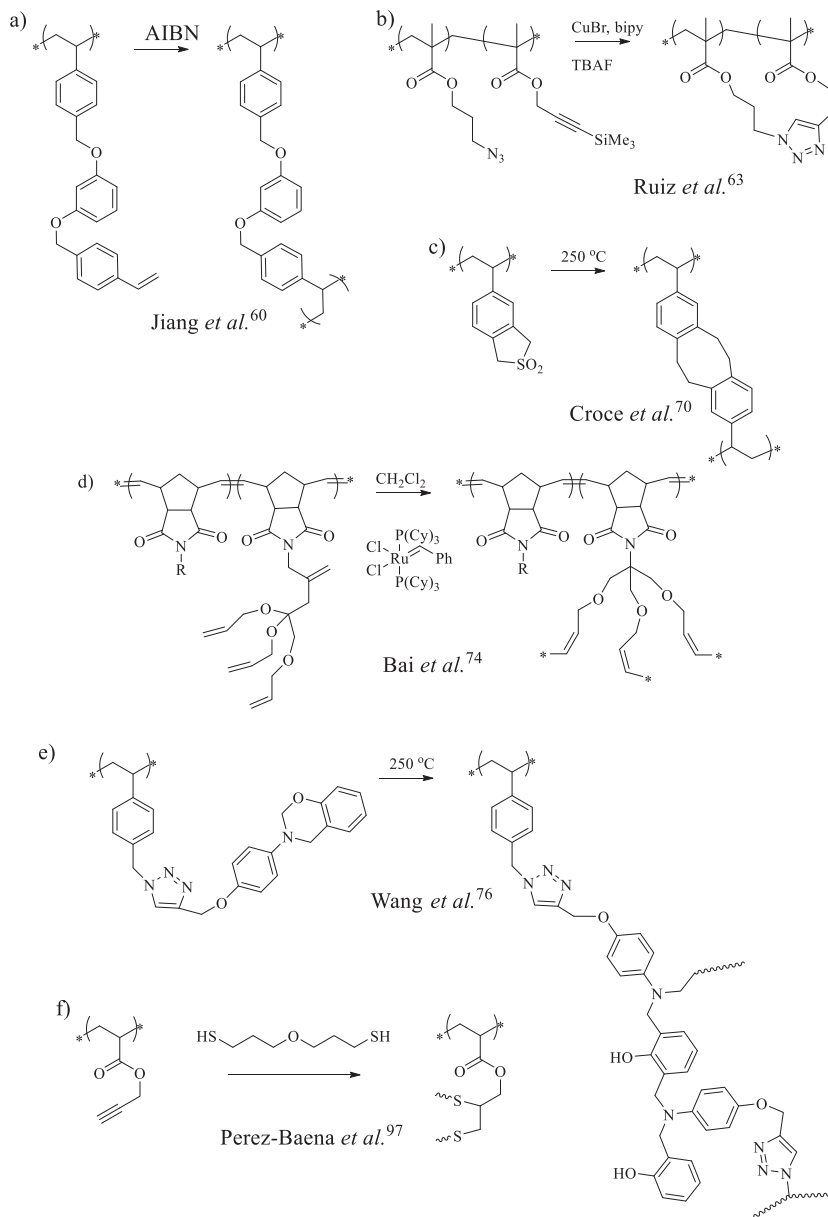


Figure 1.4 Structure of several covalent crosslinking motifs.

### 1.4 Single chain polymeric nanoparticles

In early 2000's, the first examples started to appear in which polymer chains were functionalized with reactive pendant side groups. Upon triggering a reaction, polymer chains were trapped into particles of controllable size by *interpolymer* crosslinking of the pendant

functional groups.<sup>52,53</sup> By performing these crosslinking reactions in ultra-dilute conditions, interpolymer interactions were minimized and single polymer chains could be collapsed into particles that showed restricted conformational freedom. After these first examples, many others followed and the study of single chain polymeric nanoparticles (SCPNS) became a rapidly growing field.<sup>54-58</sup> SCPNS have been designed both in a non-dynamic and a dynamic fashion. In non-dynamic SCPNS, intramolecular crosslinks are formed by covalent bonds, and the particle thus cannot rearrange into a thermodynamically favored conformation and are kinetically trapped. Alternatively, dynamic SCPNS formed by the non-covalent or dynamic covalent have the ability to rearrange into a thermodynamic equilibrium. The dynamic nature of these particles makes it possible for the particles to respond external triggers (*vide infra*).

#### 1.4.1 Non-dynamic single chain polymeric nanoparticles

In non-dynamic SCPNS, many different types of covalent bond formation have been applied successfully for the intramolecular crosslinking of the polymers such as radical coupling (Figure 1.4a),<sup>59,60</sup> copper(I)-catalyzed azide-alkyne cycloaddition (CuAAC) (Figure 1.4b)<sup>61-68</sup>, Diels-Alder (DA) reaction,<sup>69</sup> quinodimethane formation (Figure 1.4c),<sup>70-72</sup> cross-metathesis (Figure 1.4d),<sup>73,74</sup> amide formation<sup>75</sup> benzoxazine ring opening polymerization (Figure 1.4e) (ROP),<sup>76,77</sup> Bergman cyclization<sup>78,79</sup> nitrene cross-linking,<sup>80,81</sup> alkyne homocoupling,<sup>82</sup> oxidative polymerization,<sup>83</sup> thiol-ene coupling,<sup>84</sup> Michael addition<sup>85-87</sup>, lactone ROP,<sup>69,88-94</sup> urea formation,<sup>95</sup> nitrile-imine ligation,<sup>96</sup> thiol-yne coupling (Figure 1.4f)<sup>97</sup>, and tetrazine-norbornene reaction.<sup>98</sup> Non-dynamic SCPNS were shown to be particularly attractive for applications such as drug delivery, wherein biodegradable crosslinks ensure the controlled release of the molecule of interest.<sup>99-102</sup> In addition, they featured nontoxic properties due to the limited interactions of the interior moieties with the outside environment.

#### 1.4.2 Dynamic single chain polymeric nanoparticles

A disadvantage of non-dynamic SCPNS is that the polymeric chain is irreversibly ‘frozen’ in a certain conformation, preventing the nanoparticles to adapt to their environment. Introducing reversible interactions to form SCPNS, in contrast, would provide a system that remains adaptive and can respond to external triggers.

To achieve this reversibility, reversible covalent bonds such as disulfides (Figure 1.5a)<sup>103</sup> or acyl hydrazones (Figure 1.5b)<sup>104</sup> have been utilized as well as non-covalent bonds such as diamides (Figure 1.5c),<sup>37</sup> 2-ureido-pyrimidinones (UPys) (Figure 1.5d),<sup>105</sup> benzene-1,3,5-tricarboxamides (BTAs) (*vide infra*),<sup>106</sup> a combination of BTAs and UPys,<sup>107</sup> BTA-bipyridines,<sup>108</sup> thymine-diaminopyridine (Figure 1.5e),<sup>109</sup> cucurbit[8]uril (Figure 1.5f),<sup>110</sup> ureidoguanosine-diaminonaphthyridine (Figure 1.5g),<sup>111</sup> *N*-(6-(3-(2,4-dioxo-3,4-dihydropyrimidin-1(2H)-yl)-propanamido)pyridine-2-yl)undec-10-enamide dimerization,<sup>112</sup> six-point cyanuric acid-Hamilton wedge interactions (Figure 1.5h)<sup>113</sup> and a combination of the last two.<sup>114</sup> Such dynamic SCPNS respond well to triggers such as pH,<sup>115</sup> light,<sup>107</sup> heat,<sup>107,115</sup> and metals.<sup>108</sup>

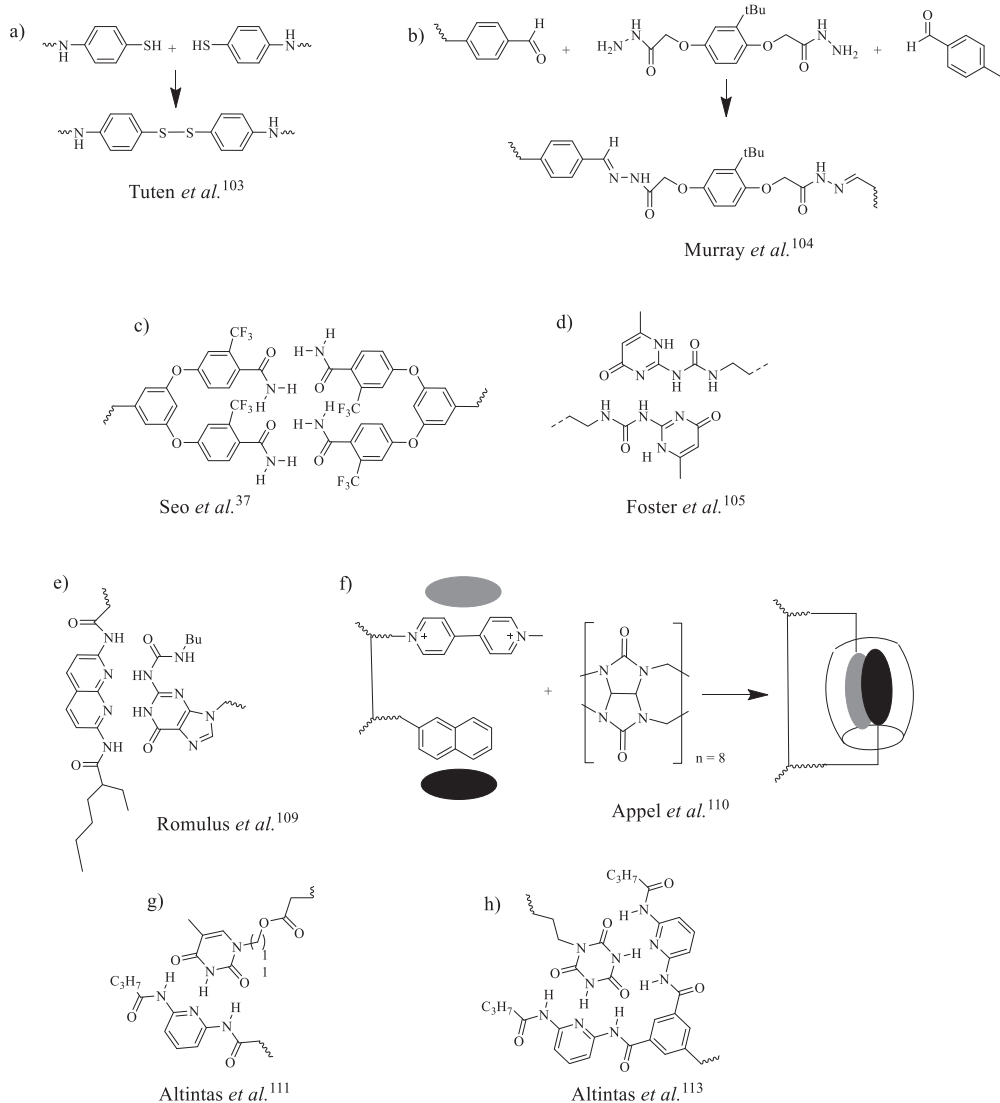


**Figure 1.5** Structure of several dynamic covalent and non-covalent crosslinking motifs.

In the Meijer group, the first examples of dynamic SCPNs were based on polynorbornenes, prepared by ROMP with a second generation Grubbs catalyst, incorporating pendant 2-ureidopyrimidinone units to a polymer backbone, and using the strong dimerization of UPys as a driving force for the collapse of one single polymer chain.<sup>105</sup> In a following approach, single-electron transfer living radical polymerization (SET-LRP) was utilized to synthesize alkyn-functionalized methacrylate-based polymers, followed by a post-modification to attach azide functionalized UPys to free alkynes on the methacrylate backbone *via* azide-alkyne 1,3-dipolar cycloaddition.<sup>116</sup> In both cases, the dimerization of the UPys was controlled



by an external trigger, the 2-ureidopyrimidinone moieties on the polymers were functionalized with *o*-nitrobenzyl ether photolabile protecting groups (phUPy) at the terminal carbonyl of the UPy.<sup>117</sup> The photolabile protecting groups were cleaved off by photoirradiation and the UPy moieties were allowed to dimerize in dilute solutions, resulting in the formation of polymeric nanoparticles (Figure 1.6). SCPN formation was demonstrated by the change in apparent hydrodynamic volume, and thus the size difference between the free polymer and the collapsed nanoparticle *via* size exclusion chromatography (SEC). The size of the SCPNs could be tuned *via* varying the molecular weight of the polymer.<sup>118</sup>

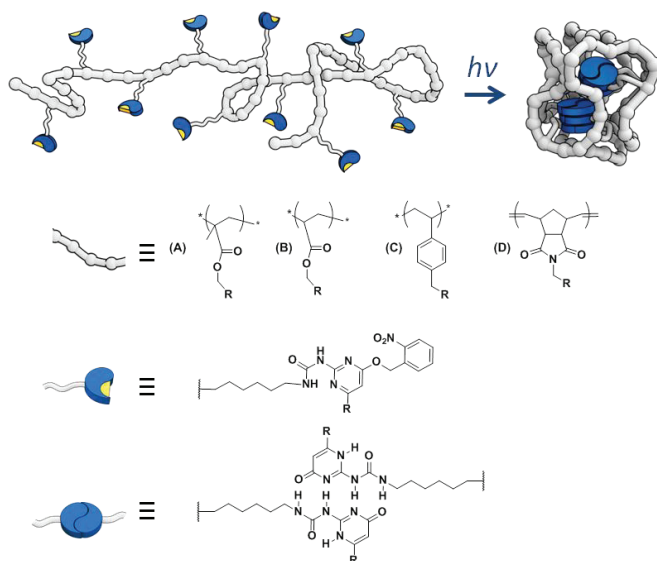


**Figure 1.6** Schematic representation of a polymer backbone (polyacrylate-, polymethacrylate-, polystyrene- or polynorbornene-based) with pendant *o*-nitrobenzyl protected (yellow dots) UPy motifs (blue half-moon) that upon UV-induced cleavage of the *o*-nitrobenzyl group forms UPy dimers (blue circles) that induce the formation of a compact conformation. Reproduced with permission from reference 119.

In a following study, Stals *et al.* prepared a library of vinyl based polymer backbones (polyacrylates, polymethacrylates, and polystyrenes) *via* CRP techniques, such as RAFT, ATRP and NMP (Figure 1.6). Next, the post-functionalization of these polymers was performed *via* either the reaction of the pendant alcohol/amine units with *o*-nitrobenzyl protected UPy isocyanates or pendant active ester groups with the reaction of *o*-nitrobenzyl protected UPy amines. Interestingly, these polymers were similarly suitable for SCPN formation *via* UPy dimerization. Crucially, the results revealed that the solvent choice was the determining factor in the intramolecular folding process; solvents that enhanced intramolecular hydrogen bonding, at the same time enhanced interparticle interactions.<sup>119</sup>

Following these examples, Mes *et al.* showed that benzene-1,3,5-tricarboxamides (BTAs) can also be utilized as a supramolecular unit to form SCPNs.<sup>106</sup> In this example, a prepolymer was synthesized *via* ATRP, using isobornyl methacrylate and silyl-protected propargyl

methacrylate as the monomers. The prepolymers, were then functionalized with azide substituted BTAs. The BTA moiety comprised one *o*-nitrobenzyl group protected amide in order to trigger the threefold hydrogen bonding into BTA aggregates *via* light.

Later, both BTA and UPy moieties were utilized in one polymer chain, by Hosono *et al.*, by which orthogonal self-assembly was introduced into SCPNs (Figure 1.7).<sup>107,120</sup> ABA and BAB triblock copolymers possessing different pendant functional groups in the A and B blocks were prepared *via* ATRP, to which a complementary BTA and phUPy moiety were ligated in a modular post-functionalization approach. Both ABA, as well as BAB block-copolymer formed BTA-based helical aggregates and UPy dimers within one SCPN, upon a two-step thermal/photoirradiation treatment under dilute conditions. The orthogonality of the BTA and UPy self-assembly was corroborated *via* variable-temperature NMR studies. The collapse of polymers after deprotection of the photolabile protecting groups of phUPys into SCPNs was indicated by significant reductions in the hydrodynamic volume by SEC and a decrease in the radius of gyration as evidenced by small-angle X-ray scattering (SAXS).

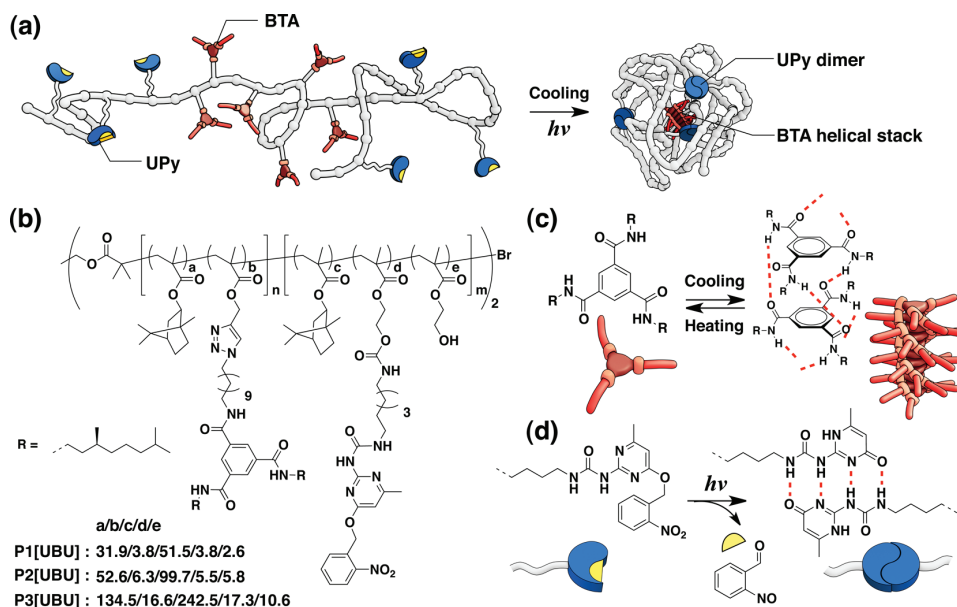


**Figure 1.7** (a) Design of a triblock copolymer with BTA and UPy moieties that folds into a single chain polymeric nanoparticle cross-linked via orthogonal self-assembly. (b) Chemical structure of the triblock copolymers. (c) Helical self-assembly of chiral BTAs via threefold, symmetric hydrogen bonding. (d) Photoinduced dimerization of *o*-nitrobenzyl protected UPys via quadruple hydrogen bonding. Reproduced with permission from reference 107.

Besides UPy and BTA motifs, the 3,3'-bis(acylamino)-2,2'-bipyridine substituted benzene-1,3,5-tricarboxamide (BiPy-BTA) unit was also utilized as a structure forming element in SCPN design by Gillissen *et al.*<sup>108</sup> and ter Huurne *et al.*<sup>121</sup> Ring-opening metathesis polymerizations were applied to prepare polynorbornene based copolymers with pendant BiPy-

BTA units using a third generation Grubbs catalyst. The polymers formed SCPNs in mixtures of tetrahydrofuran and methylcyclohexane *via*  $\pi$ - $\pi$  interactions. In the self-assembled state, a strong fluorescence was observed due to the rigidification of the bipyridine moieties, which was utilized as a sensor by using metal binding affinity that enables quenching of the emission.<sup>108</sup>

Water-solubility was first introduced into BTA-based dynamic SCPNs by Terashima *et al.*<sup>122</sup> Ru-catalyzed living radical polymerization was used to prepare a segmented amphiphilic copolymer based on oligo(ethyleneglycol)methacrylate (*o*EGMA) and a BTA-functional methacrylate (BTAMA). When the content of BTAMA was smaller than 20%, the copolymers were water-soluble. In addition, a combination of circular dichroism (CD) spectroscopy and scattering techniques showed that these copolymers fold into a SCPNs as a result of the helical self-assembly of the pendant BTA units and/or hydrophilic-hydrophobic phase separation.<sup>123</sup>

Recently, folding of the single chains was achieved *via* hydrophilic/hydrophobic phase separation without any additional non-covalent interaction and/or chemical linking, one of the simplest models in self-folding polymers. Sawamoto and coworkers reported on the single-chain folding of amphiphilic random copolymers prepared by the Ru-catalyzed living radical copolymerization of a *o*EGMA and an alkyl methacrylate (RMA) in water.<sup>124</sup> Detailed structural and chain-folding characterization on the resulting dynamic and reversible SCPNs disclosed the design rules for single chain folding as an alkyl methacrylate content between 20–40 mol% per chain. Notably, a sharp and reversible lower critical solution temperature (LCST) and phase separation in water was observed with these *p*(*o*EGMA-*co*-RMA) random copolymers. Besides tunable hydrophobicity of the compartments depending on nature and content of the alkyl methacrylate, a stimulus-responsive unfolding was observed *via* the addition of methanol.

### 1.4.3 Characterization of dynamic SCPNs

As summarized above, the broad synthetic scope of polymer chemistry in combination with the molecular recognition that supramolecular chemistry affords, enables the design of various SCPNs. However, the verification of the single chain character, and untangling the nature of the three dimensional architectures of the SCPNs has been less straightforward. In fact, it was found that a combination of characterization techniques is required in order to exclude artifacts arising when those techniques are applied separately. Direct visualization using (cryogenic) transmission electron microscopy (TEM) is possible but low contrast and the small sizes of the particles typically hamper the elucidation of the overall structure. Atomic force microscopy (AFM) images have also been frequently applied to visualize the size and shape of SCPNs. However, the method of sample preparation may yield unclear and even misleading images due to solvent evaporation effects.<sup>125</sup> In addition, polymer-surface contacts have a significant impact on the conformation of the polymer chain.<sup>125</sup> Size exclusion chromatography (SEC) is used to circumvent these issues allowing the determination of the hydrodynamic volume. However, SEC does not provide detailed information on the global conformations that the polymers adopt in solution, and undesirable interactions of polymers with the SEC column may lead to unreliable results.<sup>119</sup>

Spectroscopic techniques (nuclear magnetic resonance (NMR), fluorescence, ultraviolet (UV) and circular dichroism (CD) spectroscopy) all are useful to provide evidence on the

aggregation state of the supramolecular recognition motifs but they do not distinguish between *intra* and *inter* chain interactions. The most revealing method until now has been the combination of scattering techniques (dynamic light scattering (DLS), small angle X-ray scattering (SAXS) and small angle neutron scattering (SANS)) to analyze dynamic SCPNs.

While the first studies on SCPNs relied strongly on the use of AFM and SEC to elucidate the single chain character of the particles obtained, Stals *et al.* monitored the polymer backbone collapse of UPy functionalized SCPNs using a combination of DLS, NMR, SEC and AFM.<sup>119</sup> Hereto, a library of polymers with varying backbone structures, molecular weights and linking groups was prepared that contained between 5-10% of photoprotected pendant UPy groups. All characterizations were done in 3 different solvents, tetrahydrofuran, chloroform and dimethylformamide to assess the importance of solvent-polymer interactions in SCPN formation. After photodeprotection, UPy dimerization was observed by <sup>1</sup>H-NMR in tetrahydrofuran and chloroform, but not as strong in dimethylformamide, a solvent that suppresses hydrogen bond formation. Moreover, changes in hydrodynamic radius were observed by DLS and SEC before and after deprotection, which were very sensitive to the solvent applied. AFM showed the formation of well-defined particles. Later, complex polymeric architectures based on a block copolymer with a cylindrical brush block and a single-chain polymeric nanoparticle block with pendant UPy groups were investigated.<sup>126</sup> The self-assembly of these constructs was studied with a similar combination of techniques but in this case, only high resolution AFM images provided clear evidence of SCPN formation.<sup>126</sup>

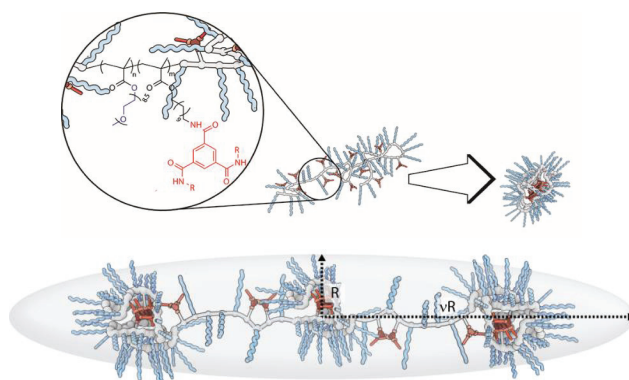


**Figure 1.8** (a) Schematic representation of the structure of amphiphilic poly(oEGMA-co-BTA) random copolymers that fold in water into compact conformations. (b) Representation of the global, ellipsoidal conformation of folded SCPNs in water; when the polymer length increases, only the major axis  $vR$  increases in length while the minor axis  $R$  remains constant. Reproduced with permission from reference 127.

For the systems in which folding is governed by BTA self-assembly, CD spectroscopy is a powerful technique as shown by Mes *et al.*<sup>106</sup> When the BTAs are non-racemic, helical aggregates of one helicity are biased and this assembly process gives rise to a signature Cotton effect. Upon attaching BTAs to the polymer chains, the Cotton effect was found to be sensitive to the loading of BTAs per polymer chain and, in later examples, to the length of the

oligo(ethyleneglycol) side chain.<sup>122</sup> In addition, the magnitude of the Cotton effect was only determined by the local BTA concentration.<sup>106,127</sup> However, the presence of a Cotton effect does not exclude interparticle interactions. Therefore, scattering techniques proved to be crucial to elucidate the single chain character in the BTA-based water-soluble systems. In recent studies, Gillissen *et al.* combined spectroscopy and small-angle neutron scattering to unravel the relation between interchain self-assembly and the polymer conformation.<sup>123</sup> SANS experiments revealed the asymmetric shape of these SCPNs with a constant cross section,  $R_{cs}$ , and variable length,  $L$ , with  $L > R_{cs}$  (Figure 1.8). Detailed investigations corroborated the elongated and highly stretched structure at room temperature, which adopts a constant cross section regardless of the increase in the degree of polymerization.<sup>127</sup>

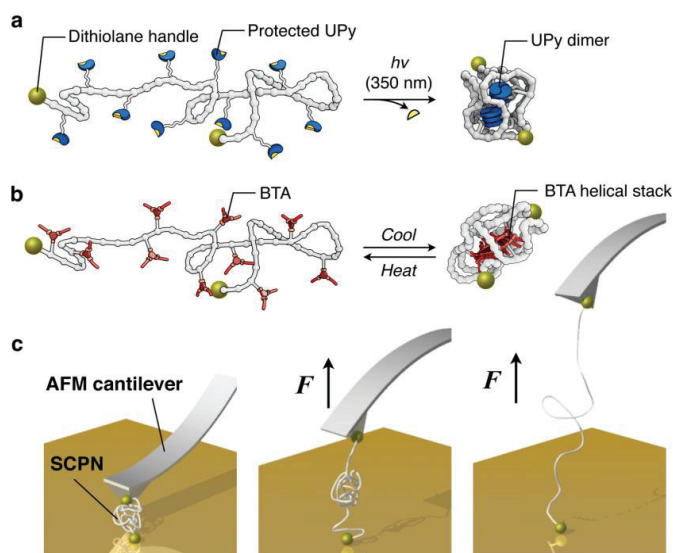


**Figure 1.9** Schematic representations of folding polymer with (a) UPy modules  $P[UPy_n]$  and (b) BTA modules  $P[BTA_n]$ , which self-assemble into dimer and helical columnar aggregates, respectively, resulting in SCPN formation. (c) Schematic illustrations of the mechanical unfolding experiment on SCPNs. Reproduced with permission from reference 128.

Very recently, Hosono *et al.* applied AFM-based single-molecule force spectroscopy (SMFS) to SCPNs in order to understand the internal folding structure of SCPNs and intrinsic kinetic parameters of polyacrylate-based polymers carrying UPy or BTA pendants (Figure 1.9a, b).<sup>128</sup> These polymers were end functionalized with dithiolane in order to provide a "molecular handle" to perform pulling experiments with AFM cantilever. The force-extension profiles of the UPy and BTA pendant polymers were obtained *via* stretching SCPNs from the dithiolane end to unfold them mechanically (Figure 1.9c). Analysis of the statistical force profiles of the polymers provided insights into the internal conformation of SCPNs and dynamic loading rate analysis allowed the determination of kinetic parameters of BTA and UPy self-assembly.

## 1.5 Catalysis in confined spaces

The advances in both the preparation and the characterization of the three-dimensional synthetic structures pave the way for achieving function in confined spaces. Active and selective catalytic conversions are particularly attractive in this respect. Achieving catalytic conversions in water with rates and selectivities approaching those of enzyme, has attracted considerable attention and many approaches have been followed to increase activity and selectivity of synthetic catalysts.<sup>129</sup> Promising strategies are the utilisation of cross-linked nanoparticles,<sup>130</sup> micellar structures,<sup>131</sup> hydrogels,<sup>132</sup> star polymers,<sup>133</sup> self-assembled systems<sup>134</sup> and dendrimers,<sup>135</sup> these examples not only show high activity in water due to the so-called “concentrator effect” but also can give high selectivities. Among these, *homogenous* water-soluble systems offer a number of advantages over heterogeneous systems, such as providing a relatively more uniform micro environment around the catalytic sites, facilitating efficient diffusion of reagents and products and allowing easy recyclability.<sup>136</sup> Polymeric nanoparticles have also been evaluated as catalysts for organic reactions. Several elegant examples have been presented in which SCPNs are catalytically active in organic media,<sup>45,137</sup> even some with high selectivity for specific substrates.<sup>137e</sup> For example, several groups applied metal loaded polymeric systems for catalysis. Cu (II) loaded methacrylate based polymers were used in the coupling reactions by Sanchez-Sanchez *et al.*<sup>137c</sup> and Willenbacher *et al.*<sup>137d</sup> applied Pd(II) loaded styrene based polymers in a Sonogashira coupling, in organic solvents. Lastly, Mavila *et al.* showed the potential of Rh(I), Ir(I) and Ni(0) loaded polycycloocta-1,5-diene based nanoparticles in the catalysis of several reactions.<sup>137e</sup> Nevertheless, a major challenge is to prepare SCPNs that show high activity and selectivity in complex, *aqueous* media. This is especially relevant in view of future biomedical applications and cascade catalytic conversions in water.

### 1.5.1 Dynamic single chain polymeric nanoparticles as compartmentalized catalysts

The water-soluble, BTA-based SCPNs discussed in Paragraph 1.4.2, offer a compact yet dynamic and responsive inner structure; in contrast to the rather dense and “frozen” interior reaction spaces that are usually employed in synthetic systems displaying confined spaces. SCPNs could therefore be a very attractive option to prepare compartmentalized, water-soluble, nanometre-sized particles with a hydrophobic interior for efficient and selective catalysis in water.

There are two main approaches that have been evaluated to access dynamic, water-soluble, catalytically active SCPNs (Figure 1.10). In the first, the catalysts or ligands that bind a metal-based catalyst contain a polymerizable group and are copolymerised with water-soluble monomers and hydrophobic/structuring monomers. Frequently, (meth)acrylates and/or styrenes have been employed in combination with controlled radical polymerisation techniques.<sup>138</sup> When there are no reactivity differences in the polymerizable monomers, random copolymers are obtained. Alternatively, segmented copolymers can be prepared by taking advantage of the reactivity differences between styrene- and methacrylate-based monomers.<sup>124</sup> However, polymerizing highly functional monomers can be rather troublesome and needs careful optimisation since functional units (i.e. ligands, organocatalysts, charged units, radicals, etc.) can hamper controlled radical polymerization processes, resulting in less well-defined products and broad molecular weight distributions of the prepared polymers.<sup>116</sup> As an alternative, the

post-polymerization modification of poly(pentafluorophenyl acrylate)<sup>139</sup> with amine derivatives carrying functional groups has been investigated.<sup>140</sup> This post-functionalization approach is a convenient way to prepare polymers with tuneable amounts of functional side chains, however, the polymer dispersity is poorly controlled and a large amount of toxic side-products are produced.<sup>140</sup> Using all of these approaches, a library of catalytically active SCPNs capable of reductions, oxidations, C-C bond forming reactions, deprotection reactions and click reactions have been evaluated (Figure 1.11).

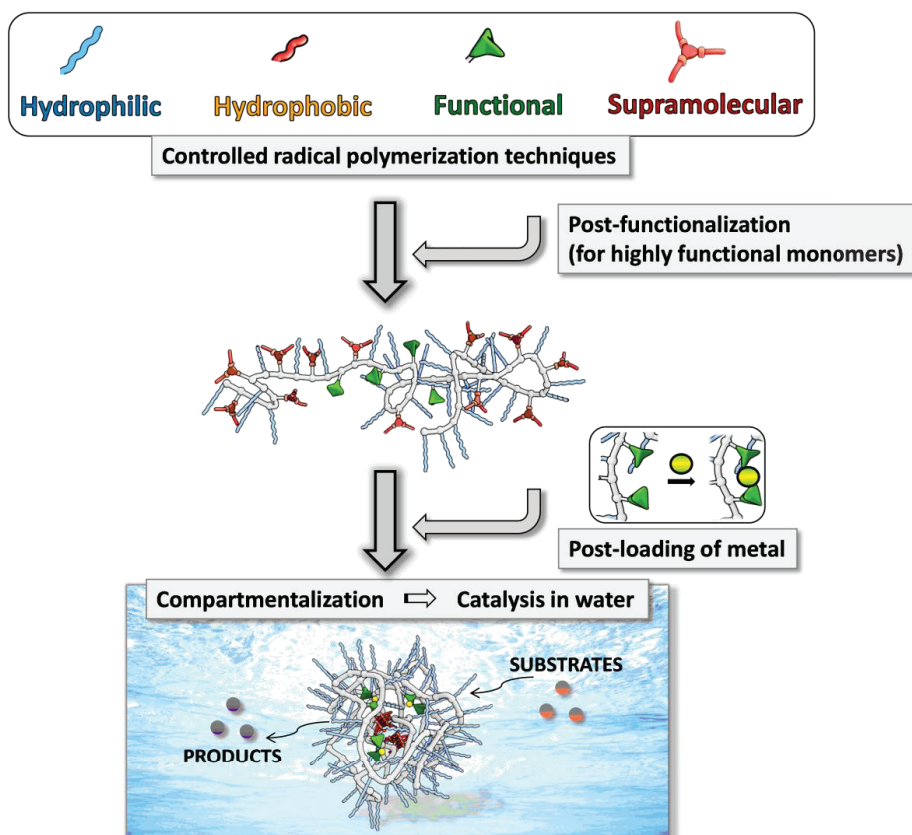


**Figure 1.10** General approach for preparing metal-based catalytically active SCPNs in water.

Terashima *et al.* prepared a water-soluble segmented copolymer using the benzene-1,3,5-tricarboxamide motif as the supramolecular unit and triphenylphosphine (SDP) pendants as ligands for complexing Ru(II) (**P1**, Figure 1.11a). This system efficiently catalysed the transfer hydrogenation of ketones in the presence of sodium formate as the hydrogen source with a turnover frequency (TOF) of  $20 \text{ h}^{-1}$ , which was high compared to previous examples of similar Ru-based complexes in water.<sup>122</sup> In another example, Huerta *et al.* reported L-proline functionalized SCPNs as highly active catalysts for the aldol reaction of cyclohexanone and *p*-nitrobenzaldehyde in water.<sup>138</sup> The BTA-based L-proline functionalized SCPN (**P2**, Figure

1.11b) showed a diastereomeric excess up to 94% and an enantiomeric excess up to 70%. The activity and stereoselectivity of the reaction was intricately linked to the L-proline loading on the polymer chain and the amount of BTA as a structuring motif: higher L-proline loading gave higher activity but lower selectivity while replacing BTAMA with LMA (**P3**, Figure 1.11c) resulted in an inactive organocatalyst. In a later study, in which a BTA functionalized L-proline was incorporated to a BTA based SCPN *via* molecular recognition, a higher stereoselectivity was observed.<sup>141</sup>

For both Ru@SCPN and proline@SCPN examples, the origin of the efficient catalysis was attributed to the high effective molarity of substrates, and catalytic sites, and shielding of the active sites *via* compartmentalization in water. Yet, the loss of catalytic activity in the absence of structuring motif in L-proline functionalized SCPNs indicated the need for a structured, conformationally adaptable pocket *via* BTA induced helical stack formation and required further investigation. Recent studies on enzyme catalysis using 2,2,6,6-tetramethyl-1-piperidinyloxyl (TEMPO) radical spin labels have helped to elucidate the role of structure and dynamics of hydration water in relation to their activity.<sup>142</sup> Therefore, polymers **P4** (Figure 1.11d) and **P5** (Figure 1.11e) were prepared as models for **P2** and **P3**, respectively. Analysis of the polymers was performed using electron paramagnetic resonance (EPR) line-shape analysis and the local water translational diffusion dynamics within 0.5-1 nm of tethered TEMPO spin labels *via* solution-state Overhauser dynamic nuclear polarization (ODNP) NMR relaxometry under ambient solution conditions by Stals and Cheng *et al.*<sup>143</sup> A stronger retardation of surface water was reported for **P4** compared to **P5** as a result of a more ordered packing of the folded core by BTA self-assembly, which consequently displays a more ordered polymer surface and solvation structure in water. The surface water diffusivity serves as an important parameter that differs for a structured and non-structured SCPN, however, further research is needed to reveal the exact reason why a more retarded hydration shell would be so critical for the activity.

Recently, a new family of BTA-based amphiphilic SCPNs was prepared using the post-polymerization modification of poly(pentafluorophenyl acrylate) (pPFPA). Ligand-containing BTA-based amphiphilic SCPNs capable of coordinating to Cu(I) (**P6**, **P8**, Figure 1.11f) or Pd(II) (**P7**, Figure 1.11f) were prepared for bio-orthogonal organometallic catalysts while porphyrin-containing SCPNs were prepared as photosensitizers (**P9**, Figure 1.11g).<sup>140</sup> **P6** and **P8** significantly accelerated azide-alkyne cycloaddition reactions while **P7** efficiently catalysed depropargylation reactions. Most importantly, these catalytic reactions proceeded efficiently in phosphate buffer at physiological pH and at low substrate concentrations, demonstrating that SCPNs are promising systems to function in complex media, e. g. cellular environments.



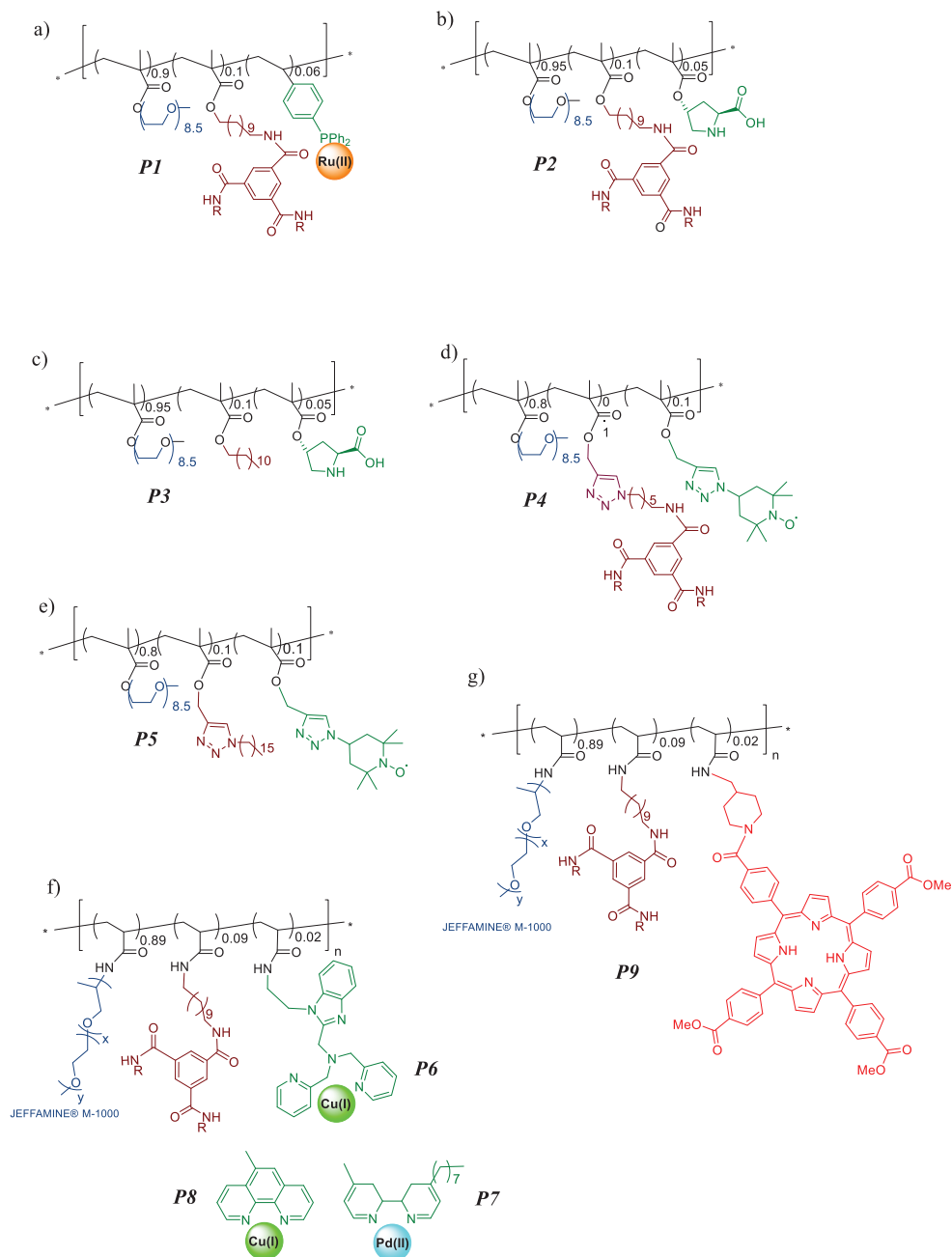


**Figure 1.11** Chemical structures of several amphiphilic SCPNs studied; (a) **P1**: Ru(II)@SCPNTA, (b) **P2**: Proline@SCPNTA, (c) **P3**: Proline@SCPNTA, (d) **P4**: TEMPO@SCPNTA, (e) **P5**: TEMPO@SCPNTA, (f) **P6-P7-P8**: Cu(I)/Pd(II)@SCPNTA, (g) **P9**: Porphyrin@SCPNTA ( $R = (S)$ -3,7-dimethyloctyl).

## 1.6 Aim and outline

Folding polymer chains *via* pendant supramolecular recognition motifs into single chain polymeric nanoparticles is an emerging field of research, crossing the boundaries between polymer chemistry, supramolecular chemistry and catalysis. The aim of this thesis is to make the next step in the complexity of folding synthetic polymers by preparing polymers that fold through orthogonal interactions into defined particles and to employ these particles as functional nano-sized reactors.

Therefore, *Chapter 2* discusses the effect of the local BTA concentration on the folding behavior of the polymers in organic solvents and their final collapsed structure. Hydrophobic methacrylate based polymers were prepared with varying BTA distributions, i.e. random, diblock and gradient, by RAFT and ATRP techniques. Folded polymers were extensively studied using a combination of CD, DLS and AFM techniques.

*Chapter 3* describes the design and synthesis of an ABC-type triblock copolymer that is decorated with complementary motifs, i.e. Hamilton wedge (HW, A block), benzene-1,3,5-tricarboxamide (BTA, B block) and cyanuric acid (CA, C block) to carry the level of complexity one step further, in order to gain more control on the folding process in organic solvents. The precursor ABC-type triblock copolymer was prepared *via* reversible addition-fragmentation chain transfer (RAFT) polymerization and structuring motifs were incorporated into the linear triblock copolymer side-chains *via* post functionalization. <sup>1</sup>H-NMR studies in combination with CD spectroscopy evidenced that the BTA and HW-CA self-assembly steps take place orthogonally in diluted solution. In addition, the final aggregates formed by these two orthogonal forces, namely HW-CA pseudo crosslinking and BTA stacking, are characterized by DLS as well as AFM.

*Chapter 4* discusses the design and synthesis of a water soluble ABA type triblock copolymer bearing both BTA and 2-ureido-4[1H]-pyrimidinone (UPy) moieties on B and A blocks, respectively. An ABA triblock copolymer possessing different pendant functional groups in the A and B blocks was efficiently prepared *via* ATRP, to which BTA and UPy moieties were ligated *via* post-functionalization. The BTA-based helical stack formation in water was evidenced *via* CD spectroscopy. The UPy dimerization in CHCl<sub>3</sub> was evidenced *via* <sup>1</sup>H-NMR studies. The collapse of polymers into nanoparticles in water was evidenced by DLS. Nile-red experiments confirmed the existence of hydrophobic environment inside the formed nanoparticles.

*Chapter 5* assesses the role of benzene-1,3,5-tricarboxamide (BTA) groups for the catalytic activity of SCPNs in water. The Ru(II) loaded SCPNs were tested in the transfer hydrogenation of cyclohexanone. The study revealed that BTA induced stack formation is not essential for SCPN formation and catalytic activity when SDP-bearing copolymers with hydrophobic pendants are present to provide hydrophobic, isolated reaction pockets around Ru(II) complexes.

Last, in *Chapter 6* the utilization of SCPNs to create selective hydrophobic reaction spaces was explored. Competition experiments were performed in which a mixture of alcohol substrates that varied in hydrophobicity (tetrahydropyranol, cyclohexanol and 4-*tert*-butylcyclohexanol) showed that the SCPN folding around an intrinsically non-selective Ru(II) centre successfully created a selective, hydrophobic, reaction space in water. A significant

selectivity was observed; both the rate as well as the end conversion differed between the three substrates. A similar selectivity was observed in the reverse reaction, namely the transfer hydrogenation of the corresponding ketones. These results demonstrated that SCPN folding around the active site provided efficient reaction spaces to achieve selectivity, based on hydrophobic effects. Finally, the potential of SCPN approach in performing one-pot multi-step reactions was introduced.

### 1.7 References

- (1) (a) C. B. Anfinsen *Science* **1973**, *181*, 223; (b) C. M. Dobson *Nature* **2003**, *426*, 884; (c) K. Lindorff-Larsen, S. Piana, R. O. Dror, D. E. Shaw *Science* **2011**, *334*, 517; (d) R. P. Cheng, S. H. Gellman, W. F. De Grado *Chem. Rev.* **2001**, *101*, 3219; (e) M. Garcia-Viloca *Science* **2004**, *303*, 186; (f) G. M. Whitesides, J. P.; Mathias, C. T. Seto *Science* **1991**, *254*, 1312; (g) M. Rief, M. Gautel, F. Oesterhelt, J. M. Fernandez, H. E. Gaub *Science* **1997**, *276*, 1109; (h) M. Oberhouser, A. F. Carrion-Vazquez, S. B. Fowler, P. E. Marszalek, S. E. Broedel, J. Clarke, J. M. Fernandez *Proc. Natl. Acad. Sci. U.S.A.* **1999**, *96*, 3694; (i) A. M. Kushner, Z. Guan *Angew. Chem. Int. Ed.* **2001**, *50*, 9026; (j) G. M. Whitesides, M. Boncheva *Proc. Natl. Acad. Sci. U.S.A.* **2002**, *99*, 4769.
- (2) G. D. Rose, P. J. Fleming, J. R. Banavar, A. Maritan *Proc. Natl. Acad. Sci. U.S.A.* **2006**, *103* 16623.
- (3) J. A. Pomposo *Polym. Int.* **2014**, *63*, 589.
- (4) Y. Imanishi, N. Naga *Prog. Polym. Sci.* **2001**, *26*, 1147.
- (5) S. Aoshima, S. Kanaoka *Chem. Rev.* **2009**, *109*, 5245.
- (6) N. Hadjichristidis, M. Pitsikalis, S. Pispas, H. Iatrou *Chem. Rev.* **2001**, *101*, 3747.
- (7) C. W. Bielawski, R. H. Grubbs *Prog. Polym. Sci.* **2007**, *32*, 1.
- (8) G. Moad, E. Rizzardo, S. H. Thang, *Acc. Chem. Res.* **2008**, *41*, 1133.
- (9) G. Moad, E. Rizzardo, S. H. Thang *Aust. J. Chem.* **2009**, *62*, 1402.
- (10) A. Gregory, M. H. Stenzel *Prog. Polym. Sci.* **2012**, *37*, 38.
- (11) D. Bertin, D. Gigmes, S. R. A. Marque, P. Tordo *Chem. Soc. Rev.* **2011**, *40*, 2189.
- (12) J. Nicolas, Y. Guillauneuf, C. Lefay, D. Bertin, D. Gigmes, B. Charleux *Prog. Polym. Sci.* **2013**, *38*, 63.
- (13) N. V. Tsarevsky, K. Matyjaszewski *Chem. Rev.* **2007**, *107*, 2270.
- (14) M. Ouchi, T. Terashima, M. Sawamoto *Chem. Rev.* **2009**, *109*, 4963.
- (15) K. Matyjaszewski *Macromolecules* **2012**, *45*, 4015.
- (16) G. Gody, T. Maschmeyer, P. B. Zetterlund, S. Perrier *Nature Commun.* **2013**, *4*, 2505.
- (17) H. K. Murnen, A. R. Khokhlov, P. G. Khalatur, R. A. Segalman, R. N. Zuckermann *Macromolecules* **2012**, *45*, 5229.
- (18) A. A. Ouahabi, L. Charles, J. F. Lutz *J. Am. Chem. Soc.* **2015**, *137*, 5629.
- (19) Z. Guan *J. Am. Chem. Soc.* **2002**, *124*, 5616.
- (20) O. W. Webster *Science* **1991**, *251*, 887.
- (21) K. Matyjaszewski *Polym. Int.* **2003**, *52*, 1559.
- (22) W. A. Braunecker, K. Matyjaszewski *Prog. Polym. Sci.* **2007**, *32*, 93.
- (23) J. F. Lutz, M. Ouchi, D. R. Liu, M. Sawamoto, *Science* **2013**, *341*, 1238149.

- (24) M. K. Georges, R. P. N. Veregin, P. M. Kazmaier, G. K. Hamer *Macromolecules* **1993**, *26*, 2987.
- (25) J. Nicolas, Y. Guillauneuf, C. Lefay, D. Bertin, D. Gigmes, B. Charleux *Prog. Polym. Sci.* **2013**, *38*, 63.
- (26) J. Chiefari, Y. K. Chong, F. Ercole, J. Krstina, J. Jeffery, T. P. T. Le, R. T. A. Mayadunne, G. F. Meijs, C. L. Moad, G. Moad, E. Rizzardo, S. H. Thang *Macromolecules* **1998**, *31*, 5559.
- (27) (a) M. Stenzel, C. Barner-Kowollik, T. P. Davis, H. M. Dalton *Macromol. Biosci.* **2004**, *4*, 445. (b) T. L. U. Nguyen, B. Farrugia, T. P. Davis, C. Barner-Kowollik, M. H. Stenzel *J. Polym. Sci. Part A: Polym. Chem.* **2007**, *45*, 3256.
- (28) S. Perrier, C. Barner-Kowollik in *Handbook of RAFT Polymerization* (Ed. C. Barner-Kowollik), Wiley-VCH, Weinheim, **2008**, 455.
- (29) M. Kato, M. Kamigaito, M. Sawamoto, T. Higashimura *Macromolecules* **1995**, *28*, 1721.
- (30) J. S. Wang, K. Matyjaszewski *J. Am. Chem. Soc.* **1995**, *117*, 5614.
- (31) B. M. Rosen, V. Percec *Chem. Rev.* **2009**, *109*, 5069.
- (32) W. Jakubowski, K. Matyjaszewski *Angew. Chem. Int. Ed.* **2006**, *45*, 4482.
- (33) K. Matyjaszewski, W. Jakubowski, K. Min, W. Tang, J. Huang, W. A. Braunecker, N. V. Tsarevsky *Proc. Natl. Acad. Sci.* **2006**, *103*, 15309.
- (34) W. Jakubowski, K. Min, K. Matyjaszewski *Macromolecules* **2006**, *39*, 39.
- (35) V. Coessens, T. Pintauer, K. Matyjaszewski *Prog. Polym. Sci.* **2001**, *26*, 337.
- (36) K. Matyjaszewski, J. Xia *Chem. Rev.* **2001**, *101*, 2921.
- (37) M. Seo, J. B. Beck, J. M. J. Paulusse, C. J. Hawker, S. Y. Kim *Macromolecules* **2008**, *41*, 6413.
- (38) D. Mecerreyes, V. Lee, C. J. Hawker, J. L. Hedrick, A. Wursch, W. Volksen, T. Magbitang, E. Huang, R. D. Miller *Adv. Mater.* **2001**, *13*, 204.
- (39) J. Meeuwissen, J. N. H. Reek *Nat. Chem.* **2010**, *2*, 615.
- (40) M. Gonzalez-Burgos, A. Latorre-Sanchez, J. A. Pomposo *Chem. Soc. Rev.* **2015**, *44*, 6122.
- (41) B. M. Rossbach, K. Leopold, R. Weberskirch *Angew. Chem. Int. Ed.* **2006**, *45*, 1309.
- (42) (a) S. Striegler, J. D. Barnett, N. A. Dunaway *ACS Catal.* **2012**, *2*, 50; (b) Z. Chen, Z. Hua, J. Wang, Y. Guan, M. Zhao, Y. Li *Appl. Catal. A* **2007**, *328*, 252; (c) G. Wulff, B.-O. Chong, U. Kolb *Angew. Chem. Int. Ed.* **2006**, *45*, 2955.
- (43) S. M. Grayson, J. M. J. Fréchet *Chem. Rev.* **2001**, *101*, 3819.
- (44) B. Zhang, H. Zhang, Y. Li, J. N. Hoskins, S. M. Grayson *ACS Macro Lett.* **2013**, *2*, 845.
- (45) A. W. Bosman, R. Vestberg, A. Heumann, J. M. J. Fréchet, C. J. Hawker *J. Am. Chem. Soc.* **2003**, *125*, 715.
- (46) T. Terashima, M. Kamigaito, K.Y. Baek, T. Ando, M. Sawamoto *J. Am. Chem. Soc.* **2003**, *125*, 5288
- (47) B. Helms, S. J. Guillaudeu, Y. Xie, M. McMurdo, C. J. Hawker, J. M. J. Fréchet *Angew. Chem. Int. Ed.* **2005**, *44*, 6384.
- (48) B. Helms, J. M. J. Fréchet *Adv. Synth. Catal.* **2006**, *348*, 1125.
- (49) Y. Chi, S. T. Scroggins, J. M. J. Fréchet *J. Am. Chem. Soc.* **2008**, *130*, 6322.

- (50) R. J. R. W. Peters, M. Marguet, S. Marais, M. W. Fraaije, J. C. M. van Hest, S. Lecommandoux *Angew. Chem. Int. Ed.* **2014**, *53*, 146.
- (51) A. Lu, R. K. O'Reilly *Curr. Op. Biotechnol.* **2013**, *24*, 639.
- (52) D. Mecerreyes, V. Lee, C. J. Hawker, J. L. Hedrick, A. Wursch, W. Volksen, T. Magbitang, E. Huang, R. D. Miller *Adv. Mater.* **2001**, *13*, 204.
- (53) J. Pyun, C. Tang, T. Kowalewski, J. M. J. Fréchet, C. J. Hawker *Macromolecules* **2005**, *38*, 2674.
- (54) O. Altintas, C. Barner-Kowollik *Macromol. Rapid Commun.* **2012**, *33*, 958.
- (55) A. Sanchez-Sanchez, I. Perez-Baena, J. A. Pomposo *Molecules* **2013**, *18*, 3339.
- (56) L. Li, K. Raghupathi, C. Song, P. Prasad, S. Thayumanavan *Chem. Commun.* **2014**, *50*, 13417.
- (57) C. K. Lyon, A. Prasher, A. M. Hanlon, B. T. Tuten, C. A. Tooley, P. G. Frank, E. B. Berda *Polym. Chem.* **2015**, *6*, 181.
- (58) M. Huo, N. Wang, T. Fang, M. Sun, Y. Wei, J. Yuan *Polymer* **2015**, *66*, 11.
- (59) K. S. Park, D. Y. Kim, S. K. Choi, D. H. Suh *Jpn. J. Appl. Phys.* **2003**, *42*, 3877.
- (60) J. Jiang, S. Thayumanavan *Macromolecules* **2005**, *38*, 5886.
- (61) A. Ruiz de Luzuriaga, N. Ormategui, H. J. Grande, I. Odriozola, J. A. Pomposo, I. Loinaz *Macromol. Rapid Commun.* **2008**, *29*, 1156.
- (62) L. Oria, R. Aguado, J. A. Pomposo, J. Colmenero *Adv. Mater.* **2010**, *22*, 3038.
- (63) A. Ruiz de Luzuriaga, I. Perez-Baena, S. Montes, I. Loinaz, I. Odriozola, I. García, J. A. Pomposo *Macromol. Symp.* **2010**, *296*, 303.
- (64) P. Khanjani, I. Pérez-Baena, L. Boruga, J. A. Pomposo *Macromol. Symp.* **2012**, *145*, 321.
- (65) H. Cengiz, B. Aydogan, S. Ates, E. Acikalin, Y. Yagci *Des. Monomers Polym.* **2011**, *14*, 68.
- (66) N. Ormategui, I. Garcia, D. Padro, G. Cabanero, H. J. Grande, I. Loinaz *Soft Matter* **2012**, *8*, 734.
- (67) I. Perez-Baena, I. Loinaz, D. Padro, I. Garcia, H. J. Grande, I. Odriozola *J. Mater. Chem.* **2010**, *20*, 6916.
- (68) J. E. F. Radu, L. Novak, J. F. Hartmann, N. Beheshti, A. L. Kjoniksen, B. Nyström, J. Borbély *Colloid Polym. Sci.* **2008**, *286*, 365.
- (69) E. Harth, B. van Horn, V. Y. Lee, D. S. Germack, C. P. Gonzales, R. D. Miller, C. J. Hawker *J. Am. Chem. Soc.* **2002**, *124*, 8653
- (70) T. A. Croce, S. K. Hamilton, M. L. Chen, H. Muchalski, E. Harth *Macromolecules* **2007**, *40*, 6028.
- (71) C. T. Adkins, H. Muchalski, E. Harth *Macromolecules* **2009**, *42*, 5786.
- (72) J. N. Dobish, S. K. Hamilton, E. Harth *Polym. Chem.* **2012**, *3*, 857.
- (73) A. E. Cherian, F. C. Sun, S. S. Sheiko, G. W. Coates *J. Am. Chem. Soc.* **2007**, *129*, 11350.
- (74) Y. Bai, H. Xing, G. A. Vincil, J. Lee, E. J. Henderson, Y. Lu, N. G. Lemcoff, S. C. Zimmerman *Chem. Sci.* **2014**, *5*, 2862.
- (75) A. Sanchez-Sanchez, J. A. Pomposo *J. Nanomater.* **2015**, *72*, 3492.
- (76) P. Wang, H. Pu, M. Jin *J. Polym. Sci., Part A: Polym. Chem.* **2011**, *49*, 5133.
- (77) P. Wang, H. Pu, J. Ge, M. Jin, H. Pan, Z. Chang, D. Wan *Mater. Lett.* **2014**, *132*, 102

- (78) B. Zhu, J. Ma, Z. Li, J. Hou, X. Cheng, G. Qian, P. Liu, A. Hu *J. Mater. Chem.* **2011**, *21*, 2679.
- (79) G. Qian, B. Zhu, Y. Wang, S. Deng, A. Hu, *Macromol. Rapid Commun.* **2012**, *33*, 1393.
- (80) X. Jiang, H. Pu, P. Wang *Polymer* **2011**, *52*, 3597.
- (81) G. Li, F. Tao, L. Wang, Y. Li, R. Bai *Polymer* **2014**, *55*, 3696.
- (82) A. Sanchez-Sanchez, I. Asenjo-Sanz, L. Buruaga, J. A. Pomposo *Macromol. Rapid Commun.* **2012**, *33*, 1262.
- (83) P. T. Dirlam, H. J. Kim, K. J. Arrington, W. J. Chung, R. Sahoo, L. J. Hill, P. J. Costanzo, P. Theato, K. Char, J. Pyun *Polym. Chem.* **2013**, *4*, 3765.
- (84) D. Chao, X. Jia, B. Tuten, C. Wang, E. B. Berda *Chem. Commun.* **2013**, *49*, 4178.
- (85) A. Sanchez-Sanchez, S. Akbari, A. Etxeberria, A. Arbe, U. Gasser, A. J. Moreno, J. Colmenero, J. A. Pomposo *ACS Macro Lett.* **2013**, *2*, 491.
- (86) A. J. Moreno, F. Lo Verso, A. Sanchez-Sanchez, A. Arbe, J. Colmenero, J. A. Pomposo *Macromolecules* **2013**, *46*, 9748.
- (87) A. Sanchez-Sanchez, S. Akbari, A. J. Moreno, F. Lo Verso, A. Arbe, J. Colmenero, J. A. Pomposo *Macromol. Rapid Commun.* **2013**, *34*, 1681.
- (88) E. H. H. Wong, S. J. Lam, E. Nam, G. G. Qiao *ACS Macro Lett.* **2014**, *3*, 524.
- (89) J. B. Beck, K. L. Killups, T. Kang, K. Sivanandan, A. Bayles, M. E. Mackay, K. L. Wooley, C. J. Hawker *Macromolecules* **2009**, *42*, 5629.
- (90) B. Zhu, J. Ma, Z. Li, J. Hou, X. Cheng, G. Qian, P. Liu, A. Hu *J. Mater. Chem.* **2011**, *21*, 2679.
- (91) J. He, L. Tremblay S. Lacelle Y. Zhao *Soft Matter* **2011**, *7*, 2380.
- (92) T. A. Croce, S. K. Hamilton, M. L. Chen, H. I. Muchalski, E. Harth *Macromolecules* **2007**, *40*, 6028.
- (93) A. Sanchez-Sanchez, I. Asenjo-Sanz, L. Buruaga, J. A. Pomposo *Macromol. Rapid Commun.* **2012**, *33*, 1262.
- (94) A. E. Cherian, F. C. Sun, S. Sheiko, G. W. Coates *J. Am. Chem. Soc.* **2007**, *129*, 11350.
- (95) J. B. Beck, K. L. Killups, T. Kang, K. Sivanandan, A. Bayles, M. E. Mackay, K. Wooley, C. J. Hawker *Macromolecules* **2009**, *42*, 5629.
- (96) J. Willenbacher, K. N. R. Wuest, J. O. Mueller, M. Kaupp, H.-A. Wagenknecht, C. Barner-Kowollik *ACS Macro Lett.* **2014**, *3*, 574.
- (97) I. Perez-Baena, I. Asenjo-Sanz, A. Arbe, A. J. Moreno, F. Lo Verso, J. Colmenero, J. A. Pomposo *Macromolecules* **2014**, *47*, 8270.
- (98) C. F. Hansell, A. Lu, J. P. Patterson, R. K. O'Reilly *Nanoscale* **2014**, *6*, 4102
- (99) W. Fan, X. Tong, Q. Yan, S. Fu, Y. Zhao *Chem. Commun.* **2014**, *50*, 13492.
- (100) S. K. Hamilton, E. Harth *ACS Nano* **2009**, *3*, 402.
- (101) G. Njjang, G. Liu, L. Hong *Langmuir* **2012** *27*, 7176.
- (102) A. Tamura, M. Oishi, Y. Nagaski *Biomacromolecules* **2009**, *10*, 1818.
- (103) B. T. Tuten, D. Chao, C. K. Lyon, E. B. Berda *Polym. Chem.* **2012**, *3*, 3068.
- (104) B. S. Murray, D. A. Fulton *Macromolecules* **2011**, *44*, 7242.
- (105) E. J. Foster, E. B. Berda, E. W. Meijer *J. Am. Chem. Soc.* **2009**, *131*, 6964.
- (106) T. Mes, R. van der Weegen, A. R. A. Palmans, E. W. Meijer *Angew. Chem. Int. Ed.* **2011**, *50*, 5085.

- (107) N. Hosono, M. A. J. Gillissen, Y. Li, S. Sheiko, A. R. A. Palmans, E. W. Meijer *J. Am. Chem. Soc.* **2013**, *135*, 501.
- (108) M. A. J. Gillissen, I. K.; Voets, E. W. Meijer, A. R. A. Palmans *Polym. Chem.* **2012**, *3*, 3166.
- (109) O. Altintas, T. Rudolph, C. Barner-Kowollik *J. Polym. Sci., Part A: Polym. Chem.* **2011**, *49*, 2566.
- (110) E. A. Appel, J. Dyson, J. del Barrio, Z. Walsh, O. A. Scherman *Angew. Chem. Int. Ed.* **2012**, *51*, 4185.
- (111) J. Romulus, M. Weck *Macromol. Rapid. Commun.* **2013**, *34*, 1518.
- (112) C. C. Cheng, F. C. Chang, H. C. Yen, D. J. Lee, C. W. Chiu, Z. Xin *ACS MacroLett.* **2015**, *4*, 1184.
- (113) O. Altintas, P. Gerstel, N. Dingenouts, C. Barner-Kowollik *Chem. Commun.* **2010**, *46*, 6291.
- (114) O. Altintas, E. Lejeune, P. Gerstel, C. Barner-Kowollik *Polym. Chem.* **2012**, *3*, 640.
- (115) D. E. Whitaker, C. S. Mahon, D. A. Fulton *Angew. Chem. Int. Ed.* **2013**, *52*, 956.
- (116) E. B. Berda, E. J. Foster, E. W. Meijer *Macromolecules* **2010**, *43*, 1430.
- (117) B. J. B. Folmer, E. Cavini, R. P. Sijbesma, E. W. Meijer *Chem. Commun.* **1998**, 1847.
- (118) E. J. Foster, E. B. Berda, E. W. Meijer *J. Polym. Sci. Part A: Polym. Chem.* **2011**, *49*, 118.
- (119) P. J. M. Stals, M. A. J. Gillissen, R. Nicolaÿ, A. R. A. Palmans, E. W. Meijer *Polym. Chem.* **2013**, *4*, 2584.
- (120) N. Hosono, P. J. M. Stals, A. R. A. Palmans, E. W. Meijer *Chem. Asian J.* **2014**, *9*, 1099.
- (121) G. M. ter Huurne, M. A. J. Gillissen, A. R. A. Palmans, I. K. Voets, E. W. Meijer *Macromolecules* **2015**, *48*, 3949.
- (122) T. Terashima, T. Mes, T. F. A. de Greef, M. A. J. Gillissen, P. Besenius, A. R. A. Palmans, E. W. Meijer *J. Am. Chem. Soc.* **2011**, *133*, 4742.
- (123) M. A. J. Gillissen, T. Terashima, E. W. Meijer, A. R. A. Palmans, I. K. Voets *Macromolecules* **2013**, *46*, 4120.
- (124) T. Terashima, T. Sugita, K. Fukae, M. Sawamoto *Macromolecules* **2014**, *47*, 589.
- (125) H. W. H. van Roekel, P. J. M. Stals, M. A. J. Gillissen, P. A. J. Hilbers, A. J. Markvoort, T. F. A. de Greef *Chem. Commun.* **2013**, *49*, 3122.
- (126) P. J. M. Stals, J. Burdyńska, R. Nicolaÿ, A. R. A. Palmans, E. W. Meijer, K. Matyjaszewski, S. S. Sheiko *J. Am. Chem. Soc.* **2013**, *135*, 11421.
- (127) P. J. M. Stals, M. A. J. Gillissen, T. F. E. Paffen, T. F. A. de Greef, P. Lindner, E. W. Meijer, A. R. A. Palmans, I. K. Voets *Macromolecules* **2014**, *47*, 2947.
- (128) N. Hosono, A. M. Kushner, J. Chung, A. R. A. Palmans, Z. Guan, E. W. Meijer *J. Am. Chem. Soc.* **2015**, *137*, 6880.
- (129) (a) C. Liang, J. M. Fréchet *J. Prog. Polym. Sci.* **2005**, *30*, 385; (b) J. Kofoed, L. Reymond *Curr. Op. Chem. Biol.* **2005**, *9*, 656; (c) T. Dwars, E. Paetzold, G. Oehme *Angew. Chem. Int. E. d.* **2005**, *44*, 7174; (d) K. Kirkorian, A. Ellis *Chem. Soc. Rev.* **2012**, *41*, 6138.
- (130) Y. Liu, Y. Wang, Y. Wang, J. Lu, V. Piñón, M. Weck *J. Am. Chem. Soc.* **2011**, *133*, 14260.

- (131) (a) Z. Ge, D. Xie, D. Chen, X. Jiang, Y. Zhang, H. Liu, S. Liu *Macromolecules* **2007**, *40*, 3538; (b) A. Lu, P. Cotanda, J. P. Patterson, D. A. Longbottom, R. K. O'Reilly *Chem. Commun.* **2012**, *48*, 9699; (c) M. C. M. van Oers, L. K. E. A. Abdelmohsen, F. P. J. T. Rutjes, J. C. M. van Hest *Chem. Commun.* **2014**, *50*, 4040; (d) A. Cardozo, C. Julcour, L. Barthe, J. F. Blanco, S. Chen, F. Gayet, E. Manoury, X. Zhang, M. Lansalot, B. Charleux, F. D'Agosto, R. Poli, H. Delmas *J. Catal.* **2015**, *324*, 1.
- (132) (a) C. Berdugo, J. F. Miravet, B. Escruder *Chem. Commun.* **2013**, *49*, 10608; (b) A. Haimov, R. Neumann *J. Am. Chem. Soc.* **2006**, *128*, 15697; (c) B. L. Moore, D. Moatsou, A. Lu, R. K. O'Reilly *Polym. Chem.* **2014**, *5*, 3487; (d) A. Lu, D. Moatsou, I. Hands-Portman, R. K. O'Reilly *ACS MacroLett.* **2014**, *3*, 1235.
- (133) T. Terashima, M. Ouchi, T. Ando, M. Sawamoto *J. Polym. Sci. A. Polym. Chem.* **2011**, *49*, 1061.
- (134) L. N. Neumann, M. B. Baker, C. M. A. Leenders, I. K. Voets, R. P. M. Lafleur, A. R. A. Palmans, E. W. Meijer *Org. Biomol. Chem.* **2015**, *13*, 7711.
- (135) (a) A. W. Bosman, H. M. Janssen, E. W. Meijer *Chem. Rev.* **1999**, *99*, 1665; (b) S. M. Grayson, J. M. J. Fréchet, *Chem. Rev.* **2001**, *101*, 3819; (c) B. Helms, E. W. Meijer, *Science* **2006**, *313*, 929; (d) J. T. V. Yu, T. V. RajanBabu, J. R. Parquette *J. Am. Chem. Soc.* **2008**, *130*, 7845.
- (136) (a) T. Frenzel, W. Solodenko, A. Kirschning, in *Polymeric Materials in Organic Synthesis and Catalysis* **2005**, p 201; (b) T. J. Dickerson, N. N. Reed, K. D. Janda *Chem. Rev.* **2002**, *102*, 3325; (c) B. Helms, J. M. J. Fréchet *Adv. Synth. Catal.* **2006**, *348*, 1125.
- (137) (a) G. Wulff, B. O. Chong, U. Kolb *Angew. Chem. Int. Ed.* **2006**, *45*, 2955; (b) I. Perez-Baena, F. Barroso-Bujans, U. Gasser, A. Arbe, A. J. Moreno, J. Colmenero, J. A. Pomposo *ACS MacroLett.* **2013**, *2*, 775; (c) S. Mavila, I. Rozenberg, N. G. Lemcoff *Chem. Sci.* **2014**, *5*, 4196; (d) A. Sanchez-Sanchez, A. Arbe, J. Colmenero, J. A. Pomposo *ACS MacroLett.* **2015**, *3*, 439; (e) J. Willenbacher, O. Altintas, V. Trouillet, N. Knoefel, M. Monteiro, P. Roesky, C. Barner-Kowollik *Polym. Chem.* **2015**, *6*, 4358.
- (138) E. Huerta, P. J. M. Stals, E. W. Meijer, A. R. A. Palmans *Angew. Chem. Int. Ed.* **2013**, *52*, 2906.
- (139) M. Eberhardt, R. Mruk, R. Zentel, P. Theato *Eur. Polym. J.* **2005**, *41*, 1569.
- (140) Y. Liu, T. Pauloehrl, S. I. Presolski, L. Albertazzi, A. R. A. Palmans, E. W. Meijer *J. Am. Chem. Soc.* **2015**, *137*, 13096.
- (141) E. Huerta, B. van Genabeek, P. J. M. Stals, E. W. Meijer, A. R. A. Palmans *Macromol. Rapid. Commun.* **2014**, *35*, 1320.
- (142) (a) B. D. Armstrong, S. Han *J. Am. Chem. Soc.* **2009**, *131*, 4641; (b) J. M. Franck, A. Pavlova, J. A. Scott, S. Han *Prog. Nucl. Mag. Res. Sp.* **2013**, *74*, 33.
- (143) P. J. M. Stals, C. Y. Cheng, L. van Beek, A. C. Wauters, A.R.A. Palmans, S. Han, E. W. Meijer *Chem. Sci.* **2016**, *7*, 2011.





# Chapter 2

## *Exploring the self-assembly of polymer pendant benzene-1,3,5 tricarboxamides*

**Abstract:** Two sets of benzene-1,3,5-tricarboxamide (BTA) pendant methacrylate copolymers were prepared with the aim to elucidate the effects of molar mass dispersity and the distribution of pendant BTAs along the polymer backbone on the folding behavior of the copolymers. In the first set, 2-ethylhexylmethacrylate (EHMA) was copolymerized with BTA-methacrylate (BTAMA) to afford random copolymers with molar mass dispersities  $D$  varying from 1.06 to 2.27. In the second set, the distribution of the BTA monomer along the copolymer backbone was tuned by preparing a random, a diblock and a gradient EHMA/BTAMA-based copolymer. The self-assembly behavior of the pendant BTAs was studied by temperature-dependent circular dichroism (CD) experiments in 1,2-dichloroethane. The first set of polymers showed almost identical CD cooling curves, suggesting that the self-assembly of the pendant BTA moieties was independent of the molar mass dispersity of the copolymers. In contrast, the copolymers that varied in microstructure showed differently shaped CD cooling curves, and a more intense CD effect was observed for the gradient copolymer. In addition, dynamic light scattering (DLS) and atomic force microscopy (AFM) experiments indicated that the block copolymers formed large, multi-chain aggregates whereas the random and gradient copolymers predominantly formed single chain polymeric nanoparticles. These results indicate that the distribution and local density of pendant BTAs affect the folding behavior of the copolymers whereas the molar dispersity does not, if the distribution of the BTAs remains random. Moreover, interparticle interactions are enhanced by increasing the local density of BTAs in one block of the copolymers.

## 2.1 Introduction

Enantiomerically pure benzene-1,3,5-tricarboxamides (BTAs) are supramolecular units that self-assemble into helical stacks with a preferred helicity due to strong intermolecular threefold hydrogen bonds between the amides of adjacent BTAs.<sup>1-3</sup> Detailed mechanistic studies on BTA self-assembly showed that a highly cooperative process was operative, in which the unfavorable formation of a critical sized aggregate (nucleation) is followed by a favorable elongation process.<sup>4</sup> Later, BTAs were incorporated to polymer chains, with the aim to use these units as a structuring motif for controlling the global conformation of polymer chains. Interestingly, BTA moieties retained their propensity to self-assemble when randomly distributed on a polymer chain as pendant motifs in organic<sup>5,6</sup> and in aqueous solvents.<sup>7,8</sup> Both hydrophobic<sup>5</sup> and amphiphilic polymers<sup>7,9,10</sup> folded reversibly as shown *via* temperature-dependent circular dichroism experiments and the amphiphilic copolymers formed single chain particles of nanometer-sized dimensions. However, detailed studies on both amphiphilic and hydrophobic copolymers with an *increasing degree of polymerization*, but constant BTA content, showed that the folding of these polymers was a non-cooperative process,<sup>10-12</sup> in contrast to the cooperative nature of molecular BTA aggregation.<sup>4,13</sup> This is also very different from the folding of natural polymers such as proteins, and synthetic systems such as foldamers<sup>14-16</sup> and polyisocyanides,<sup>17</sup> which all fold highly cooperatively. The lack of cooperative folding in BTA-based systems was attributed to the tendency of the pendant BTA units to form multiple, segregated stacks in the SCPNs, as recently confirmed by the ‘Sergeant-and-Soldiers’ experiments on isobornyl methacrylate/BTA-methacrylate (BTAMA) based block-copolymers.<sup>11</sup> In addition, for amphiphilic random *o*EGMA/BTAMA copolymers with increasing polymer chain length but constant BTA ratio, an elongated shape was observed *via* SAXS experiments in water.<sup>10</sup> This elongation was assumed to result in a constant local BTA concentration within local domains of the folded aggregate as the copolymer increases in length.

One could argue that the dispersity of the polymers and the lack of exact localization of the BTAs along the polymer chain could affect the folding of the polymers. Although controlled radical polymerization techniques were applied to prepare polymers in these aforementioned studies, the end products were still a mixture of oligomers with varying lengths and sequences. Thus the observed folding behaviour is a summation of a large number of cooling-curves of a polymer ensemble.

For perfectly defined polymers or oligomers the importance of length has been shown in the past. For example, a direct correlation between  $\epsilon$ -caprolactone oligomer length and thermal properties, as a result of the change in the crystal behaviour, was shown by Hawker and coworkers.<sup>18</sup> Nowick and coworkers demonstrated the translation of precise control on the length of the building blocks to final structures *via* preparation of rod-like peptide architectures (1 to 10 nm), by using well-defined nanometer sized amino acids (1 nm) as building blocks.<sup>19</sup> Moore *et al.* showed a trend in physical and chemical properties associated with chain-length of poly(phenyleneethynylenes) *via* extensive chain-length dependence tests.<sup>20</sup> Therefore, it is reasonable to expect that if we increase or decrease the number of the different species in the summation (i.e. the molar mass dispersity), that also a difference in folding behavior can be observed.

While these aforementioned examples highlight the importance of the dispersity *via* length control, Zuckermann and coworkers showed the impact of the hydrophobic unit sequence along a polymer backbone for coil-to-globule transition in water. Increased cooperativity was found for a ‘protein like’ sequence compared to a repeating pattern of the hydrophobic unit distribution.<sup>21</sup> Also, Torkelson *et al.* demonstrated the dependence of glass transition temperature ( $T_g$ ) behavior on the monomer sequence of styrene and acrylic acid based copolymers with similar compositions.<sup>22</sup> The random copolymers displayed one narrow  $T_g$ , while diblock copolymers with similar monomer compositions displayed two narrow  $T_g$ 's ( $T_g$ 's matching with the homopolymers of the each comonomer) and the gradient copolymer exhibited a unusually broad  $T_g$  with an improved upper limit compared to the high  $T_g$  of the diblock copolymer.

In this chapter, we aim to gain a deeper insight into the folding behavior of the hydrophobic EHMA/BTAMA based copolymers by investigating the effect of two important factors; molar mass dispersity of the polymer backbone, and different distributions of BTA units along the polymer chain; *e.g.* randomly over the entire chain, randomly on half of the chain and in a gradient fashion over the entire chain (Figure 2.1). Temperature-dependent CD measurements were performed to elucidate the folding behavior of the obtained copolymers. In addition, atomic force microscopy (AFM) and dynamic light scattering (DLS) experiments were performed to elucidate the size of the formed aggregates in dry and dissolved states, respectively. Part of the work described in this chapter was performed in collaboration with Marly J. G. M. Hummelink, while the gradient polymer described in the second part was prepared in collaboration with Yusuke Ogura and Dr. Takaya Terashima of Kyoto University, Japan.

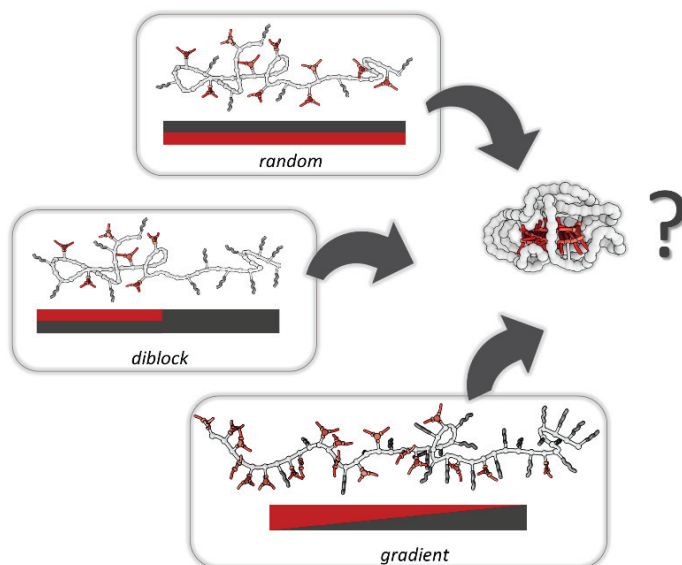
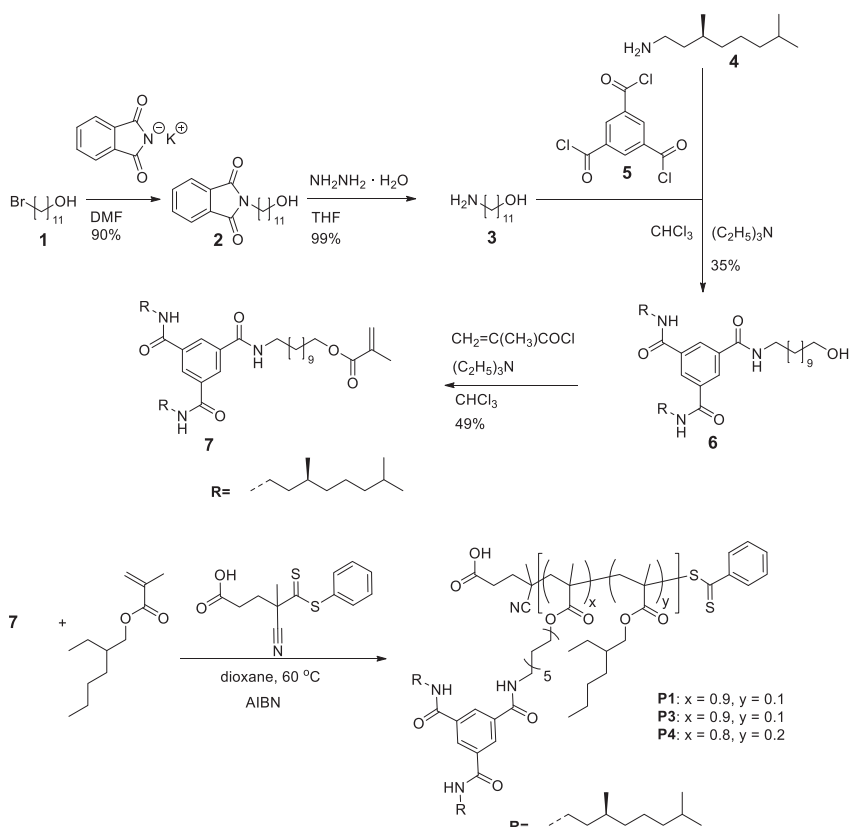


**Figure 2.1** Schematic representation of the folding of BTA functionalized polymers studied in this chapter.

## 2.2 Effect of molar mass dispersity on folding of poly(EHMA-co-BTAMA)

To investigate the effect of molar mass dispersity on the self-assembly of the pendant BTA units, a range of random BTA containing copolymers, with narrow and broad molar mass dispersities, were synthesized *via* a reversible addition fragmentation transfer (RAFT) polymerization and characterized *via*  $^1\text{H-NMR}$  and SEC.

RAFT was applied as a polymerization technique due to its tolerance towards a variety of functional groups and also for its metal-free nature that makes it easy to apply.<sup>23,24</sup> Polymers with a *DP* of  $\sim 250$  were prepared in order to form particles with sizes that can be observed easily by scattering techniques and AFM. BTA methacrylate (BTAMA) was prepared *via* a well-known route,<sup>7</sup> which is depicted in Scheme 2.1. This route is based on a statistical Schotten-Baumann reaction of benzene-1,3,5-tricarboxylic acid chloride with 11-aminoundecanol (obtained from 11-bromoundecanol in a Gabriel synthesis) and (*S*)-3,7-dimethyloctylamine. This latter amine was found to have an enantiomeric excess (*ee*) of 98.4%.<sup>25</sup> Alcohol **6** was isolated from the resulting reaction mixture with column chromatography and reacted in a second Schotten-Baumann reaction with methacryloyl chloride to form BTAMA **7**.



Scheme 2.1 Synthesis of **7**, **P1**, **P3** and **P4**.

As a comonomer, we chose 2-ethylhexylmethacrylate, since this monomer is known to solubilize BTA-containing copolymers in pure solvent, 1,2-dichloroethane (DCE).<sup>12</sup> DCE is also able to create an environment wherein BTA units can aggregate as, shown in previous circular dichroism (CD) studies,<sup>12</sup> while having boiling point that is high enough for the BTA to reach the unaggregated state. A total BTA incorporation of around 10 % was applied to ensure good polymer solubility while providing a sufficient amount of BTA units per polymer chain to induce the folding.

### 2.2.1 Synthesis of poly(EHMA-co-BTAMA) with a narrow molar mass dispersity

A EHMA/BTAMA based copolymer **P1** with a degree of polymerization ( $DP$ ) around 250 was synthesized using 4-cyano-4-((phenylcarbonothioyl)thio)pentanoic acid as chain transfer agent (CTA), azobisisobutyronitrile (AIBN) as initiator, and dioxane as a solvent (Scheme 2.1). The polymerization was stopped around 80% monomer conversion, as determined by the comparison of monomer and polymer peak integrals of corresponding monomers in the crude polymerization mixture. The SEC trace (THF, relative to polystyrene (PS) standards) of **P1** showed a monomodal peak with narrow molar mass dispersity ( $D = 1.12$ ) and a molecular weight  $M_n$  of 36.0 kDa (THF-SEC). Furthermore, **P1** was characterized by <sup>1</sup>H-NMR to determine the incorporation of EHMA and BTAMA monomers (Figure 2.2). The results are summarized in Table 2.1. The observed polymer composition matched very well with the composition of the monomer feed.

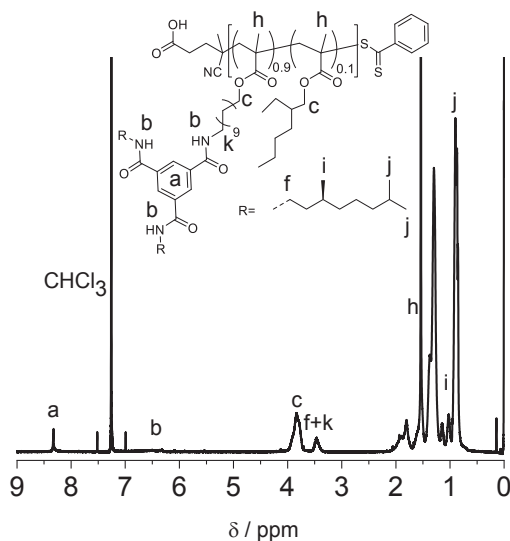


**Figure 2.2** Typical example of a <sup>1</sup>H-NMR spectrum for an EHMA/BTAMA random copolymer in CDCl<sub>3</sub> with assignment of the most important peaks (shown here is **P3**, see Table 2.2 for details).

To reduce the molar mass dispersity, recycling-SEC was used. Prior to the fractionation, SEC was applied in CHCl<sub>3</sub> on **P1**. CHCl<sub>3</sub> was confirmed to be a suitable solvent for the fractionation based on the observed narrow  $D$  value (1.23), even though a slight increase in  $D$  was observed in the CHCl<sub>3</sub>-SEC compared to THF-SEC ( $D = 1.06$ ), indicating some interaction

between the amide groups of the BTAs and the SEC column. The recycling SEC was applied on **P1** with  $\text{CHCl}_3$  as the mobile phase. After fractionation of **P1** in one recycling cycle, **P1a** ( $M_n = 40.3$  kDa,  $\bar{D} = 1.06$ , THF-SEC) was obtained, which indeed showed a smaller molar mass dispersity than that of starting polymer **P1** ( $\bar{D} = 1.12$ , THF-SEC), as shown in Figure 2.3.

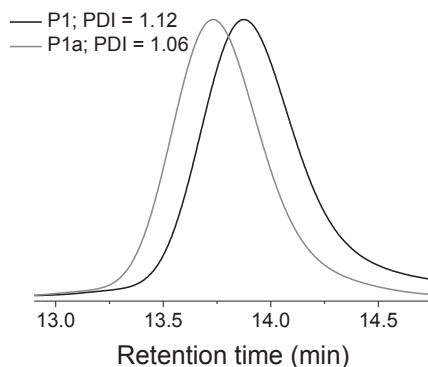


**Figure 2.3** THF-SEC trace of polymer **P1** and **P1a**.

Since the tailing on the low molecular weight side of the SEC trace was eliminated via the fractionation process, an increase in the molecular weight of **P1a** ( $M_n = 40.3$  kDa, THF-SEC, Table 2.1) compared to **P1** ( $M_n = 36.0$  kDa, Table 2.1) was observed. The average number of BTA moieties per polymer chain for **P1a** was determined as 12% via  $^1\text{H-NMR}$  and this fits well within the range of the target BTA content of  $10 (\pm 2)\%$ .

**Table 2.1** Conditions and results for the copolymer preparation.

	Feed ratio [% BTA]	Feed DP [-]	Observed ratio <sup>a</sup> [% BTA]	Conversion <sup>a</sup> [%]	BTAs <sup>b</sup> [#]	DP <sup>a</sup> [-]	$M_n^a$ [kDa]	$M_n^c$ [kDa]	$\bar{D}^c$ [-]
<b>P1</b>	8	259	8	83	17	215	51.4	36.0	1.12
<b>P1a</b>	n. a.	n. a.	12	n. a.	n. d.	n. d.	n. d.	40.3	1.06
<b>P2</b>	8	250	9	76	15	190	46.6	49.9	2.27

*a: Determined by  $^1\text{H-NMR}$ , b: Average number of BTAs per polymer chain, and c: Determined by THF-SEC relative to PS standards. n.a.: not applicable.*

### 2.2.2 Synthesis of poly(EHMA-co-BTAMA) with broad molar mass dispersity

A broad dispersity EHMA/BTAMA copolymer was prepared to compare with the folding behavior of random copolymers **P1** ( $\bar{D} = 1.12$ , THF-SEC) and **P1a** ( $\bar{D} = 1.06$ , THF-SEC). Hereto, the same RAFT procedure was applied, except that the mixture was not degassed. As a result, the control during the polymerization process is reduced due to the oxidation of the RAFT-CTA and/or the presence of oxygen-radicals, resulting in a broader dispersity. We preferred this method compared to a normal free radical polymerization process because it avoids the

Trommsdorff-effect. The copolymerization of EHMA and BTAMA was stopped at 76% total monomer conversion, affording copolymer **P2** which showed a  $D$  of 2.27 and a  $M_n$  of 49.9 kDa (SEC-THF). **P2** comprised 9% of BTA units as evidenced by  $^1\text{H-NMR}$  (Table 2.1).

### 2.2.3 Circular dichroism studies

Circular dichroism (CD) spectroscopy is a powerful technique to assess the presence of helical BTA-based aggregates within the SCPNs. Previously, it was shown that a stereogenic center with an (*S*) configuration in the BTA side chain gives rise to a negative Cotton effect, with a maximum at  $\lambda = 223$  nm, indicative of a bias for the *M* helical sense.<sup>3</sup> Especially, the shape and the magnitude of a CD spectrum in combination with the temperature dependent behaviour can provide insights into the folding process of the studied self-assembling system.<sup>26</sup>

The folding behavior of the synthesized copolymers was investigated *via* temperature-dependent CD in DCE ( $[\text{BTA}] = 5 \cdot 10^{-5}$  M,  $l = 0.5$  cm, cooling rate = 60 °C/h), a representative CD-spectrum at 20 °C is shown in Figure 2.4, left. The cooling curves of the three copolymers are almost identical (Figure 2.4, right), at high temperatures the BTAs on the polymers are not aggregated in a helical aggregate, while cooling results in the aggregation of the BTAs into a helical aggregate, and thus a CD-effect is observed. Reducing the cooling rate from 60 °C/h to 30 °C/h for **P2** did not affect the shape of the cooling curve, indicating that the polymer is in thermodynamic equilibrium.

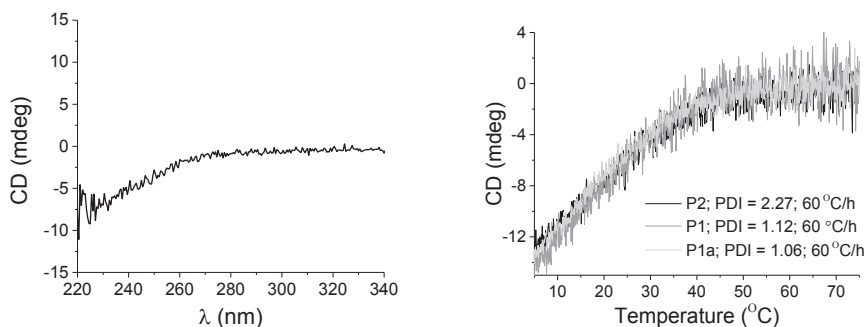


**Figure 2.4** CD spectrum of **P1** measured at 20 °C in DCE ( $[\text{BTA}] = 50 \mu\text{M}$ ,  $l = 0.5$  cm) (left). Temperature - dependent CD effect of 2-EHMA/BTAMA random copolymers **P1**, **P1a**, and **P2** in DCE ( $\lambda = 223$  nm,  $[\text{BTA}] = 50 \mu\text{M}$ ,  $l = 0.5$  cm). The cooling runs were performed at a cooling rate of 60 °C/hour (right).

The super-imposable cooling curves indicate that the self-assembly of the pendant BTA moieties, probed by CD spectroscopy, is independent of the dispersity of the copolymers. Since copolymers that are similar to **P1** previously showed non-cooperative assembly,<sup>12</sup> we can conclude that also these three copolymers show non-cooperative folding. It should be considered, however, that although polymer dispersities are controlled, the observed cooling curves for BTA functionalized polymers here are still a summation of a large number of cooling-curves of a polymer ensemble with varying lengths and random composition/distributions.



### 2.3 Investigating the effect of distribution over the polymer chain on the self-assembly of pendant-BTAs

In order to avoid polarity changes due to the differences in concentration of BTAs per polymer chain, we prepared polymers in which the BTA incorporation ratio and *DP* of the copolymers were kept constant, while the *distribution* of pendant BTA units was varied. This was achieved by using random, diblock and gradient copolymer structures with constant *DP*s and BTA incorporations. This allowed the average distance between adjacent pendant BTA units to be varied from concentrated only in one block of the diblock structure, to a gradient distribution along the entire chain, and finally to a random distribution. Random and diblock copolymers were prepared *via* the RAFT technique and the gradient copolymer was prepared *via* the synchronization of the ruthenium-catalyzed living radical polymerization and in-situ transesterification of methacrylates. To confirm the effect of the higher BTA concentrations on folding, a random copolymer with 20% BTA incorporation and a *DP* of 250 was also prepared.

#### 2.3.1 Synthesis of random copolymers

2-EHMA/BTAMA random copolymers **P3** and **P4** with ~10% and ~20% BTA incorporation were synthesized in a similar way as described for random copolymer **P1** (Scheme 2.1). To avoid termination, polymerizations were stopped around 80% total monomer conversion. **P3** was obtained with  $\bar{D} = 1.24$ ,  $M_n = 56.4$  kDa and 8% BTAs, and **P4** was obtained with  $\bar{D} = 1.32$ ,  $M_n = 45.7$  kDa and 19% BTAs as was evidenced by SEC (THF, relative to PS standards) and  $^1\text{H-NMR}$  (Table 2.2). As a typical example of a  $^1\text{H-NMR}$  spectrum for a random EHMA/BTAMA based polymer, **P3**, in  $\text{CDCl}_3$  is shown in Figure 2.2 (*vide supra*).

Table 2.2 Conditions and results for the copolymer preparation.

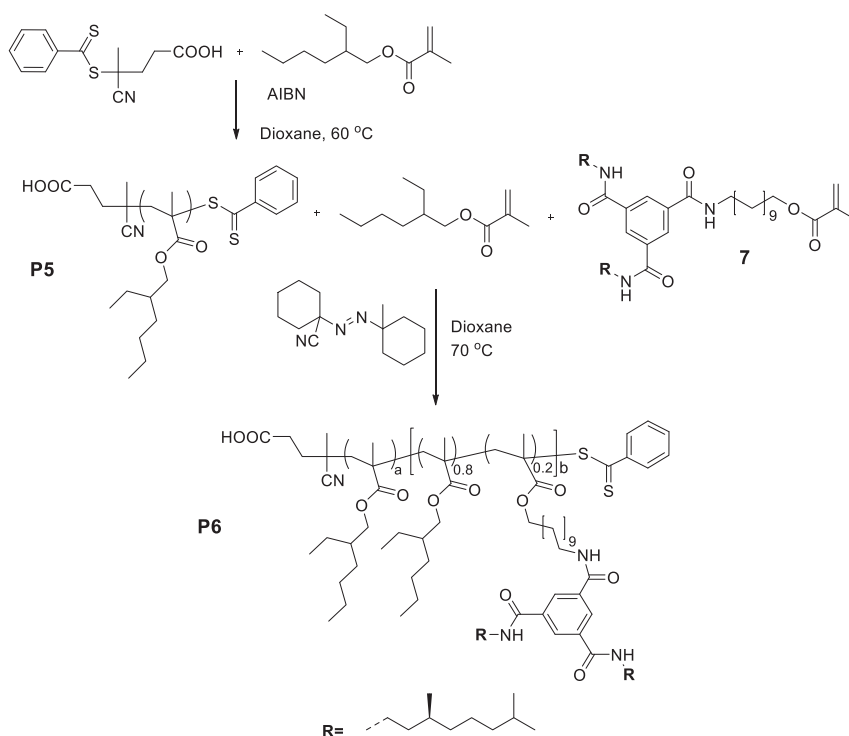
	Feed BTA [%]	Feed <i>DP</i> [-]	Obs. ratio <sup>a</sup> [%]	Conv. <sup>a</sup> [%]	BTAs <sup>b</sup> [#]	<i>DP</i> <sup>a</sup> [-]	$M_n$ <sup>a</sup> [kDa]	$M_n$ <sup>c</sup> [kDa]	$\bar{D}$ <sup>c</sup> [-]	$R_{\text{H}}$ <sup>d</sup> [nm]	$R_{\text{H}}$ <sup>e</sup> [nm]
<b>P3</b>	8	301	8	83	20	250	65.7	56.4	1.24	8.0	7.8
<b>P4</b>	8	335	10	58	26	256	59.9	46.6	1.41	48	7.5
<b>P5</b>	0	271	0	57	0	154	30.5	26.7	1.12	n. d.	n. d.
<b>P6</b>	20	295	19	80	45	236	70.5	45.7	1.32	159	7.2
<b>P7</b>	12	297	8	74	17	220	52.7	45.0	1.34	11.3 <sup>f</sup>	n. d.

<sup>a</sup> Determined by  $^1\text{H NMR}$ . <sup>b</sup> Average number of BTAs per polymer chain. <sup>c</sup> Determined by THF-SEC related to PS standard. <sup>d</sup> In 1,2-dichloroethane, and <sup>e</sup> in THF, <sup>f</sup> A small contribution of larger particles observed. n.d.: not determined.

#### 2.3.2 Synthesis of diblock copolymers

The most commonly used technique to synthesize diblock copolymers by RAFT polymerization, is the chain extension of a macro-RAFT agent.<sup>27</sup> The diblock copolymer **P6** was synthesized *via* chain extension of a macro-RAFT agent from a 2-EHMA homopolymer (**P5**). For the synthesis of the macro-RAFT, 4-cyano-4-((phenylcarbonothioyl)thio)pentanoic acid was used as RAFT-

CTA (Scheme 2.2). To avoid termination of the living chains and to keep a high number of active CTAs, the polymerization of the macro-RAFT agent was stopped around 60% monomer conversion. No purification of the macro-RAFT agent was performed in order to avoid the loss of activity of the macro-RAFT. **P5** was analyzed by  $^1\text{H}$  NMR and THF-SEC ( $DP = 154$ ,  $M_n = 26.7$  kDa,  $D = 1.12$ ). The remaining excess of 2-EHMA in the reaction mixture of **P5** was also used for the chain extension reaction. Since the half-life of AIBN is 10 hours at  $65^\circ\text{C}$ ,<sup>28</sup> and initiation of the RAFT-CTA is preferred due to the inherently high chain-transfer constant, we assumed that no AIBN or unreacted RAFT-CTA remained in the solution.<sup>29</sup> To obtain a higher efficiency of the chain-extension reaction, the reaction temperature during the polymerization of the second block was raised from  $60^\circ\text{C}$  to  $70^\circ\text{C}$ , a radical source with a more suitable half-life was used (V-40, Scheme 2.2) and a monomer feed was added to the reaction mixture to reach in the extension a feed-ratio of 80/20 EHMA/BTAMA.

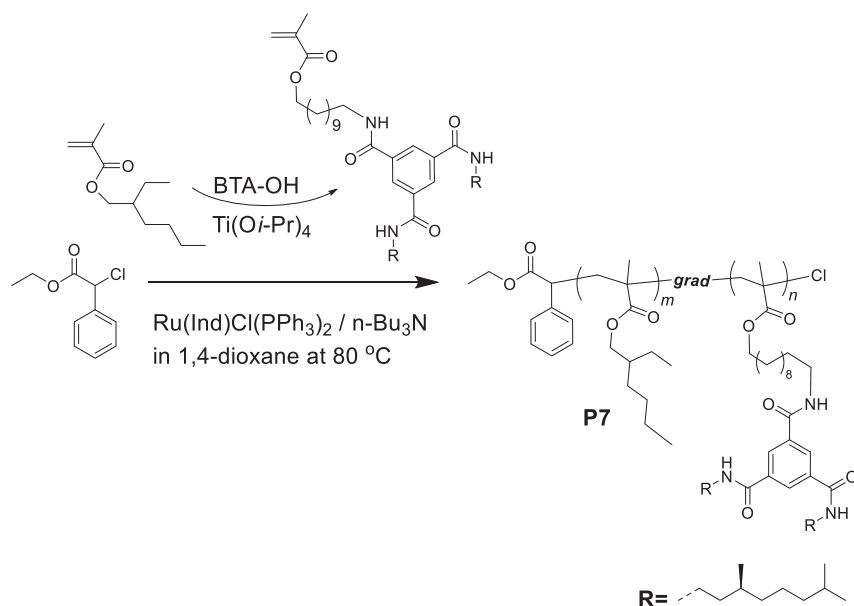


The polymerization was stopped at 60% monomer conversion, leading to block copolymer **P6**. The SEC trace of **P6** in THF showed no shoulder, indicative for the success of the chain-extension, and a decent polydispersity was obtained ( $M_n = 46.6$  kDa,  $D = 1.41$ ). Furthermore,  $^1\text{H}$ -NMR was used to analyze the purified block copolymer, indicating an overall 10% BTAs per polymer chain and a  $DP$  of 256 (Table 2.2).

### 2.3.3 Synthesis of gradient copolymers

Recently, Sawamoto and Terashima *et al* reported the preparation of tailor-made sequence-regulated copolymers *via* tandem catalysis of living radical polymerization and in-situ transesterification.<sup>30</sup> Gradient, block random, random-gradient and random-block structures are readily available by this one-pot tandem technique which is catalytically controlled by the reaction conditions, e.g. temperature, concentration and/or catalysts, alcohols, or monomers.

For this study, a gradient sequence is very interesting since it would result in a change of BTA concentration *along* the polymer-chain. The approach for the preparation of a gradient sequence lies in including the metal oxides ( $\text{Ti}(\text{O}i\text{-Pr})_4$ ) and alcohols (*i.e.* BTAOH) in the ruthenium mediated living radical polymerization of unsaturated ester monomers (EHMA).  $\text{Ti}(\text{O}i\text{-Pr})_4$  can (co)catalyze both the ruthenium mediated living radical polymerization and also the transesterification of unsaturated ester monomers (EHMA) with alcohols (BTAOH, *vide infra*). When  $\text{Ti}(\text{O}i\text{-Pr})_4$  and BTAOH are included in the ruthenium mediated living radical polymerization of EHMA, transesterification of the pendant esters of the EHMA is induced by BTAOH selectively in the monomers, not in the polymers, and therefore results in a gradual change in the monomer feed in favor of BTAMA. This gradual increase in the BTAMA feed ratio is reflected on the copolymer (EHMA/BTAMA) composition along the polymer chain to give a gradient structure.<sup>30,31</sup>



**Scheme 2.3** Synthesis of the gradient copolymer **P7**.

In collaboration with Yusuke Ogura of Kyoto University, we investigated the introduction of highly functional BTA alcohols (compound **6**, Scheme 2.1) into a gradient copolymer structure with EHMA *via* careful tuning of the reaction conditions. Gradient EHMA/BTAMA based copolymer **P7** was synthesized in the presence of ethyl  $\alpha$ -chlorophenylacetate (ECPA) as the

initiator, and  $[\text{Ru}(\text{Ind})\text{Cl}(\text{PPh}_3)_2]$  and  $n\text{-Bu}_3\text{N}$  as the catalyst for the living radical polymerization in dioxane at  $80\text{ }^\circ\text{C}$ .  $\text{Ti}(\text{O}i\text{-Pr})_4$  was added as the metal alkoxide to perform the transesterification, four hours after the initiation of the polymerization (Scheme 2.3). The polymerization solution was analyzed by  $^1\text{H-NMR}$  to confirm synchronization of the living radical polymerization and in-situ transesterification of monomers from the initial stage (Figure 2.6, left), and to directly determine EHMA and BTAMA contents in polymer **P7** (Figure 2.6, right). Figure 2.6, right, shows the BTAMA contents in monomers ( $100 \times [\text{BTAMA}]_t / ([\text{EHMA}]_t + [\text{BTAMA}]_t)$ ) as a function of total monomer conversion. BTAMA was gradually generated in the solutions by the in-situ transesterification of BTA-alcohol as the polymerization proceeded. Such a conversion profile points to a gradient distribution of BTAMA monomer along the polymer chain as previously shown by extensive kinetic studies.<sup>30</sup> The polymerization was stopped at 74% monomer conversion, leading to gradient copolymer **P7** with 8% BTA incorporation and a  $DP$  of 220 ( $M_n = 45.0\text{ kDa}$ , with  $D = 1.34$  (Table 2.2)).

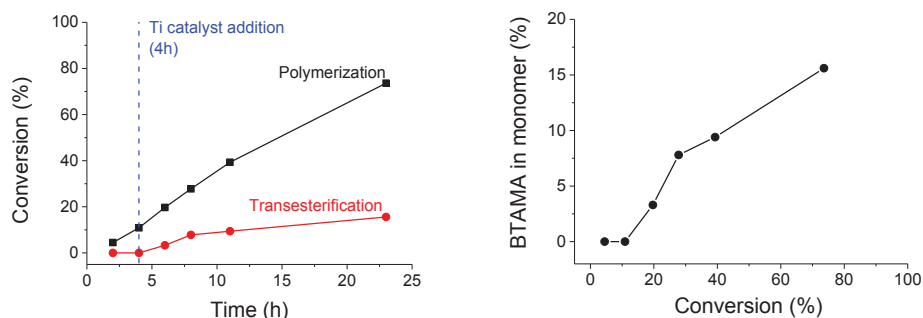


**Figure 2.6** Conversion vs time of polymerization and transesterification during the synthesis of **P7** (left) and the incorporation of BTAs vs conversion during the synthesis of **P7** (right).

### 2.3.4 Circular dichroism studies

Temperature-dependent CD measurements in DCE ( $[\text{BTA}] = 5 \cdot 10^{-5}\text{ M}$ ,  $l = 0.5\text{ cm}$ ) with a cooling rate of  $60\text{ }^\circ\text{C/h}$  were performed to investigate the folding behavior of random **P3** (8% BTA) and **P4** (19% BTA), diblock **P6** (8 % BTA) and gradient **P7** (8% BTA) copolymers (Figure 2.7). Polymers **P3**, **P6** and **P4** showed a similar maximum Cotton-effect around  $-14\text{ mdeg}$  at  $5\text{ }^\circ\text{C}$  while **P7** showed a maximum Cotton-effect of  $-22\text{ mdeg}$  at  $5\text{ }^\circ\text{C}$  (Figure 2.7). A remarkable higher maximum Cotton-effect was observed for the gradient copolymer **P7** compared to copolymers **P3**, **P4** and **P6** with random pendant BTA distribution. To be able to compare the maximum CD-effect of **P3**, **P4** and **P6** with known values, the molar circular dichroism,  $\Delta\epsilon$ , was determined using equation 2.1:

$$\Delta\epsilon = \frac{\text{CD-effect}}{32980 \cdot c \cdot l} \quad (2.1)$$

wherein  $c$  is the concentration of BTAs in  $\text{mol L}^{-1}$  and  $l$  is the optical path length in cm. **P3**, **P4** and **P6** showed  $\Delta\epsilon$  values around  $-18\text{ L mol}^{-1}\text{ cm}^{-1}$  while **P7** showed a  $\Delta\epsilon$  of  $-27\text{ L mol}^{-1}\text{ cm}^{-1}$  at  $5\text{ }^\circ\text{C}$ . Random (**P3**, **P4**) and diblock (**P6**) copolymers showed a  $\Delta\epsilon$  that is in the range of  $\Delta\epsilon$ s for previously studied random amphiphilic copolymers with 10 mol% BTAs with values varying

between  $-13$  and  $-20 \text{ L mol}^{-1} \text{ cm}^{-1}$ .<sup>32</sup> Interestingly, also the shape of the cooling curves of **P4**, **P6**, and **P7** is different than that of **P3**, and especially the cooling curve for **P7** is much steeper than those of the other polymers.

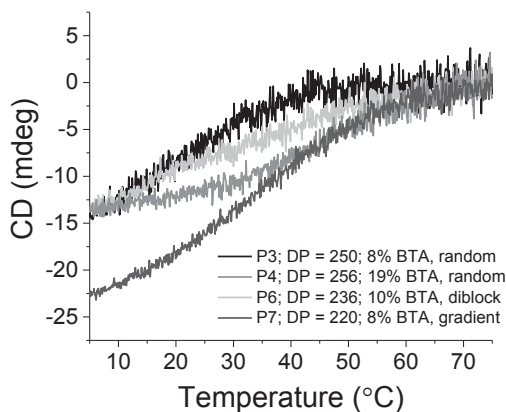


**Figure 2.7** Temperature-dependent CD effect of **P3**, **P4**, **P6**, and **P7** in DCE ( $\lambda = 223 \text{ nm}$ ,  $[\text{BTA}] = 50 \mu\text{M}$ ,  $l = 0.5 \text{ cm}$ ) at a cooling rate of  $60 \text{ }^\circ\text{C per hour}$ .

A closer look to the temperature at which the BTA self-assembly starts, reveals that **P4** (19% random) and **P7** (8% gradient) start self-assembling first, then **P6** (8% diblock) follows, and **P3** (8% random) starts last. For **P4**, the higher temperature at which aggregation started compared to **P3** is in line with earlier observations for increased total BTA concentration.<sup>33</sup> For **P6** and **P7**, the higher temperature at which aggregation starts compared to **P3** can be explained by the increase in local BTA concentration compared to **P3**. Since the average distance between two BTA moieties is smaller in **P4**, **P6**, and **P7** as compared to **P3**, it is energetically more favorable to form aggregates at higher temperatures. The fact that the aggregation of **P6** does start at lower temperatures than that of **P7** and **P4** can be explained by the presence of the unfunctionalized EHMA block, which probably gives an additional entropic penalty to the folding.

### 2.3.5 Dynamic light scattering

In order to investigate how different polymer architectures influence the size of folded polymers, DLS measurements were performed on **P3**, **P4**, **P6**, and **P7** in DCE (1 mg/mL), a solvent in which the CD experiments were performed, and in which the pendant BTAs can stack (*vide supra*). At  $20 \text{ }^\circ\text{C}$ , an  $R_H$  of 8 nm for **P3**, an  $R_H$  of 48 nm for **P4**, an  $R_H$  of 159 nm for **P4**, and a  $R_H$  of 11.3 nm and of 96.8 nm for **P7** were observed (Figure 2.8). For **P7**, due to the fact that large particles scatter significantly more than smaller particles (the intensity scales with  $R^6$ ) we can assume that the fraction of larger aggregates will be close to negligible. **P3** and **P7**

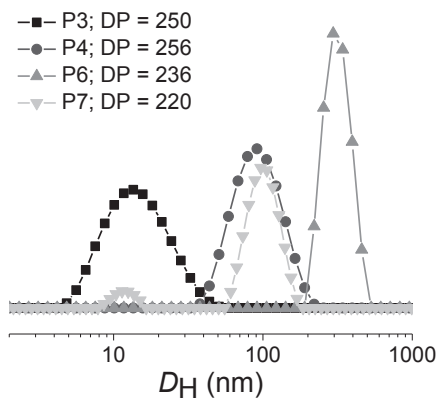


**Figure 2.8** DLS size distribution traces of **P3**, **P6**, and **P4** in DCE (1 mg/mL) at 20 °C.

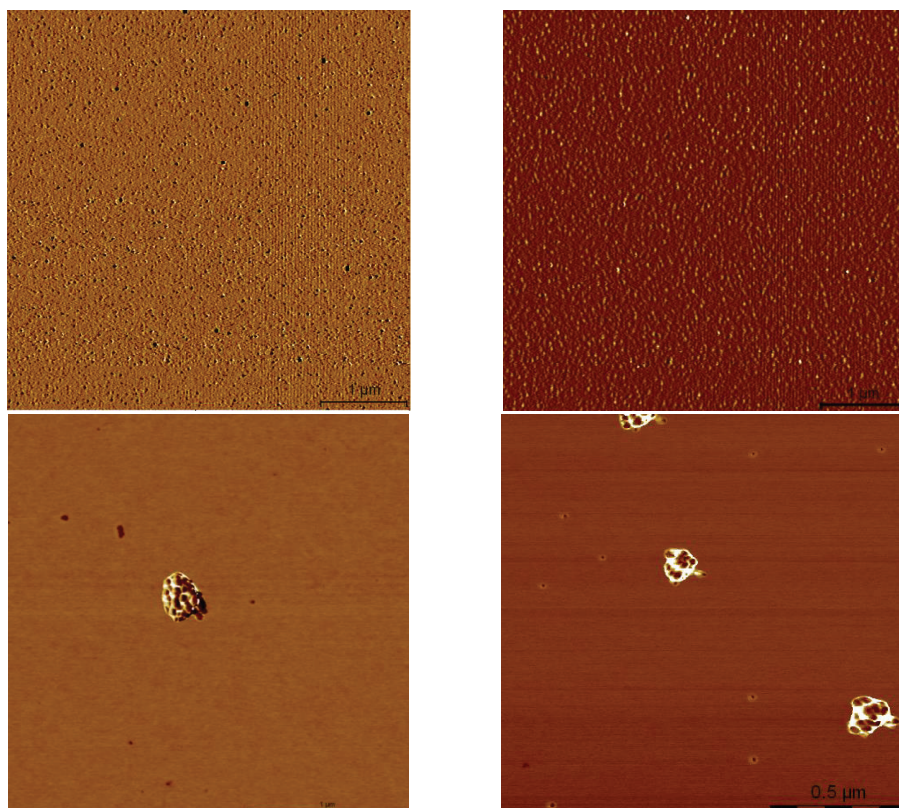


**Figure 2.9** AFM images of **P3** (random) (top left: height; top right: phase) and **P6** (diblock) (bottom left: height; bottom right: phase) (0.01 mg/mL, spincoated 4500 rpm from DCE).

showed a diameter matching with that of previously reported SCPN in organic solvents, with similar BTA incorporations and lengths;<sup>11</sup> while **P6** and **P4** showed multi-chain aggregation.

In order to understand the effect of supramolecular BTA interactions on multi-chain aggregation behavior, additional DLS experiments were performed on **P4** and **P6** in THF, a solvent wherein BTA stack formation is suppressed.<sup>10,33</sup> The size of the aggregates decreased to 7.5 and 7.2 nm for **P4** and **P6**, respectively (Table 2.2), indicating the influence of the BTAs on the aggregation of **P4** and **P6** in DCE.

### 2.3.6 Atomic force microscopy

Finally, atomic force microscopy (AFM) measurements were performed for **P3** and **P6**. These polymers were chosen since they represent the polymers that formed nanoparticles either *via* folding of a single chain (**P3**) or multi-chains (**P6**). Samples were prepared by drop-casting on freshly cleaved mica from a 0.01 mg/mL solution in DCE. The measurement showed well-defined nanoparticles with a narrow polydispersity and diameters of 50 nm for **P3** and 250 nm for **P6** (Figure 2.9). The measurement showed significantly larger particles for **P6** than for **P3**, and this increase in particle size is probably because of aggregation of multiple polymer chains. It is possible that the more hydrophobic 2-EHMA/BTAMA block cluster together, resulting in an increase of the particle size. Taking the flattening effect of surface-nanoparticle interactions into account, these results are in agreement with the values obtained from DLS.

## 2.4 Discussion and conclusion

The random EHMA/BTAMA based copolymers with varying molar mass dispersities and constant BTA incorporations, showed an almost identical self-assembly of their pendant BTA, as was confirmed by the superimposable cooling curves. Thus, decreasing the polymer length distribution from a  $D$  of 2.27 to a  $D$  of 1.06, does not affect the BTA self-assembly in an observable way *via* CD. Therefore we can conclude that dispersity does not influence the apparent non-cooperativity of the self-assembly of the pendant BTAs. It should be taken into account that although the studied polymers with different molar mass distributions have similar *average* BTA contents, the BTA content and distribution of the individual polymer chains cannot be controlled or determined since the monomers are polymerized in a random manner during synthesis.

However, copolymers with varying pendant BTA distributions on the copolymer backbone showed very differently shaped cooling curves in CD measurements, and thus self-assembly behavior. The difference in the temperature at which the self-assembly of pendant BTAs starts could be due to the difference in distribution of the BTAs along the polymer backbone; the higher local concentration of the BTAs on **P4** makes it energetically more favorable for the BTAs to self-assemble at higher temperatures than for the BTAs on **P3**. Diblock polymer **P6** also has a higher BTA concentration in the second block than **P3**, accounting for the higher temperature at which self-assembly starts. Self-assembly was, however, disturbed to a large extent by the unfunctionalized block, accounting for the lower temperature at which BTA self-assembly starts compared to **P4**. For **P7**, the gradient distribution of the BTAs along the polymer chain implies that there are sections with high BTA concentration, making the initial self-assembly of these sections energetically more favorable compared to **P3** and **P6**.

Furthermore, a higher maximum Cotton effect was observed for the gradient copolymer **P7** compared to copolymers **P3**, **P6** and **P4**, that had random pendant BTA distribution. This could indicate a more favorable positioning of BTA units in a gradient type of distribution. A possible cooperativity in the self-assembly of the BTAs on this gradient polymer could, however, not be confirmed for these polymers, since a comparison with similar polymers, only differing in  $DP$ , is needed to elucidate this.

Random copolymer **P3** and gradient copolymer **P7** formed predominantly single chain nanoparticles in DCE, as evidenced by their  $D_H$ , while **P4** and **P6** showed multi-chain aggregation, as evidenced by the higher  $D_H$ . For **P4**, multi-chain aggregation could be explained by the high BTA incorporation, which increases the interparticle interactions. Similarly, for diblock copolymer **P6**, multi-chain aggregation could be explained by the increased local BTA concentration in one block, due to the diblock structure. The role of BTA stacking in the multi-chain aggregation is confirmed by the dramatic decrease in  $R_H$  of **P4** and **P6** in THF, where BTA interactions are suppressed.

Previously, it was shown that varying the length of EHMA/BTAMA based copolymers with a constant BTA incorporation ratio ( $DP$ s between 100-500), did not affect the self-assembly behavior of the pendant BTA units, as was evidenced by the superimposable temperature dependent CD curves.<sup>12</sup> There is a close similarity between increasing the polymer length and increasing the number of polymer chains in one aggregate; in both cases the BTAs do not self-assemble into one single aggregate, but instead self-assemble into isolated aggregates.<sup>10,11</sup> Therefore, the particle size is not expected to affect the self-assembly behavior of pendant BTAs for **P4** and **P6**.

Here we used polymer pendant BTAs as probes to gain insight in the folding behavior of different polymers. However, it should be noted that CD spectroscopy can only monitor the self-assembly of the pendant BTA units, but not the entire polymer folding process. Thus, the changes in the BTA helical self-assembly behavior of the pendant BTA moieties do not necessarily reflect the changes in the polymer's global conformation.

These findings serve as a starting point to understand the self-assembly of polymer pendant BTAs. Nonetheless, a better understanding on the polymer pendant BTA self-assembly can be gained by using a model system that comprise of monodisperse polymers with BTAs at exactly defined positions to eliminate the contribution the poorly defined polymer lengths and sequences.

## 2.5 Experimental

### 2.5.1 Instrumentation, materials and methods

#### Materials

All reagents were purchased from Aldrich, Fluka, or Acros and all solvents were obtained from Biosolve. Triethylamine was stored over KOH pellets and chloroform was dried over molecular sieves. 2-Ethylhexyl methacrylate (2-EHMA) was purified by passing through an inhibitor removal column. BTAMA and BTA-alcohol were prepared according to literature procedures.<sup>7</sup> 4-Cyano-4-methyl-5-(phenylthio)-5-thioxopentanoic acid was kindly provided by SyMO-Chem (Eindhoven, the Netherlands). Compounds **3** and **4** were kindly provided by Marly Hummelink.

#### Methods



<sup>1</sup>H-NMR spectra were recorded on a Varian Mercury Vx 400 MHz and/or a Varian 400MR 400 MHz (400 MHz for <sup>1</sup>H-NMR and 100 MHz for <sup>13</sup>C-NMR) and/or JEOL JNM-ECA500 (500 MHz for <sup>1</sup>H-NMR). <sup>1</sup>H chemical shifts are reported in ppm downfield from tetramethylsilane (TMS). <sup>13</sup>C chemical shifts are reported in ppm downfield of TMS using the resonance of the deuterated solvent as internal standard. Abbreviations used are s: singlet, d: doublet, dd: double doublet, t: triplet, m: multiplet, b: broad. Flash column chromatography was performed on a Biotage Isolera Spektra One Flash Chromatography system using KP-Sil Silica Gel SNAP columns. MALDI-TOF MS was performed using a Perspective Biosystem Voyager-DE PRO spectrometer (matrix material:  $\alpha$ -cyano-4-hydroxycinnamic acid). SEC-measurements were performed on a Shimadzu-system with two PolymerLabs columns in serie (PLgel 5 $\mu$ m mixed C [200–2000000 Da] and PLgel 5 $\mu$ m mixed D [200–40000 Da]) and equipped with a RI (Shimadzu RID-10A) and a PDA detector (Shimadzu SPD-M10A), with THF or CHCl<sub>3</sub> as eluent at a constant flow rate of 1.0 mL/min. Number averaged molecular weights and molecular weight distribution ( $D$ ) were obtained relative to PS standards (Polymer Laboratories). The molecular weight  $M_n$  and  $D$  ratios of the gradient polymer (**P7**) was measured by SEC in THF (flow rate = 1 mL/min) on three linear-type polystyrene gel columns (Shodex KF-805L; exclusion limit =  $4 \times 10^6$ , pore size = 5000 Å, 0.8 cm i.d. x 30 cm) that were connected to a Jasco PU-2080 precision pump, a Jasco RI-2031 refractive index detector, and a Jasco UV-2075 UV-vis detector set at 270 nm. The columns were calibrated against 10 standard PMMA samples, (Polymer Laboratories;  $M_n = 1680$ -1,200,000,  $D = 1.06$ -1.22). The recycling SEC was performed using two JALGEL columns (20 mm x 600 mm) connected in series (JAIGEL-2H MW till 5.000 and JAIGEL-2.5H MW till 20.000) with chloroform at 3.5 mL/min as the mobile phase. A Shimadzu LC-10AD pump was used for delivering the solvent, and a Shimadzu SPD-10AV UV-Vis detector for detection. CD measurements were performed on a Jasco J-815 spectropolarimeter where the sensitivity, time constant and scan range were chosen appropriately (sensitivity: standard, response: 4 s, band width: 1 nm, data pitch: 1 nm, scanning speed: 20 nm/min). Corresponding temperature-dependent measurements (data pitch: 0.1 °C) were performed with a PFD-425S/15 Peltier temperature controller with a temperature range of -10 °C to 110 °C and adjustable temperature slope.

Dynamic light scattering measurements were performed on a Malvern  $\mu$ V Zetasizer equipped with a 830 nm laser. Samples were prepared by filtering solutions in spectroscopy grade solvents through a 0.45  $\mu$ m PTFE-filter (Whatman) in a fluorescence cell with a path length of pathlength 10x2 mm and a chamber volume of 100  $\mu$ L. Samples for dynamic and static light scattering measurements were prepared by first dissolving the polymer in spectroscopy grade solvent and then sonicating for 2 hours in a Cole Parmer 8891 sonification bath. Immediately after the sonification, a 0.2  $\mu$ m PTFE-filter (Whatman) was first washed by filtering spectroscopy grade solvent through and then the polymer solution was filtered in a fluorescence cell with a path length of 10x2 mm and chamber volume of 100  $\mu$ L. Prepared solutions were measured immediately.

Atomic force micrographs were recorded under ambient conditions with silicon cantilever tips (PPP-NCH, 300-330 kHz, 42 N/m from Nanosensors) using an Asylum Research MFP-3D in AC (tapping) mode. AFM samples were spincoated at 4500 rpm from DCE polymer solution (0.01 mg/mL).

### 2.5.2 Synthesis

#### 2-(Hydroxyundecyl)isoindoline-1,3-dione (2)

11-Bromoundecanol **1** (40.00 mmol, 10.0485 g) and potassium phthalimide (52.05 mmol, 9.6406 g) were placed in a 500 mL flask and dissolved in DMF (200 mL). The resulting mixture was stirred at 70 °C for 20 hours. The mixture was cooled to room temperature, filtered and the precipitate was washed with ethyl acetate (500 mL). The filtrate combined with the EtOAc fraction was washed with H<sub>2</sub>O (3 x 150 mL) and saturated KCl (2 x 75 mL). The organic layer was dried with MgSO<sub>4</sub> and the solvent was evaporated *in vacuo* to yield a white powder (10.84 g, 85%). <sup>1</sup>H-NMR (CDCl<sub>3</sub>): δ = 7.84 (dd, 2H, Ar-H), 7.70 (dd, 2H, Ar-H), 3.67 (t, 2H, CH<sub>2</sub>N), 3.63 (t, 2H, CH<sub>2</sub>OH), 1.67 (t, 2H, aliphatic), 1.55 (t, 2H, aliphatic) 1.40-1.21 (m, 14H, aliphatic). <sup>13</sup>C-NMR (CDCl<sub>3</sub>): δ = 168.5, 133.8, 132.2, 123.1, 63.1, 38.1, 32.8, 29.5, 29.4, 29.4, 29.3, 28.6, 26.8, 25.7 MALDI-TOF-MS (m/z) calc for C<sub>11</sub>H<sub>25</sub>NO 187.32, found 188.49 (M+H)<sup>+</sup>.

#### 11-Aminoundecanol (3)

Compound **2** (35.12 mmol, 11.15 g) was placed in a 500 mL flask and dissolved in dry THF (200 mL). Hydrazine monohydrate (0.55 mol, 27.5 mL) was added to the mixture and the solution was heated at reflux temperature for 20 hours. The solvent and the excess of hydrazine were removed *in vacuo*. CHCl<sub>3</sub> (500 mL) and 3 M NaOH (500 mL) were added to the residue. The organic layer was separated and washed with 3 M NaOH (1 x 100 mL), H<sub>2</sub>O (1 x 100 mL) and brine (1 x 100 mL). The organic layer was dried over MgSO<sub>4</sub> and the solvent was removed *in vacuo* to afford a white solid (6.49 g, 99%). <sup>1</sup>H-NMR (CDCl<sub>3</sub>): δ = 3.63 (t, 2H, CH<sub>2</sub>OH), 2.68 (t, 2H, CH<sub>2</sub>NH<sub>2</sub>), 1.67-1.08 (m, 18H, aliphatic protons). <sup>13</sup>C-NMR (CDCl<sub>3</sub>): δ = 63.0, 42.3, 33.9, 32.8, 29.6, 29.6, 29.5, 29.5, 29.4, 26.9, 25.7 MALDI-TOF-MS (m/z) calc for C<sub>19</sub>H<sub>27</sub>NO<sub>3</sub> 317.42, found 318.28 (M+H)<sup>+</sup> 340.24 (M+Na)<sup>+</sup>.

#### Hydroxyundecyl-3,5-bis((3S)-3,7-dimethyloctylcarbamoyl)benzoate (6)

In a 1000 mL flask compound **3** (21.75 mmol, 4.07 g), (S)-3,7-dimethyloctanamine **4** (43.50 mmol, 7.80 g) and triethylamine (205.54 mmol, 20.78 g) were dissolved in dry CHCl<sub>3</sub> (375 mL). The resulting solution was cooled with an ice-water-salt bath while stirring and under an argon atmosphere. Benzene-1,3,5-tricarbonyl trichloride (18.13 mmol, 4.81 g) was dissolved in dry CHCl<sub>3</sub> (65 mL) and added dropwise to the cooled solution. After the ice-water-salt bath was completely melted, the solution was stirred at room temperature. The chloroform and the excess of triethylamine were removed *in vacuo*. The residue was dissolved in chloroform (250 mL) and washed with 1 M HCl (2 x 350 mL) and brine (1 x 350 mL). The organic layer was evaporated *in vacuo* and further purification by column chromatography (ethyl acetate/chloroform: 30/70) was performed to obtain a sticky white solid (3.51 g, 35%). <sup>1</sup>H-NMR (CDCl<sub>3</sub>): δ = 8.41 (s, 2H, Ar-H), 8.34 (s, 1H, Ar-H), 6.32 (b, 1H, NH), 6.75 (b, 2H, NH), 3.63 (m, 2H, OCH<sub>2</sub>-) 3.49 (m, 6H, -NHCH<sub>2</sub>-), 1.71-0.7 (mm, 56H, aliphatic). <sup>13</sup>C-NMR (CDCl<sub>3</sub>): δ = 165.8, 165.7, 165.7, 135.2, 135.2, 135.2, 128.0, 128.0, 127.9, 63.0, 63.0, 40.3, 39.3, 39.2, 38.5, 37.1, 36.6, 32.8, 32.7, 30.8, 30.7, 29.5, 29.4, 29.4, 29.4, 29.3, 29.3, 29.2, 29.2, 29.2, 29.1, 27.9, 26.8, 25.7, 25.6, 24.6, 22.7, 22.6, 19.5, MALDI-TOF-MS (m/z) calc for C<sub>40</sub>H<sub>71</sub>N<sub>3</sub>O<sub>4</sub> 658.01, found 658.67 (M+H)<sup>+</sup> 680.65 (M+Na)<sup>+</sup> 666.62 (M+K)<sup>+</sup>.

#### 11-(3,5-Bis((3S)-3,7-dimethyloctylcarbamoyl)benzamido)undecyl methacrylate (7)

In a 100 mL three-necked round-bottom flask compound **6** (4.54 mmol, 2.98 g) and triethylamine (5.14 mmol, 0.52 g) were dissolved in dry CH<sub>2</sub>Cl<sub>2</sub> (60 mL). The solution was cooled with an ice bath and placed under argon atmosphere. Methacryloyl chloride (5.06 mmol, 0.49 mL) was dissolved in dry CH<sub>2</sub>Cl<sub>2</sub> (20 mL) and added dropwise to the reaction flask. After 20 h stirring, the crude mixture was washed with 0.1 M HCl (2 x 40 mL) and saturated NaHCO<sub>3</sub> (1 x 40 mL). The product was purified by column chromatography three times (ethyl acetate/chloroform; 30/70, methanol/chloroform; 2/98 and ethyl acetate/chloroform; gradient 0/100 – 60/40) to afford a sticky white solid (1.62 g, 49%). <sup>1</sup>H-NMR (CDCl<sub>3</sub>): δ = 8.33 (s, 3H, Ar-*H*), 6.37 (s, 3H, *NH*), 6.09 (s, 1H, CCHH), 5.54 (s, 1H, - CCHH), 4.21 (t, 2H, -OCH<sub>2</sub>), 3.46 (m, 6H, -NHCH<sub>2</sub>), 1.94 (s, 3H, -CCH<sub>3</sub>), 1.75-0.91 (m, 56H, aliphatic). <sup>13</sup>C-NMR (CDCl<sub>3</sub>): δ = 167.6, 165.6, 136.6, 135.3, 127.9, 125.2, 64.8, 60.4, 39.2, 38.5, 37.1, 36.6, 30.8, 29.5, 29.2, 28.6, 28.0, 26.0, 24.6, 22.7, 22.6, 19.5, 14.2. MALDI-TOF-MS (m/z) calc for C<sub>44</sub>H<sub>75</sub>N<sub>3</sub>O<sub>5</sub> 726.08, found 726.58 (M+H)<sup>+</sup> 748.55 (M+Na)<sup>+</sup> 764.53 (M+K)<sup>+</sup>.

*2-EHMA/BTAMA random copolymer P1 (DP = 215)*

In a Schlenk-tube were 2-ethylhexyl methacrylate (2.03 mmol, 402.4 mg), BTAMA **7** (177 μmol, 128.2 mg), RAFT-CTA **8** (8.53 μmol, 2.38 mg) and AIBN (1.75 μmol, 0.29 mg) dissolved in dry dioxane (2 mL). The mixture was subjected to four freeze–pump–thaw cycles, backfilled with argon and placed in a preheated oil-bath at 60 °C for 46 hours while stirring. The polymerization was stopped by quenching the polymerization solution in a water bath. Purification was performed by dialysis in THF to yield a pink solid (312 mg). <sup>1</sup>H-NMR (CDCl<sub>3</sub>): δ = 8.32 (s, Ar-*H*: BTAMA), 6.49 (b, *NH*), 6.32 (b, *NH*), 3.83 (b, CO<sub>2</sub>-CH<sub>2</sub>), 3.46 (b, NH-CH<sub>2</sub>), 2.05-0.75 (m, aliphatic, backbone). THF-GPC: *M<sub>n</sub>* = 36.0, *D* = 1.12.

*2-EHMA/BTAMA random copolymer P2 (DP = 190)*

In a Schlenk-tube was 2-ethylhexyl methacrylate (2.005 mmol, 397.6 mg), BTAMA **7** (0.175 mmol, 127.1 mg), RAFT-CTA **8** (8.73 μmol, 2.44 mg) and AIBN (1.86 μmol, 0.306 mg) dissolved in dry dioxane (2 mL). The Schlenk-tube was filled with argon and placed in a preheated oil-bath at 60 °C for 25 hours while stirring. The polymerization was stopped by quenching the polymerization solution in a water bath. Purification was performed by dialysis in THF and precipitation in cold methanol to yield a white solid (133 mg). Spectroscopic data was similar to the data of **P1**. THF-SEC: *M<sub>n</sub>* = 49.9 kDa, *D* = 2.27.

*2-EHMA/BTAMA random copolymer P3 (DP = 250)*

In a Schlenk-tube were 2-ethylhexyl methacrylate (2.38 mmol, 471.6 mg), BTAMA **7** (207 μmol, 150.1 mg), RAFT-CTA **8** (8.60 μmol, 2.40 mg) and AIBN (1.80 μmol, 0.30 mg) dissolved in dry dioxane (2.4 mL). The mixture was subjected to four freeze–pump–thaw cycles, backfilled with argon and placed in a preheated oil-bath at 60 °C for 46 hours while stirring. The polymerization was stopped by quenching the polymerization solution in a water bath. Purification was performed by dialysis in THF to yield a pink solid (381 mg). Spectroscopic data was similar to the data of **P1**. THF-SEC: *M<sub>n</sub>* = 56.4 kDa, *D* = 1.24.

*2-EHMA/BTAMA random copolymer P4 (DP = 256)*

In a Schlenk-tube 2-ethylhexyl methacrylate (1.058 mmol, 209.9 mg), BTAMA **7** (0.253 mmol, 183.7 mg), RAFT-CTA **8** (4.446 μmol, 1.242 mg) and AIBN (0.926 μmol, 0.152 mg) were charged and dissolved in dry dioxane (1.5 mL). The Schlenk-tube was subjected to six consecutive freeze–pump–thaw cycles, backfilled with argon and placed in a preheated oil-bath at

60 °C for 43 hours while stirring. The polymerization was stopped by quenching the polymerization solution in a water bath. Purification was performed by dialysis in THF and precipitation in cold methanol to yield a white solid (185 mg). Spectroscopic data was similar to the data of **P1**. THF-SEC:  $M_n = 46.6$  kDa,  $D = 1.41$ .

*2-EHMA macro-RAFT agent P5 (DP = 154)*

In a Schlenk-tube were 2-EHMA (11.73 mmol; 2.326 g), AIBN (8.91  $\mu$ mol; 1.463 mg), and RAFT-CTA (43.31  $\mu$ mol; 12.10 mg) dissolved in dry dioxane (1.8 mL). The Schlenk-tube was subjected to four consecutive freeze-pump-thaw cycles, backfilled with argon and placed in a preheated oil-bath at 60 °C for 22 hours while stirring. The reaction was stopped by quenching the Schlenk-tube in a cold water-bath. No purification was performed.  $^1\text{H-NMR}$  ( $\text{CDCl}_3$ ):  $\delta = 7.36$  (b, NH), 3.84 (b,  $\text{CO}_2\text{-CH}_2$ ), 2.10-0.75 (m, aliphatic, backbone). THF-SEC: THF-SEC:  $M_n = 26.7$  kDa,  $D = 1.12$ .

*2-EHMA / (2-EHMA/BTAMA) diblock copolymer P6 (DP = 236)*

In a Schlenk-tube were 2-EHMA macro-RAFT agent in dioxane (0.259 g/mL; 5.974 mmol; 1.24 mL), V-40 (0.753  $\mu$ mol; 0.181 mg), 2-EHMA (0.877 mmol; 174.0 mg), and BTAMA (0.206 mmol; 149.7 mg) dissolved in dry dioxane (4 mL). The Schlenk-tube was subjected to eight consecutive freeze-pump-thaw cycles, backfilled with argon and placed in a preheated oil-bath at 70 °C for 16 hours while stirring. The reaction was stopped by quenching the reaction mixture in a water-bath. Purification was performed by dialysis in THF (2 days) and precipitation in methanol cooled with  $\text{N}_2$  (once) resulting in a light pink solid (374 mg). Spectroscopic data was similar to the data of **P1**. THF-SEC:  $M_n = 45.7$  kDa,  $D = 1.32$ .

*2-EHMA/BTAMA gradient copolymer P7 (DP = 220)*

BTA-OH (0.15 mmol, 0.10 g) was first placed in a 30 mL glass tube. Then,  $\text{Ru}(\text{Ind})\text{Cl}(\text{PPh}_3)_2$  (0.0024 mmol, 1.86 mg) was charged, and 1,4-dioxane (0.52 mL), tetralin (0.04 mL), EHMA (1.2 mmol, 0.27 mL), a solution of  $n\text{-Bu}_3\text{N}$  (400 mM, 0.06 mL,  $n\text{-Bu}_3\text{N} = 0.024$  mmol) in toluene and a solution of ECPA (50 mM, 0.19 mL, ECPA = 0.0095 mmol) in 1,4-dioxane were added sequentially at 25 °C, under argon. The total volume of the reaction mixture was thus 1.2 mL. After polymerization initiated (4 h, conv. = 11%), a solution of  $\text{Ti}(\text{O}i\text{-Pr})_4$  (50 mM, 0.19 mL,  $\text{Ti}(\text{O}i\text{-Pr})_4 = 0.0095$  mmol) in 1,4-dioxane was added to the reaction mixture at 80 °C under argon. The glass tube was placed in an oil bath kept at 80 °C. At predetermined intervals, the mixture was sampled with a syringe under dry argon and cooled to -78 °C to terminate the reaction. The total monomer conversion, BTAMA content in monomer, and cumulative BTAMA content in polymer ( $F_{\text{cum,BTAMA}}$ ) were directly determined by  $^1\text{H-NMR}$  measurements of the terminated reaction solution in  $\text{CDCl}_3$  at r.t. with tetralin as an internal standard.

Instantaneous BTAMA content in polymer **P7** ( $F_{\text{inst,BTAMA}}$ ) was estimated according to the following equation:  $F_{\text{inst,BTAMA}} = [\text{Conv}_{\text{total}, i} \times F_{\text{cum,BTAMA}, i} - \text{Conv}_{\text{total}, i-1} \times F_{\text{cum,BTAMA}, i-1}] / [\text{Conv}_{\text{total}, i} - \text{Conv}_{\text{total}, i-1}]$ , where  $\text{Conv}_{\text{total}}$  is the total conversion of both monomers. The quenched reaction solutions were evaporated to dryness to give the crude product. The product was then fractionated by preparative SEC in THF containing 2,6-di-*t*-butyl-4-methylphenol as stabilizer. Obtained polymer was fractionated by preparative SEC in  $\text{CHCl}_3$  to remove 2,6-di-*t*-butyl-4-methylphenol for analysis. THF-SEC:  $M_n = 45,0$  kDa;  $D = 1.34$ .  $^1\text{H-NMR}$  ( $\text{CD}_2\text{Cl}_2$ )  $\delta = 8.25$  (s, Ar-H: BTAMA), 7.30-7.15 (aromatic: ECPA), 4.20-3.55 ( $-\text{COOCH}_2-$ ), 3.55-3.05 (-

CONHCH<sub>2</sub>-), 2.15-1.45 (-CH<sub>2</sub>C(CH<sub>3</sub>)-), 1.45-0.40 (-CH<sub>2</sub>C(CH<sub>3</sub>)-).  $M_{n,NMR} = 52.7$  kDa;  $DP_{EHMA}/DP_{BTAMA} = 202/17$ ;  $F_{cum,BTAMA} = 8\%$ .

## 2.6 References

- (1) S. Cantekin, T. F. A. de Greef, A. R. A. Palmans. *Chem. Soc. Rev.* **2012**, *41*, 6125.
- (2) P. J. M. Stals, M. M. J. Smulders, R. Martín-Rapún, A. R. A. Palmans, E. W. Meijer *Chem. Eur. J.* **2009**, *15*, 2071.
- (3) Y. Nakano, T. Hirose, P. J. M. Stals, E. W. Meijer, A. R. A. Palmans *Chem. Sci.* **2012**, *3*, 148.
- (4) M. M. J. Smulders, A. P. H. J. Schenning, E. W. Meijer *J. Am. Chem. Soc.* **2008**, *130*, 606.
- (5) T. Mes, R. van der Weegen, A.R.A. Palmans, E.W. Meijer *Angew. Chem. Int. Ed.* **2011**, *50*, 5085.
- (6) N. Hosono, M. A. J. Gillissen, Y. Li, S. S. Sheiko, A. R. A. Palmans, E. W. Meijer *J. Am. Chem. Soc.* **2013**, *135*, 501.
- (7) T. Terashima, T. Mes, T. F. A. de Greef, M. A. J. Gillissen, P. Besenius, A. R. A. Palmans, E. W. Meijer *J. Am. Chem. Soc.* **2011**, *133*, 4742.
- (8) E. Huerta, P. J. M. Stals, E. W. Meijer, A. R. A. Palmans *Angew. Chem. Int. Ed.* **2013**, *52*, 2906.
- (9) M. A. J. Gillissen, T. Terashima, E. W. Meijer, A. R. A. Palmans, I. K. Voets *Macromolecules* **2013**, *46*, 4120.
- (10) P. J. M. Stals, M. A. J. Gillissen, T. F. E. Paffen, T. F. A. de Greef, P. Lindner, E. W. Meijer, A. R. A. Palmans, I. K. Voets *Macromolecules* **2014**, *47*, 2947.
- (11) N. Hosono, A. R. A. Palmans, E. W. Meijer *Chem. Commun.* **2014**, *50*, 7990.
- (12) P. J. M. Stals, PhD Thesis, Eindhoven University of Technology, **2013**.
- (13) P. Jonkheijm, P. van der Schoot, A. P. H. J. Schenning, E. W. Meijer *Science* **2006**, *313*, 80.
- (14) D. J. Hill, M. J. Mio, R. B. Prince, T. S. Hughes, J. S. Moore *Chem. Rev.* **2001**, *101*, 3893.
- (15) R. B. Prince, J. G. Saven, P. G. Wolynes, J. S. Moore *J. Am. Chem. Soc.* **1999**, *121*, 3114.
- (16) J. W. Wackerly, J. S. Moore *Macromolecules* **2006**, *39*, 7269.
- (17) J. J. L. M. Cornelissen, J. J. J. M. Donners, R. de Gelder, W. S. Graswinckel, G. A. Metselaar, A. E. Rowan, N. A. J. M. Sommerdijk, R. J. M. Nolte *Science* **2001**, *293*, 676.
- (18) K. Takizawa, C. Tang, C. J. Hawker *J. Am. Chem. Soc.* **2008**, *130*, 1718.
- (19) C. M. Gothard, N. A. Rao, J. S. Nowick *J. Am. Chem. Soc.* **2007**, *129*, 7272.
- (20) M. T. Stone, J. M. Heemstra, J. S. Moore *Acc. Chem. Res.* **2006**, *39*, 11.
- (21) H. K. Murnen, A. R. Khokhlov, P. G. Khalatur, R. A. Segalman, R. N. Zuckermann *Macromolecules* **2012**, *45*, 5229.
- (22) C. L. H. Wong, J. Kim, J. M. Torkelson *J. Polym. Sci., Part B: Polym. Phys.* **2007**, *45*, 2842.
- (23) J. Chiefari, Y. K. Chong, F. Ercole, J. Krstina, J. Jeffery, T. P. T. Le, R. T. A. Mayadunne, G. F. Meijs, C. L. Moad, G. Moad, E. Rizzardo, S. H. Thang *Macromolecules* **1998**, *31*, 5559.
- (24) G. Moad, E. Rizzardo, S. H. Thang *Austr. J. Chem.* **2009**, *11*, 1402.
- (25) A. R. A. Palmans *Personal Communication*.
- (26) M. M. J. Smulders, M. M. L. Nieuwenhuizen, T. F. A. de Greef, P. van der Schoot, A. P. H. J. Schenning, E. W. Meijer *Chem. Eur. J.* **2010**, *16*, 362.
- (27) M. H. Stenzel, in *Handbook of RAFT polymerization* (Ed: C. Barner-Kowollik), WILEY-VCH, Weinheim, **2008**, 3165.

- 
- (28) G. Moad, D. H. Solomon, *The Chemistry of Radical Polymerization*, Elsevier, Amsterdam, **2006**, p 66.
- (29) A. B. Lowe, C. L. McCormick, in *Handbook of RAFT polymerization* (Ed: C. Barner-Kowollik), WILEY- VCH, Weinheim, **2008**, p. 237.
- (30) K. Nakatani, T. Terashima, M. Sawamoto *J. Am. Chem. Soc.* **2009**, *131*, 13600.
- (31) K. Nakatani, Y. Ogura, Y. Koda, T. Terashima, M. Sawamoto *J. Am. Chem. Soc.* **2012**, *134*, 4373.
- (32) N. Hosono, P. J. M. Stals, A. R. A. Palmans, E. W. Meijer *Chem. Asian J.* **2014**, *9*, 1099.
- (33) T. Mes, PhD Thesis, Eindhoven University of Technology, **2011**.



# Chapter 3

## *Triblock copolymers for creating complex secondary structures by orthogonal self-assembly*

**Abstract:** *The synthesis and characterization of ABC-type triblock copolymers containing two complementary association motifs is reported and their folding into well-defined polymeric nanoparticles under diluted conditions via intramolecular orthogonal hydrogen bonding has been investigated. The precursor ABC-type triblock copolymers are prepared via reversible addition-fragmentation chain transfer (RAFT) polymerization bearing primary alkyl bromide on A, protected alkyne on B and protected hydroxyl pendant groups on the C units. The complementary motifs, i.e. Hamilton wedge (HW, A block), benzene-1,3,5-tricarboxamide (BTA, B block) and cyanuric acid (CA, C block) are incorporated into the linear triblock copolymer side-chains via post functionalization. The self-folding processes are followed by nuclear magnetic resonance (<sup>1</sup>H-NMR) spectroscopy focused on the respective recognition pairs at ambient temperature in various solvents. The intramolecular chain collapse via helical stack formation is monitored by circular dichroism (CD) spectroscopy. In addition, the final aggregates formed by these two orthogonal forces, namely HW-CA pseudo crosslinking and BTA stacking, are characterized by static and dynamic light scattering (SLS and DLS) as well as atomic force microscopy (AFM).*

*Part of this work has been published:*

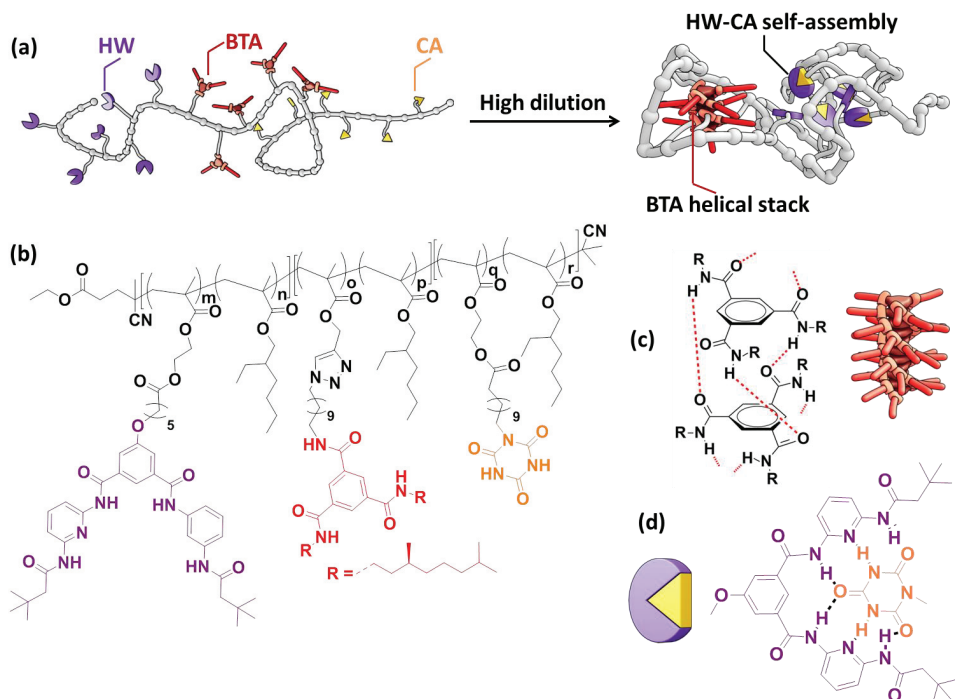
O. Altintas, M. Artar, G. ter Huurne, I. K. Voets, A. R. A. Palmans, C. Barner-Kowollik, E. W. Meijer *Macromolecules* **2015**, *48*, 8921-8932.



### **3.1 Introduction**

The study and application of single chain polymeric nanoparticles (SCPNs), generated by collapsing of a well-defined macromolecule into nanometer sized particles, is a dynamic new area that – potentially – opens a pathway to synthetic responsive nanoparticles able to mimic naturally occurring functions.<sup>1-13</sup> In the last years, a wide array of synthetic methodologies for the generation of SCPNs has been developed focusing on covalent,<sup>14-20</sup> dynamic covalent,<sup>21-24</sup> or non-covalent bonds, as summarized in Chapter 1.<sup>25-31</sup> In most cases, only one type of interaction was applied to induce chain collapse and a combination of analytical techniques revealed that the structures of the nanoparticles formed became more compact after single-chain folding, although their conformations remain relatively sparse and open.<sup>32,33</sup> Intriguingly, recent computational results revealed that using *multiple*, orthogonal intramolecular interactions can result in more compact, globular SCPNs.<sup>45</sup> Recently, the combination of two orthogonally assembling supramolecular motifs, the BTA motif and the (ureidopyrimidinone) UPy motif, attached to a poly(methacrylate) backbone resulted in polymer conformations that reversibly fold and unfold in apolar organic media.<sup>34-36</sup> While the UPy unit is self-complementary and dimerizes *via* quadruple hydrogen bonding,<sup>37,38</sup> the BTA unit forms helical aggregates stabilized by 3-fold hydrogen bonding.<sup>39,40</sup> Interestingly, differences in the topology of the prepared triblock copolymer, ABA or BAB (A = UPy units and B = BTA units), indicated a more loose packing for the BAB-type folded nanoparticles than for the ABA-type,<sup>36</sup> implying that topological differences in the polymer architecture do affect the folding behavior when using self-complementary motifs.

In this Chapter, we explore the cyanuric acid (CA)–Hamilton wedge (HW) couple, inspired by the possibilities that motifs forming heterodimers instead of homodimers offer. This pair has been used successfully to induce single chain collapse.<sup>41-43</sup> In addition, the use of hetero-complexing motifs attached to polymer backbones have been proposed to form hairpin-type structures in collapsed macromolecules.<sup>44</sup> Thus, in the present study, the formation of SCPNs using a combination of the BTA and HW-CA system is carefully investigated. Consequently, the synthesis and characterization of an ABC triblock copolymer that is designed to fold into a single-chain polymeric nanoparticle by intramolecular self-assembly is reported. The compartmentalized architecture was successfully synthesized by incorporating the HW, BTA and CA motifs into the A, B and C blocks, respectively (Scheme 3.1). A secondary structure was achieved *via* restricted interblock interactions between the A and C blocks *via* HW-CA dimerization together with BTA induced helical folding of the B block. The work described in this chapter was performed in close collaboration with Dr. Özcan Altıntaş and Prof. Dr. Christopher Barner-Kowollik of Karlsruhe Institute of Technology, Germany.



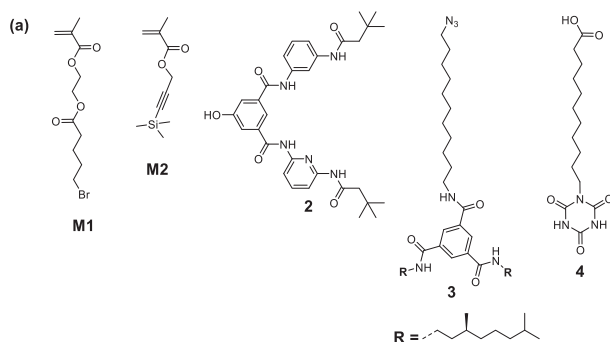
**Scheme 3.1** (a) Design of a triblock copolymer with orthogonal complementary motifs (HW, BTA and CA) alongside the polymer chain, which folds into a compartmentalized structure via orthogonal self-assembly. (b) Chemical structure of the functionalized triblock copolymers. (c) Self-assembly of BTA units via threefold symmetric hydrogen bonding. (d) Self-assembly of HW and CA via multiple hydrogen bonding.

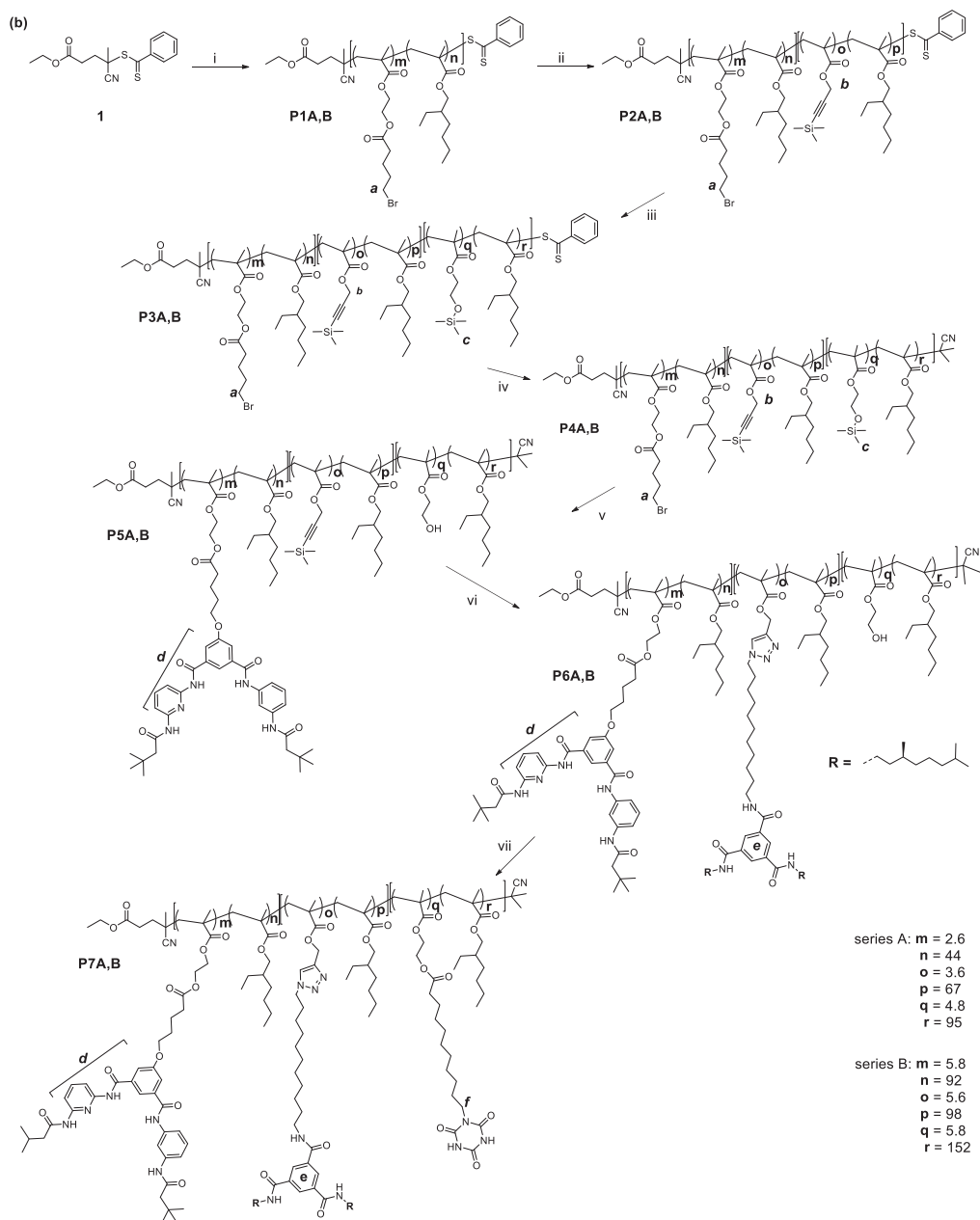
### 3.2 Design and synthesis of ABC triblock copolymers carrying pendant supramolecular motifs in the side chains

The ABC triblock copolymers **P7A,B** featuring (*S*) chiral BTA moieties in the middle (B) block and HW and CA moieties in the outer (A and C, respectively) blocks were designed and prepared (Schemes 3.1 and 3.2). In addition, **P8A**, lacking the HW-CA motifs, and **P9A**, lacking the BTA units, were prepared as reference polymers to help elucidate the contributions of both the hydrogen-bonding groups (Scheme 3.3). A post-polymerization functionalization approach was employed to introduce the HW, BTA and CA motifs. The reversible addition fragmentation transfer (RAFT) technique was selected to prepare well-defined linear precursors due to its tolerance towards many functional groups. After careful consideration, we copolymerized the post-functionalizable monomers comprising a primary alkyl bromide (**M1**), silyl-protected propargyl methacrylate (**M2**) and silyl-protected hydroxyethyl methacrylate (**M3**) with 2-ethylhexyl methacrylate (EHMA). EHMA was chosen as the comonomer to enhance the solubility of the resulting copolymers. The desired ABC precursor polymers are accessible using a chain extension technique in which 2-ethyl hexyl methacrylate is copolymerized with the appropriate first functional vinyl monomer (**M1**), followed by re-initiation with the second and

third functional vinyl monomer (**M2** and **M3**). In addition, hydroxyl functional HW, azide functional BTA and carboxyl functional CA are readily accessible *via* standard procedures and can be coupled *via* etherification, copper-catalyzed azide-alkyne cycloadditions (CuAAC) and an esterification process, respectively, to the ABC precursor copolymers. The complete synthesis route to obtain the ABC triblock copolymer **P7A** or **P7B** is depicted in Scheme 3.2. We prepared two series of polymers **P1A-P7A** and **P1B-P7B**, in which the final degrees of polymerization differed ( $DP \sim 220$  for the A series and  $DP \sim 360$  for the B series). The average number of incorporated functional groups is close to 5% in both series (see Table 1 for details).

The post-functionalizable triblock copolymers with primary alkyl halide groups in the A block, protected acetylene groups in the B block and protected hydroxyl groups in the C block were readily prepared by three-step RAFT polymerization. The trimethylsilyl (TMS)-protected monomers **M2** and **M3** were used to avoid undesirable interactions of the alkyn-termini. For the B-series polymers, the synthesis commences with the chain transfer agent (CTA) **1**, which is an esterified version of the commercially available CTA, 4-cyano-4-((phenylcarbonothioyl)-thio)pentanoic acid, in order to avoid possible side reactions.<sup>61</sup> We subsequently polymerized a mixture of monomer **M1** and ethyl hexylmethacrylate (EHMA) (ratios = EHMA/**M1**/**1** = 190/10/1) in 1,4-dioxane at 60 °C with **1** as CTA, affording **P1B**. Figure 3.1a shows the <sup>1</sup>H-NMR spectrum of the purified random copolymer **P1B**. The resonances at 7.85-7.33 ppm are associated with the aromatic protons in the CTA units, which show that the RAFT agent is still attached to the end of the polymer chain. The absence of resonances associated with the vinyl protons of the methacrylate around 6.13 and 5.60 ppm and appearance of broad resonances of EHMA close 3.82 ppm as well as the protons adjacent to bromide around 3.43 ppm indicate the successful polymerization. The SEC chromatogram of **P1B** shows a monomodal molar mass distribution (Figure 3.1b,  $M_n = 28.7$  kDa,  $D = 1.05$ ).  $DP$  was calculated by following the work of Matyjaszewski and co-workers on spontaneous gradient copolymerization for brush polymers.<sup>48,49</sup> From the monomer feed ratio, the final composition of functionalized monomers in the polymer backbone was calculated to be 5% in any part of polymer. For example, the incorporation of **M1** can be calculated by the integral area of the resonances of the  $CH_2$  next to bromine at 3.43 ppm and the two proton resonances of the CTA at 7.83 ppm. The total  $DP$  was calculated as the sum of all, and those are calculated in an analogous way.





**Scheme 3.2** (a) Monomers and functional units. (b) Synthetic strategy for the preparation of the ABC triblock with complementary motifs attached to the polymer chain. (i) 2-Ethylhexyl methacrylate (EHMA), **M1**, AIBN, dioxane, 60 °C; (ii) EHMA, **M2**, AIBN, dioxane, 60 °C; (iii) EHMA, **M3**, AIBN, dioxane, 60 °C; (iv) AIBN, lauroyl peroxide (LPO), toluene, 80 °C; (v) **2**, K<sub>2</sub>CO<sub>3</sub>, DMF/THF, 50 °C; (vi) **3**, CuSO<sub>x</sub>5H<sub>2</sub>O, Na ascorbate, DMF/THF, r.t.; (vii) **4**, DCC/DMAP, DCM, r.t.

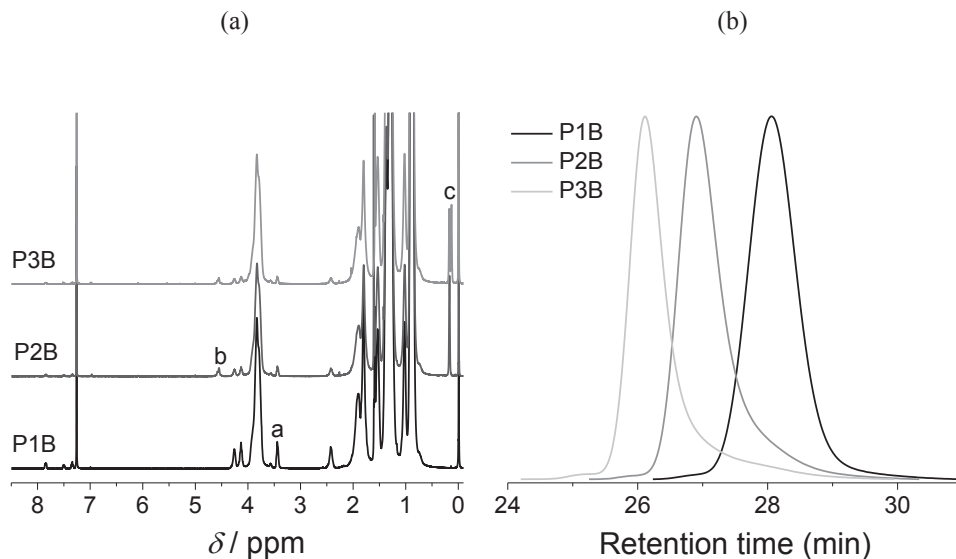


**Figure 3.1** (a)  $^1\text{H-NMR}$  spectra of **P1B**, **P2B**, and **P3B** in  $\text{CDCl}_3$  at ambient temperature. The chemical structures of the related polymers and  $^1\text{H-NMR}$  spectra labels can be found in Scheme 3.2. (b) SEC traces of the precursor polymers **P1B** (side-chain alkyl bromide), **P2B** (side-chain alkyl bromide/protected alkyne) as well as **P3B** (side-chain alkyl bromide/protected alkyne/protected hydroxyl).

In the next step, side-chain protected alkyne-containing diblock copolymer **P2B** was prepared by using **P1B** as a macro-RAFT agent. **P1B** was mixed with 3-(trimethylsilyl)prop-2-yn-1-yl methacrylate (TMS-alkyne MA, **M2**) and EHMA (EHMA/**M2**/**P1B** = 190/10/1). The chain extension was carried out in 1,4-dioxane at 60 °C. As shown in the  $^1\text{H-NMR}$  spectrum after purification of **P2B** (Figure 3.1a, middle), the disappearance of the vinyl proton resonances at 5.6 and 6.1 ppm and the appearance of resonances at 4.54 and 0.16 ppm suggests that **M2** was successfully polymerized. The number of the units of the **M2** can be calculated by the integral area of the  $\text{CH}_2$  resonance next to alkyne resonance at 4.54 ppm and the two protons of the CTA at 7.83 ppm (Figure 3.1a, middle), indicating the composition of **M2** maintained a constant value of ~5%. As shown in Figure 3.1b, the SEC trace of **P2B** shifted to higher molecular weight, confirming the successful chain extension ( $M_n = 48.9$  kDa,  $\mathcal{D} = 1.09$ ). Subsequently, the RAFT polymerization of 2-(trimethylsilyloxy)ethyl methacrylate (protected-HEMA, **M3**) was carried out using diblock copolymer **P2B** as the macro-RAFT agent and AIBN as the initiator. The signal in the  $^1\text{H-NMR}$  spectrum at 0.14 ppm is associated with the TMS group of **M3** in the side chain demonstrating the successful preparation of triblock copolymer **P3B** (Figure 3.1a, top). The number of the units of **M3** can be calculated by the integral area of the TMS group at 0.14 ppm and the two proton resonances of the CTA at 7.83 ppm, demonstrating the composition of **M3** to be at a constant value of ~5%. As shown in Figure 3.1b, SEC traces shifted to higher molecular weight, confirming the successful chain extension ( $M_n = 74.7$  kDa,  $\mathcal{D} = 1.13$ ). A slight increase was observed in the molar mass dispersity of **P3B** (from 1.05 in **P1B** to 1.13 in **P3B**). This is attributed to the presence of a small tailing peak in the SEC trace. The SEC trace of triblock

copolymer **P3** indicates the presence of very small amounts of precursor polymer, associated with some unavoidable loss of end group functionality during the synthesis of diblock copolymer (**P2**). For A-series polymers an analogues synthesis approach was followed. The data are collected in Table 1.

**Table 3.1** Conditions and results for the triblock copolymer preparation via RAFT.

Precursor polymer	A block <sup>a</sup>		B block <sup>a</sup>		C block <sup>a</sup>		$M_{n,NMR}^b$ kDa	$M_{n,SEC}^c$ kDa	$\bar{D}^c$	$D_H^d$ nm
	<i>n</i> EHMA	<i>n</i> M1	<i>n</i> EHMA	<i>n</i> M2	<i>n</i> EHMA	<i>n</i> M3				
<b>P1A</b>	44	2.6					10.5	14.8	1.04	n.d.
<b>P2A</b>	44	2.6	67	3.6			25.6	31.0	1.06	n.d.
<b>P3A</b>	44	2.6	67	3.6	95	4.8	47.0	45.5	1.12	n.d.
<b>P4A</b>	44	2.6	67	3.6	95	4.8	46.7	46.0	1.15	11.7 <sup>e</sup>
<b>P1B</b>	92	5.8					21.8	28.7	1.05	n.d.
<b>P2B</b>	92	5.8	98	5.6			43.9	48.9	1.09	n.d.
<b>P3B</b>	92	5.8	98	5.6	152	5.8	77.7	74.7	1.13	n.d.
<b>P4B</b>	92	5.8	98	5.6	152	5.8	77.6	77.0	1.14	15.6
Final polymer	<i>n</i> EHMA	<i>n</i> HW	<i>n</i> EHMA	<i>n</i> BTA	<i>n</i> EHMA	<i>n</i> CA	$M_{n,NMR}^b$ kDa	$M_{n,SEC}^c$ kDa	$\bar{D}^c$	$D_H^d$ nm
<b>P7A</b>	44	2.6	67	3.6	95	4.8	51.4	51.2	1.14	11.7 <sup>e</sup>
<b>P7B</b>	92	5.8	98	5.6	152	5.8	85.1	82.3	1.22	24.4
<b>P8A</b>	44	-	67	3.6	95	-	49.1	50.9	1.11	20.1
<b>P9A</b>	44	2.6	67	-	95	4.8	50.3	50.0	1.12	10.1

<sup>a</sup> *n* is the average number of incorporated 2-ethyl hexylmethacrylate (EHMA) or functional monomers (M1-M3) in the polymer chain as determined by <sup>1</sup>H-NMR by integration of the end-groups and / or relative intensities of selected signals.

<sup>b</sup> Calculated value for the molecular weight based on the molecular weights of the respective monomers and the average number of incorporated monomers.

<sup>c</sup> Determined via SEC using THF as the eluent, calibrated with polystyrene standards.

<sup>d</sup> The hydrodynamic diameter ( $D_H$ ) in MCH, determined from the translational diffusion coefficient, obtained via an Inverse Laplace Transform analysis of the second order correlation function, using the Stokes-Einstein equation ( $\theta = 90^\circ$ ,  $T = 20^\circ\text{C}$ ,  $c_{polymer} = 1\text{ mg mL}^{-1}$ ).

<sup>e</sup> A small fraction of larger aggregates was observed.

After the successful preparation of the triblock precursor polymers **P3A,B** with three different reactive side groups, the pendant primary alkyl bromide, acetylene and hydroxyl groups were functionalized with a hydroxyl functional HW, an azide-functionalized BTA and a carboxyl functional CA, respectively, affording the desired triblock copolymers (**P7A,B**) bearing both self-

assembling motifs. We attempted to attach the BTA unit on the side chain of **P3B** via copper-catalyzed azide–alkyne cycloaddition (CuAAC) reaction between the azide functional BTA and **P3B**. However, it was observed that the presence of the dithiobenzoate end-group was not compatible with the CuAAC reaction and caused crosslinking of the polymer chains.<sup>61</sup> Thus, it was decided to first remove the RAFT agent through a radical-induced reaction before conducting any further polymer functionalization reactions. Pink solutions of the triblock copolymer **P3A,B** with a dithiobenzoate end group were reacted with 20 molar equivalents of AIBN and 2 molar equivalents of lauroyl peroxide in toluene, affording white triblock copolymer **P4A,B**.<sup>50</sup> As an example, the SEC chromatogram and <sup>1</sup>H-NMR of **P4B** are presented in Figure 3.2. The <sup>1</sup>H-NMR spectrum indicates that aromatic protons of RAFT agent completely disappeared, indicating the complete removal of the dithiobenzoate group (Figure 3.2a, bottom). The SEC trace shows the presence of a small high molecular weight peak approximately twice that of the precursor polymer **P3B** due to chain-chain coupling (Figure 3.2b).

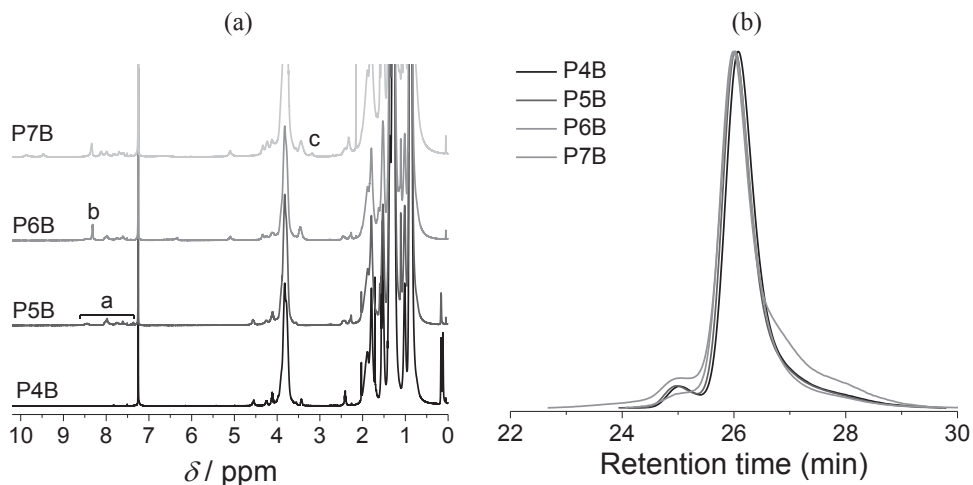
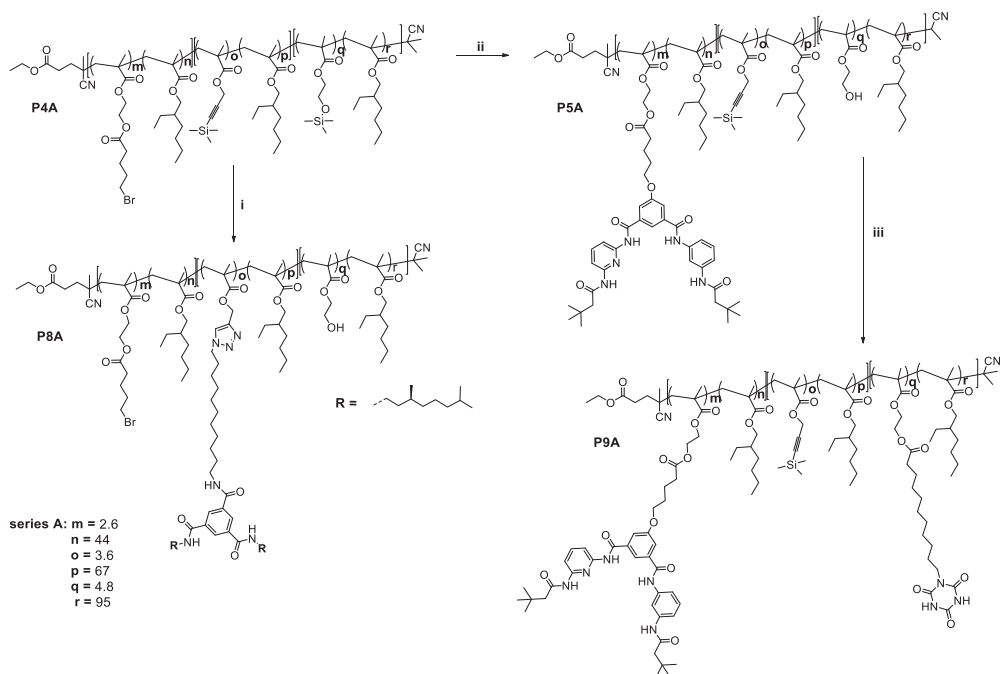


**Figure 3.2** (a) <sup>1</sup>H-NMR spectra of **P4B**, **P5B**, **P6B** and **P7B** in CDCl<sub>3</sub> at ambient temperature. The chemical structures of the related polymers and <sup>1</sup>H-NMR spectra labels can be found in Scheme 3.3. (b) SEC traces of the precursor polymers **P4B**, **P5B** (side-chain HW), **P6B** (side-chain HW/BTA) as well as **P7B** (side-chain HW/BTA/CA).

After the dithiobenzoate group was successfully removed, an etherification reaction was carried out in order to attach the HW moiety on the side-chain of the triblock copolymer **P4A,B**. The hydroxyl-functional HW (**3**) was successfully introduced into the preformed triblock copolymer backbone **P4A,B**, as confirmed by <sup>1</sup>H-NMR spectroscopy. A close inspection of Figure 3.2a of **P5B** clearly indicates the quantitative conversion of the alkyl bromide into its HW derivative as the resonance at 3.43 ppm – corresponding to CH<sub>2</sub>Br – has completely disappeared and the new resonances of the HW moiety are detected between 7.5 and 8.5 ppm. During the substitution, potassium carbonate also deprotected the TMS group of HEMA as confirmed by <sup>1</sup>H-NMR.<sup>51</sup> Subsequently, a direct CuAAC reaction between the **P5A,B**, containing TMS-protected acetylenes, and the azide functional BTA (**3**) was performed.<sup>52,53</sup> <sup>1</sup>H-NMR

spectroscopy (Figure 3.2a) showed a new resonance emerging for the  $CH_2$  protons next to the triazole ring at 5.09 ppm, indicating the successful coupling. Next, in order to install the cyanuric acid moieties onto the previously obtained polymers, **P5A,B** were esterified with a slight excess of **4** per hydroxyl group of HEMA. A new resonance arose at 3.21 ppm, which can be assigned to the  $CH_2$  protons next to the CA moiety. The  $^1H$ -NMR spectrum reveals a strong shift of the amide protons of the HW to lower field resonance signals at 9.44 and 9.87 ppm indicating an interaction between HW and CA. Additionally, the SEC trace of the conjugated product shifted to shorter retention times after each functionalization, which is related to an increase in molar mass (Figure 3.2b). The numbers of incorporated HW, BTA and CA moieties in the polymer were determined by  $^1H$ -NMR spectroscopy. Reference polymer **P8A** was prepared from precursor **P4A** by a modified procedure,<sup>34</sup> while **P9A** was prepared in analogy to **P7B** (Scheme 3.3). The results for the characterization of **P7A**, **P8A** and **P9A** are summarized in Table 1.



**Scheme 3.3** Synthetic strategy for the preparation of the reference triblock copolymer with orthogonal complementary motifs alongside the polymer chain. (i) **3**,  $CuSO_4 \cdot xH_2O$ , Na ascorbate, DMF/THF, room temperature; (ii) **2**,  $K_2CO_3$ , DMF/THF, 50 °C; (iii) **4**, DCC/DMAP, DCM, ambient temperature.

### 3.3 Folding of the triblock copolymers via multiple hydrogen bonds

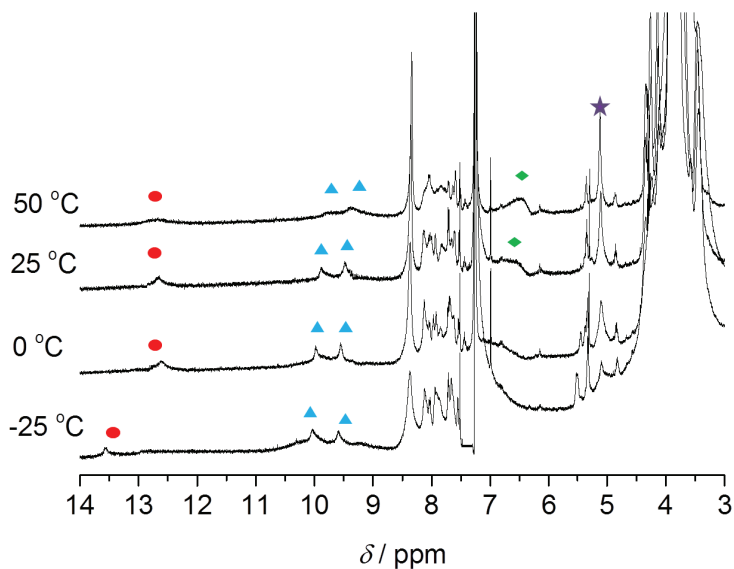
The dynamic nature of single-chain polymers in their folded state makes them challenging to be characterized using conventional polymer analysis techniques. A combination of several techniques for the characterization of non-covalent interactions is required to provide convincing evidence of the single-chain folding of synthetic polymers. Therefore, the hydrogen-bonding directed single-chain folding of linear polymers was first characterized by  $^1H$ -NMR



spectroscopy, allowing the study of dynamic interactions in a wide range of concentrations and temperatures. We selected chloroform, a solvent in which the HW-CA interaction has been characterized in detail.<sup>41-43,54-57</sup> Thus, we performed VT-NMR analysis<sup>34,42</sup> of **P7B** in CDCl<sub>3</sub> at a concentration of 1 mg/mL (Figure 3.3a). The <sup>1</sup>H-NMR spectra were recorded between 50 and –25 °C. At 50 °C, the broad resonance at 6.45 ppm is attributed to the amide protons on the BTA moieties, and the signals at 12.72, 9.75 and 9.36 to the NHs in the CA and HW units, respectively. Upon cooling the sample, all NH signals shifted downfield. The further broadening and shifting of the BTA-NH resonance is a result of threefold hydrogen-bond formation in agreement with previous reports.<sup>34</sup> In the absence of self-assembly between the HW and CA motifs, the corresponding protons of the HW and the CA units appear between 7.9 ppm and 8.5 ppm.<sup>55-57</sup> In **P7B**, the CA resonance at 12.65 ppm shifts to 13.58 ppm upon cooling, which corresponds to the CA unit binding increasingly strong to the HW unit. At the same time, the amide protons of the Hamilton wedge shift to 9.62 and 10.08 ppm when going from 50 °C to –25 °C, evidencing that supramolecular assembly is operational for these two complementary recognition units.

In addition, the self-assembly process between these motifs was investigated in 1,2-dichloroethane-d<sub>2</sub> (DCE-d<sub>2</sub>) and methyl cyclohexane-d<sub>14</sub> (MCH d<sub>14</sub>) via <sup>1</sup>H-NMR spectroscopy at a concentration of 1 mg mL<sup>-1</sup>. While DCE and CHCl<sub>3</sub> are of medium polarity ( $\mu = 1.15$  and 1.83 D for CHCl<sub>3</sub> and DCE, respectively), MCH is apolar ( $\mu = 0$  D). Especially MCH is expected to enhance the hydrogen-bond formation between the supramolecular motifs. As shown in Figure 3.4a, the resonances from protons of CA in DCE-d<sub>2</sub> strongly shifted downfield to 16.98 ppm, and the resonances corresponding to the amide protons of HW also displayed a significant downfield shift to 12.94 and 9.38 ppm. In addition, the <sup>1</sup>H-NMR spectrum in MCH-d<sub>14</sub> (Figure 3.3b and Figure 3.4b) showed that the resonances associated with the amide protons of the HW and the CA are very broad and appeared at 10.01, 9.76, and 12.78 ppm, respectively. These observations evidence that hydrogen-bonded self-assemblies are formed between HW and CA in DCE and MCH. The <sup>1</sup>H-NMR spectrum of **P7A** was also evaluated in MCH-d<sub>14</sub> at higher temperatures (Figure 3.3b). The data show that the resonances of the aromatic protons and the NH protons of the HW wedge shift very little upon increasing the temperature to 60 °C and remain broad, indicating that the hydrogen bonds remain. The resonance of the CH<sub>2</sub>-triazole at 5 ppm, on the other hand, became sharper with increasing temperature, suggesting an increase in the mobility of the polymer backbone.

(a)



(b)

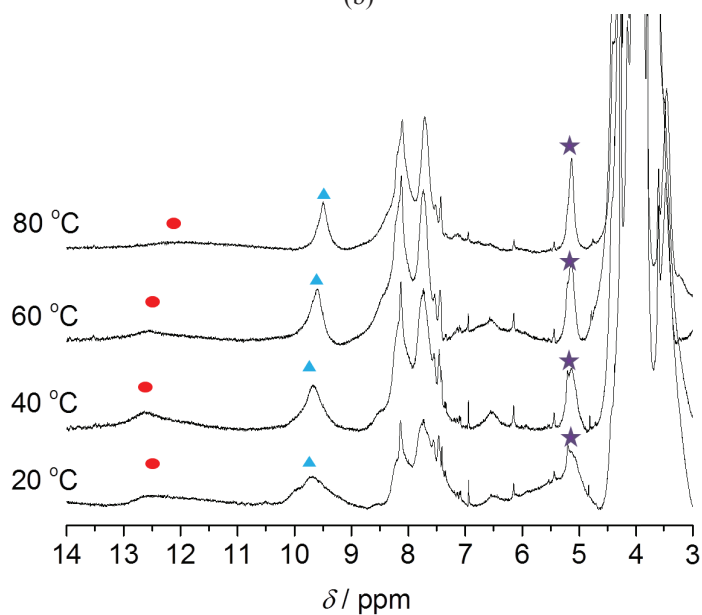
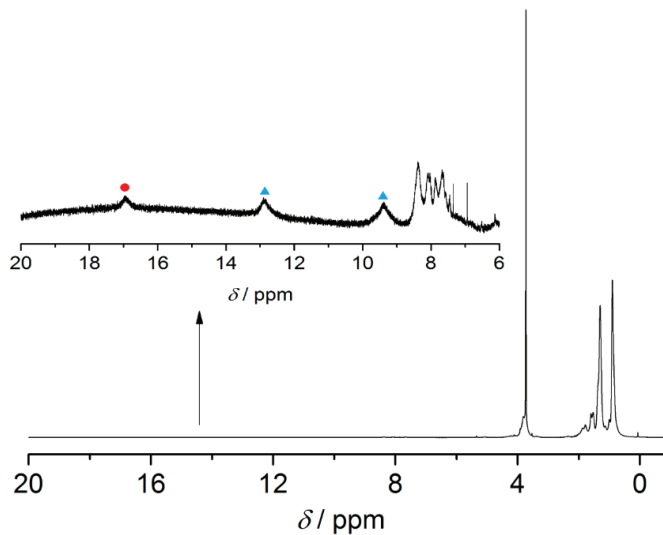


**Figure 3.3** (a) Arrays of VT-NMR spectra recorded for 1 mg mL<sup>-1</sup> solutions in CDCl<sub>3</sub> upon cooling from 50 to -25 °C for P7B. (b) Arrays of VT-NMR spectra recorded for 15 mg mL<sup>-1</sup> solutions in MCH-d<sub>14</sub> upon cooling from 20 to 80 °C for P7A. The solvent peak was used as an internal standard. The insets depict the assignments of protons on BTA (green), HW (blue), CA (red) and CH<sub>2</sub>-triazole (purple).

(a)



(b)

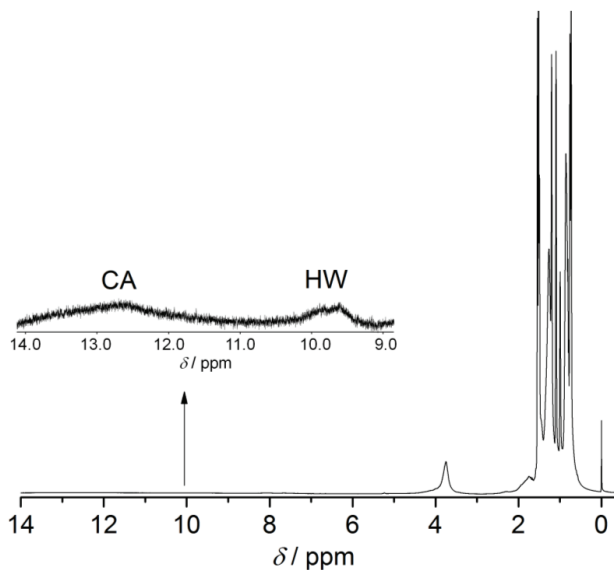


**Figure 3.4** (a)  $^1\text{H-NMR}$  spectrum of SCNPs **P7B** in 1,2-dichloroethane- $d_2$  at 25  $^\circ\text{C}$  showing the resonances associated with the bound imide protons of cyanuric acid (CA, red) as well as the resonances of the amide protons of the Hamilton wedge (HW, blue). (b)  $^1\text{H-NMR}$  spectrum of the SCNPs **P7B** in methyl cyclohexane- $d_{14}$  (MCH- $d_{14}$ ) at 25  $^\circ\text{C}$  showing the resonances associated with the bound imide protons of cyanuric acid (CA) as well as the resonances of the amide protons of the Hamilton wedge (HW). The concentration of polymer **P7B** was kept constant at 1  $\text{mg mL}^{-1}$ .

While Hamilton wedge-cyanuric acid or thymine-diaminopyridine systems dimerize in various halogenated solvents such as chloroform, dichloromethane and tetrachloroethane,<sup>41,42,54</sup>

chiral BTA units are known to be highly sensitive to solvent polarity.<sup>39</sup> To better understand the effect of solvent on self-assembly of the pendant supramolecular units and SCPN formation through hydrogen-bond induced folding, circular dichroism (CD) spectroscopy was performed on **P7A,B** which differ in degree of polymerization and total number of functional units. As a reference to better elucidate the contributions of both the hydrogen-bonding groups, **P8A**, lacking the HW-CA motifs, was investigated as well.

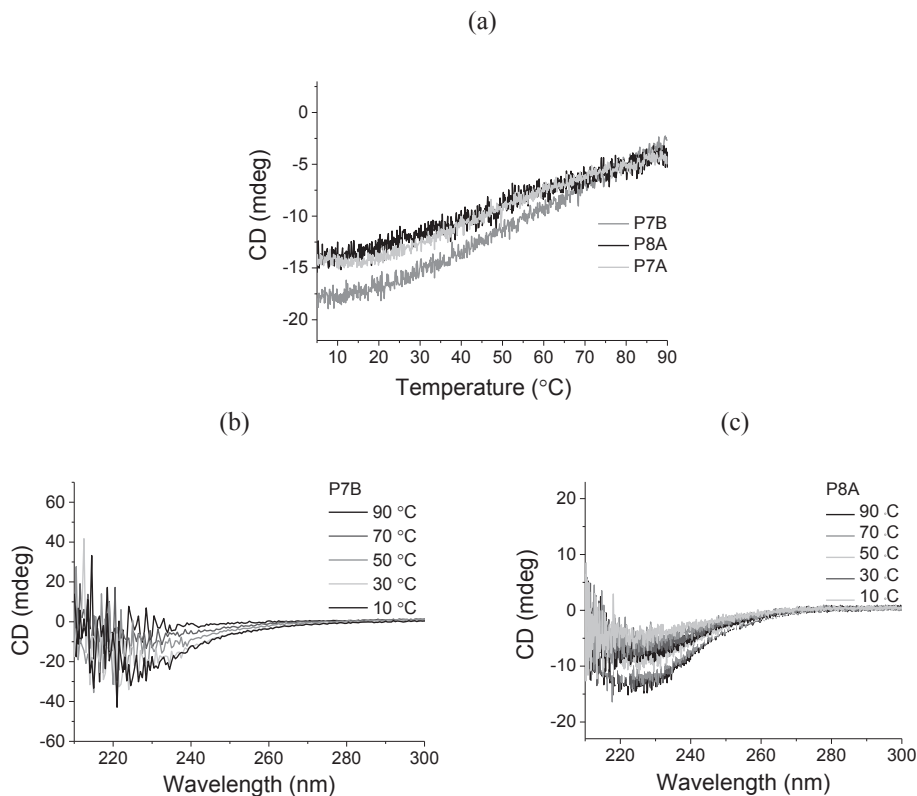


**Figure 3.5** (a) CD cooling curves of **P7A,B** and **P8A** ( $c_{BTA} = 35 \mu\text{M}$ ,  $l = 0.5 \text{ cm}$ ) monitored at  $\lambda = 225 \text{ nm}$  in methyl cyclohexane (MCH) at temperatures from 90 to 5 °C (cooling rate 1 C  $\text{min}^{-1}$ ). (b) CD spectra in MCH of **P7B** (wavelength scan) and (c) **P8A** (wavelength scan) for different temperatures ( $c_{BTA} = 35 \mu\text{M}$ ,  $l = 0.5 \text{ cm}$ ).

The self-assembly of (*S*) chiral BTA moieties of the **P7A,B** and **P8A** as well as the orthogonality of BTA stacking and HW-CA self-assembly were assessed using temperature-dependent CD spectroscopy. The experiments were performed at a 35  $\mu\text{M}$  total BTA concentration ( $c_{\text{polymer}}$  around 0.5  $\text{mg mL}^{-1}$ ) in MCH. The cooling curves were recorded at 225 nm upon cooling from 90 to 5 °C, and a slow cooling rate (1 K  $\text{min}^{-1}$ ) was applied. The transition from the unfolded state (high temperatures, no BTA aggregation, no Cotton effect) to the folded state (low temperature, aggregated BTAs, negative Cotton effect) of polymers **P7A,B** and **P8A** in MCH is clearly evidenced in the CD spectra (Figure 3.5). Upon cooling, all cooling traces are

rather similar and negative Cotton effects were observed for both the polymers **P7A,B** and **P8A**, indicating helical aggregates with a preferred left-handed (*M*) helical sense. At 20°C, the molar ellipticity  $\Delta\epsilon$  is -23, -29 and -24 L mol<sup>-1</sup> cm<sup>-1</sup> for **P7A**, **P7B** and **P8A**, respectively. The slightly different  $\Delta\epsilon$  for **P7B** compared to **P7A** is a result of the different loading of BTAs in the two polymers. Together with the HW-CA dimerization observed in MCH by NMR, we can conclude that BTA stacking and HW-CA dimerization act in an orthogonal manner. Previously, for a UPy-BTA-UPy polymer with a similar BTA concentration in the middle block and similar degree of polymerization, Hosono *et al.* reported a  $\Delta\epsilon$  of -30 L mol<sup>-1</sup> cm<sup>-1</sup> for ABA triblock polymers functionalized with BTAs in the middle B block and self-complementary ureidopyrimidinones (UPys) in the A and C blocks and isobornyl moieties as hydrophobic units.<sup>34</sup> Moreover, random amphiphilic copolymers with 10 mol% BTAs typically display  $\Delta\epsilon$  values between -13 and -20 L mol<sup>-1</sup> cm<sup>-1</sup> in water.<sup>28,40,58,59</sup>

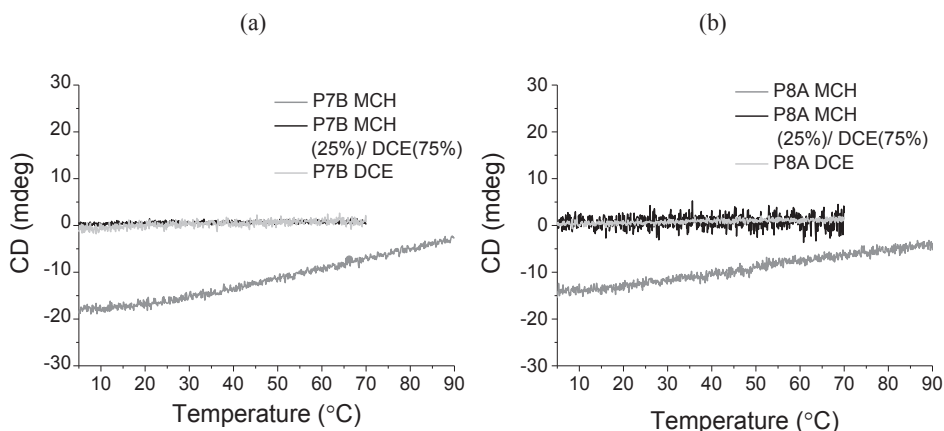


**Figure 3.6** CD cooling curves of **P8A** (a) and **P7B** (b) at  $\lambda = 225$  nm in wavelength scan in MCH, DCE and MCH/DCE (25:75) mixture ( $[BTA] = 35 \mu\text{M}$ ,  $l = 0.5$  cm).

In contrast, no CD effect was observed for the polymers (**P7B** and **P8A**) in DCE and DCE/MCH (75/25) mixtures (Figure 3.6a, b), indicating that the BTAs are not able to *helically* aggregate under these solvent conditions. This is in contrast to the observations by Mes *et al.*<sup>39</sup> and Hosono *et al.*<sup>34</sup> who reported helical BTA stack formation in DCE/MCH mixtures for random BTA-containing copolymers and for ABA triblock polymers functionalized with BTAs in the middle B block and self-complementary ureidopyrimidinones in the A blocks. This difference in the ability to form helical BTA aggregates in these two types of polymers in solvent mixtures containing DCE is remarkable and points to a significant sensitivity of the BTAs to their direct, local environment. In the current study, self-assembly is only possible between the HW functionalized A block and the CA functionalized C block of the ABC triblock copolymers, while in the previous study UPy-UPy dimerization also could occur within one block. Possibly, a tweezer structure arises from intramolecular dimerization, which could destabilize helical BTA aggregate formation, by relaying more entropic strain to fold the polymer backbone. This effect could make BTA aggregation more susceptible to an enhanced polarity of the solvent.

While orthogonality of the HW-CA self-assembly and BTA stacking in MCH is shown *via*  $^1\text{H-NMR}$  and CD spectroscopy, these techniques do not permit to conclude if one polymer chain folds into one single chain polymeric nanoparticle or if more polymer chains are present within the formed nanoparticles. Therefore, we performed dynamic light scattering (DLS) and static light scattering (SLS) experiments in collaboration with ir. Gijs ter Huurne. DLS experiments were carried out in MCH to determine the hydrodynamic diameters ( $D_{\text{H}}$ ) of unfunctionalized **P4A,B**, BTA functionalized **P8A**, HW and CA functionalized **P9A**, and fully functionalized **P7A,B**, the results are collated in Table 1. The hydrodynamic diameters vary between 10 nm (for **P9A**) and 24 nm (for **P7B**). While the autocorrelation curves show a monomodal decay for all functionalized polymers, the autocorrelation curve for **P4A** is not monomodal and a small fraction of particles with a larger  $D_{\text{H}}$  of 91 nm is observed (Figure 3.7a). As an example the intensity distributions obtained for the series **P4A**, **P7A**, **P8A**, and **P9A** are shown in Figure 3.8a. These intensity distributions at 20 °C are rather broad and in combination with the rather high values for  $D_{\text{H}}$  may suggest that multi-chain aggregation is present in some of the functionalized polymers.

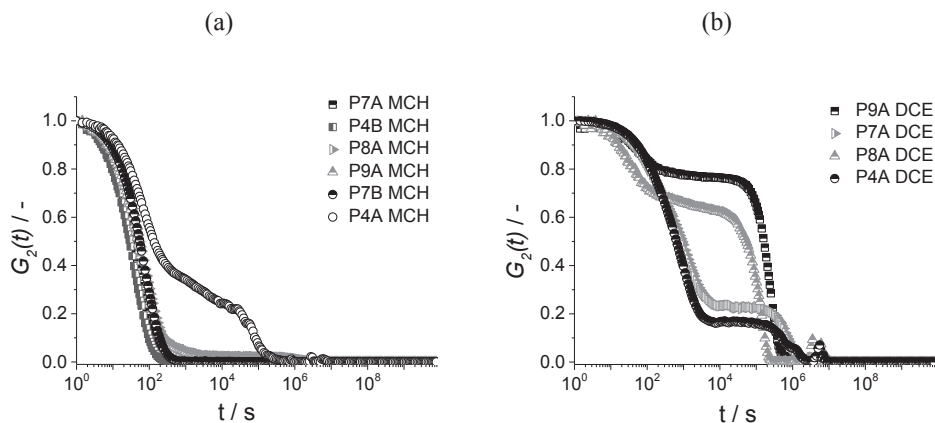


**Figure 3.7** Dynamic light scattering intensity autocorrelation functions of (a) **P7A**, **P4B**, **P8A**, **P9A**, **P7B** and **P4A** in MCH and (b) **P9A**, **P7A**, **P8A**, and **P4A** in DCE in  $1 \text{ mg mL}^{-1}$  at room temperature.

To investigate in more detail whether the formed particles comprise of one or more polymer chains, SLS was measured for **P4A**, **P7A**, **P8A**, and **P9A** in MCH ( $c_{\text{polymer}} = 1 \text{ mg mL}^{-1}$ ). The results show an angle-independent excess scattered intensity for polymers **P4A**, **P8A**, and **P9A** suggesting very small ( $< 25 \text{ nm}$ ) particles. For **P7A** a slight angle-dependence is observed, suggesting a small fraction of larger aggregates (Figure 3.8b). In addition, an increase in the scattered intensity is observed in the series **P4A**, **P9A**, **P8A**, and **P7A**, the increments are, however, larger than expected based on the molecular weight increases as a result of functionalization of the polymers. Neglecting small differences in the refractive index increment ( $dn/dc$ ), the polymers contain at most 5% of functional groups per polymer chain, the relative molecular weight of **P7A** is almost four times higher than that of **P4A** (Figure 3.8b). These

results suggest that on average more than one polymer is involved in the nanoparticle formation once the polymers are functionalized.

We also measured DLS in DCE, a solvent in which BTA aggregation is absent at ambient temperature as evidenced by CD measurements. Interestingly, now all polymers clearly show decay curves that are not monomodal, indicative of the presence of large multi-chain aggregates (Figure 3.7b). We hypothesize that a chlorinated solvent of medium polarity results in weakened intra-particle interactions and this more dynamic structure may enhance inter-particle interactions. It is important to note that these observations are in line with the previous studies on SCPNs comprising UPy motifs where solvent played a crucial role in the type of aggregate (single chain or multi-chain) that was formed.<sup>27</sup>

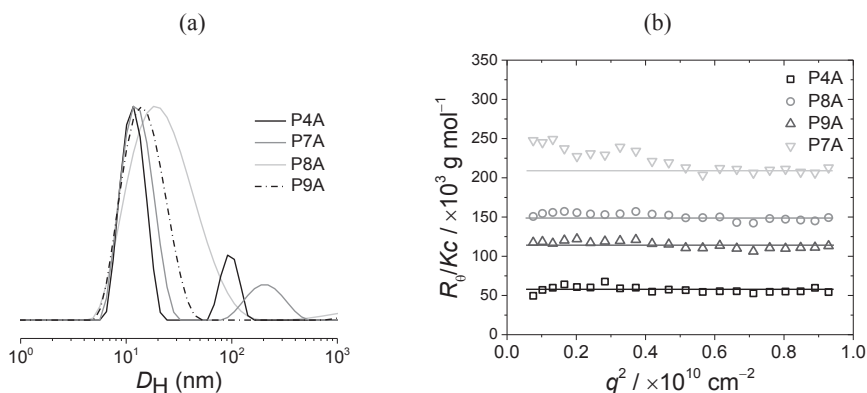


**Figure 3.8** (a) DLS intensity distributions measured at  $\theta = 90^\circ$  for **P4A**, **P7A**, **P8A**, **P9A**, and **P7A** at  $20^\circ\text{C}$  in MCH. (b) SLS results for **P4A**, **P7A**, **P8A**, and **P9A** in MCH. In all cases, the measurements were carried out at  $20^\circ\text{C}$  at a polymer concentration of  $c_{\text{polymer}} = 1\text{ mg mL}^{-1}$ .

Finally, we conducted a preliminary study on the effect of temperature on the stability of the nanoparticles formed in MCH. From the NMR results in combination with CD, an increase in temperature is expected to result in a higher mobility of the polymer backbone and, at the same time, weakening of the hydrogen-bond interactions, especially those related to helical hydrogen-bond formation between the BTAs. Interestingly, in all cases an increase in temperature results in a change in shape of the autocorrelation function due to a secondary decay. This strongly points to the formation of multi-chain aggregates. Above  $30^\circ\text{C}$ , **P8A** and **P9A** start forming large multi-chain aggregates (Figure 3.9 c,d), while this occurs at a temperature of  $60^\circ\text{C}$  for **P7B** (Figure 3.9 e). The latter could be related to the slightly higher number of BTA and HW-CA units present in **P7B**, stabilizing *intra*-particle interactions. The formation of more and larger multi-chain aggregates at higher temperatures was corroborated by SLS measurements and is in line with the observations made in DCE. However, the exact origin of this behavior is currently not clear and subject of further investigations.

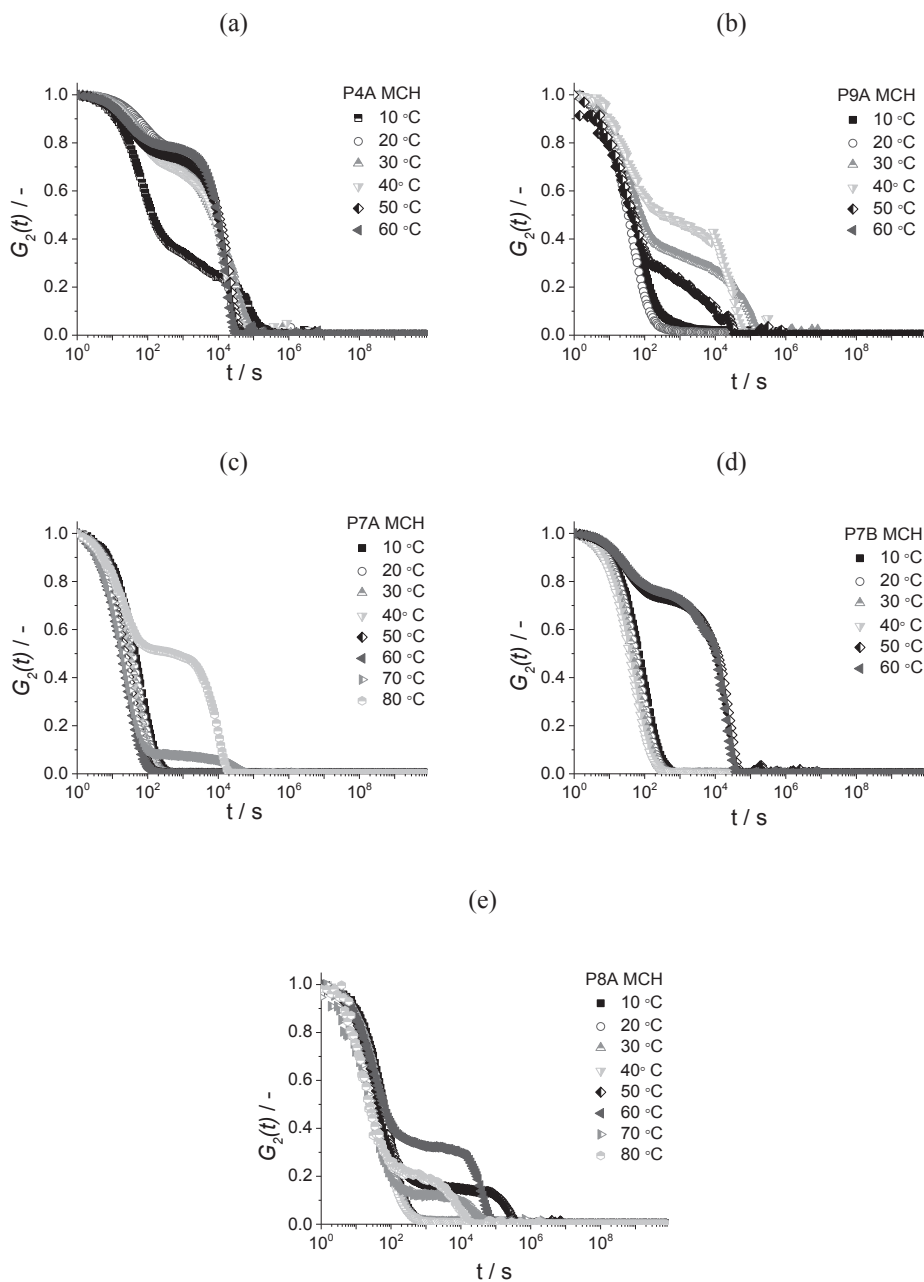


**Figure 3.9** Dynamic light scattering intensity autocorrelation functions of (a) **P4A**, (b) **P7A**, (c) **P9A**, (d) **P8A**, and (e) **P7B** in MCH at a polymer concentration of  $1 \text{ mg mL}^{-1}$  at various temperatures.

Finally, atomic force microscopy (AFM) was measured for **P7B**. Samples were prepared by drop-casting from a  $0.01 \text{ mg mL}^{-1}$  solution on freshly cleaved mica in MCH (Figure 3.10,



height image). Here, we observed a particle diameter between 25 and 30 nm, which is in good agreement with the values obtained from DLS, taken the flattening of the SCNP on the surface into account. Additionally, no large, undefined aggregates were observed.

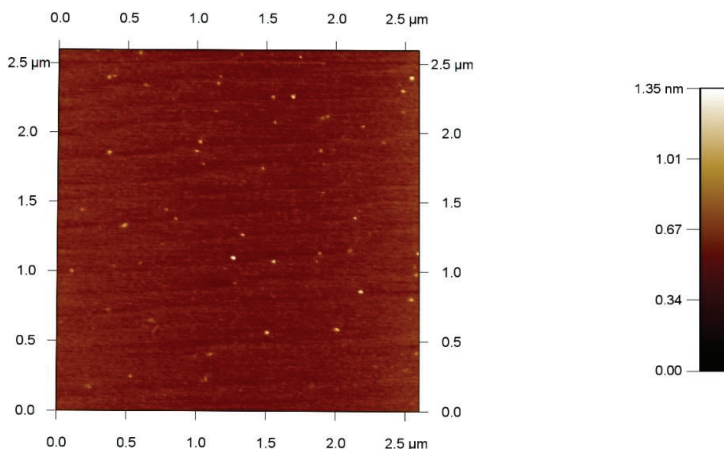


**Figure 3.10** AFM (height) image of **P7B** ( $0.01 \text{ mg mL}^{-1}$ , dropcasted on freshly cleaved mica from MCH).

### 3.4 Conclusions

We presented a modular synthetic strategy to access well-defined triblock copolymer systems featuring orthogonal hydrogen bonding motifs by combining reversible addition fragmentation chain transfer (RAFT) polymerization with a three step post-functionalization. In this way, an ABC-type triblock copolymer was constructed with restricted intrablock interaction of the B block *via* BTA stacking and A to C interblock interaction *via* Hamilton wedge (HW) (A block) and cyanuric acid (CA) (C block) driven self-assembly. In methylenecyclohexane, temperature-dependent CD experiments show that the presence of HW-CA units does not disturb the helical self-assembly of the BTA aggregates, while NMR indicates that the HW-CA dimerization is not affected by the presence of BTA units. As a result, the triblock copolymers fold through the orthogonal self-assembly of two independently aggregating supramolecular motifs. Interestingly, the BTA helical aggregation in the triblock copolymers is highly sensitive to the addition of more polar 1,2-dichloroethane.

The scattering results in MCH suggest that the triblock copolymers form well-defined particles of uniform size comprising a few polymer chains at the concentrations applied in this study (1 mg/mL). In contrast, very large multichain aggregates are observed in more polar 1,2-dichloroethane, in which no BTA aggregation is present. The combined results evidence that the ABC-triblock copolymer design results in a system that is more sensitive to the polarity of its environment than systems we previously investigated. In addition, the nature of the solvent is of crucial importance to balance inter- vs intramolecular self-assembly in the ABC-triblock copolymers. Nevertheless, well-defined particles with orthogonally self-assembling domains mimicking, in a simplified way, an  $\alpha$ -helix and a  $\beta$ -sheet are accessible with the procedures outlined in the current study. The solution behavior of the current system as a function of solvent

polarity and temperature is complex and subject to further detailed investigations. It is anticipated that the rapid advances made in precision polymer synthesis are crucial to implement the construction of complex polymers with pendant supramolecular motifs, leading to controlled folding of polymer chains into perfectly defined aggregates.<sup>6</sup>

### 3.5 Experimental

#### 3.5.1 Materials

2-Ethylhexyl methacrylate (EHMA, 98%, Aldrich), 2-hydroxyethyl methacrylate (HEMA, 97%, Aldrich), 2-(trimethylsilyloxy)ethyl methacrylate (**M3**, 96%, Aldrich) were passed through a column of inhibitor remover (Aldrich) prior to use and subsequently stored at -19°C. The initiator, azobisisobutyronitrile (AIBN, Merck), was purified by recrystallization from methanol. 11-Bromoundecanoic acid (99%, Aldrich), ethylenediaminetetraacetic acid disodium salt (EDTA) (99%, Acros), cyanuric acid (CA) (99%, ABCR GmbH and Co. KG), 4-dimethylamino pyridine (DMAP) (99%, Acros), *N,N*-dicyclohexylcarbodiimide (DCC) (99%, Acros), *N,N*-dimethylformamide extra dry (DMF) (99.8%, Acros), tetrahydrofuran extra dry (THF) (99.8%, Acros), sodium azide (99.8%, Acros), 5-bromovaleryl chloride (97%, Aldrich), hydrochloric acid (37%, Carl Roth GmbH and Co. KG), benzoyl chloride (99%, Aldrich), oxalyl chloride (99%, Aldrich), sodium hydroxide (98%, Carl Roth GmbH and Co. KG), 5-hydroxyisophthalic acid (97%, Aldrich), sulfuric acid (95%, Carl Roth GmbH and Co. KG), 3,3-dimethylbutyryl chloride (99%, Aldrich), 2,6-diamino pyridine (98%, Aldrich), triethylamine (99.7%, ABCR GmbH and Co. KG), cupric sulfate pentahydrate (99.5%, Aldrich), (+)-sodium L-ascorbate (98%, Aldrich), 4-cyano-4-((phenylcarbonothioyl)thio)pentanoic acid (97%, Aldrich) and lauroyl peroxide (LPO, 97%, Aldrich) were used as received. All solvents were purchased from Biosolve. Lauryl methacrylate (LMA: Aldrich, purity >96%), purified by an inhibitor removal column (Aldrich). The synthesis of chiral BTA azide was performed as described elsewhere, starting from (*S*)-citronellol with an enantiomeric excess (*ee*) of 98.4%.<sup>60</sup>

#### 3.5.2 Instrumentation

SEC measurements were performed on a Polymer Laboratories PL-GPC 50 Plus Integrated System, comprising an autosampler, a PLgel 5  $\mu\text{m}$  bead-size guard column (50  $\times$  7.5 mm) followed by three PLgel 5  $\mu\text{m}$  Mixed-C and one PLgel 3  $\mu\text{m}$  Mixed-E columns (300  $\times$  7.5 mm) and a differential refractive index detector using THF as the eluent at 35 °C with a flow rate of 1 mL min<sup>-1</sup>. The SEC system was calibrated using linear poly(styrene) (PS) standards ranging from 476 to 2.5·10<sup>6</sup> g mol<sup>-1</sup>.

The structures of the synthesized compounds were confirmed *via* <sup>1</sup>H-NMR and <sup>13</sup>C-NMR spectroscopy using a Bruker AM 400 MHz spectrometer, a Varian Mercury Vx 400 MHz or a Varian 400MR 400 MHz (in all cases 400 MHz for <sup>1</sup>H measurements and 100 MHz for <sup>13</sup>C measurements), temperature-dependent experiments on **P7A** were performed on a Varian Unity Inova 500 MHz spectrometer. To improve signal to noise ratio, polymer sample of **P7A** was measured at concentrations of 15 mg/mL of polymer with a delay time of 5 seconds. Samples were dissolved in CDCl<sub>3</sub> or CD<sub>2</sub>Cl<sub>2</sub>. Proton chemical shifts are reported in ppm relative to tetramethylsilane (TMS).

Dynamic light scattering measurements were performed on a Malvern  $\mu$ V Zetasizer equipped with a 830 nm laser. Samples were prepared by filtering solutions in spectroscopy grade solvents through a 0.45  $\mu$ m PTFE-filter (Whatman) in a fluorescence cell with a path length of pathlength 10x2 mm and chamber volume of 100  $\mu$ L. Static light scattering (SLS) measurements were carried out on an ALV/CGS-3 MD-4 compact goniometer system equipped with a multiple tau digital real time correlator (ALV- 7004, solid state laser:  $\lambda = 532$  nm; 40 mW). Measurements were performed over an angular range of 30° to 130° in steps of 5°, performing 10  $\times$  5 seconds acquisitions at  $T = 20$  °C.<sup>61</sup> Samples for dynamic and static light scattering measurements were prepared by first dissolving the polymer in spectroscopy grade solvent and then sonicating for 2 hours in a Cole Parmer 8891 sonification bath. Immediately after the sonification, a 0.45  $\mu$ m PTFE-filter (Whatman) was first washed by filtering spectroscopy grade solvent through, and then the polymer solution was filtered in a fluorescence cell with a path length of 10x2 mm and chamber volume of 100  $\mu$ L. Prepared solutions were measured immediately.

Circular dichroism (CD) measurements were performed on a Jasco J-815 spectropolarimeter where the sensitivity, time constant and scan rate were chosen appropriately (sensitivity: standard; response: 2 sec; band width: 1 nm; data pitch: 0.1 nm; scanning speed: 20 nm min<sup>-1</sup>). Corresponding temperature-dependent measurements (data pitch: 0.1 °C) were performed with a PFD-425S/15 Peltier-type temperature controller with a temperature range of 263-383 K and adjustable temperature slope, in all cases temperature slope of 1 K/min was used. In all experiments the linear dichroism was also measured and in all cases no linear dichroism was observed. Separate UV/Vis spectra were obtained from a Perkin-Elmer UV/Vis spectrometer Lambda 40 (optical path length = 0.5 cm).

Atomic force micrographs were recorded under ambient conditions with silicon cantilever tips (PPP-NCH, 300-330 kHz, 42 N/m from Nanosensors) using an Asylum Research MFP-3D in AC (tapping) mode.

### 3.5.3 Synthesis

2-(Methacryloyloxy)ethyl 5-bromopentanoate (**M1**),<sup>61</sup> 3-(trimethylsilyl)prop-2-yn-1-yl methacrylate (**M2**),<sup>46</sup> ethyl 4-cyano-4-((phenylcarbonothioyl)thio)pentanoate (**1**),<sup>61</sup> *N*<sup>1</sup>-(3-(3,3-dimethylbutanamido)phenyl)-*N*<sup>3</sup>-(6-(3,3-dimethylbutanamido)pyridin-2-yl)-5-hydroxyiso-phthalamide (**2**),<sup>47</sup> *N*<sup>1</sup>-(11-azidoundecyl)-*N*<sup>3</sup>,*N*<sup>5</sup>-bis((S)-3,7-dimethyloctyl)benzene-1,3,5-tricarboxamide (**3**),<sup>34</sup> 11-(2,4,6-trioxo-1,3,5-triazinan-1-yl)undecanoic acid (**4**)<sup>47</sup> were synthesized according to literature procedures.

*Synthesis of side-chain alkyl bromide functional homopolymer (PIB):*

2-Ethylhexyl methacrylate (EHMA, 2.02 g, 10.2 mmol), **1** (CTA, 16.5 mg, 0.0535 mmol), **M1** (0.157 g, 0.54 mmol) and azobisisobutyronitrile (AIBN, 1.75 mg, 0.01 mmol), dioxane (2.5 mL) and a stirring-bar were added into a Schlenk-tube. After three freeze–pump–thaw cycles the tube was backfilled with argon, sealed, placed in an oil bath at 60 °C and removed after 16 h. The tube was subsequently cooled with liquid nitrogen to stop the reaction. The reaction mixture was diluted with THF and subsequently precipitated three times into 200 mL cold methanol. The polymer was dried overnight under high vacuum and isolated as a pink solid (**PIB**, 1.31 g, 59%). <sup>1</sup>H-NMR (CDCl<sub>3</sub>):  $\delta = 7.85$ -7.33 (aromatic protons of CTA), 4.26-4.13 (4H, ester protons of M1),

3.82 (backbone protons of EHMA), 3.43 (2H, protons adjacent to bromide).  $M_{n,NMR} = 21.8$  kDa,  $M_{n,SEC} = 28.7$  kDa,  $D = 1.05$ .

*Synthesis of diblock copolymer bearing alkyl bromide and protected alkyne functionalities (P2B):*

Macro-CTA (**P1B**, 1.2 g, 0.042 mmol), EHMA (1.58 g, 7.98 mmol), **M2** (0.083 g, 0.42 mmol), AIBN (0.92 mg, 5.6  $\mu$ mol), dioxane (6.7 mL) and a stirring bar were added into a Schlenk tube. After three freeze–pump–thaw cycles the tube was backfilled with argon, sealed, placed into an oil bath at 60 °C, and removed after 16 h. The tube was subsequently cooled with liquid nitrogen to stop the reaction. The reaction mixture was diluted with THF and subsequently precipitated three times into 200 mL cold methanol. The polymer was dried overnight under high vacuum and isolated as a pink solid (**P2B**, 2.08 g, 53%).  $^1\text{H-NMR}$  ( $\text{CDCl}_3$ ):  $\delta = 7.85\text{--}7.33$  (aromatic protons of CTA), 4.54 (2H, adjacent protons of alkyne), 4.25–4.12 (4H, ester protons of M1), 3.82 (backbone protons of EHMA), 3.43 (2H, protons adjacent to bromide), 0.16 (9H, TMS protection protons of alkyne).  $M_{n,NMR} = 43.9$  kDa,  $M_{n,SEC} = 48.9$  kDa,  $D = 1.09$ .

*Synthesis of triblock copolymer bearing alkyl bromide/protected alkyne/protected hydroxyl functionalities (P3B):*

Macro-CTA (**P2B**, 1 g, 0.021 mmol), EHMA (0.79 g, 4 mmol), **M3** (0.043 g, 0.21 mmol), AIBN (0.28 mg, 1.7  $\mu$ mol), dioxane (3.4 mL) and a stirring-bar were added into a Schlenk-tube. After three freeze–pump–thaw cycles the tube was backfilled with argon, sealed, placed in an oil bath at 60 °C and removed after 48 h. The tube was subsequently cooled with liquid nitrogen to cease the reaction. The reaction mixture was diluted with THF and subsequently precipitated three times into 200 mL cold methanol. The polymer was dried overnight under high vacuum and isolated as a white-pink solid (**P3B**, 1.6 g, 72%).  $^1\text{H-NMR}$  ( $\text{CDCl}_3$ ):  $\delta = 7.85\text{--}7.33$  (aromatic protons of CTA), 4.55 (2H, adjacent protons of alkyne), 4.25–4.12 (4H, ester protons of M1), 3.82 (backbone protons of EHMA), 3.43 (2H, protons adjacent to bromide), 0.16 (9H, TMS protection protons of alkyne), 0.13 (9H, TMS protection protons of hydroxyl).  $M_{n,NMR} = 77.7$  kDa,  $M_{n,SEC} = 74.7$  kDa,  $D = 1.13$ .

*Synthesis of triblock copolymer bearing alkyl bromide/protected alkyne/protected hydroxyl functionalities (P3A):*

**P3A** was procured in an analogous manner as **P3B** except that the degrees of polymerization for the A, B and C block were lower (see Table 1 for details). The  $^1\text{H-NMR}$  data were identical.  $M_{n,NMR} = 47.0$  kDa,  $M_{n,SEC} = 45.5$  kDa,  $D = 1.12$ .

*Removal of the dithioester group via a radical-induced process (P4A,B):*

As an example, the procedure is described for **P4B**. In a Schlenk tube equipped with a stirring bar, **P3B** (1 g, 0.013 mmol), AIBN (43.7 mg, 0.26 mmol) and lauroyl peroxide (LPO, 10.3 mg, 0.026 mmol) were dissolved in toluene (20 mL). The solution was degassed *via* three freeze–pump–thaw cycles, sealed, and heated at 80 °C. After 4 h, the reaction vessel was cooled with liquid nitrogen to stop the reaction. The solvent was removed under reduced pressure. The reaction mixture was diluted with THF and subsequently precipitated into 200 mL cold methanol (**P4B**, 0.95 g, 95%).  $^1\text{H-NMR}$  ( $\text{CDCl}_3$ ):  $\delta = 4.55$  (2H, adjacent protons of alkyne), 4.25–4.12 (4H, ester protons of M1), 3.82 (backbone protons of EHMA), 3.43 (2H, protons adjacent to bromide), 0.16 (9H, TMS protection protons of alkyne), 0.13 (9H, TMS protection protons of hydroxyl).

$M_{n,NMR} = 77.6$  kDa,  $M_{n,SEC} = 77.0$  kDa,  $D = 1.14$ . Polymer **P4A** was prepared in an identical manner from **P3A**.  $M_{n,NMR} = 46.9$  kDa,  $M_{n,SEC} = 46.0$  kDa,  $D = 1.15$ .

*Synthesis of triblock copolymer bearing HW functionality (P5B):*

**P4B** (0.9 g, 0.011 mmol), **2** (0.185 g, 0.33 mmol), potassium carbonate (0.46 g, 3.3 mmol) and DMF/THF (10 mL, v:v = 1:1) were stirred at 50 °C for 48 h. The solution was diluted with ethyl acetate and subsequently extracted twice with water. The combined organic phases were dried over Na<sub>2</sub>SO<sub>4</sub>, filtered and evaporated. The mixture was diluted with THF and subsequently precipitated twice into 100 mL cold methanol. The polymer was dried overnight under high vacuum and isolated as a yellowish solid (**P5B**, 0.75 g, 85%). <sup>1</sup>H-NMR (CDCl<sub>3</sub>):  $\delta = 8.15$ -7.71 (aromatic protons of HW), 4.55 (2H, adjacent protons of alkyne), 4.25-4.12 (4H, ester protons of M1), 3.82 (backbone protons of EHMA), 2.27 (4H, protons adjacent *t*-butyl groups of HW),  $M_{n,NMR} = 74.9$  kDa,  $M_{n,SEC} = 80.3$  kDa,  $D = 1.15$ .

*Synthesis of triblock copolymer bearing HW/BTA functionalities (P6B):*

Following by a modified procedure,<sup>34</sup> **P5B** (0.6 g, 7.45  $\mu$ mol), **3** (0.1 g, 0.15 mmol), copper (II) sulfate pentahydrate (0.1 g, 0.4 mmol) and sodium ascorbate (0.1 g, 0.5 mmol) were dissolved in DMF/THF (10 mL, v:v = 1:1). The resulting mixture was stirred at ambient temperature for 24 h and subsequently diluted with the addition of CH<sub>2</sub>Cl<sub>2</sub> and extracted with 5% EDTA solution to remove the copper (a catalyst also complexed by the recognition units). The organic phase was dried over Na<sub>2</sub>SO<sub>4</sub>, concentrated and subsequently precipitated twice into 100 mL cold methanol. The polymer was dried for 24 h under high vacuum resulting in a white powder (**P6B**, 0.45 g, 75%). <sup>1</sup>H-NMR (CDCl<sub>3</sub>):  $\delta = 8.30$  (aromatic protons of BTA), 8.15-7.71 (aromatic protons of HW), 5.10 (2H, adjacent protons of the triazole ring), 4.25-4.12 (4H, ester protons of M1), 3.82 (backbone protons of EHMA), 2.27 (4H, protons adjacent *t*-butyl groups of HW).  $M_{n,NMR} = 78.4$  kDa,  $M_{n,SEC} = 84.3$  kDa,  $D = 1.20$ .

*Synthesis of triblock copolymer bearing HW/BTA/CA functionalities (P7B):*

**P6B** (0.4 g, 4.75  $\mu$ mol), **4** (0.075 g, 0.23 mmol), DMAP (0.056 g, 0.46 mmol) were dissolved in anhydrous DCM (10 mL) in a 25 mL Schlenk-flask. A solution of DCC (0.12 g, 0.59 mmol) in anhydrous DCM (5 mL) was added at 0 °C. After one hour, the solution was warmed to ambient temperature, stirred for 2 days, filtered and concentrated under reduced pressure. The mixture was diluted with THF and subsequently precipitated three times into 200 mL cold methanol. The polymer was dried overnight under high vacuum and isolated as a white solid (**P7B**, 0.2 g, 50%). <sup>1</sup>H-NMR (CDCl<sub>3</sub>):  $\delta = 9.87$ -9.46 (interacted amide protons of HW with CA), 8.30 (aromatic protons of BTA), 8.15-7.71 (aromatic protons of HW), 5.10 (2H, adjacent protons of the triazole ring), 4.25-4.12 (4H, ester protons of M1), 3.82 (backbone protons of EHMA), 2.27 (4H, protons adjacent *t*-butyl groups of HW).  $M_{n,NMR} = 85.1$  kDa,  $M_{n,SEC} = 82.3$  kDa,  $D = 1.22$ .

*Synthesis of triblock copolymer bearing HW/BTA/CA functionalities (P7A):*

**P7A** was procured starting from **P3A** in an analogous manner as **P7B**. <sup>1</sup>H-NMR showed an identical spectrum as found for **P7B**.  $M_{n,NMR} = 51.4$  kDa,  $M_{n,SEC} = 51.2$  kDa,  $D = 1.14$ .

*Synthesis of triblock copolymer bearing BTA functionalities (P8A):*

Following a modified procedure,<sup>34</sup> **P4A** (0.3 g, 6.12  $\mu$ mol), **3** (0.05 g, 0.075 mmol), copper (II) sulfate pentahydrate (0.05 g, 0.2 mmol) and sodium ascorbate (0.05 g, 0.25 mmol) were dissolved in DMF/THF (10 mL, v:v = 1:1). The resulting mixture was stirred at ambient temperature for 24 h and subsequently diluted with the addition of CH<sub>2</sub>Cl<sub>2</sub> and extracted with 5% EDTA solution

to remove the copper (a catalyst also complexed by the recognition units). The organic phase was dried over  $\text{Na}_2\text{SO}_4$ , concentrated and subsequently precipitated twice into 100 mL cold methanol. The polymer was dried for 24 h under high vacuum resulting in a white powder (0.23 g, 75%).  $^1\text{H-NMR}$  ( $\text{CDCl}_3$ ):  $\delta = 8.30$  (aromatic protons of BTA), 5.10 (2H, adjacent protons of the triazole ring), 4.25–4.12 (4H, ester protons of M1), 3.82 (backbone protons of EHMA)  $M_{n,\text{NMR}} = 49.1$  kDa,  $M_{n,\text{SEC}} = 50.9$  kDa,  $D = 1.11$

*Synthesis of triblock copolymer bearing HW and CA functionalities (P9A):*

**P4A** (0.3 g, 6.12  $\mu\text{mol}$ ), **2** (0.093 g, 0.17 mmol), potassium carbonate (0.28 g, 2 mmol) and DMF/THF (10 mL, v:v = 1:1) were stirred at 50 °C for 48 h. The solution was diluted with ethyl acetate and subsequently extracted twice with water. The combined organic phases were dried over  $\text{Na}_2\text{SO}_4$ , filtered and evaporated. The mixture was diluted with THF and subsequently precipitated twice into 100 mL cold methanol. The polymer was dried overnight under high vacuum and isolated as a yellowish solid (**P5A**, 0.25 g, 85%). **P5A** (0.2 g, 4.1  $\mu\text{mol}$ ), **4** (0.065 g, 0.21 mmol), DMAP (0.026 g, 0.22 mmol) were dissolved in anhydrous DCM (10 mL) in a 25 mL Schlenk-flask. A solution of DCC (0.12 g, 0.59 mmol) in anhydrous DCM (5 mL) was added at 0 °C. After one hour, the solution was warmed to ambient temperature, stirred for 2 days, filtered and concentrated under reduced pressure. The mixture was diluted with THF and subsequently precipitated three times into 200 mL cold methanol. The polymer was dried overnight under high vacuum and isolated as a white solid (**P9A**, 0.2 g, 50%).  $^1\text{H-NMR}$  ( $\text{CDCl}_3$ ):  $\delta = 12.78$  (interacted amide protons of CA with HW), 9.89–9.48 (interacted amide protons of HW with CA), 8.15–7.71 (aromatic protons of HW), 4.25–4.12 (4H, ester protons of M1), 3.82 (backbone protons of EHMA), 2.27 (4H, protons adjacent *t*-butyl groups of HW).  $M_{n,\text{NMR}} = 50.3$  kDa,  $M_{n,\text{SEC}} = 50.0$  kDa,  $D = 1.12$ .

### 3.6 References

- (1) C. B. Anfinsen *Science* **1973**, *181*, 223.
- (2) C. M. Dobson *Nature* **2003**, *426*, 884.
- (3) C. T. J. Branden *Introduction to Protein Structure*, Garland Publishing, New York, **1998**.
- (4) O. Altintas, C. Barner-Kowollik *Macromol. Rapid Commun.* **2012**, *33*, 958.
- (5) M. Ouchi, N. Badi, J.-F. Lutz, M. Sawamoto *Nat. Chem.* **2011**, *3*, 917.
- (6) J.-F. Lutz, M. Ouchi, D. R. Liu, M. Sawamoto *Science* **2013**, *341*, 1238149.
- (7) C. K. Lyon, A. Prasher, A. M. Hanlon, B. T. Tuten, C. A. Tooley, P. G. Frank, E. B. Berda *Polym. Chem.* **2015**, *6*, 181.
- (8) M. Gonzalez-Burgos, A. Latorre-Sanchez, J. A. Pomposo *Chem. Soc. Rev.* **2015**, *44*, 6122.
- (9) O. Altintas, C. Barner-Kowollik *Macromol. Rapid Commun.* **2016**, *37*, 29.
- (10) M. Elsbahy, K. L. Wooley *Chem. Soc. Rev.* **2012**, *41*, 2545.
- (11) M. Artar, E. Huerta, E. W. Meijer, A. R. A. Palmans, in *Sequence-Controlled Polymers: Synthesis, Self-Assembly, and Properties* (Eds.: J.-F. Lutz, T. Y. Meyer, M. Ouchi, M. Sawamoto), American Chemical Society, Washington, DC, **2014**, *1170*, 313.
- (12) J. P. Rao, K. E. Geckeler *Prog. Polym. Sci.* **2011**, *36*, 887.
- (13) A. Sanchez-Sanchez, I. Pérez-Baena, J. A. Pomposo *Molecules* **2013**, *18*, 3339.
- (14) I. Perez-Baena, I. Asenjo-Sanz, A. Arbe, A. J. Moreno, F. Lo Verso, J. Colmenero, J. A. Pomposo *Macromolecules* **2014**.
- (15) C. F. Hansell, A. Lu, J. P. Patterson, R. K. O'Reilly *Nanoscale* **2014**, *6*, 4102.
- (16) J. Willenbacher, K. N. R. Wuest, J. O. Mueller, M. Kaupp, H.-A. Wagenknecht, C. Barner-Kowollik *ACS Macro Lett.* **2014**, *3*, 574.

- (17) J. Willenbacher, O. Altintas, P. W. Roesky, C. Barner-Kowollik *Macromol. Rapid Commun.* **2014**, *35*, 45.
- (18) O. Shishkan, M. Zamfir, M. A. Gauthier, H. G. Borner, J.-F. Lutz *Chem. Commun.* **2014**, *50*, 1570.
- (19) A. Sanchez-Sanchez, A. Arbe, J. Colmenero, J. A. Pomposo *ACS Macro Lett.* **2014**, *3*, 439.
- (20) P. G. Frank, B. T. Tuten, A. Prasher, D. Chao, E. B. Berda *Macromol. Rapid Commun.* **2014**, *35*, 249.
- (21) A. Sanchez-Sanchez, D. A. Fulton, J. A. Pomposo *Chem. Commun.* **2014**, *50*, 1871.
- (22) D. E. Whitaker, C. S. Mahon, D. A. Fulton *Angew. Chem., Int. Ed.* **2013**, *52*, 956.
- (23) B. T. Tuten, D. Chao, C. K. Lyon, E. B. Berda *Polym. Chem.* **2012**, *3*, 3068.
- (24) B. S. Murray, D. A. Fulton *Macromolecules* **2011**, *44*, 7242.
- (25) J. Lu, N. ten Brummelhuis, M. Weck *Chem. Commun.* **2014**, *50*, 6225.
- (26) J. Willenbacher, B. V. K. J. Schmidt, D. Schulze-Suenninghausen, O. Altintas, B. Luy, G. Delaittre, C. Barner-Kowollik *Chem. Commun.* **2014**, *50*, 7056.
- (27) P. J. M. Stals, M. A. J. Gillissen, R. Nicolay, A. R. A. Palmans, E. W. Meijer *Polym. Chem.* **2013**, *4*, 2584.
- (28) M. Artar, T. Terashima, M. Sawamoto, E. W. Meijer, A. R. A. Palmans *J. Polym. Sci., Part A: Polym. Chem.* **2014**, *52*, 12.
- (29) M. Artar, E. R. J. Souren, T. Terashima, E. W. Meijer, A. R. A. Palmans *ACS Macro Lett.*, **2015**, *4*, 1099.
- (30) Y. Liu, T. Pauloehrl, S. I. Presolski, L. Albertazzi, A. R. A. Palmans, E. W. Meijer *J. Am. Chem. Soc.* **2015**, *137*, 13096.
- (31) G. ter Huurne, M. A. J. Gillissen, A. R. A. Palmans, I. K. Voets, E. W. Meijer *Macromolecules* **2015**, *48*, 3949.
- (32) F. Lo Verso, J. A. Pomposo, J. Colmenero, A. J. Moreno *Soft Matter* **2014**, *10*, 4813.
- (33) A. J. Moreno, F. Lo Verso, A. Sanchez-Sanchez, A. Arbe, J. Colmenero, J. A. Pomposo *Macromolecules* **2013**, *46*, 9748.
- (34) N. Hosono, M. A. J. Gillissen, Y. Li, S. S. Sheiko, A. R. A. Palmans, E. W. Meijer *J. Am. Chem. Soc.* **2013**, *135*, 501.
- (35) N. Hosono, A. R. A. Palmans, E. W. Meijer *Chem. Commun.* **2014**, *50*, 7990.
- (36) N. Hosono, P. J. M. Stals, A. R. A. Palmans, E. W. Meijer *Chem. Asian J.* **2014**, *9*, 1099.
- (37) E. B. Berda, E. J. Foster, E. W. Meijer *Macromolecules* **2010**, *43*, 1430.
- (38) E. J. Foster, E. B. Berda, E. W. Meijer *J. Am. Chem. Soc.* **2009**, *131*, 6964.
- (39) T. Mes, R. van der Weegen, A. R. A. Palmans, E. W. Meijer *Angew. Chem., Int. Ed.* **2011**, *50*, 5085.
- (40) T. Terashima, T. Mes, T. F. A. de Greef, M. A. J. Gillissen, P. Besenius, A. R. A. Palmans, E. W. Meijer *J. Am. Chem. Soc.* **2011**, *133*, 4742.
- (41) O. Altintas, P. Gerstel, N. Dingenouts, C. Barner-Kowollik *Chem. Commun.* **2010**, *46*, 6291.
- (42) O. Altintas, E. Lejeune, P. Gerstel, C. Barner-Kowollik *Polym. Chem.* **2012**, *3*, 640.
- (43) O. Altintas, P. Krolla-Sidenstein, H. Gliemann, C. Barner-Kowollik *Macromolecules* **2014**, *47*, 5877.
- (44) J. Romulus, M. Weck *Macromol. Rapid Commun.* **2013**, *34*, 1518.
- (45) J. A. Pomposo, I. Perez-Baena, F. Lo Verso, A. J. Moreno, A. Arbe, J. Colmenero *ACS Macro Lett.* **2014**, *3*, 767.
- (46) V. Ladmiral, G. Mantovani, G. J. Clarkson, S. Cauet, J. L. Irwin, D. M. Haddleton *J. Am. Chem. Soc.* **2006**, *128*, 4823.
- (47) O. Altintas, T. Muller, E. Lejeune, O. Plietzsch, S. Bräse, C. Barner-Kowollik *Macromol. Rapid Commun.* **2012**, *33*, 977.

- (48) H. G. Börner, D. Duran, K. Matyjaszewski, M. da Silva, S. S. Sheiko *Macromolecules* **2002**, *35*, 3387.
- (49) H.-i. Lee, K. Matyjaszewski, S. Yu, S. S. Sheiko *Macromolecules* **2005**, *38*, 8264.
- (50) M. Chen, G. Moad, E. Rizzardo *J. Polym. Sci., Part A: Polym. Chem.* **2009**, *47*, 6704.
- (51) K. Khanna, S. Varshney, A. Kakkar *Macromolecules* **2010**, *43*, 5688.
- (52) P. J. M. Stals, C.-Y. Cheng, L. van Beek, A. C. Wauters, A. R. A. Palmans, S. Han, E. W. Meijer *Chemical Science* **2016**, *7*, 2011.
- (53) H. Ito, K. Arimoto, H.-o Sensul, A. Hosomi *Tetrahedron Lett.* **1997**, *38*, 3977.
- (54) O. Altintas, T. Rudolph, C. Barner-Kowollik *J. Polym. Sci., Part A: Polym. Chem.* **2011**, *49*, 2566.
- (55) O. Altintas, D. Schulze-Suenninghausen, B. Luy, C. Barner-Kowollik *ACS Macro Lett.* **2013**, *2*, 211.
- (56) O. Altintas, D. Schulze-Suenninghausen, B. Luy, C. Barner-Kowollik *Eur. Polym. J.* **2015**, *62*, 409.
- (57) O. Altintas, U. Tunca, C. Barner-Kowollik *Polym. Chem.* **2011**, *2*, 1146.
- (58) M. A. J. Gillissen, T. Terashima, E. W. Meijer, A. R. A. Palmans, I. K. Voets *Macromolecules* **2013**, *46*, 4120.
- (59) P. J. M. Stals, M. A. J. Gillissen, T. F. E. Paffen, T. F. A. de Greef, P. Lindner, E. W. Meijer, A. R. A. Palmans, I. K. Voets *Macromolecules* **2014**, *47*, 2947.
- (60) T. Mes, PhD Thesis, Eindhoven University of Technology, Eindhoven, The Netherlands, **2011**.
- (61) O. Altintas, M. Artar, G. ter Huurne, I. K. Voets, A. R. A. Palmans, C. Barner-Kowollik, E. W. Meijer *Macromolecules*. **2015**, *48*, 8921.





# Chapter 4

## *Exploring orthogonal self-assembly of amphiphilic triblock polymers*

**Abstract:** Here, we report the synthesis and characterization of ABA type, amphiphilic triblock copolymers decorated with 1,3,5-benzene tricarboxamide (BTA) and photoprotected 2-ureido-4[1H]-pyrimidinone (phUPy) self-assembly motifs in the B and A blocks, respectively, with the aim to create complex, stimuli-responsive, compartmentalized structures in aqueous media. Precursor ABA type triblock copolymers were prepared via copper catalyzed atom transfer radical polymerization (ATRP). The obtained triblock copolymers were subsequently functionalized in a two-step post-functionalization approach with BTAs and phUPys and fully characterized using <sup>1</sup>H-NMR and SEC. As a reference, a random, amphiphilic copolymer comprising phUPy groups was prepared. <sup>1</sup>H-NMR studies in CDCl<sub>3</sub> showed that the UPy groups are capable of dimerization when attached to an amphiphilic polymer backbone. In addition, BTA helical stacking was operative in these systems in water and independent of the presence of phUPy and UPy groups. However, it remained unclear whether the UPy groups are capable of dimerization in water. Nile Red experiments revealed that all amphiphilic polymers form compartmentalized structures with a hydrophobic interior in water and fully functionalized UPy-BTA-UPy triblock copolymer appeared to form particles with the most hydrophobic environment. Finally, dynamic light scattering (DLS) revealed that the functionalized triblock copolymers form multichain aggregates in water, but also that deprotection of the UPy moieties results in a reduction of the hydrodynamic radius.

#### 4.1 Introduction

Synthetic, water-soluble functional polymers are used in a wide range of industrial applications, including coatings, inks, papers, adhesives, cosmetics and personal care products.<sup>1</sup> Recently, the control of the composition, length, and sequence of polymer chains has received a great deal of attention, resulting in well-defined and tailor-made derivatives that are applicable in homogenous catalysis,<sup>2</sup> sensing,<sup>3,4</sup> various biomedical applications,<sup>5,6,7</sup> and thermoresponsive materials.<sup>8-15</sup> Among water-soluble polymers, amphiphilic derivatives attract particular interest due to their hydrophilic/hydrophobic composition that acts as a carrier system to bring hydrophobic moieties in water while providing the solubility with the hydrophilic parts.<sup>13</sup>

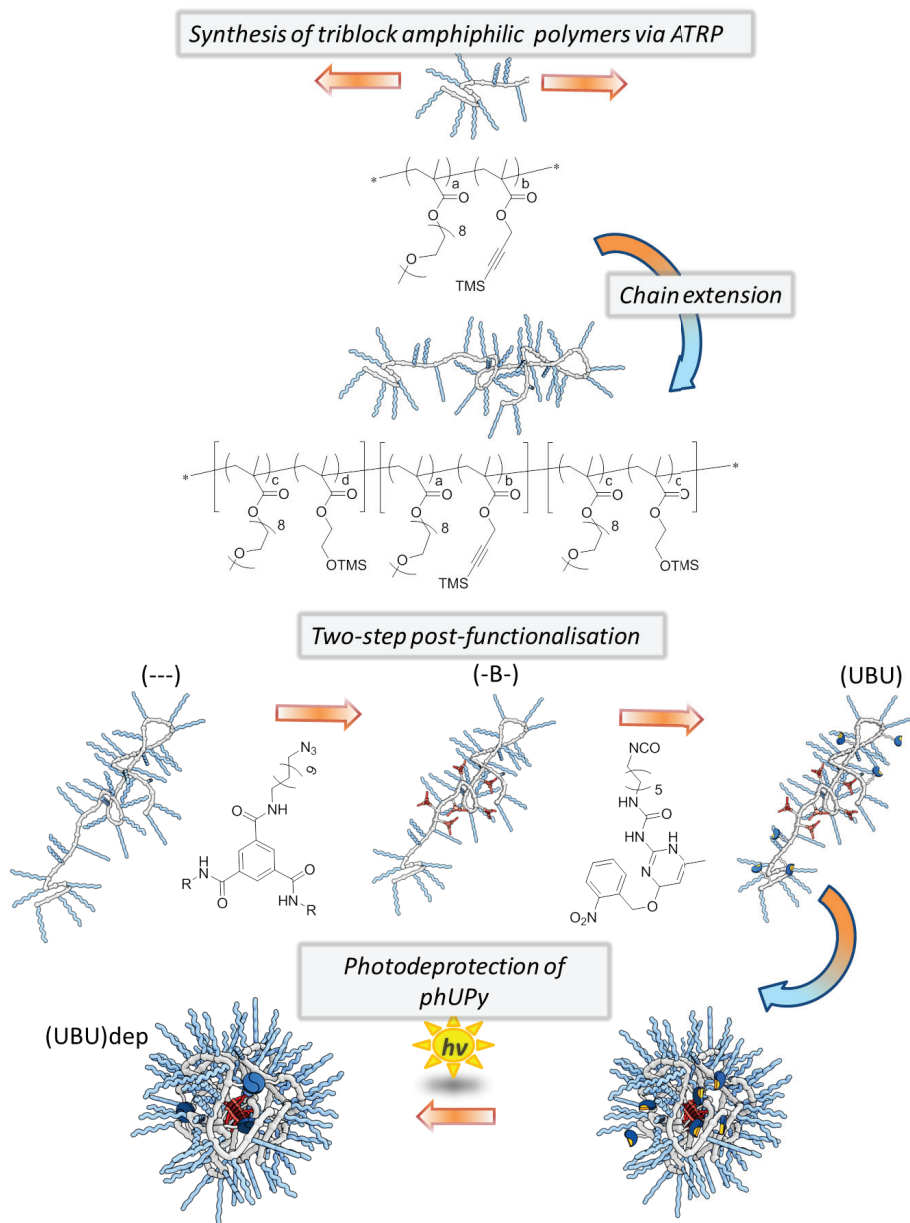
First described by Staudinger in 1929,<sup>14</sup> poly(ethylene glycol) (PEG) derivatives are nowadays widely used as building blocks for water soluble polymeric systems owing to the availability of polymerizable PEG macromonomers,<sup>10,15,16</sup> biocompatibility<sup>17,18</sup> and interesting thermoresponsive features of PEG derivatives.<sup>19,20</sup> However, polymerization of PEG and derivatives, presents several challenges such as (i) the low solubility of the ethylene glycol units in some organic solvents at mild temperatures,<sup>21</sup> and (ii) side reactions due to the interactions of the PEG units with other polar species, which limits the use of anionic polymerization techniques.<sup>22,23</sup> Therefore, atom transfer radical polymerization (ATRP), single electron transfer living radical polymerization (SET LRP) and reversible addition fragmentation transfer (RAFT) have been the most widely applied techniques, owing to their applicability on a wide library of monomers, including water soluble ones.<sup>13</sup>

In an elegant example, Percec *et al.* performed the polymerization of PEG methacrylate with a narrow molecular weight distribution in water/MeOH mixtures in the presence of air, by employing the SET-LRP technique, thereby demonstrating the tolerance of living radical polymerization techniques towards challenging monomers and conditions.<sup>24</sup> Haddleton and coworkers showed the preparation of water soluble acrylate based multiblock copolymers in water *via* iterative chain extension with narrow molecular weight distribution, by light induced SET-LRP.<sup>25</sup> Perrier and coworkers applied a RAFT polymerization at room temperature for the preparation of amphiphilic multiblock copolymers.<sup>26</sup> Sawamoto and coworkers applied Ru-mediated ATRP to prepare methacrylate based amphiphilic random<sup>27</sup> and gradient copolymers.<sup>28</sup> Lutz and coworkers,<sup>29</sup> Neoh and coworkers<sup>30</sup> and Zhao and coworkers<sup>31</sup> reported the preparation of amphiphilic brush polymers *via* RAFT in combination with ATRP. Even more complex amphiphilic polymeric structures, i.e. covalent amphiphilic polymer networks, were achieved *via* RAFT by using PEG based chain transfer agents.<sup>32</sup> Interestingly, most examples focus on polymers with low degrees of polymerization, and block copolymers consist of homopolymer blocks.

In addition, as discussed in the previous chapters, the controlled folding of synthetic polymers, often prepared by the polymerization techniques mentioned above, *via* the self-assembly of pendant structuring motifs has emerged as an important topic of interest since it is a process reminiscent of protein folding.<sup>33</sup> In contrast to the growing number of polymeric systems that are folded by one structuring interaction, only a few elegant examples demonstrated dynamic folding of synthetic polymers by multiple, orthogonal structuring interaction. The orthogonal action of multiple non-covalent interactions has been used to create novel materials, *i.e.* supramolecular block copolymers,<sup>34-41</sup> cross-linked nanorods,<sup>42</sup> cross-linked polymers<sup>43</sup>

dendrimers,<sup>44</sup> nanostructured materials<sup>45,46</sup> and self-assembled fibrillar networks with encapsulated micelles.<sup>47,48</sup> As a transition from molecular to polymer-pendant self-assembly, Weck *et al* showed the orthogonal self-assembly of Hamilton wedge (HW) and diaminopyridines with polymer pendant thymine and cyanuric acid (CA) units, respectively, in organic media.<sup>49</sup> A first attempt to introduce orthogonal self-assembly within a single polymer chain was made by Barner-Kowollik *et al.* by insertion of orthogonally acting pairs of CA-HW and thymine (Thy)-diaminopyridine (DAP) on a styrene/acrylate based diblock copolymer.<sup>50</sup> Recently, Hosono *et al* combined block copolymer formation with orthogonal self-assembly to prepare folded structures in organic media. ABA-type triblock copolymers of different lengths were prepared *via* copper mediated ATRP and a two-step post-functionalization of these polymers gave triblock copolymers decorated with BTA units in the B and with *o*-nitrobenzyl protected 2-ureido-4[1H]-pyrimidinone (phUPy) moieties in the A segments.<sup>51-52</sup> Apart from the use of BTAs and UPys, a hairpin-like structure by orthogonal action of BTA stacking in the middle segment and HW-CA dimerization on two separate outer segments of an ABC type triblock copolymer was investigated in Chapter 3.

While the examples above demonstrate the successful orthogonal self-assembly of supramolecular motifs in complex block copolymer structures in organic media, exploring their potential in biological environments requires compatibilization of the dynamic, orthogonal folding of synthetic polymers with water. In addition, water as a medium presents additional challenges to the formation of supramolecular complexes based on hydrogen bonds. Whereas it was previously shown that BTA helical self-assembly is operative in water if a sufficiently hydrophobic pocket is formed<sup>53-59</sup> the dimerization of UPy groups in water is less well explored although preliminary results suggest that UPy dimerization in water is feasible in micelles<sup>60</sup> and UPy functionalized polymers.<sup>61</sup> In this chapter we show i) the synthesis and characterization of ABA type amphiphilic triblock copolymers **P1**(---) ( $DP = 265$ ) and **P2**(---) ( $DP = 533$ ), ii) decorate the high  $DP$  polymer **P2** (---) with UPys and BTAs in the A and B blocks, respectively (Scheme 1) and iii) study the self-assembly of **P2**(UBU). As a reference, random block copolymers **P3**(-) ( $DP = 405$ ) and **P4**(-) ( $DP = 100$ ) were prepared and functionalized with only UPy moieties (see Scheme 4.1 for explanation of the abbreviations).

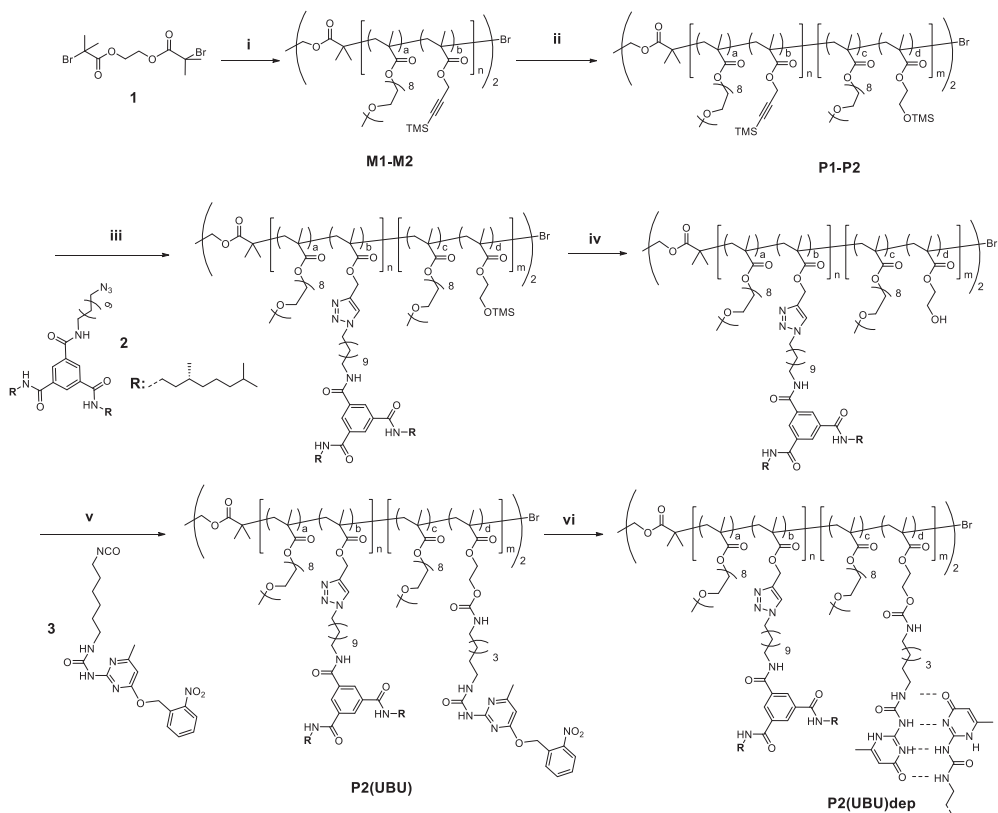


**Scheme 4.1** Approach for the preparation of amphiphilic polymers that are introduced in this Chapter. Unfunctionalized polymers are shown as (---) for triblock copolymers and (-) used for the random copolymers; for BTA functionalization (-B-) and for UPy functionalization (U-U) or (U) is used. For photo-deprotected polymers (UBU)dep and (U)dep notations are used for clarity.

#### 4.2 Design of amphiphilic triblock (UBU) and random (U) copolymers

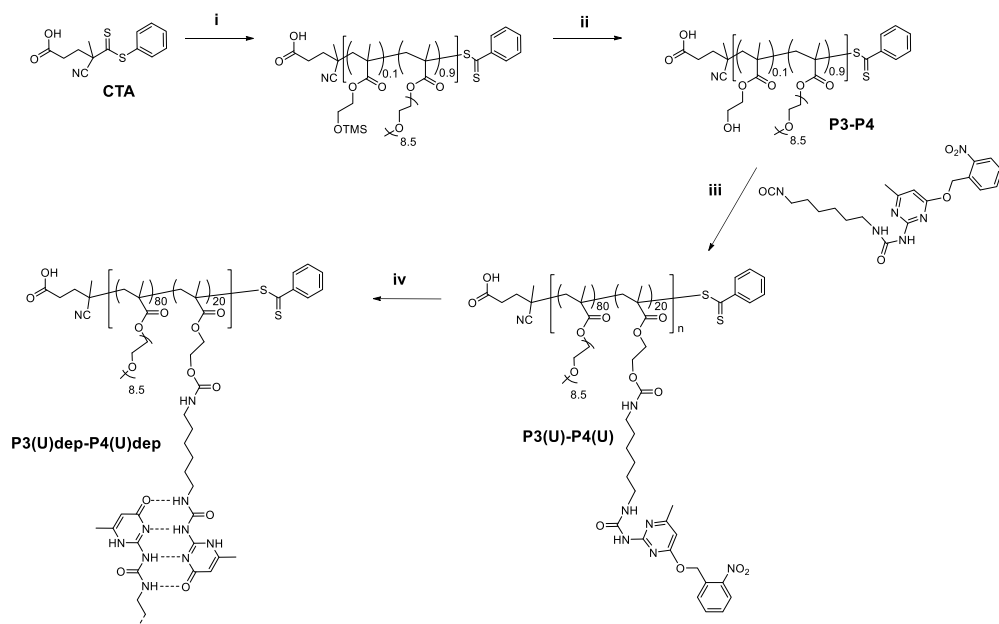
The synthesis of the highly functionalized, water-soluble polymers containing oligomeric ethyleneglycol pendants, shown in Scheme 4.1, *via* controlled radical polymerizations is not trivial, since functional units (i.e. ligands, organocatalysts, charged units, radicals and etc.) can potentially hamper the controlled radical polymerization process. Undesired side reactions and limited solubility of the monomers at high concentration typically results in poorly defined products and broad molecular weight distributions of the prepared polymers.<sup>70</sup> Especially in block copolymer synthesis, it is crucial to have a well-controlled polymerization process to preserve the active chain ends for the sequential chain extensions. Among the three well-known controlled living radical polymerization techniques i.e. nitroxide mediated polymerization (NMP), reversible addition-fragmentation technique (RAFT) and atom-transfer radical-polymerization (ATRP), NMP usually requires high polymerization temperatures, long reaction times and has a limited monomer selection with initiators that are not easily accessible.<sup>62</sup> In contrast, RAFT permits to use a larger monomer library, however, the presence of radical initiator sources in the process makes it less favorable for chain extensions, due to homo polymer formation *via* free radical polymerization route as a side reaction.<sup>63</sup> Methacrylates are known to be very efficiently polymerized by ATRP, and during the chain extension process, side reactions can be minimized, owing to a process in which metal mediated halogen group transfer of the macroinitiator itself enables preparation of high molecular weight block copolymers.<sup>64-65</sup>

As a result, we selected Cu(I)-catalyzed ATRP to access ABA type, methacrylate-based amphiphilic triblock copolymers (Scheme 4.2). Oligo(ethylene glycol) methyl ether methacrylate (oEGMA) was selected as a comonomer and applied as 85% of the total monomer composition to ensure solubility in water, and 15 % of all segments were reserved for post-functionalizable units. These consisted of monomers with silyl-protected alkynes (TMS-PMA) or alcohols (TMS-HEMA), known to be compatible with controlled radical polymerization techniques.<sup>66</sup> The silyl protection group was selected for both units because silyl protected alcohols are deprotected under mild conditions, and silyl protected alkynes can be directly functionalized with azides *via* a copper-catalyzed Huisgen 1,3-dipolar cycloaddition reaction.<sup>57,67,68</sup> After preparation of the precursor triblock copolymers **P1**(---) and **P2**(---), a two-step post-functionalization was applied. First, a copper-mediated Huisgen 1,3-dipolar cycloaddition reaction with azide-substituted BTA (**2**) was performed directly on the silyl-protected alkynes. Next, after deprotection of the silyl-protected alcohols, the polymer pendant alcohols were reacted with *o*-nitrobenzyl protected UPy isocyanate (**3**).<sup>51,55,69</sup> The *o*-nitrobenzyl unit was applied as a protection unit for the UPy synthon to improve its solubility and, most importantly, to enable control of the dimerization process by UV-light as the external trigger.



**Scheme 4.2** Preparation of **P1(---)** and **P2(UBU)dep**. Reagents and conditions: (i) *o*EGMA, TMS-PMA, Cu(I)Br, PMDETA, toluene, 50 °C; (ii) *o*EGMA, TMS-HEMA, Cu(I)Br, PMDETA, toluene, 60 °C; (iii) **2**, Cu(II)SO<sub>4</sub>, 2-propylamine, DMSO/water (1/1); (iv) TFA, DCM, RT; (v) **3**, DBTDL, THF, 50 °C; (vi) *hν* (350 nm), 4 h.

To investigate if UPy-pendant polymers are capable of folding in water as a result of UPy dimerization, we prepared and characterized *o*EGMA-UPy random copolymers. In this case, a RAFT polymerization was selected for the copolymerization of *o*EGMA and TMS-HEMA (Scheme 4.3). After deprotection of the silyl-protecting units, the polymer pendant alcohols were reacted with *o*-nitrobenzyl protected UPy isocyanate (**3**). **P3(U)** serves as a reference polymer of **P2(UBU)** in terms of length to study the effect of UPy unit segmentation in folding, while **P4(U)** is a shorter *o*EGMA-UPy random copolymer to study the effect of length on the folding of UPy functionalized polymers.



**Scheme 4.3** Preparation of **P3(U)dep** and **P4(U)dep**. Reagents and conditions: (i) *o*EGMA, TMS-HEMA, AIBN, dioxane, 70 °C; (ii) TFA, CH<sub>2</sub>Cl<sub>2</sub>; (iii) **3**, DBTDL, THF, 50 °C; (vi) hv (350 nm), 4 h.

### 4.3 Synthesis and post-functionalization of amphiphilic block copolymers

The synthetic strategy of low (**P1**(---),  $DP = 265$ ) and high (**P2**(---),  $DP = 533$ ) molecular weight amphiphilic ABA type triblock copolymers using Cu(I)-catalyzed ATRP, is depicted in Scheme 4.2. We used difunctional dibromide **1** as an initiator in the radical polymerization process and *N,N,N',N',N''*-pentamethyldiethylenetriamine (PMDETA) as the ligand at 50 °C in toluene. A ratio of 1:1:1 ([CuBr]<sub>0</sub>:[initiator]<sub>0</sub>:[PMDETA]<sub>0</sub>) was applied for **M1** and **M2**. The middle A block copolymers (**M1**,  $DP = 60$ ; **M2**,  $DP = 120$ ) were obtained by copolymerization of TMS-protected propargyl methacrylate (TMS-PMA) and *o*EGMA with a TMS-PMA ratio of 17% for **M1** and 20% for **M2**. The macro-initiators obtained showed an  $M_n$  around 7 kDa, with a  $D$  of 1.12 for **M1** and an  $M_n$  around 29 kDa, with a  $D$  of 1.35 for **M2**.

In the next step, the two B blocks were grown from the halogen-capped ends of the macroinitiators **M1** and **M2** in the presence of PMDETA as ligand at 50 °C in toluene. The polymerization conditions previously used for **M1** and **M2** (1:1:1 ([CuBr]<sub>0</sub>:[macroinitiator]<sub>0</sub>:[PMDETA]<sub>0</sub>)) were inefficient for the chain extensions. For the chain extension of **M1**, the presence of remaining macroinitiator peak in SEC trace confirmed the poor initiation (Figure 4.1a). An attempt to achieve a more efficient initiation by increasing the polymerization temperature to 70 °C resulted in a poorly controlled process, as confirmed by the formation of both high and low molecular weight species in SEC trace shown for the extension of **M1** (Figure 4.1b).

However, efficient chain extension of **M1** was achieved by increasing the ligand concentration two fold to 1:1:2 ([CuBr]<sub>0</sub>:[macroinitiator]<sub>0</sub>:[PMDETA]<sub>0</sub>) (Figure 4.1c). For the



chain extension of **M2**, the catalyst concentration was increased two-fold and ligand concentration was increased four-fold, to 2:1:4, since a much longer chain extension was targeted. The triblock copolymers (**P1**(---),  $DP = 265$ ; **P2**(---),  $DP = 533$ ) were obtained by copolymerization of TMS-protected hydroxyethyl methacrylate (TMS-HEMA) and *o*EGMA with a TMS-HEMA ratio of 13% for **P1**(---) and 12% for **P2**(---). The obtained triblock prepolymers showed an  $M_n$  around 11 kDa, with a  $D$  of 1.08 for **P1**(---) and an  $M_n$  around 56 kDa, with a  $D$  of 1.45 for **P2**(---).

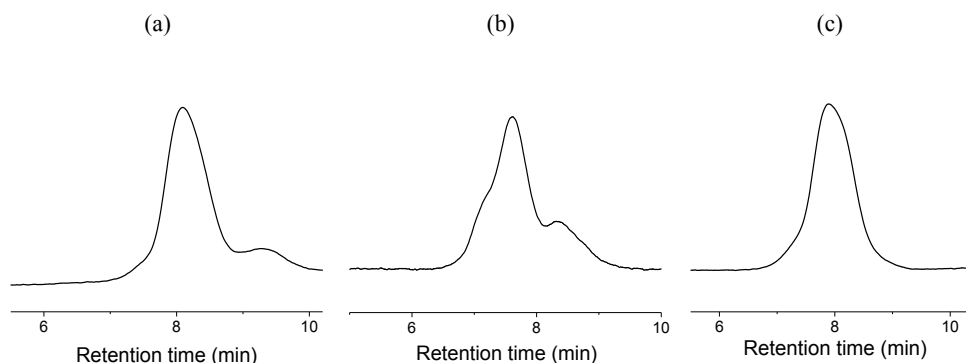


**Figure 4.1** SEC traces (DMF+LiBr) for chain extension trials of the preparation of **P1**. (a) 1:1:1 ([CuBr]<sub>0</sub>:[initiator]<sub>0</sub>:[PMDETA]<sub>0</sub>) at 60 °C, (b) 1:1:1 ([CuBr]<sub>0</sub>:[initiator]<sub>0</sub>:[PMDETA]<sub>0</sub>) conditions at 70 °C, (c) 1:1:2 ([CuBr]<sub>0</sub>:[initiator]<sub>0</sub>:[PMDETA]<sub>0</sub>) conditions at 60 °C.

Macroinitiators **M1**, **M2** and prepolymers **P1**(---) and **P2**(---) were characterized by <sup>1</sup>H-NMR and SEC (DMF+LiBr) (Figure 4.2, Figure 4.3). In all cases, we observed polymer compositions matching those of the feed ratios. The results are summarized in Table 4.1. As an example, the <sup>1</sup>H-NMR spectra of **M2**, **P2**(---), **P2**(-B-) and **P2**(UBU) are shown in Figure 4.2. The spectrum depicted in Figure 4.2A shows the presence of the *o*EGMA units, with characteristic peaks of the closest methylene to the ester bonds -O-CH<sub>2</sub>- (peak labeled as h<sub>1</sub>) and methyl units -O-CH<sub>3</sub> (peak labeled as j), TMS-PMA units with characteristic peaks of the methylene units -CH<sub>2</sub>-C≡C- (peak labeled as v) and TMS methyl units -Si-(CH<sub>3</sub>)<sub>3</sub> (peak labeled as t). Figure 4.2B depicts the triblock polymer after chain extension, and shows the presence of *o*EGMA and TMS-HEMA peaks of the closest methylene to the ester bonds -O-CH<sub>2</sub>- (peak labeled as h<sub>2</sub> for *o*EGMA, and peak labeled as s for TMS-HEMA) and a singlet at 0.19 ppm appeared which is assigned to the TMS methyl units O-Si-(CH<sub>3</sub>)<sub>3</sub> (peak labeled as u).

**Table 4.1** Conditions and results for the triblock copolymer preparation via ATRP.

	A block		A block		B block		B block		$M_{n, NMR}$ kDa <sup>l</sup>	$M_{n, SEC}$ kDa <sup>g</sup>	$\bar{D}^g$
	<i>N</i>	<i>N</i>	<i>n</i>	<i>n</i>	<i>N</i>	<i>N</i>	<i>n</i>	<i>n</i>			
	<i>o</i> EGMA <sup>c</sup>	TMS-PMA <sup>d</sup>	<i>o</i> EGMA <sup>h</sup>	TMS-PMA <sup>i</sup>	<i>o</i> EGMA <sup>e</sup>	TMS-HEMA <sup>f</sup>	<i>o</i> EGMA <sup>j</sup>	TMS-HEMA <sup>k</sup>			
<b>M1</b> <sup>a</sup>	127	23	50	10	-	-	-	-	26.7	7.5	1.12
<b>M2</b> <sup>a</sup>	160	40	96	24	-	-	-	-	52.4	29.3	1.35
<b>P1</b> (---) <sup>b</sup>	-	-	-	-	426	75	178	27	118.7	11.1	1.08
<b>P2</b> (---) <sup>b</sup>	-	-	-	-	501	89	365	48	239.6	56.7	1.45

<sup>a</sup> ATRP polymerization:  $[CuBr]_0:[I]_0:[PMDETA]_0 = 1:1:1$  (**M1/M2**), where **I** is the initiator. ( $[M_{tot}]$ :  $[oEGMA]_0 + [PMA]_0$ ) (**M1-M2**) in toluene at 50 °C.

<sup>b</sup>  $[CuBr]_0:[I]_0:[PMDETA]_0 = 1:1:2$  (**P1**),  $[CuBr]_0:[I]_0:[PMDETA]_0 = 2:1:4$  (**P2**) where **I** is the initiator.  $[CuBr]_0:[I]_0:[PMDETA]_0 = 2:1:4$  (**P2**), where **I** is the initiator. ( $[M_{tot}]$ :  $[oEGMA]_0 + [HEMA]_0$ ) (**P1-P2**) in toluene at 60 °C.

<sup>c</sup>  $N_{oEGMA} = [oEGMA]_0/[I]_0$ . <sup>d</sup>  $N_{PMA} = [PMA]_0/[I]_0$ . <sup>e</sup>  $N_{oEGMA} = [oEGMA]_0/[I]_0$ . <sup>f</sup>  $N_{HEMA} = [HEMA]_0/[I]_0$ .

<sup>g</sup> Analyzed by SEC in DMF (10 mM LiBr) with PEO standard;  $\bar{D} = M_w/M_n$ .

<sup>h</sup>  $n_{oEGMA} = [oEGMA]_0 \times Conv./[I]_0$ . <sup>i</sup>  $n_{PMA} = [PMA]_0 \times Conv./[I]_0$ . <sup>j</sup>  $n_{oEGMA} = [oEGMA]_0 \times Conv./[I]_0$ .

<sup>k</sup>  $n_{HEMA} = [HEMA]_0 \times Conv./[I]_0$ . Conversion is determined by <sup>1</sup>H-NMR in CDCl<sub>3</sub>.

<sup>l</sup>  $M_n, calcd = F_w, oEGMA \times n_{oEGMA} + F_w, I + F_w, PMA \times n_{PMA} + F_w, oEGMA \times n_{oEGMA} + F_w, HEMA \times n_{HEMA}$ .

The degree of polymerization for **M1-M2** was determined by comparing the integrals of the residual monomer peaks (5-5.5 ppm) of the fed *o*EGMA and TMS-PMA with the polymer peak assigned as *h*<sub>1</sub> and *v* of the crude polymerization mixture. Incorporation ratios of the monomers were calculated by comparing the intensity of the peak labeled as *h*<sub>1</sub> and *v* as follows: TMS-PMA% = 100 × [*I*<sub>v</sub>/(*I*<sub>v</sub>+*I*<sub>h1</sub>)] and *o*EGMA<sub>1</sub>% = 100 × [*I*<sub>h1</sub>/(*I*<sub>h1</sub>+*I*<sub>v</sub>)] (see Figure 4.2A for assignments).

For triblocks **P1(---)** and **P2(---)**, the degree of polymerization was determined based on the conversion of fed *o*EGMA and TMS-HEMA by using residual monomer peaks. Here, assignment of **P2(---)** is explained as an example. The intensity of the peak assigned as *s*, *I*<sub>s</sub>, was determined by using the intensity of the methyl peak of TMS-HEMA (Si-(CH<sub>3</sub>)<sub>3</sub>), assigned as *u*, as follows: *I*<sub>s</sub> = 2 × (*I*<sub>u</sub>/9). Since (-O-CH<sub>2</sub>-) peaks for both *o*EGMA (peak labeled as *h*<sub>2</sub>) and TMS-HEMA (peak labeled as *s*) are at the same position with *o*EGMA (peak labeled as *h*<sub>1</sub>) on macroinitiator **M2**; the intensity of *o*EGMA (-O-CH<sub>2</sub>-) peaks of macroinitiator (*h*<sub>1</sub>) and methylene peaks of TMS-HEMA (-O-CH<sub>2</sub>-) peaks (*s*) were subtracted from the peak labeled as (*I*<sub>h2</sub>+*I*<sub>h1</sub>+*I*<sub>s</sub>) to calculate the intensity of the peak *h*<sub>2</sub>. Finally, the incorporation ratios of the *o*EGMA<sub>2</sub> and TMS-HEMA were calculated as explained for **M1**. (Figure 4.2B).

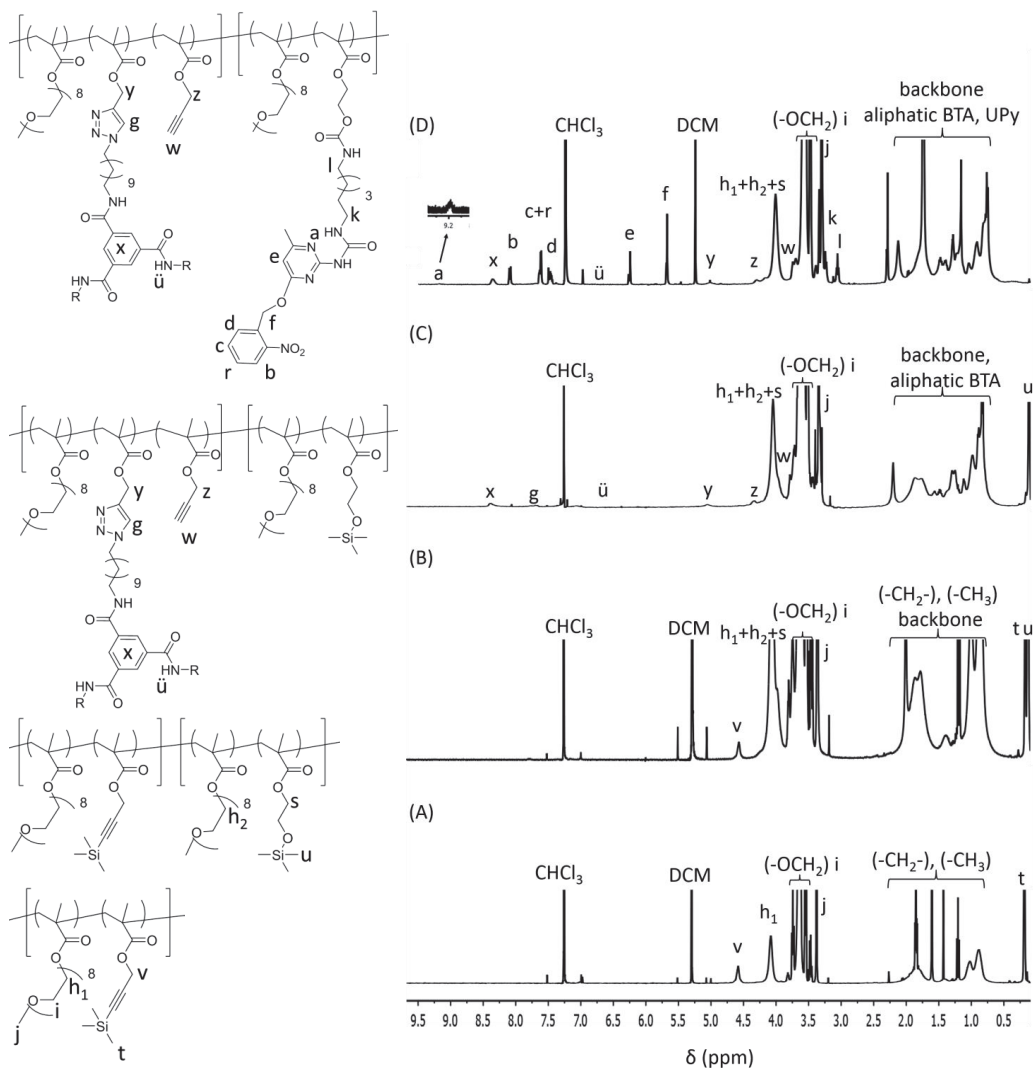


**Figure 4.2**  $^1\text{H-NMR}$  of **M2** (A), **P2(-)** (B), **P2(-B-)** (C) and **P2(UBU)** (D) in  $\text{CDCl}_3$ .

For the preparation of **P3(U)** and **P4(U)**, we followed the synthetic route depicted in Scheme 4.2. Precursor polymer **P3(-)** was obtained through copolymerization of *o*EGMA and TMS-HEMA *via* RAFT in the presence of 4-cyano-4-methyl-5-(phenylthio)-5-thioxopentanoic acid as chain transfer agent (see Chapter 5 and 6 for details, *vide infra*). The amount of TMS-HEMA in the monomer mixture was 20% for **P3(-)** and 21% for **P4(-)**. SEC showed an  $M_n$  of 45 kDa ( $\mathcal{D} = 1.21$ ) and  $M_n$  of 16 kDa ( $\mathcal{D} = 1.11$ ), for **P3(-)** and **P4(-)**, respectively (Table 4.2).

**Table 4.2** Conditions and results for the random copolymer preparation via RAFT.

	$N_{oEGMA}^b$	$N_{HEMA}^c$	$n_{oEGMA}^e$	$n_{HEMA}^f$	$M_{n,NMR}$ kDa <sup>g</sup>	$M_{n,SEC}$ kDa <sup>d</sup>	$\mathcal{D}^d$
<b>P3(-)</b> <sup>a</sup>	344	86	324	81	178.9	44.9	1.21
<b>P4(-)</b> <sup>a</sup>	120	30	80	20	30.1	8	1.13

<sup>a</sup> RAFT polymerization: ( $[M_{tot}]_0/[CTA]_0/[AIBN]_0 = 530/5.2/2.5$  mM) ( $[M_{tot}]_0: [oEGMA]_0 + [HEMA]_0$ ) (**P3** and **P4**) in dioxane at 60 °C.

<sup>b</sup>  $N_{oEGMA} = [oEGMA]_0/[CTA]_0$ . <sup>c</sup>  $N_{HEMA} = [HEMA]_0/[CTA]_0$ .

<sup>d</sup> Analyzed by SEC in DMF (10 mM LiBr) with PEO standard;  $\mathcal{D} = M_w/M_n$ .

<sup>e</sup>  $n_{oEGMA} = ([oEGMA]_0/[CTA]_0) \times \text{Conv.}$ . Conversions are determined by <sup>1</sup>H-NMR in CDCl<sub>3</sub>.

<sup>f</sup>  $n_{HEMA} = ([HEMA]_0/[CTA]_0) \times \text{Conv.}$ . Conversions are determined by <sup>1</sup>H-NMR in CDCl<sub>3</sub>.

<sup>g</sup>  $M_{n, calcd} = Fw, oEGMA \times n_{oEGMA} + Fw, CTA + Fw, HEMA \times n_{HEMA}$ .

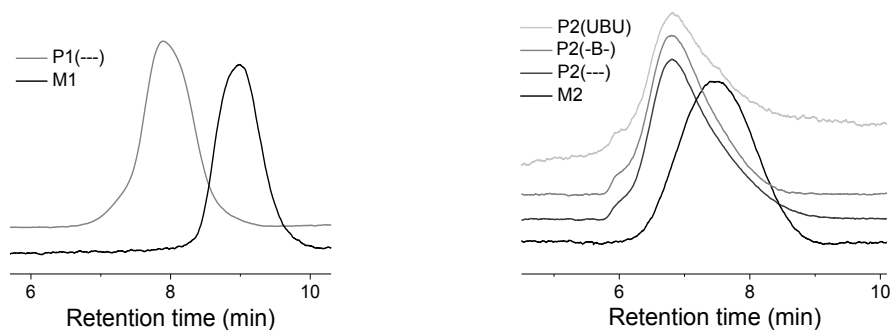


**Figure 4.3** SEC traces for polymers **M1/P1(---)** (left) and **M2/P2/P2(-B-)/P2(UBU)** (right).

Triblock copolymer **P2(---)** was subsequently selected for further functionalization steps. First, a direct copper-catalyzed Huisgen 1,3-dipolar cycloaddition reaction was done on the TMS protected PMA units of **P2(---)** with azide-substituted (R)-chiral BTA (**2**).<sup>57,67</sup> The functionalization of the TMS-protected alkynes in **P2(---)** was not complete. The incorporation of the BTA units was confirmed by <sup>1</sup>H-NMR by the presence of resonances at 8.3, 7.7, 7.0-6.3 and 5.1 ppm (peaks x, g, ü and y in Figure 4.2C) while the comparison of the integrals of peaks y and z indicated a 47 % functionalization of the total alkyl units of the prepolymer **P2(---)** (Figure 4.2C). Subsequently, all TMS groups on HEMA units were removed *via* dialysis against DCM/TFA to yield the corresponding free alcohols. The polymer was further dialyzed against pure DCM to remove free TMS and TFA. The complete removal of the TMS units was evidenced by the disappearance of the peaks at 0.16 ppm. After rigorous drying of the polymer in the presence of P<sub>2</sub>O<sub>5</sub> at low pressure, **P2(---)** was reacted with phUPy-isocyanate (**3**), added in excess, using dibutyltin dilaurate (DBTDL) as the catalyst. The conversion of the alcohol groups was quantitative as shown by <sup>1</sup>H-NMR. The incorporation of the UPy units was confirmed with the presence of peaks labeled as a-f. The peak labeled as l indicated urea linker groups while

comparison of the integrals of peaks labeled as  $h_1$ ,  $h_2$  and  $l$  showed a quantitative reaction of the alcohols of prepolymer **P2(-B-)** with UPy isocyanates (Figure 4.2D). Key to the success of the complete functionalization, which is contrast to earlier reports on functionalization of HEMA with phUPy-isocyanates,<sup>51,55</sup> was the use of a large excess of phUPy-isocyanate, around two phUPy-isocyanates per alcohol functionality. The functionalization was followed by a rigorous purification by first treating the reaction mixture with an aminomethylated-polystyrene resin (200-400 mesh) to remove unreacted UPy isocyanate, and then dialyzing it against DCM for 2 days.

Apart from  $^1\text{H-NMR}$  to follow the functionalization of **P2(---)**, SEC (DMF+LiBr, PEO standards) measurements were performed on all triblock copolymers to assess changes in the hydrodynamic volume (Figure 4.3, right). For both functionalization steps, an increase in molecular weight was observed from 56.6 kDa in **P2(---)** to 57.2 in **P2(-B-)** and 68.5 in **P2(UBU)** indicating the successful functionalization, while the molar mass dispersity remained narrow.

**Table 4.3** Results of the analysis of **P2(---)**, **P3(-)** and **P4(-)** before and after post functionalization.

Polymer	$n_{\text{EGMA}}^c$	$n_{\text{C=C}}^c$	$n_{\text{OH}}^c$	$n_{\text{UPy}}^c$	$n_{\text{BTA}}^c$	$M_{n,\text{exp}}$ (kDa) <sup>a</sup>	$D_H^d$ (nm)	$D_{H\text{-dep}}^d$ (nm)	$\bar{D}^b$
<b>P2(---)</b>	461	24	48	-	-	56.6	-	-	1.45
<b>P2(-B-)</b>	461	11	48	-	15	57.2	-	-	1.26
<b>P2(UBU)</b>	461	11	-	48	15	68.5	295	220	1.24
<b>P3(-)</b>	324	-	81	-	-	44.7	-	-	1.21
<b>P3(U)</b>	324	-	20	60	-	54.5	105	58	1.47
<b>P4(-)</b>	77	-	23	-	-	9.7	-	-	1.09
<b>P4(U)</b>	77	-	6	17	-	10.1	105	18 <sup>e</sup>	1.11

<sup>a</sup> Analyzed by SEC in DMF (10 mM LiBr) with PEO standard; <sup>b</sup>  $\bar{D} = M_w/M_n$ . <sup>c</sup> Number of units determined via the conversion that is determined by  $^1\text{H-NMR}$  in  $\text{CDCl}_3$ . <sup>d</sup> Determined by DLS at angle of  $90^\circ$  at  $25^\circ\text{C}$  (1 mg/mL) in water. <sup>e</sup> Contribution of a peak with a  $D_H$  of 141 nm was observed.

Random copolymers **P3(-)** and **P4(-)** were functionalized with UPy isocyanate (**3**) in a similar approach as was applied to **P2(-B-)**.  $^1\text{H-NMR}$  analysis on **P3(-)** and **P4(-)** showed 75 % and 73 % functionalization of the pendant alcohol moieties, respectively. It is important to note that after UPy functionalization, the increase in molecular weight was accompanied with a decrease in signal strength and broadening was observed in the SEC traces of **P2(UBU)** (Figure 4.3, right), **P3(U)** (Figure 5A) and **P4(U)** (Figure 4.4, left). This was attributed to the increased interaction of the polymer chains with the SEC column after incorporation of highly functional units, even though the LiBr salt is present in DMF to suppress the interactions. The relevant data are summarized in Table 4.3.

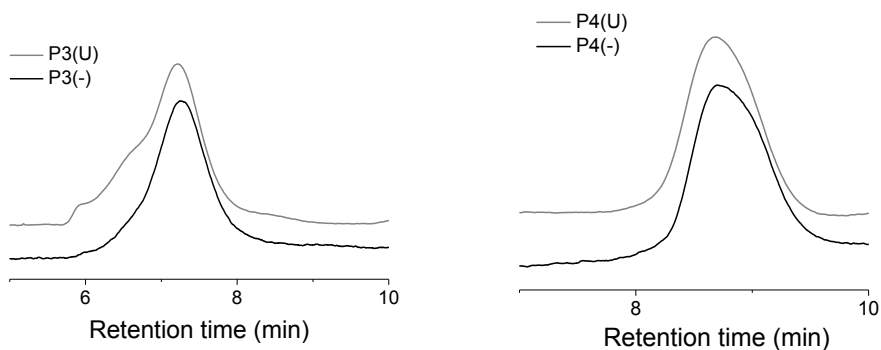


**Figure 4.4** SEC traces for polymers **P3(-)/P3(U)** (left) and **P4(-)/P4(U)** (right) in DMF/LiBr).

#### 4.4 Monitoring BTA helical self-assembly with CD spectroscopy

In order to investigate the capability of the BTA units in the middle part of the triblock copolymers to form helical aggregates, in the absence and in the presence, of the UPy units incorporated in the outer parts, circular dichroism (CD) experiments were performed after BTA functionalization (**P2(-B-)**), after phUPy functionalization (**P2(UBU)**) and after UPy deprotection (**P2(UBU)dep**) (Figure 4.5). The BTA applied here has two stereogenic centra in the alkyl chains with an *R* configuration, which is expected to result in a positive Cotton effect, indicative of predominantly *P* helical stacks.<sup>70</sup> The CD effect of all polymers was indeed positive with values for  $\Delta\epsilon$  of 18, 16 and 18 L mol<sup>-1</sup> cm<sup>-1</sup> observed for **P2(-B-)**, **P2(UBU)** and **P2(UBU)dep**, respectively. Importantly, the magnitude of the Cotton effect with and without UPy incorporation, and before and after UV irradiation remained almost the same (Figure 4.5, right). Furthermore, the cooling curves of **P2(-B-)**, **P2(UBU)** and **P2(UBU)dep** were almost superimposable (Figure 4.5, left). These observations indicate that triblock copolymers with BTAs incorporated in their middle segment (around 8%), show a very similar stacking behavior compared to previously studied amphiphilic copolymers with 10 mol % randomly distributed BTA units, which typically show  $|\Delta\epsilon|$  values between 13 and 20 L mol<sup>-1</sup> cm<sup>-1</sup>.<sup>53,54</sup> Therefore, we can conclude that the presence of BTA free blocks on the outer blocks of triblock polymer **P2** does not significantly hamper the self-assembly of the BTAs on the inner-block.

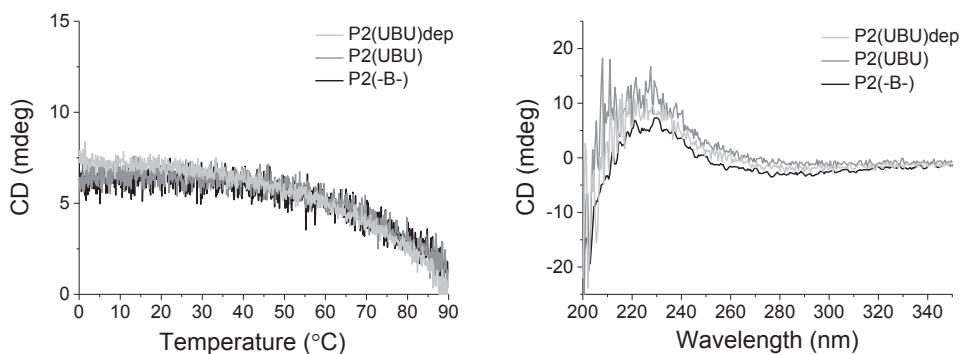
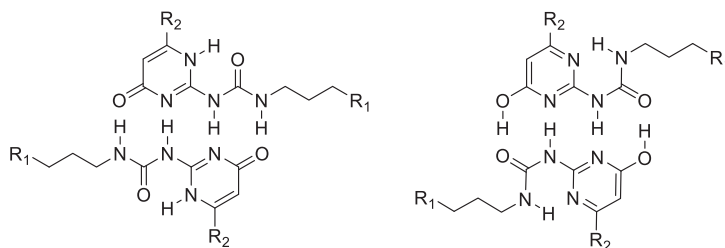


**Figure 4.5** Temperature-wavelength scan measured with 60 K/h at  $\lambda = 223$  nm (left) and wavelength scan measured at 10 °C (right) for 25  $\mu$ M BTA solutions of **P2(-B-)**, **P2(UBU)** and **P2(UBU)dep** in water,  $l = 0.5$  cm.

#### 4.5 Monitoring UPy dimerization via $^1\text{H-NMR}$

Previously, it was shown that UPy derivatives form 4[1H]-pyrimidinone dimers through strong four-fold hydrogen bonds in relatively apolar solvents, while in more polar and competitive solvents they either form the weaker pyrimidin-4-ol dimers (Scheme 4.4) or no dimer formation is observed.<sup>71-73</sup> On the other hand, polymer pendant UPys could form strong 4[1H]-pyrimidinone dimers in organic solvents with varying polarities, regardless of the chemical nature of the backbone, most probably due to the increased local concentration of the self-assembly units and the microenvironment inside the collapsed aggregate in dilute solutions.<sup>51,52,55,74</sup> However, despite the considerable number of reports utilizing UPy containing materials in aqueous systems,<sup>75</sup> direct observation of the UPy dimerization in water *via*  $^1\text{H-NMR}$  has remained a challenge due to proton exchange of H-bonding units with deuterium of the solvent.

In this section, we discuss the results of the  $^1\text{H-NMR}$  experiments performed on **P2(UBU)**, **P3(U)** and **P4(U)** before and after UV irradiation. To induce the UPy dimerization by an external trigger, the 2-ureidopyrimidinone moieties on the polymers were functionalized with *o*-nitrobenzyl-ether photolabile protecting groups at the terminal carbonyl of the UPy.<sup>73</sup> To cleave off the protection groups, we irradiated aqueous solutions of **P2(UBU)**, **P3(U)** and **P4(U)** ( $c = 1$  mg/mL) with UV light (UV-A,  $\lambda_{\text{max}} = 350$  nm) in a Luzchem photoreactor for 4 hours, where after the UPy moieties have the possibility to dimerize.



**Scheme 4.4.** 4[1H]-pyrimidinone dimer (left) and pyrimidin-4-ol dimer (right).

$\text{CDCl}_3$ , in which UPy units are generally able to strongly dimerize,<sup>72</sup> was first used as a solvent to investigate the polymers before and after deprotection of the pendant UPy moieties *via*  $^1\text{H-NMR}$ . Before deprotection, both **P2(UBU)** and **P3(U)** showed the intramolecular H-bonded proton peak that belongs to the urea of the protected UPy, as observed at 9.2 ppm (Figure 4.6, Figure 4.7, bottom, respectively, peak assigned with an empty square). It should be noted that for **P2(UBU)**, an intramolecular hydrogen bonding signal with a lower intensity, compared to the one for **P3(U)**, was observed (Figure 4.6, bottom, empty square). This might indicate a more pronounced interference of oligoethylene glycol units with intramolecular hydrogen bonding on **P2(UBU)**, where phUPy units are segregated into two B blocks, compared to **P3(U)** which has a random distribution of phUPy units. A similar effect of oligoethylene glycols on hydrogen bonding in UPy derivatives was reported by De Greef *et al.*, who reported a decrease of the association constant for UPy derivatives with a *o*EG functionality attached compared to hydrophobic UPy derivatives, *via* changes in the dimerization peaks in  $\text{CHCl}_3$ .<sup>76</sup>

After deprotection, an upfield shift was observed for alkylidene protons of pendant UPy of **P2(UBU)** and **P3(U)** due to the cleavage of *o*-nitrobenzyl unit (Figure 4.6, Figure 4.7, respectively, peaks assigned with an open star). In addition, three broad main peaks were observed around 10.3, 11.9 and 13.1 ppm (Figure 4.6, Figure 4.7, top, respectively, peaks assigned with a filled circle). Those are ascribed to the UPy dimers in their 4[1H]-pyrimidinone tautomer. The observed broadening of the dimerization peaks indicates a decreased mobility of pendant UPy units, in line with the previous UPy based SCPNs in apolar solvents.<sup>55</sup> Smaller sub-peaks around the main broad dimerization peaks indicate subtle microenvironment differences provided by the polymers. For **P2(UBU)**, a lower intensity was observed for the dimerization peaks between 10-13 ppm. This could again be due to the pronounced interference of oligoethylene glycol units with the dimerization in the triblock architecture, *vide supra*.

In order to obtain a direct evidence on the dimerization of the pendant UPy units in water,  $^1\text{H-NMR}$  experiments were performed on **P2(UBU)** and **P3(U)** in water/ $\text{D}_2\text{O}$  mixtures in collaboration with Prof. Dr. Oliver Zerbe (Department of Chemistry, University of Zurich, Switzerland). In these experiments it was attempted to suppress the exchange between acidic protons and deuterium of the solvent. Unfortunately, these attempts were not yet successful.



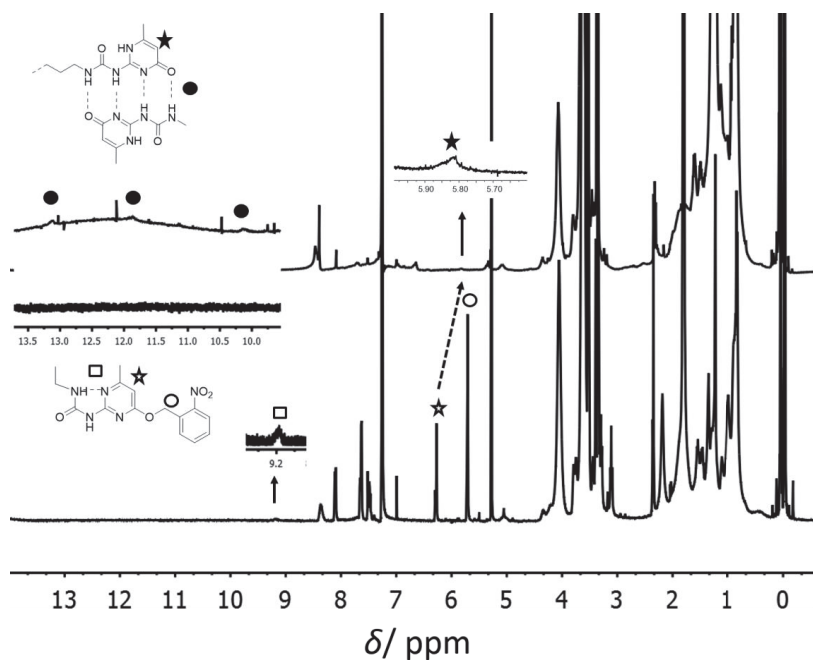


Figure 4.6  $^1\text{H-NMR}$  spectrum of **P2(UBU)** in  $\text{CDCl}_3$  before (bottom) and after (top) deprotection.

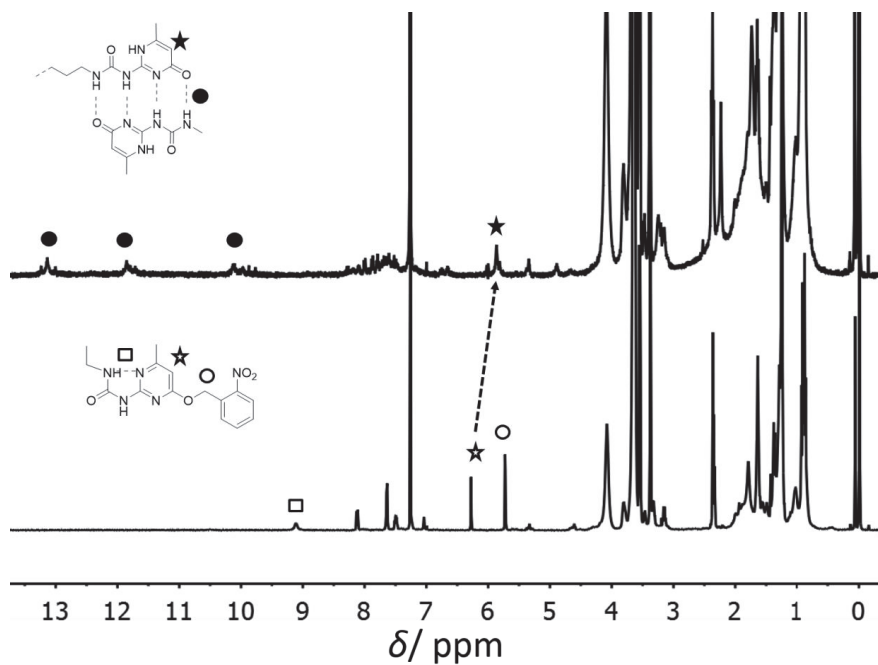
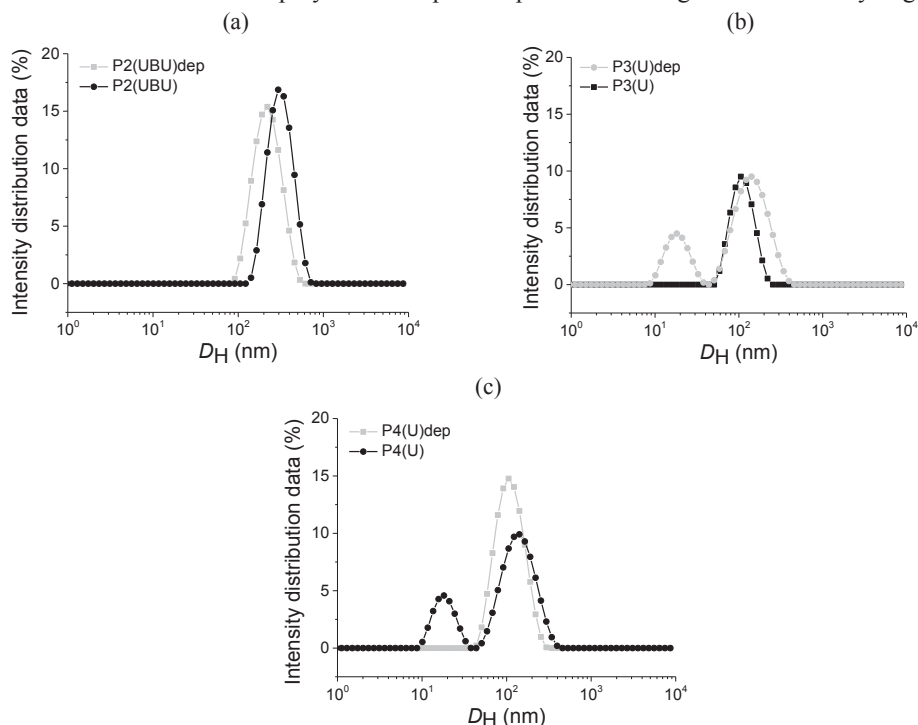


Figure 4.7  $^1\text{H-NMR}$  spectrum of **P3(U)** in  $\text{CDCl}_3$  before (bottom) and after (top) deprotection.

#### 4.6 Monitoring the size of the functionalized polymers via DLS

Dynamic light scattering (DLS) was performed on the polymer solutions ( $c = 1$  mg/mL) to determine the hydrodynamic diameter ( $D_H$ ) before and after photodeprotection of **P2(UBU)**, **P3(U)** and **P4(U)** in water (Table 4.3 and Figure 4.8). Before deprotection, a  $D_H$  of 295 nm for **P2(UBU)**, a  $D_H$  of 105 nm for **P3(U)** and a  $D_H$  of 105 nm for **P4(U)** were observed, implying multi-chain aggregation for all polymers. After photodeprotection, a  $D_H$  of 220 nm for **P2(UBU)dep**, a  $D_H$  of 58 nm for **P3(U)dep** and a  $D_H$  of 18 nm for **P4(U)dep** were observed for the polymers, indicating a decrease in  $D_H$  of 25 %, of 44% and of 88% for **P2(UBU)dep**, **P3(U)dep** and **P4(U)dep**, respectively. For **P4(U)dep**, an additional peak with a  $D_H$  of 141 nm was observed, however, since it is known that large particles scatter significantly more than smaller particles (intensity scales with  $R^6$ ) the fraction of these larger aggregates can be assumed to be small. To understand the origin of the reduction in size, we currently perform SLS and SEC-MALLS experiments to determine the number polymer chains in the aggregate before and after photodeprotection. The larger decrease in  $D_H$  (44%) after the photodeprotection of **P3(U)**, with a  $DP$  of 405, could be due to the change in the number of the polymer chains in the aggregates before and after photo deprotection. However, it could also be due to the compaction of the polymer *via* supramolecular forces. Finally, it should be noted that the multi-chain aggregation behavior was retained for all polymers after photodeprotection owing to their relatively large  $D_{HS}$ .



**Figure 4.8** Intensity distribution vs. hydrodynamic diameter ( $D_h$ ) comparisons of **P2(UBU)/P2(UBU)dep** (a), **P3(U)/P3(U)dep** (b) and **P4(U)/P4(U)dep** (c) measured at a  $90^\circ$  angle at  $20^\circ\text{C}$  for 1 mg/mL solutions in  $\text{H}_2\text{O}$ .

#### 4.7 Probing hydrophobicity via Nile Red experiments

The presence and extent of the hydrophobicity of the formed aggregates were probed with a solvatochromic dye, Nile Red. In pure water, Nile Red displays low fluorescence intensity with an emission maximum ( $\lambda_{\max,em}$ ) at 660 nm. Decreasing the polarity of the medium results in a shift of  $\lambda_{\max,em}$  to lower wavelengths. This tool has been widely used to probe the formation of hydrophobic pockets within self-assembled structures.<sup>77,78</sup> The Nile red solutions with **P2(---)**, **P2(-B-)**, **P2(UBU)** and **P2(UBU)dep** showed a  $\lambda_{\max}$  between 629-633 nm similar to that of Nile Red in MeOH ( $\lambda_{\max,em} = 632$  nm). This indicates that hydrophobic pockets are formed in all polymer solutions, owing to a blue-shift around 30 nm compared to  $\lambda_{\max,em}$  in water at 660 nm. The fluorescence intensity also increased significantly in the presence of the polymers (Figure 4.9). The solutions of polymers **P2(UBU)dep** and **P2(UBU)** showed a stronger increase in fluorescence intensity compared to solutions of polymers **P2(-B-)** which lack UPy units and bare polymer **P2(---)**. This suggests that a more stabilized hydrophobic cavity upon incorporation of both BTA and UPy units in a triblock copolymer, can better accommodate Nile Red molecules compared to a triblock copolymer lacking UPy or any functionalization.

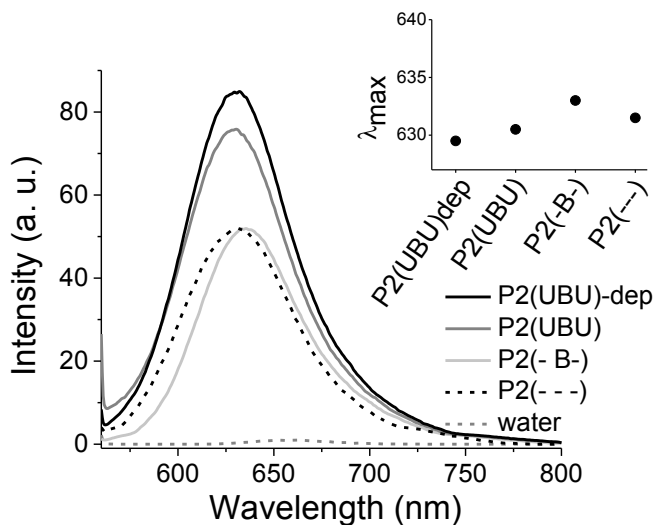


**Figure 4.9** Fluorescence spectra of **P2(---)**, **P2(-B-)**, **P(UBU)** and **P2(UBU)dep** Nile Red solutions in water at 20 °C ( $C_{\text{Nile Red}} = 5 \mu\text{M}$ ,  $C_{\text{polymer}} = 2 \mu\text{M}$ ).

The Nile red solutions with **P3(U)** and **P3(U)dep** also showed a  $\lambda_{\max}$  between 634-636 nm, close to that of Nile Red in MeOH ( $\lambda_{\max,em} = 632$  nm). This indicates that hydrophobic pockets are formed in all polymer solutions. However, the fluorescence intensity increased in the presence of the polymers to a lesser degree compared to **P2(UBU)** and **P2(UBU)dep** (Figure 4.10). Since **P3** and **P2** series have similar  $DP$ s of around 400 and 500, respectively, with functional unit incorporations around 15-20%, a larger increase in the emission intensity for **P2(UBU)** and **P2(UBU)dep** suggests that Nile Red molecules can be better accommodated by a triblock (UPy-BTA-UPy) copolymer than a random (UPy) copolymer.

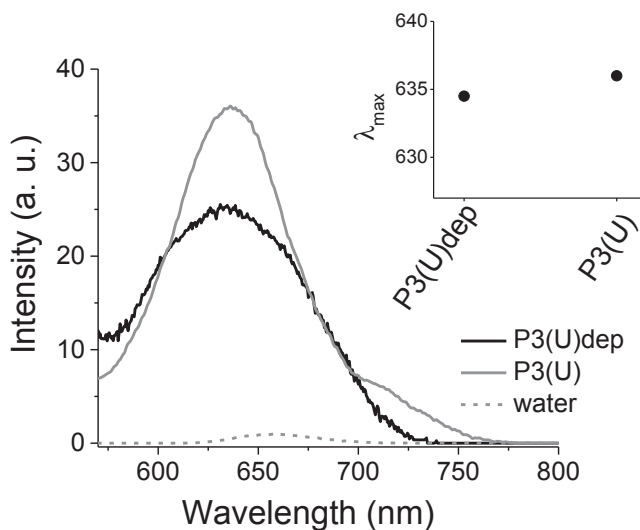


**Figure 4.10** Fluorescence spectra of **P3(U)** and **P3(U)dep**/Nile Red solutions in water at 20 °C ( $C_{\text{Nile Red}} = 5 \mu\text{M}$ ,  $C_{\text{polymer}} = 2 \mu\text{M}$ ).

#### 4.8 Conclusions

In conclusion, we have shown the successful synthesis of highly complex, low and high molecular weight *amphiphilic* ABA type triblock copolymers *via* copper catalyzed ATRP. The post-functionalization of the obtained triblock copolymers with BTA on the B and phUPy on the A segments proved to be efficient. All polymers are soluble in water.

Pendant BTAs on the polymer chains showed a temperature-dependent stacking behavior in water, as confirmed *via* CD spectroscopy, *independent* of the presence of the phUPy *or* UPy moieties, which contain a high number of hydrogen-bond donor and accepting functionalities. After the successful deprotection of the pendant phUPy units, the dimerization of the UPy-moieties was confirmed by  $^1\text{H-NMR}$  for triblock and random UPy functionalized polymers, in  $\text{CDCl}_3$ . Although an indirect confirmation for the UPy dimerization in water was provided by the further reduction of the  $D_{\text{H}}$  after deprotection of pendant phUPy units, the orthogonality of the pendant BTA and UPy self-assembly could not be fully confirmed, since  $^1\text{H-NMR}$  experiments in water were as of yet unsuccessful.

Both triblock and random BTA and/or UPy functionalized copolymers showed multi-chain aggregation, with a relatively narrow dispersity, as shown by DLS in water. The particle size decreased after deprotection of the photo protected UPy units. The presence and relative degree of the hydrophobicity in the triblock copolymers was shown *via* Nile Red experiments, and an overall, relative, hydrophobicity around MeOH was observed for amphiphilic UPy-BTA-UPy and UPy polymers.

From the results described in this chapter it becomes clear that while we have shown the successful preparation of a water soluble system with several, distinct, supramolecular units, their orthogonality still remains challenging to be proven. However, achieving the controlled folding of amphiphilic triblock UPy-BTA-UPy polymer is a step forward in creating synthetic analogues

of natural systems, e.g. proteins, which are held together with a combination of non-covalent forces.

## 4.9 Experimental

### 4.9.1 Materials

Oligo(ethylene glycol) methyl ether methacrylate (*o*EGMA,  $M_n \approx 475$ ) and 2-(trimethylsilyloxy)ethyl methacrylate (TMS-HEMA) (96%) were of commercial source (Aldrich), and purified by an inhibitor removal column (Aldrich) and degassed by reduced pressure before use. Ethylene bis(2-bromoisobutyrate) (97%) (**1**) and *N,N,N',N'',N'''*-pentamethyldiethylenetriamine (PMDETA) (>99), copper(I) bromide (99.999%), copper(II) sulfate (99.999%), (+)-sodium L-ascorbate, dibutyltin dilaurate (DBTDL) and toluene (anhydrous, 99.8%) were purchased from Aldrich Chemicals and used as received. Azobisisobutyronitrile (AIBN) was recrystallized from methanol. 4-Cyano-4-methyl-5-(phenylthio)-5-thioxopentanoic acid was kindly provided by SyMO-Chem (Eindhoven, the Netherlands). All other solvents were obtained from Biosolve. 2-Methyl-acrylic acid 3-trimethylsilylanyl-prop-2-ynyl ester (TMS protected propargyl methacrylate: TMS-PMA) was prepared according to a literature procedure.<sup>79</sup> Deuterated solvents for NMR spectroscopy were purchased from Cambridge Isotope Laboratories. All other materials were purchased from Aldrich Chemicals and used without any further purification. The synthesis of (R,R)-chiral benzene-1,3,5-tricarboxamide (BTA) azide (**2**),<sup>51</sup> and *o*-nitrobenzyl-protected 2-ureidopyrimidinone (UPy) (**3**) were performed as described elsewhere.<sup>55</sup>

### 4.9.2 Methods

Polymerizations were carried out by the syringe technique under dry argon in baked glass tubes equipped with a three-way stopcock. Alumina column purification was performed using Aldrich 58 Å pore size aluminium oxide. DMF-SEC measurements were carried out in PL-GPC-50 plus from Polymer Laboratories (Agilent Technologies) with refractive index detector working in DMF containing 10 mM LiBr at 50 °C at a constant flow rate of 1 mL/min on a Shodex GPC-KD-804 column (exclusion limit = 400000 Da.; 0.8 cm i.d. × 300 mL) which was calibrated with polyethyleneoxide (PEO) samples with a range from 282 - 77350 Da (Polymer Laboratories - Agilent Technologies). <sup>1</sup>H-NMR spectra were recorded at 25°C on a Varian Mercury Vx 400 MHz, operating at 400 MHz, where chemical shifts ( $\delta$  in ppm) were determined with respect to tetramethylsilane (TMS) as an internal reference.

Dynamic light scattering measurements were performed on a Malvern  $\mu$ V Zetasizer equipped with a 830 nm laser. Samples were prepared by first dissolving the polymer in MilliQ quality water and then sonificating for 2 hours in a Cole Parmer 8891 sonification bath. Immediately after the sonification, a 0.2  $\mu$ m PVDF-filter (Whatman) was first washed by filtering MilliQ quality water through and then the polymer solution was filtered in a fluorescence cell with a path length of path length 10x2 mm and chamber volume of 100  $\mu$ L. Prepared DLS solutions were measured immediately.

CD spectra were recorded on a Jasco J-815 CD spectrometer equipped with a Jasco PTC-348 WI temperature controller. Cells with an optical path length of 0.5 cm were applied. Fluorescence data were recorded on a Varian Cary Eclipse fluorescence spectrometer.

Photoirradiation experiments were performed in a Luzchem LZC-4V UV reactor equipped with 8 x 8 Watt light bulbs ( $\lambda_{\text{max}} = 350$  nm). The photo irradiation reactions were performed in a quartz cuvet or NMR tube at 25 °C.

#### 4.10 Synthesis

##### Synthesis of **M1**

Cu(I)Br (13.67 mg, 0.095 mmol), *o*EGMA (5.5 g, 12.15 mmol), TMS-PMA (0.42 g, 2.144 mmol), PMDETA (16.51 mg, 0.095 mmol) and dry toluene (23 mL) were placed in a Schlenk tube (50 mL) capped with a three-way stopcock. The mixture was degassed by freeze-pump-thaw cycles (eight times) and the tube was placed in an oil bath thermostated at 50 °C. A stock solution of difunctional initiator **1** (in toluene) was degassed by Ar bubbling for 20 min. 0.5 mL of this stock solution (34,3 mg, 0.095 mmol) was added under dry argon to the polymerization mixture, and the mixture was stirred at 50 °C. After 2 hours, the reaction mixture was cooled down to room temperature and diluted with DCM (10 mL). <sup>1</sup>H-NMR analysis gave a total monomer conversion of 40 %. The solution was filtered through neutral alumina to remove the copper catalyst. The product was dialyzed against pure DCM for two days. After complete removal of the monomers was verified *via* <sup>1</sup>H-NMR, the solution was concentrated *in vacuo* and dried under a reduced pressure at room temperature to give **M1** (1.40 g) as a sticky white gum. <sup>1</sup>H-NMR (CDCl<sub>3</sub>):  $\delta$  (ppm) = 4.70–4.20 (m, 41.9H, -C(O)O-CH<sub>2</sub>-: TMS-PMA), 4.13-3.89 (m, CO<sub>2</sub>CH<sub>2</sub>CH<sub>2</sub>: *o*EGMA), 3.66-3.43 (s, broad, OC<sub>2</sub>H<sub>4</sub>O), 3.37-3.22 (s, broad, -OCH<sub>3</sub>), 2.25-1.48 (m, CH<sub>2</sub> backbone, *o*EGMA and TMS-PMA), 1.38-0.70 (m, broad, CCH<sub>3</sub> backbone, *o*EGMA and TMS-PMA), 0.19 (s, 34.2H, -Si(CH<sub>3</sub>)<sub>3</sub>). Apparent molecular weight was assigned *via* SEC analysis (DMF + 10 mM LiBr, PEO standards):  $M_n = 7,5$  kDa;  $D = 1.12$ . Degree of polymerization was determined based on <sup>1</sup>H-NMR,  $DP = 59.9$  (*o*EGMA 49.5 + PMA 10.4).

##### Synthesis of **M2**

Cu(I)Br (6.8 mg, 0.047 mmol), *o*EGMA (5.5 g, 12.15 mmol), TMS-PMA (0.42 g, 2.144 mmol), PMDETA (8.3 mg, 0.047 mmol) and toluene (23 mL) were placed in a Schlenk tube (50 mL) capped with a three-way stopcock. The mixture was degassed by freeze-pump-thaw cycles (eight times) and the tube was placed in an oil bath thermostated at 50 °C. A stock solution of difunctional initiator **1** (in toluene) was degassed by Ar bubbling for 20 min. 0.5 mL of this stock solution (17.2 mg, 0.047 mmol) was added under dry argon to the polymerization mixture and the mixture was stirred at 50 °C. After 5 hours, the reaction mixture was cooled down to room temperature and diluted with DCM (10 mL). <sup>1</sup>H-NMR analysis gave a total monomer conversion of 59 %. The solution was filtered through neutral alumina to remove the copper catalyst. The product was dialyzed against pure DCM for two days. After complete removal of the monomers were verified *via* <sup>1</sup>H-NMR, the solution was concentrated *in vacuo* and dried under a reduced pressure at room temperature to give **M2** (1.90 g) as a sticky white gum. <sup>1</sup>H-NMR (CDCl<sub>3</sub>):  $\delta$  (ppm) = 4.70-4.20 (m, 41.9H, -C(O)O-CH<sub>2</sub>-: TMS-PMA), 4.13-3.89 (m, CO<sub>2</sub>CH<sub>2</sub>CH<sub>2</sub>: *o*EGMA), 3.66-3.43 (s, broad, OC<sub>2</sub>H<sub>4</sub>O), 3.37-3.22 (s, broad, -OCH<sub>3</sub>), 2.25-1.48 (m, CH<sub>2</sub> backbone, *o*EGMA and TMS-PMA), 1.38-0.70 (m, broad, CCH<sub>3</sub> backbone, *o*EGMA and TMS-PMA), 0.19 (s, 34.2H, -Si(CH<sub>3</sub>)<sub>3</sub>). Apparent molecular weight was assigned *via* SEC analysis (DMF + 10 mM LiBr, PEO standards):  $M_n = 29,3$  kDa;  $D = 1.35$ . Degree of

polymerization was determined based on conversion *via*  $^1\text{H-NMR}$ ,  $DP = 119.8$  (*o*EGMA 95.7 + PMA 24.1).

#### Synthesis of **P1(---)**

Due to the poor initiation rate and low polymerization speed, this copolymerization was performed with the catalyst ratio of  $[\text{Cu}]_0:[\text{I}]_0:[\text{L}]_0 = 1:1:2$  instead of 1:1:1 used for **M1** and **M2**. Difunctional macroinitiator **M1** (0.540 g, 0.02 mmol), Cu(I)Br (3.0 mg, 0.02 mmol), *o*EGMA (5.63 g, 12.44 mmol), TMS-HEMA (0.444 g, 2.1 mmol) and toluene (0.75 mL) were placed in a Schlenk tube (25 mL) capped with a three-way stopcock. The mixture was degassed by freeze-pump-thaw cycles (eight times) and the flask was placed in an oil bath thermostated at 50 °C. 0.5 mL of a stock solution of PMDETA (0.04 mmol) was added under dry argon to the above polymerization mixture after degassing by Ar bubbling for 20 min and the mixture was stirred at 60 °C. After 5 hours, the reaction mixture was cooled down to room temperature and diluted with DCM (10 mL).  $^1\text{H-NMR}$  analysis gave a total monomer conversion of 31 %. The solution was filtered through neutral alumina to remove the copper catalyst. The product was dialyzed against pure DCM for two days. After complete removal of the monomers were verified *via*  $^1\text{H-NMR}$ , the solution was concentrated *in vacuo* and dried under a reduced pressure at room temperature to give **P1(---)** (0.50 g) as a sticky white gum.

$^1\text{H-NMR}$  ( $\text{CDCl}_3$ ):  $\delta$  (ppm) = 4.70–4.20 (m, 41.9H,  $-\text{C}(\text{O})\text{O}-\text{CH}_2-$ : TMS-PMA), 4.15–3.89 (m,  $\text{CO}_2\text{CH}_2\text{CH}_2$ : *o*EGMA, TMS-HEMA), 3.66–3.43 (s, broad,  $\text{OC}_2\text{H}_4\text{O}$ ), 3.37–3.22 (s, broad,  $-\text{OCH}_3$ ), 2.25–1.48 (m,  $\text{CH}_2$  backbone, *o*EGMA and TMS-PMA), 1.38–0.70 (m, broad,  $\text{CCH}_3$  backbone, *o*EGMA and TMS-PMA), 0.19 (s, 34.2H,  $-\text{Si}(\text{CH}_3)_3$ ), 0.15 (s, 42.8H,  $-\text{Si}(\text{CH}_3)_3$ : TMS-HEMA). Apparent molecular weight was assigned *via* SEC analysis (DMF + 10 mM LiBr, PEO standards):  $M_n = 11,1$  kDa;  $D = 1.08$ . Degree of polymerization was determined based on conversion *via*  $^1\text{H-NMR}$ ,  $DP = 265.02$  (**M1** + *o*EGMA 178.45 + HEMA 26.6). Degree of polymerization was determined based on conversion of the fed *o*EGMA (h) and TMS-HEMA (u) compared to the initial number of TMS-PMA (t) and *o*EGMA ( $h_1$ ) *via*  $^1\text{H-NMR}$ ,  $DP = 265.02$  (**M1** + *o*EGMA 178.45 + HEMA 26.6). ( $\text{TMS-HEMA} = u/9$ ;  $o\text{EGMA}_2 = [h - (v \cdot 4.75)]/2 - (u/9)$ ).

#### Synthesis of **P2(---)**

Due to the poor initiation rate and low polymerization speed, this copolymerization was performed with the catalyst ratio of  $[\text{Cu}]_0:[\text{I}]_0:[\text{L}]_0 = 2:1:4$  instead of 1:1:2 used for **P1(---)**. Difunctional macroinitiator **M2** (0.500 g, 0.0095 mmol), Cu(I)Br (2.8 mg, 0.02 mmol), *o*EGMA (2.96 g, 6.54 mmol), TMS-HEMA (0.233 g, 1.15 mmol) and toluene (13 mL) were placed in a Schlenk tube (25 mL) capped with a three-way stopcock. The mixture was degassed by freeze-pump-thaw cycles (eight times) and the flask was placed in an oil bath thermostated at 60 °C. 0.5 mL of a stock solution of PMDETA (0.04 mmol) was added under dry argon to the above polymerization mixture after degassing by Ar bubbling for 20 min and the mixture was stirred at 50 °C. After 13 hours, the reaction mixture was cooled down to room temperature and diluted with DCM (10 mL).  $^1\text{H-NMR}$  analysis gave a total monomer conversion of 57 %. The solution was filtered through neutral alumina to remove the copper catalyst. The product was dialyzed against pure DCM for two days. After complete removal of the monomers were verified *via*  $^1\text{H-NMR}$ , the solution was concentrated *in vacuo* and dried under a reduced pressure at room temperature to give **P2(---)** (0.50 g) as a sticky white gum.

$^1\text{H-NMR}$  ( $\text{CDCl}_3$ ):  $\delta$  (ppm) = 4.70–4.20 (m, 41.9H,  $-\text{C}(\text{O})\text{O}-\text{CH}_2-$ : TMS-PMA), 4.15–3.89 (m,  $\text{CO}_2\text{CH}_2\text{CH}_2$ : *o*EGMA and TMS-HEMA), 3.66–3.43 (s, broad,  $\text{OC}_2\text{H}_4\text{O}$ ), 3.37–3.22 (s, broad,  $-\text{OCH}_3$ ), 2.25–1.48 (m,  $\text{CH}_2$  backbone, *o*EGMA, TMS-PMA and TMS-HEMA), 1.38–0.70 (m, broad,  $\text{CCH}_3$  backbone, *o*EGMA, TMS-PMA and TMS-HEMA), 0.19 (s, 34.2H,  $-\text{Si}(\text{CH}_3)_3$ : TMS-PMA), 0.15 (s, 42.8H,  $-\text{Si}(\text{CH}_3)_3$ : TMS-HEMA). Apparent molecular weight was assigned *via* SEC analysis (DMF+ 10 mM LiBr, PEO standards):  $M_n = 56,7$  kDa;  $D = 1.45$ . Degree of polymerization was determined based on conversion of the fed *o*EGMA ( $h_2$ ) and TMS HEMA ( $u$ ) compared to the initial number of TMS-PMA ( $t$ ) and *o*EGMA ( $h_1$ ) *via*  $^1\text{H-NMR}$ ,  $DP = 532.8$  ( $\text{M2} + \text{oEGMA } 365 + \text{HEMA } 48$ ). (TMS-HEMA =  $u/9$ ;  $\text{oEGMA}_2 = [h - (v \cdot 3.98)]/2 - (u/9)$ ).

#### Synthesis of **P3(-)** and **P4(-)**

CTA (4.2 mg, 0.015 mmol), *o*EGMA (2.96 g, 6.54 mmol), HEMA (0.33 g, 1.635 mmol), AIBN (0.42 mg, 0.0026 mmol) and dioxane (6.5 mL) was added into the tube and the solution was stirred. Immediately after mixing, the polymerization mixture was placed in an oil bath at 70 °C. The reaction was terminated after 8 h by cooling the mixture to room temperature (conv.  $\approx$  94%;  $^1\text{H-NMR}$ ). The monomer conversion was determined from the concentration of residual monomer measured by  $^1\text{H-NMR}$ . The quenched reaction solutions were evaporated under vacuum and subsequently dissolved in DCM. The product was dialyzed against pure DCM for two days. After complete removal of the monomers were verified *via*  $^1\text{H-NMR}$ , the solution was concentrated *in vacuo* and dried under a reduced pressure at room temperature to give **P3(-)** (2.40 g) as a sticky white gum.

$^1\text{H-NMR}$  ( $\text{CDCl}_3$ ):  $\delta$  (ppm) = 4.15–3.89 (m,  $\text{CO}_2\text{CH}_2\text{CH}_2$ : *o*EGMA, TMS-HEMA), 3.66–3.43 (s, broad,  $\text{OC}_2\text{H}_4\text{O}$ ), 3.37–3.22 (s, broad,  $-\text{OCH}_3$ ), 2.25–1.48 (m,  $\text{CH}_2$  backbone, *o*EGMA and TMS-HEMA), 1.38–0.70 (m, broad,  $\text{CCH}_3$  backbone, *o*EGMA and TMS-HEMA), 0.19 (s, 34.2H,  $-\text{Si}(\text{CH}_3)_3$ ), 0.15 (s, 42.8H,  $-\text{Si}(\text{CH}_3)_3$ : TMS-HEMA). Apparent molecular weight was assigned *via* SEC analysis (DMF+ 10 mM LiBr, PEO standards):  $M_n = 44,9$  kDa;  $D = 1.21$ . Degree of polymerization was determined based on conversion by  $^1\text{H-NMR}$ ,  $DP = 405$  (*o*EGMA 324 + HEMA 81).

For **P4(-)**, the procedure was identical to that described for **P3(-)** except that CTA (8.4 mg, 0.030 mmol), *o*EGMA (2.96 g, 6.54 mmol), AIBN (0.84 mg, 0.006 mmol) were added and the polymerization quenched around 50% conversion and **P4(-)** was afforded as a sticky white gum (2.40 g). Apparent molecular weight was assigned *via* SEC analysis (DMF + 10 mM LiBr, PEO standards):  $M_n = 9,7$  kDa;  $D = 1.09$ . Degree of polymerization was determined based on conversion by  $^1\text{H-NMR}$ ,  $DP = 100.5$  (*o*EGMA 80.1 + HEMA 20.4).

#### Synthesis of **P2(-B-)**

The polymer **P2(—)** (0.5 g, 11  $\mu\text{mol}$ ), **3** (0.072 g, 0.1 mmol), copper (II) sulfate pentahydrate (0.025 g, 0.1 mmol), isopropylamine and sodium ascorbate (0.02 g, 0.1 mmol) were dissolved in DMSO/water (10 mL, v:v = 1:1). The resulting mixture was stirred at room temperature for 24 h and subsequently diluted with the addition of DCM, extracted with 5% EDTA solution to remove the copper and dialyzed against first 5% EDTA solution for 2 days and then DCM for 5 days to remove the excess azide. After complete removal of the azide was verified *via*  $^1\text{H-NMR}$ , the solution was concentrated *in vacuo* and dried under reduced pressure in the presence of  $\text{P}_2\text{O}_5$  at room temperature to give **P2(-B-)**<sub>1</sub> (0.30 g) as a sticky white gum.



$^1\text{H-NMR}$  ( $\text{CDCl}_3$ ):  $\delta$  (ppm) = 8.40-8.29 (s, Ar-*H*: BTAMA), 7.83-7.77 (s, broad, *NHCO*), 5.12 (br, 3.1H, -O- $\text{CH}_2\text{-C}=\text{C}$ -), 4.70-4.20 (m, 41.9H, -C(O)O- $\text{CH}_2$ -: PMA), 4.15-3.89 (m,  $\text{CO}_2\text{CH}_2\text{CH}_2$ : *o*EGMA and TMS-HEMA), 3.66-3.43 (s, broad,  $\text{OC}_2\text{H}_4\text{O}$ ), 3.37-3.22 (s, broad, - $\text{OCH}_3$ ), 2.25-1.48 (m,  $\text{CH}_2$  backbone, *o*EGMA, PMA and TMS-HEMA), 1.38-0.70 (m, broad,  $\text{CCH}_3$  backbone, *o*EGMA, PMA and TMS-HEMA), 0.15 (s, 42.8H, -Si( $\text{CH}_3$ ) $_3$ : TMS-HEMA). SEC analysis (DMF+ 10 mM LiBr, PEO standards):  $M_n = 57,2$  kDa;  $D = 1.26$ . The average number of BTA per chain is 12.3, which is determined by the ratio between acetylene and triazole units and the initial incorporation number of PMA *via*  $^1\text{H-NMR}$  of **P2(---)**.

#### Synthesis of **P2(UBU)**

**P2(-B-)<sub>1</sub>** (0.50 g, 9.0  $\mu\text{mol}$ ), DCM (5 mL) and TFA (0.2 mL) were placed in a round bottom flask (25 mL) and the mixture was stirred for 2 hours. After complete removal of TMS units on HEMA was verified *via*  $^1\text{H-NMR}$ , TFA was removed *via* consecutive evaporations *in vacuo* and dried under reduced pressure in the presence of  $\text{P}_2\text{O}_5$  at room temperature to give **P2(-B-)<sub>2</sub>** (0.30 g) as a sticky white gum.

$^1\text{H-NMR}$  ( $\text{CDCl}_3$ ):  $\delta$  (ppm) = 8.40-8.29 (s, Ar-*H*: BTAMA), 7.83-7.77 (s, broad, *NHCO*), 5.12 (br, 3.1H, -O- $\text{CH}_2\text{-C}=\text{C}$ -), 4.70-4.20 (m, 41.9H, -C(O)O- $\text{CH}_2$ -: PMA), 4.15-3.89 (m,  $\text{CO}_2\text{CH}_2\text{CH}_2$ : *o*EGMA and TMS-HEMA), 3.66-3.43 (s, broad,  $\text{OC}_2\text{H}_4\text{O}$ ), 3.37-3.22 (s, broad, - $\text{OCH}_3$ ), 2.25-1.48 (m,  $\text{CH}_2$  backbone, *o*EGMA, PMA and TMS-HEMA), 1.38-0.70 (m, broad,  $\text{CCH}_3$  backbone, *o*EGMA, PMA and HEMA).

**P2(-B-)<sub>2</sub>** (0.10 g, 1.75  $\mu\text{mol}$ ), **3** (40 mg, 90  $\mu\text{mol}$ ), and DBTDL (1 drop) were placed in a round bottom flask (25 mL) capped with a three-way stopcock, and the inner atmosphere was purged with Ar. Dry DCM (2.0 mL) was added using a syringe to the above flask, and the mixture was stirred at 50 °C. After 12 hours, an aminomethylated-polystyrene resin (200–400 mesh) was added and the mixture was stirred for another 8 h. The solution was filtered and the solvent was removed *in vacuo*. The crude polymer was dialyzed against DCM for 2 days. The resultant polymer was concentrated *in vacuo* and dried at 25 °C under a reduced pressure to give **P2(UBU)** (100 mg) as a slightly yellow sticky gum.

$^1\text{H-NMR}$  ( $\text{CDCl}_3$ ):  $\delta$  (ppm) = 9.16 (s, broad, *N-H*), 8.40-8.29 (s, Ar-*H*: BTAMA), 8.14 (d, Ar-*H*), 7.83-7.77 (s, broad, *NHCO*), 7.65 (d, 2 x Ar-*H*), 7.51 (m, Ar-*H*), 7.16 (s, *N-H*), 6.29 (s, broad, 1H, Ar-*H*), 5.88 (s, broad, *N-H*), 5.74 (s, Ar- $\text{CH}_2\text{-O}$ ), 5.12 (br, 3.1H, -O- $\text{CH}_2\text{-C}=\text{C}$ -), 4.70-4.20 (m, 41.9H, -C(O)O- $\text{CH}_2$ -: PMA), 4.15-3.89 (m,  $\text{CO}_2\text{CH}_2\text{CH}_2$ : *o*EGMA and HEMA), 3.66-3.43 (s, broad,  $\text{OC}_2\text{H}_4\text{O}$ ), 3.37-3.22 (s, broad, - $\text{OCH}_3$ ), 3.33 (m,  $\text{NH-CH}_2$ , UPy), 3.18 (s, broad, O-CO-NH- $\text{CH}_2$ ), 2.25-1.48 (m,  $\text{CH}_2$  backbone, *o*EGMA, PMA and HEMA), 1.38-0.70 (m, broad,  $\text{CCH}_3$  backbone, *o*EGMA, PMA and HEMA). SEC analysis (DMF + 10 mM LiBr, PEO standards):  $M_n = 68,5$  kDa;  $D = 1.24$ . The average number of UPy per chains 46, which is determined by the incorporation efficiency of UPy compared to BTA units and the initial incorporation number of HEMA in **P2** of 48.

#### Synthesis of **P3(U)** and **P4(U)**

**P3(-)** (0.50 g, 9.0  $\mu\text{mol}$ ), DCM (5 mL) and TFA (0.2 mL) were placed in a round bottom flask (25 mL) and the mixture was stirred for 2 hours. After complete removal of TMS units on HEMA were verified *via*  $^1\text{H-NMR}$ , TFA was removed *via* consecutive evaporations *in vacuo* and dried under reduced pressure in the presence of  $\text{P}_2\text{O}_5$  at room temperature to give **P3(-)<sub>2</sub>** with deprotected TMS-HEMA units (0.30 g) as a sticky white gum.

$^1\text{H-NMR}$  ( $\text{CDCl}_3$ ):  $\delta$  (ppm) = 4.15-3.89 (m,  $\text{CO}_2\text{CH}_2\text{CH}_2$ : *o*EGMA, HEMA), 3.66-3.43 (s, broad,  $\text{OC}_2\text{H}_4\text{O}$ ), 3.37-3.22 (s, broad,  $-\text{OCH}_3$ ), 2.25-1.48 (m,  $\text{CH}_2$  backbone, *o*EGMA and HEMA), 1.38-0.70 (m, broad,  $\text{CCH}_3$  backbone, *o*EGMA and HEMA).

**P3(-)** (0.10 g, 1.75  $\mu\text{mol}$ ), **3** (40 mg, 90  $\mu\text{mol}$ ), and DBTDL (1 drop) were placed in a round bottom flask (25 mL) capped with a three-way stopcock, and the inner atmosphere was purged with Ar. Dry DCM (2.0 mL) was added using a syringe to the above flask, and the mixture was stirred at 50 °C. After 12 hours, an aminomethylated-polystyrene resin (200–400 mesh) was added and the mixture was stirred for another 8 h. The solution was filtered and the solvent was removed *in vacuo*. The crude polymer was dialyzed against DCM for 2 days. The resultant polymer was concentrated *in vacuo* and dried at 25 °C under a reduced pressure to give **P3(U)** (150 mg) as a slightly yellow sticky gum. For **P4(U)**, an identical procedure was applied and similar characteristics were observed as those obtained for **P3(U)**.

$^1\text{H-NMR}$  ( $\text{CDCl}_3$ ):  $\delta$  (ppm) = 9.16 (s, broad, N-H), 8.14 (d, Ar-H), 7.65 (d, 2 x Ar-H), 7.51 (m, Ar-H), 7.16 (s, N-H), 6.29 (s, broad, 1H, Ar-H), 5.88 (s, broad, N-H), 5.74 (s, Ar- $\text{CH}_2$ -O), 4.15-3.89 (m,  $\text{CO}_2\text{CH}_2\text{CH}_2$ : *o*EGMA, HEMA), 3.66-3.43 (s, broad,  $\text{OC}_2\text{H}_4\text{O}$ ), 3.33 (m, NH- $\text{CH}_2$ , UPy), 3.18 (s, broad, O-CO-NH- $\text{CH}_2$ ), 3.37-3.22 (s, broad,  $-\text{OCH}_3$ ), 2.25-1.48 (m,  $\text{CH}_2$  backbone, *o*EGMA and HEMA), 1.38-0.70 (m, broad,  $\text{CCH}_3$  backbone, *o*EGMA and HEMA). SEC analysis (DMF + 10 mM LiBr, PEO standards):  $M_n = 54,5$  kDa ( $D = 1.47$ ) for **P3(U)** and  $M_n = 10,1$  kDa ( $D = 1.11$ ) **P4(U)**. The average number of UPy per chains is 60.8 for **P3(U)** and 17 for **P4(U)**, which is determined by the incorporation efficiency of UPy compared to *o*EGMA units and the initial incorporation number of HEMA in **P3(-)** and **P4(-)**.

#### 4.11 References

- (1) *Handbook of Industrial Water Soluble Polymers* (Ed.: P. A. Williams), Wiley-Blackwell, Oxford, **2007**.
- (2) T. Terashima, M. Ouchi, T. Ando, M. Kamigaito, M. Sawamoto *Macromolecules* **2007**, *40*, 3581.
- (3) M. A. J. Gillissen, I. K. Voets, E. W. Meijer, A. R. A. Palmans *Polym. Chem.* **2012**, *3*, 3166.
- (4) W. Fan, X. Tong, Q. Yan, S. Fu, Y. Zhao *Chem. Commun.* **2014**, *50*, 13492.
- (5) E. H. H. Wong, S. J. Lam, E. Nam, G. G. Qiao *ACS Macro Lett.* **2014**, *3*, 524.
- (6) N. Nasongkla, B. Chen, N. Macaraeg, M. E. Fox, J. M. J. Frechet, F. C. Szoka *J. Am. Chem. Soc.* **2009**, *131*, 3842.
- (7) Y. Koda, T. Terashima, M. Sawamoto, H. D. Maynard *Polym. Chem.* **2015**, *6*, 240.
- (8) H. Wei, S. Perrier, S. Dehn, R. Ravarian, F. Dehghani *Soft Matter* **2012**, *8*, 9526.
- (9) Y. Koda, T. Terashima, M. Sawamoto *ACS Macro Lett.* **2015**, *4*, 1366.
- (10) J.-F. Lutz, A. Hoth *Macromolecules* **2006**, *39*, 893.
- (11) S. Han, M. Hagiwara, T. Ishizone *Macromolecules* **2003**, *36*, 8312.
- (12) D. Neugebauer, M. Theis, T. Pakula, G. Wegner, K. Matyjaszewski *Macromolecules* **2006**, *39*, 584.
- (13) J. F. Lutz *J. Polym. Sci. Part A: Polym. Chem.* **2008**, 3459.
- (14) H. Staudinger, O. Schweitzer *Chem. Ges.* **1929**, *62*, 2395.
- (15) D. Neugebauer *Polym. Int.* **2007**, *56*, 1469.
- (16) B. Zhao, D. Li, F. Hua, D. R. Green *Macromolecules* **2005**, *38*, 9509.

- (17) E. Schütz *Arzneim Forsch* **1953**, *3*, 451.
- (18) G. Mantovani, F. Lecolley, L. Tao, D. M. Haddleton, J. Clerx, J. J. L. M. Cornelissen, K. J. Velonia *J. Am. Chem. Soc.* **2005**, *127*, 2966.
- (19) J.-F. Lutz, K. Weichenhan, Ö. Akdemir, A. Hoth *Macromolecules* **2007**, *40*, 2503.
- (20) Y. Maeda, T. Kubota, H. Yamauchi, T. Nakaji, H. Kitano *Langmuir* **2007**, *23*, 11259.
- (21) A. H. E. Müller, in *Recent Advances in Anionic Polymerization* (Eds.: T. E. Hogen-Esch, J. Smid), Elsevier, New York, **1987**, 205.
- (22) H. Reuter, I. V. Berlinova, S. Höring, J. Ulbricht *Eur. Polym. J.* **1991**, *27*, 673.
- (23) T. Suzuki, Y. Murakami, Y. Takegami *Polym. J.* **1980**, *12*, 183.
- (24) N. H. Nguyen, X. Leng, H. J. Sun, V. Percec *J. Polym. Sci. Part A: Polym. Chem.* **2013**, *51*, 3110.
- (25) A. Anastasaki, V. Nikolaou, N. W. McCaul, A. Simula, J. Godfrey, C. Waldron, P. Wilson, K. Kempe, D. M. Haddleton *Macromolecules* **2015**, *48*, 1404.
- (26) L. Martin, G. Gody, S. Perrier *Polym. Chem.* **2015**, *6*, 4875.
- (27) T. Terashima, T. Sugita, K. Fukae, M. Sawamoto *Macromolecules*, **2014**, *47*, 589.
- (28) K. Nakatani, T. Terashima, M. Sawamoto *J. Am. Chem. Soc.* **2009**, *131*, 13600.
- (29) D. Zehm, A. Laschewsky, P. Heunemann, M. Gradzielski, S. Prévost, H. Liang, J. P. Rabe, J.-F. Lutz *Polym. Chem.* **2011**, *2*, 137.
- (30) Zhenping, Xiulin, E. T. Kang, K. G. Neoh *Langmuir* **2005**, *21*, 7180.
- (31) X. Lian, D. Wu, X. Song, H. Zhao *Macromolecules* **2010**, *43*, 7434.
- (32) M. Achilleos, T. M. Legge, S. Perrier, C. S. Patrickios *J. Polym. Sci. Part A: Polym. Chem.* **2008**, *46*, 7556.
- (33) M. Gonzalez-Burgos, A. Latorre-Sanchez, J. A. Pomposo *Chem. Soc. Rev.* **2015**, *44*, 6122.
- (34) A. V. Ambade, S. K. Yang, M. Weck, *Angew. Chem., Int. Ed.* **2009**, *48*, 2894.
- (35) S. K. Yang, A. V. Ambade, M. Weck *J. Am. Chem. Soc.* **2010**, *132*, 1637.
- (36) H. Hofmeier, R. Hoogenboom, M. E. L. Wouters, U. S. Schubert *J. Am. Chem. Soc.* **2005**, *127*, 2913.
- (37) S. L. Li, T. X. Xiao, Y. F. Wu, J. L. Jiang, L. Y. Wang *Chem. Commun.* **2011**, *47*, 6903.
- (38) F. Wang, C. Y. Han, C. L. He, Q. Z. Zhou, J. Q. Zhang, C. Wang, N. Li, F. H. J. Huang *J. Am. Chem. Soc.* **2008**, *130*, 11254.
- (39) U. Mansfeld, M. D. Hager, R. Hoogenboom, C. Ott, A. Winter, U. S. Schubert *Chem. Commun.* **2009**, 3386.
- (40) G. Groger, V. Stepanenko, F. Wurthner, C. Schmuck *Chem. Commun.* **2009**, 698.
- (41) B. D. Mather, M. B. Baker, F. L. Beyer, M. A. G. Berg, M. D. Green, T. E. Long *Macromolecules* **2007**, *40*, 6834
- (42) T. Mes, M. M. E. Koenigs, V. F. Scalfani, T. B. Bailey, A.R.A. Palmans, E.W. Meijer *ACS Macro Letters* **2012**, *1*, 105.
- (43) L. Yu, Z. Wang, J. Wu, S. Tu, K. Ding *Angew. Chem., Int. Ed.* **2010**, *49*, 3627.
- (44) F. Grimm, K. Hartnagel, F. Wessendorf, A. Hirsch *Chem. Commun.* **2009**, 1331.
- (45) C. F. C. Fitie, I. Tomatsu, D. Byelov, W. H. de Jeu, R. P. Sijbesma *Chem. Mater.* **2008**, *20*, 2394.
- (46) J. van Herrikhuyzen, A. Syamakumari, A. P. H. J. Schenning, E. W. Meijer *J. Am. Chem. Soc.* **2004**, *126*, 10021.

- (47) A. Heeres, C. van der Pol, M. C. A. Stuart, A. Friggeri, B. L. Feringa, J. van Esch *J. Am. Chem. Soc.* **2003**, *125*, 14252.
- (48) A. Brizard, M. Stuart, K. van Bommel, A. Friggeri, M. de Jong, J. van Esch *Angew. Chem., Int. Ed.* **2008**, *47*, 2063.
- (49) C. Burd, M. Weck *Macromolecules* **2005**, *38*, 7225.
- (50) O. Altintas, P. Krolla-Sidenstein, H. Gliemann, C. Barner-Kowollik *Macromolecules* **2014**, *47*, 5877.
- (51) N. Hosono, M. A. J. Gillissen, Y. Li, S. S. Sheiko, A. R. A. Palmans, E. W. Meijer *J. Am. Chem. Soc.* **2013**, *135*, 501.
- (52) N. Hosono, P. J. M. Stals, A. R. A. Palmans, E. W. Meijer *Chem. Asian J.* **2014**, *9*, 1099.
- (53) T. Terashima, T. Mes, T. F. A. de Greef, M. A. J. Gillissen, P. Besenius, A. R. A. Palmans, E. W. Meijer *J. Am. Chem. Soc.* **2011**, *133*, 4742.
- (54) (a) M. A. J. Gillissen, T. Terashima, E. W. Meijer, A. R. A. Palmans, I. K. Voets *Macromolecules* **2013**, *46*, 4120; (b) P. J. M. Stals, M. A. J. Gillissen, T. F. E. Paffen, T. F. A. de Greef, P. Lindner, E. W. Meijer, A. R. A. Palmans, I. K. Voets *Macromolecules* **2014**, *47*, 2947.
- (55) P. J. M. Stals, M. A. J. Gillissen, R. Nicolaÿ, A. R. A. Palmans, E. W. Meijer *Polym. Chem.* **2013**, *4*, 2584.
- (56) E. Huerta, P. J. M. Stals, E. W. Meijer, A. R. A. Palmans *Angew. Chem. Int. Ed.* **2013**, *52*, 2906.
- (57) P. J. M. Stals, C. Y. Cheng, L. van Beek, A. C. Wauters, A.R.A. Palmans, S. Han, E. W. Meijer *Chem. Sci.* **2016**, *7*, 2011.
- (58) L. N. Neumann, M. B. Baker, C. M. A. Leenders, I. K. Voets, R. P. M. Lafleur, A. R. A. Palmans, E. W. Meijer *Org. Biomol. Chem.* **2015**, *13*, 7711.
- (59) C. M. A. Leenders, L. Albertazzi, T. Mes, M. M. E. Koenigs, A. R. A. Palmans, E. W. Meijer *Chem. Commun.* **2013**, *49*, 1963
- (60) D. J. M. van Beek, PhD Thesis, Eindhoven University of Technology, **2007**.
- (61) D. Bandera *Personal Communication*.
- (62) (a) D. Bertin, D. Gignes, S. R. A. Marque, P. Tordo *Chem. Soc. Rev.* **2011**, *40*, 2189. (b) J. Nicolas, Y. Guillaneuf, C. Lefay, D. Bertin, D. Gignes, B. Charleux *Prog. Polym. Sci.* **2013**, *38*, 63.
- (63) (a) G. Moad, E. Rizzardo, S. H. Thang *Acc. Chem. Res.* **2008**, *41*, 1133. (b) G. Moad, E. Rizzardo, S. H. Thang *Aust. J. Chem.* **2009**, *62*, 1402. (c) A. Gregory, M. H. Stenzel *Prog. Polym. Sci.* **2012**, *37*, 38.
- (64) (a) M. Ouchi, T. Terashima, M. Sawamoto *Chem. Rev.* **2009**, *109*, 4963-5050. (b) K. Matyjaszewski *Macromolecules* **2012**, *45*, 4015.
- (65) N. V. Tsarevsky, K. Matyjaszewski *Chem. Rev.* **2007**, *107*, 2270.
- (66) P. J. M. Stals, T. N. T. Phan, D. Gignes, T. F. E. Paffen, E. W. Meijer, A. R. A. Palmans *J. Polym. Sci. Part A: Polym. Chem.* **2012**, *50*, 780.
- (67) H. Ito, K. Arimoto, H.-o. Sensul, A. Hosomi *Tetrahedron Lett.* **1997**, *38*, 3977.
- (68) C. Barner-Kowollik, F. E. Du Prez, P. Espeel, C. J. Hawker, T. Junkers, H. Schlaad, W. van Camp *Angew. Chem., Int. Ed.* **2011**, *50*, 60.
- (69) E. B. Berda, E. J. Foster, E. W. Meijer *Macromolecules* **2010**, *43*, 1430.

- (70) Y. Nakano, T. Hirose, P. J. M. Stals, E. W. Meijer, A. R. A. Palmans *Chem. Sci.* **2012**, *3*, 148.
- (71) F. H. Beijer, R. P. Sijbesma, H. Kooijman, A. L. Spek, E. W. Meijer *J. Am. Chem. Soc.* **1998**, *120*, 6761.
- (72) S. H. M. Söntjens, R. P. Sijbesma, M. H. P. van Genderen, E. W. Meijer *J. Am. Chem. Soc.* **2000**, *122*, 7487.
- (73) B. J. B. Folmer, E. Cavini, R. P. Sijbesma, E. W. Meijer *Chem. Commun.* **1998**, 1847.
- (74) (a) E. J. Foster, E. B. Berda, E. W. Meijer *J. Am. Chem. Soc.* **2009**, *131*, 6964. (b) E. J. Foster, E. B. Berda, E. W. Meijer *J. Polym. Sci. Part A: Polym. Chem.* **2011**, *49*, 118.
- (75) (a) P. Y. W. Dankers, M. C. Harmsen, L. A. Brouwer, M. J. A. van Luyn, E. W. Meijer *Nat. Mater.* **2005**, *4*, 568. (b) B. B. Mollet, Y. Nakano, P. C. M. M. Magusin. A. J. H. Spiering, J. A. J. M. Vekemans, P. Y. W. Dankers, E. W. Meijer *J. Polym. Sci. Part A: Polym. Chem.* **2015**, *54*, 81.
- (76) T. F. A. de Greef, M. M. L. Nieuwenhuizen, P. J. M. Stals, C. F. C. Fitié, A. R. A. Palmans, R. P. Sijbesma, E. W. Meijer *Chem. Commun.* **2008**, 4306.
- (77) C. B. Minkenberg, L. Florusse, R. Eelkema, G. J. M. Koper, J. H. van Esch *J. Am. Chem. Soc.* **2009**, *131*, 11274.
- (78) C. B. Minkenberg, F. Li, P. van Rijn, L. Florusse, J. Boekhoven, M. C. A. Stuart, G. J. M. Koper, R. Eelkema, J. H. van Esch *Angew. Chem. Int. Ed.* **2011**, *50*, 3421.
- (79) V. Ladmiral, G. Mantovani, G. J. Clarkson, S. Cauet, J. L. Irwin, D. M. Haddleton, *J. Am. Chem. Soc.* **2006**, *128*, 4823.

# Chapter 5

## *Understanding the catalytic activity of single-chain polymeric nanoparticles in water*

**Abstract:** *The structuring role of benzene-1,3,5-tricarboxamides (BTAs), with (S)-chirality, on the catalytic activity of single chain polymeric nanoparticles (SCNPs) in water was investigated in the transfer hydrogenation of ketones. To this end, a set of segmented, amphiphilic copolymers was prepared, which comprised oligo(ethylene glycol) side chains to impart water solubility, BTA and/or lauryl side chains to induce hydrophobicity and diphenylphosphinostyrene (SDP) units in the middle part as a ligand to bind a ruthenium catalyst. All copolymers were obtained by reversible addition-fragmentation chain transfer (RAFT) polymerization and showed low dispersities ( $\bar{D} = 1.23-1.38$ ) and controlled molecular weights ( $M_n = 28-44$  kDa). A combination of circular dichroism (CD) spectroscopy and dynamic light scattering (DLS) showed that all copolymers fold into SCPNs as a result of the helical self-assembly of the pendant BTA units and/or hydrophilic-hydrophobic phase separation. To create catalytic sites,  $\text{RuCl}_2(\text{PPh}_3)_3$  was loaded into the copolymers via the ligand exchange between the Ru(II) salt and polymer pendant SDP units. The Cotton effect of the copolymers before and after Ru(II) loading was identical, indicating that the helical self-assembly of the BTA units and the complexation of SDP ligands and Ru(II) occurs in an orthogonal manner. DLS revealed that after Ru(II) loading, SDP-bearing copolymers retained their single chain character in water, while copolymers lacking SDP units clustered into larger aggregates. The Ru(II) loaded SCPNs were tested in the transfer hydrogenation of cyclohexanone. This revealed that BTA induced stack formation was not crucial for SCPN formation and catalytic activity; SDP-bearing copolymers folded by Ru(II) complexation and hydrophobic pendants sufficed to provide hydrophobic, isolated reaction pockets around Ru(II) complexes.*

*Part of this work has been published:*

M. Artar, T. Terashima, M. Sawamoto, E. W. Meijer, A. R. A. Palmans *J. Polym. Sci., Part A: Polym. Chem.* **2014**, *52*, 12.

## **Introduction**

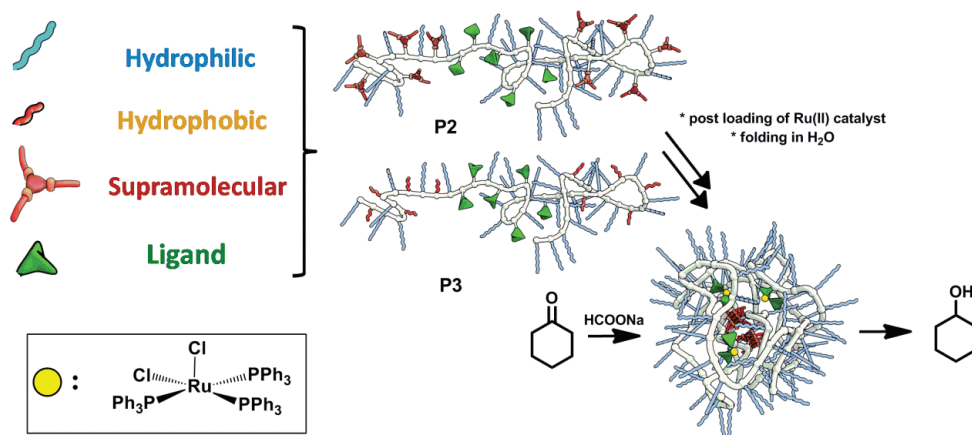
Enzymes are highly attractive for performing reactions in water on an industrial scale, and are source of inspiration to design novel catalytic systems. On the other hand, creating sufficiently hydrophobic domains around catalytic sites to ensure compatibility of the homogeneous organo- or metal-based catalysts with aqueous environments has remained a major challenge.<sup>1-3</sup> For this reason, artificial metalloenzymes,<sup>4-6</sup> DNA-based catalysts,<sup>7</sup> amphiphilic copolymers,<sup>8-10</sup> star polymers<sup>11-15</sup>, micellar systems<sup>16-20</sup>, molecularly imprinted nano- and microgels<sup>21-23</sup> and dendrimers<sup>24-28</sup> were designed to achieve the necessary compartmentalization for efficient catalysis in water. Many others applied metal loaded polymeric systems for catalysis. For example, Cu (II) loaded methacrylate based polymers were used in the coupling reactions by Sanchez-Sanchez *et al.*<sup>29</sup> and Willenbacher *et al.* applied Pd(II) loaded styrene based polymers in the Sonogashira coupling, in organic solvents.<sup>30</sup> Lastly, Mavila *et al.* showed the potential of Rh(I), Ir(I) and Ni(0) loaded polycycloocta-1,5-diene based nanoparticles in the catalysis of several reactions.<sup>31</sup>

Supramolecular folding of polymer chains into single chain polymeric nanoparticles (SCPNS) is an attractive alternative to prepare compartmentalized, water-soluble, nanometer-sized particles with a hydrophobic interior.<sup>32-35</sup> Notably, the benzene-1,3,5-tricarboxamide (BTA) is an attractive unit to form SCPNS with well-defined, conformationally adaptable, three-dimensional structures as a result of the hydrogen-bond-driven, helical self-assembly of the BTA units.<sup>32</sup> Detailed scattering studies revealed that water-soluble copolymers based on oligo(ethylene glycol) methacrylate (*o*EGMA) and benzene-1,3,5-tricarboxamide methacrylate (BTAMA) fold in water into compact conformations consisting of a single polymer chain, and having a slightly elongated shape as a result of the BTA self-assembly.<sup>32</sup>

Recently, catalytically active moieties were inserted into BTA-based amphiphilic copolymers.<sup>34,36</sup> A set of random amphiphilic copolymers comprising *o*EGMA/BTAMA and *L*-proline units was prepared *via* reversible addition-fragmentation chain transfer (RAFT) polymerization.<sup>36</sup> The copolymers efficiently catalyzed aldol reactions with good diastereo- and enantioselectivities in water.<sup>36</sup> Remarkably, BTA self-assembly was crucial for effective catalysis in these copolymers, indicating that the creation of a stable but conformationally flexible hydrophobic interior in the SCPNS was crucial for catalysis to occur.<sup>36</sup> In addition, Ru-catalyzed living free radical polymerization (LRP) was used to prepare a segmented amphiphilic *o*EGMA/BTAMA-based copolymer comprising diphenyl phosphinostyrene (SDP) units in the middle part, in which a ruthenium-based catalyst was simultaneously formed around the pendant SDP units *via* ligand exchange. The segmented copolymers formed SCPNS in water and catalyzed transfer hydrogenations of ketones.<sup>34</sup> In the Ru-based SCPNS, both the Ru-SDP complexation and the BTA stacking are elements that induce supramolecular folding of the polymer chain. Hence, it is intriguing to study in how far the BTA units are necessary as an additional structuring element for efficient catalysis, since this was so crucial in the *L*-proline-based organocatalytic system.<sup>34</sup>

In this chapter, detailed investigations are performed to understand how far the directional, structuring role of BTA groups with (*S*)-chirality is important for the catalytic activity in transfer hydrogenation reactions catalyzed by Ru(II)-based SCPNS. A set of segmented, amphiphilic copolymers (Scheme 5.1) with a varying BTA content were designed and synthesized. The

copolymers were obtained *via* RAFT, an easy to apply, metal-free living radical polymerization (LRP) technique, and then post-loading of the Ru(II) catalyst was applied to create catalytic centers. Copolymers **P1-P5** were studied using spectroscopic techniques (circular dichroism and fluorescence spectroscopy) and dynamic light scattering (DLS) before and after Ru(II) loading. The activity of the copolymers was assessed in the transfer hydrogenation of cyclohexanone derivatives. The results show that BTA self-assembly is not required for the stabilization of the hydrophobic pocket when SDP-Ru complexes are present; hydrophobic monomers and SDP ligands effectively provide isolated, hydrophobic reaction pockets around ruthenium catalysts to induce efficient catalysis.



**Scheme 5.1** Design of catalytically active SCPNs for transfer hydrogenation of ketones in water. Only the folded structure of **P2** is illustrated as the folded structure above for clarity.

## 5.2 Design and synthesis of catalytically active SCPNs

Amphiphilic copolymers (**P1-P5**) were synthesized by RAFT polymerization in dioxane at 70 °C in the presence of 4-cyano-4-methyl-5-(phenylthio)-5 thioxopentanoic acid as a chain transfer agent and azobisisobutyronitrile (AIBN) as an initiator. Copolymers with (**P1-P3**) and without (**P4-P5**) SDP ligands and copolymers with (**P1,P2,P5**) and without (**P3,P4**) BTA units were prepared. Lauryl methacrylate (LMA)—lacking structuring abilities—was chosen as a hydrophobic, non-hydrogen-bonding comonomer to replace the BTA units. To obtain SCPNs with comparable sizes and similar amphiphilic character, the theoretical degree of polymerization of methacrylates was kept constant ( $DP_{th} = 100$ ) and the  $DP_{th}$ s for hydrophilic *o*EGMA and hydrophobic chiral BTAMA with (*S*)-chirality and/or LMA were set as 90 and 10, respectively. For ligand-bearing copolymers (**P1-P3**), the SDP content was around 5.6 mol% of the total. The compositions of *o*EGMA, LMA and/or BTAMA in the final copolymers are summarized in Table 5.1. To concentrate the SDP ligands in the middle of the polymer chain, SDP was directly added to the solution at around 30 % conversion of methacrylates (after 1 h) for **P1-P3**. The reaction temperature was raised to 80 °C since styrene-based monomers require a higher polymerization temperature than methacrylates.



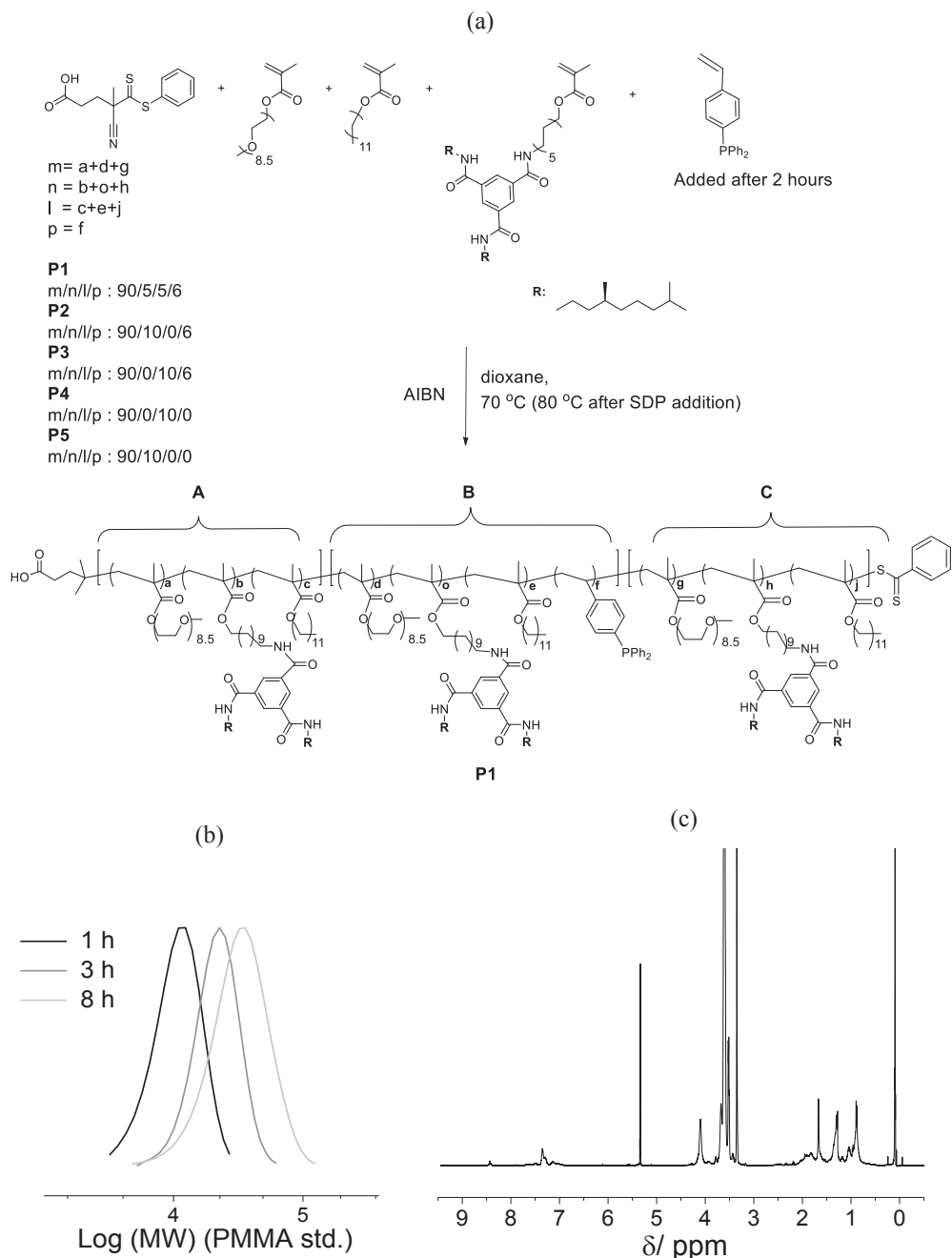


**Figure 5.1** (a) Synthesis of a segmented copolymer ligand (**P1**) by RAFT polymerization; (b) SEC (PMMA std) curves of the samples obtained after 1, 3, and 8 hr polymerization time; (c)  $^1\text{H-NMR}$  spectrum of **P1**. Conditions:  $[\text{oEGMA}]_0/[\text{BTAMA}]_0/[\text{LMA}]_0/[\text{SDP}]_0/[\text{CTA}]_0/[\text{AIBN}]_0 = 478/27/27/32/5.2/2.5 \text{ mM}$  in dioxane at 70°C (80°C after SDP addition).

The results for the polymerizations to afford **P1-P4** are shown in Figure 5.2. Conversion of the monomers was quantified by the disappearance of the vinyl peaks *via* <sup>1</sup>H-NMR. After addition, SDP was rapidly consumed within 2 hours, followed by full conversion of the remaining methacrylates in 8 hours. The rapid consumption of SDP is attributed to the reactivity ratios of SDP with methyl methacrylate (as a reference monomer for *o*EGMA) as  $r_{SDP} \approx 0.9$  and  $r_{MMA} \approx 0.3$  which explains the preference of *o*EGMA for SDP monomer.<sup>37</sup> It should be noted that although SDP units were built in rapidly, more *o*EGMA units were built in due to almost ten times higher monomer concentration, resulting in a sparsely distributed SDP in the middle segment. The molecular weights determined by SEC (relative to PMMA standards) increased with increasing conversion, SEC curves at different reaction times were shown in Figure 5.1b for **P1**, and the molecular mass distribution ( $\mathcal{D}$ ) remained narrow (<1.4) (Figure 5.2).

Almost identical consumption of the three different methacrylates, together with the rapid consumption of SDP (Figure 5.2a), indicates that a sequential, one-pot segmentation is achieved by the formation of two random end blocks of methacrylates and one middle, random, SDP/methacrylate block, with incorporations matching with feed ratios (Figure 5.1c for a representative NMR spectrum of **P1**, Table 5.1). Copolymers **P2-P5** were obtained using RAFT polymerization with varying monomer incorporations in molecular weights between 28-33 kDa (SEC DMF with 10 mM LiBr, PMMA standards) and narrow dispersities (1.2-1.4) as shown in Figure 5.2.

**Table 5.1** Characterization of amphiphilic copolymers<sup>a</sup>

Polymer	Composition	$DP_0$	$M_n^c$	$\mathcal{D}^c$	$DP_{calcd}$	$M_{n, calcd}^c$	$M_w^f$
		(m/n/l/p) <sup>b</sup>	(kDa)		(m/n/l/p) <sup>d</sup>	(kDa)	(kDa)
<b>P1</b>	<i>o</i> EGMA/BTA/LMA/SDP	90/5/5/6	28.3	1.37	81/4.5/4.5/6	44.6	55.9
<b>P2</b>	<i>o</i> EGMA/BTA/SDP	90/10/-/6	30.3	1.38	84.6/9.3/-/6	48.9	76.9
<b>P3</b>	<i>o</i> EGMA/LMA/SDP	90/-/10/6	30.1	1.36	83.7/-/9.3/6	43.8	68.5
<b>P4</b>	<i>o</i> EGMA/LMA	90/-/10/-	30.2	1.23	81.9/-/9/-	41.2	62.7
<b>P5</b>	<i>o</i> EGMA/BTA	90/10/-/-	32.2	1.34	87/8/-/-	47.1	n.d.

<sup>a</sup>RAFT polymerization: ( $[M_{10}]_0/[CTA]_0/[AIBN]_0 = 530/5.2/2.5$  mM) ( $[M_{10}]$ : [*o*EGMA]<sub>0</sub>+ [BTAMA]<sub>0</sub>+ [LMA]<sub>0</sub>+ [SDP]<sub>0</sub>) (**P1-P5**) in dioxane at 70 °C (increased to 80 °C after SDP addition).

<sup>b</sup>Degree of polymerization ( $DP_0$ ):  $m=[oEGMA]_0/[CTA]_0$ ;  $n=[BTAMA]_0/[CTA]_0$ ;  $l=[LMA]_0/[CTA]_0$ ;  $p=[SDP]_0/[CTA]_0$ .

<sup>c</sup>Analyzed by SEC in DMF (10 mM LiBr) with PMMA standards;  $\mathcal{D} = M_w/M_n$ .

<sup>d</sup> $DP_{calcd}$ :  $m=( [oEGMA]_0 \times Conv. )/[CTA]_0$ ;  $n=( [BTAMA]_0 \times Conv. )/[CTA]_0$ ;  $l=( [LMA]_0 \times Conv. )/[CTA]_0$ ;  $p = ( [SDP]_0 \times Conv. )/[CTA]_0$ . Conversion is determined by <sup>1</sup>H-NMR in CD<sub>3</sub>Cl at 25 °C.

<sup>e</sup> $M_{n, calcd} = F_{w, oEGMA} \times DP_{calcd, oEGMA} + F_{w, CTAI} + F_{w, BTAMA} \times DP_{calcd, BTAMA} + F_{w, LMA} \times DP_{calcd, LMA} + F_{w, SDP} \times DP_{calcd, SDP}$ .

<sup>f</sup>Analyzed by SEC-MALLS in DMF. n.d. = not determined.

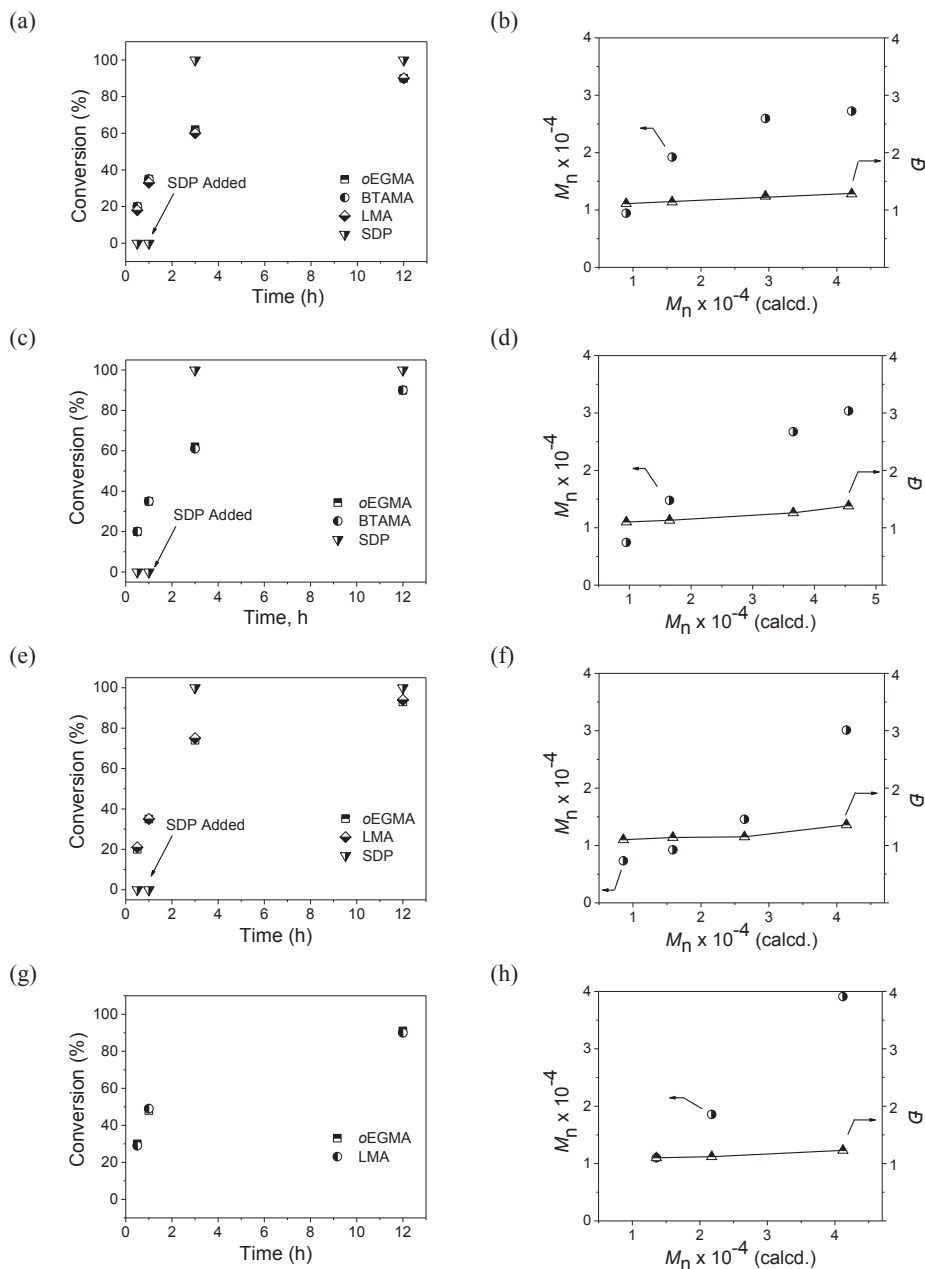


**Figure 5.2** Synthesis of copolymers **P1** (a, b), **P2** (c, d), **P3** (e, f), **P4** (g, h) by RAFT polymerization. (a, c, e, g) Conversion of monomers (oEGMA, BTAMA, LMA and SDP) as a function of time, determined with  $^1\text{H-NMR}$ ; (b, d, f, h) number-average molecular weight ( $M_n$ ) and molar mass distribution  $G$ , determined by SEC (PMMA std) as a function of the number averaged molecular weights calculated from monomer conversion.

Previously, Ru(II)-loaded terpolymers were prepared *via*  $\text{RuCl}_2(\text{PPh}_3)_3$ -catalyzed LRP by Terashima *et al.*<sup>34</sup> Efficient encapsulation of the polymerization catalyst resulted from the exchange of ligands around the Ru(II) catalyst from  $\text{PPh}_3$  units to SDP during the polymerization. As an alternative to this elegant, one-pot approach, we here introduce a post-encapsulation approach of the metal catalyst into the polymers that was applied to create catalytic centers, which permits control over the loaded amount of metal catalyst and ultimately, will permit to introduce different metal catalysts. SDP units can form complexes with various metals and catalyze a number of reactions as recently addressed by Poli *et al.* in Rh-SDP catalyzed hydroformylations by using styrene based polymers with SDP ligands.<sup>38,39</sup>

By Terashima *et al.*, the number of ruthenium atoms per chain was found to be 2.5 (determined by ICP-AES), which is close to the maximum number of the available coordination sites (3) assuming that one ruthenium is at least supported by two SDP units.<sup>34</sup> In order to obtain an analogous system, we here apply an equivalent of 2.5 ruthenium atoms per chain for post-loading of the SCPNs. The coordination of  $\text{RuCl}_2(\text{PPh}_3)_3$  (dichlorotris(triphenylphosphine) ruthenium(II) to **P3** was examined by  $^{31}\text{P}$ -NMR (Figure 5.3). Bare **P3** exhibited a  $^{31}\text{P}$ -NMR signal at -1 ppm originating from the pendant SDP (Figure 5.3).

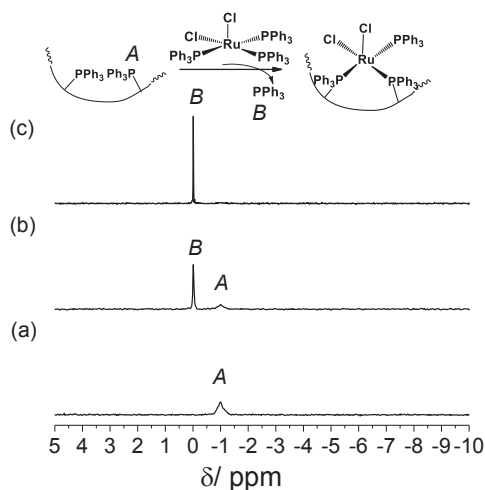


**Figure 5.3**  $^{31}\text{P}$ -NMR spectra of polymer solutions (2 mM in toluene- $d_6$ ) 2.5 equivalents of Ru(II) (a), 1 equivalent of Ru(II) (b) and bare **P3** (c) in toluene- $d_6$  at r.t.

Upon catalyst loading, the SDP signal decreased due to Ru(II) coordination and a new signal appeared at 0.2 ppm. The signal at 0.2 ppm is attributed to free  $\text{PPh}_3$ , released from Ru(II) *via* the ligand exchange with **P3**-bound SDP.  $^1\text{H}$ -NMR showed broadening of the phenyl proton signals for polymer-bound SDP after Ru(II) loading, owing to the low mobility, confirming the ligand exchange between SDP and  $\text{PPh}_3$ . No signal for free  $\text{RuCl}_2(\text{PPh}_3)_3$  was observed around 50 ppm in all cases, implying quantitative immobilization of the fed Ru(II) catalyst. The same procedure was applied to other copolymers (**P1**, **P2**, **P4**, **P5**) and successful loading was

confirmed by ICP-AES measurements (43-60  $\mu\text{mol Ru/g-polymer}$ ), which were kindly performed by A. M. Elemans-Mehring.

### 5.3 CD, DLS and fluorescence characterization of P1-P5 in solution

Circular dichroism (CD) spectroscopy is a powerful technique to assess the presence of helical BTA-based aggregates within the SCPNs. Previously, it was shown that a stereogenic center with an (*S*) configuration on an odd-carbon with respect to the amide of the BTA side chain, gives rise to a negative Cotton effect at  $\lambda = 223 \text{ nm}$ , indicative of bias for the *M* helical sense.<sup>41-44</sup>

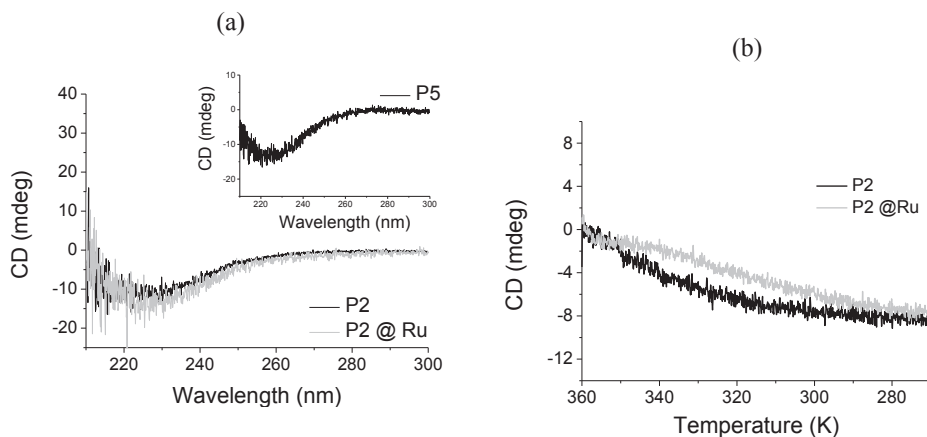


**Figure 5.4.** (a) CD spectra of **P2**, **P2@Ru(II)** and **P5** in  $\text{H}_2\text{O}$  ( $c_{\text{BTA}} = 25 \mu\text{M}$  at 313 K). (b) CD temperature-wavelength scan of **P2**, **P2@Ru(II)** measured with 60 K/h at  $\lambda = 223 \text{ nm}$  in  $\text{H}_2\text{O}$  ( $c_{\text{BTA}} = 25 \mu\text{M}$ ).

Circular dichroism experiments were performed on the *S*-BTA functionalized **P1**, **P2** and **P5** to evaluate the effect of SDP unit and Ru(II) catalysts on the helical self-assembly of the pendant BTA units before and after Ru(II) loading. The CD spectra of BTA-containing **P5**, SDP-containing **P2**, and Ru-bearing **P2** (Figure 5.4a, b) showed a  $\Delta\epsilon$  of around  $-19 \text{ L mol}^{-1}\text{cm}^{-1}$ . Since the magnitude of the Cotton effect is determined by the BTA concentration in BTA-based SCPNs,<sup>32,34</sup> the superimposable CD curves indicate that the SDP units do not affect the aggregation behavior of the pendant BTA units. Moreover, pseudo-crosslinking of the middle segment *via* the complexation of Ru(II) and the SDP ligands does not alter the magnitude of the Cotton effect, indicating that Ru(II)-SDP complexes do not significantly affect BTA aggregation. The sign and magnitude of the CD effect accord nicely with earlier observations.<sup>32,34,36</sup> These results suggest that the controlled topology of the polymer chains allows the self-assembly motifs, i.e. BTA units and Ru(II)-SDP units, to act in an orthogonal way.<sup>27,42</sup>

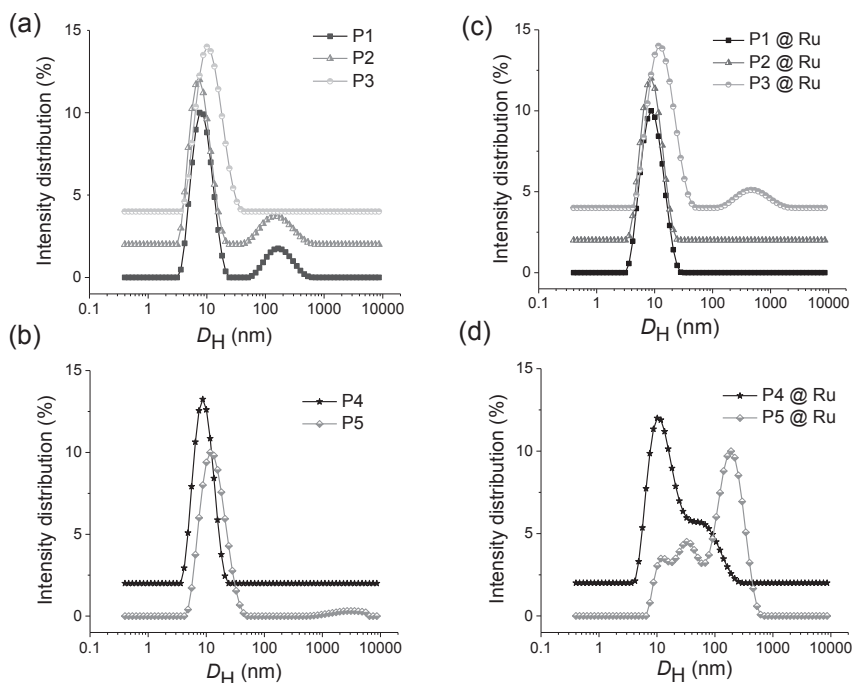


**Figure 5.5** DLS intensity distribution for **P1-P5** before (a,b) and after (c,d) catalyst loading in  $H_2O$  at  $40^\circ C$ ,  $C_{polymer} = 18 \text{ mg mL}^{-1}$ .

Dynamic light scattering (DLS) experiments were performed to elucidate the single chain folding of the prepared copolymers. When linear polymers fold into SCPNs, hydrodynamic diameters ( $D_H$ ) of around 10 nm are expected.<sup>32,34,36</sup> DLS studies of **P1-P5** were performed before and after Ru(II) loading (Figure 5.5); the values for  $D_H$  are summarized in Table 5.2. In all cases, a polymer concentration of  $18 \text{ mg mL}^{-1}$  was applied, identical to the concentrations used in the catalytic experiments (*vide infra*). The bare copolymers (**P1-P5**) show predominantly a single peak around 10 nm in DLS. The values for  $D_H$  vary between 7.5 to 11.7 nm (Table 5.2) and are in good correspondence to previously reported values. After Ru(II) loading, **P1-P3** kept a single chain character as evidenced by the presence of (predominantly) single peaks in Figure 5.5c. Interestingly, for **P4** and **P5**—polymers that lack SDP ligands—large aggregates with sizes of 32-58 nm are observed after Ru(II) loading, indicative of multiple chain aggregation (Table 5.2, entries 4 and 5, Figure 5.5d). This is most probably caused by the Ru(II) catalyst that coordinates to available lone pairs of, for example, several BTA amides or *o*EG chains, thereby crosslinking a number of different polymer chains.

Finally, the presence of a hydrophobic interior in the SCPNs was evaluated with a solvatochromic dye, Nile Red. In pure water Nile Red displays low fluorescence intensity with an emission maximum of 660 nm. Decreasing the polarity of the medium results in an increase of the emission intensity, and a shift of the emission maximum to lower wavelengths. This tool has been widely used to probe the formation of hydrophobic pockets within self-assembled structures.<sup>45-47</sup> The addition of copolymers (**P1-P5**) resulted in a blue shift of 27 nm for the

emission wavelength of Nile Red in water. The fluorescence intensity also increased significantly in the presence of the polymers (Figure 5.6). Both observations corroborate the presence of hydrophobic pockets in all polymer solutions. The solutions of polymers **P1**, **P2** and **P5** with a BTA incorporation of 5, 10 and 10%, respectively, showed a stronger increase in fluorescence intensity compared to solutions of polymers **P3** and **P4**, which lack BTA units. This suggests that a more stabilized hydrophobic cavity upon incorporation of BTAs in a polymer can better accommodate Nile Red molecules compared to a polymer with LMA. In fact, judging from the intensity of fluorescence of polymers **P1-P5** that have identical *DPs*, the fluorescence intensity seems to be proportional to the BTA content. This can be rationalized by the fact that the concentration of hydrophobic groups in BTA units is larger than in LMA units. Remarkably, polymer **P2**, which has the same 10% BTA content as **P5**, displayed a much higher fluorescence intensity compared to **P5**. This stabilization of the hydrophobic cavity is induced by the SDP units present in **P2**.

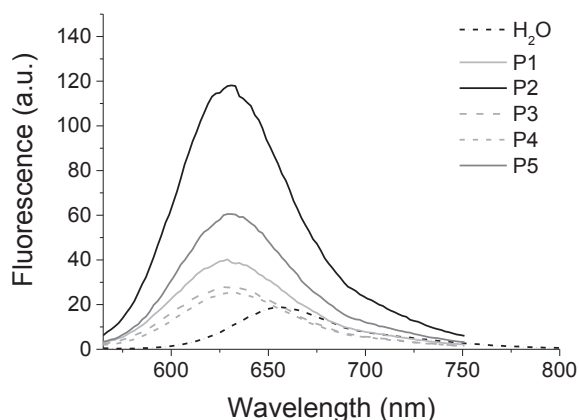


**Figure 5.6.** Fluorescence spectra of polymer/Nile Red solutions in water at 20 °C ( $c_{\text{Nile Red}} = 5 \mu\text{M}$ ,  $c_{\text{polymer}} = 2 \mu\text{M}$ ).

#### 5.4 Transfer hydrogenation of cyclohexanone in water

The catalytic activity of all copolymers was first evaluated in the transfer hydrogenation of cyclohexanone in water at 40 °C ( $[\text{substrate}]/[\text{HCOONa}]/[\text{Ru}] = 0.2/0.5/0.001 \text{ M}$ ). From the conversions after 40 h, the turnover frequencies (TOF) were calculated; the results are summarized in Table 5.2. Ru(II)-bearing copolymers, **P1@Ru-P3@Ru**, showed TOF values of around  $4.4 \text{ h}^{-1}$ , indicating that the transfer hydrogenations proceeded efficiently in the presence of SDP ligand and BTA or LMA hydrophobic units (Table 5.2, entries 1-3). The values are smaller than those previously reported ( $\text{TOF} = 10\text{-}20 \text{ h}^{-1}$ ),<sup>34</sup> which is likely caused by the different method of Ru(II) incorporation. In addition, non SDP-bearing polymers with Ru(II), **P4@Ru** and **P5@Ru**, showed a TOF of  $1.4$  and  $0 \text{ h}^{-1}$ , respectively.

**Table 5.2** Hydrodynamic radius ( $D_H$ ) of **P1-P5** before and after Ru(II) complexation and turnover frequencies (TOF) obtained in the transfer hydrogenation of cyclohexanone.

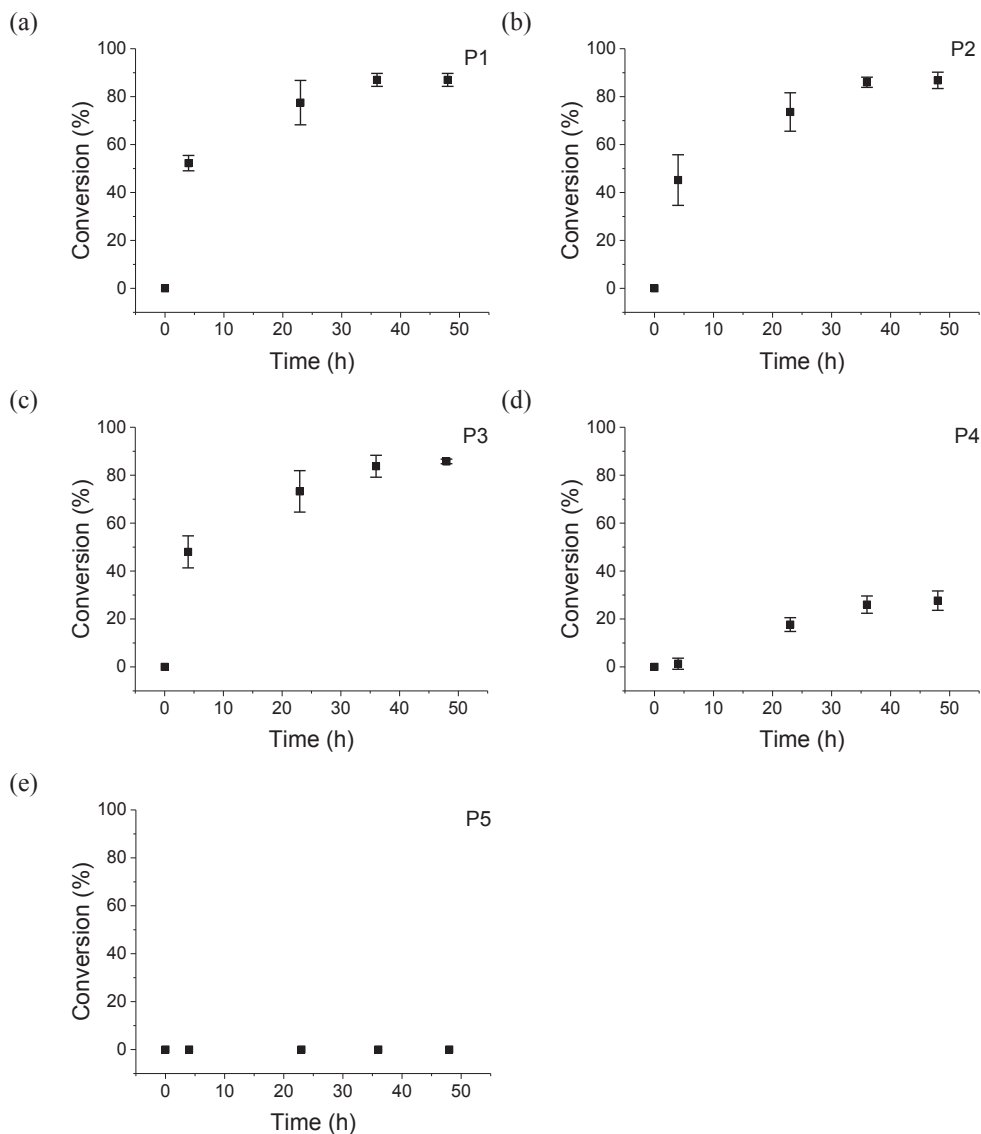
Entry	Code	$D_H^a$ , nm (bare)	$D_H^a$ , nm (Ru loaded)	TOF <sup>b</sup> , h <sup>-1</sup>
1	P1	10.0	8.7	4.4
2	P2	7.5	8.8	4.4
3	P3	8.7	11.6	4.3
4	P4	11.7	10.1; 58.8	1.4
5	P5	8.7	11.6; 32.6	0

(Ru/cyclohexanone/HCOONa): 0.001/0.2/0.5 M in H<sub>2</sub>O at 40 °C). <sup>a</sup>  $c_{polymer} = 18$  mg/mL in H<sub>2</sub>O at 40 °C. <sup>b</sup> TOF = The amount of products (mol)/(The amount of the catalyst active sites (mol) x Time(h)).

These results indicate that in the presence of SDP units, a further stabilization of the hydrophobic pocket *via* BTA self-assembly is not essential for catalytic activity. Almost no difference was observed in the activities between BTA-pendant polymers (**P1@Ru** and **P2@Ru**) and an LMA counterpart (**P3@Ru**) (Table 5.2, entries 1-3). We propose that the pseudo-crosslinking of the SCPN by SDP-Ru(II) coordination sufficiently stabilizes the hydrophobic reaction spaces around the ruthenium complexes to shield and isolate the catalytic centers from the outer environments, thereby leading to efficient catalysis. Considering both the particle size distributions and TOF values with different polymers, it becomes clear that SDP-bearing SCPNs (**P1@Ru-P3@Ru** versus **P4@Ru**) lead to the highest catalytic activity. Non SDP-bearing polymers show aggregation of several chains after the addition of Ru(II), resulting in poor isolation of catalytic sites. This may result in undesired bimetallic interactions as a deactivating factor.<sup>48</sup> It is important to note that the catalysis results are reproducible, judging from the narrow error margins based on three separate catalysis experiments for each polymer, as shown below (Figure 5.7).

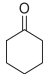
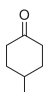
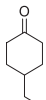
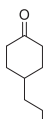
More hydrophobic substrates, 4-methyl-, 4-ethyl- and 4-propyl-cyclohexanone, were also subjected to transfer hydrogenation using **P3@Ru**. All of the substrates were efficiently converted into the corresponding alcohols with TOF values comparably to those of cyclohexanone (Table 5.3). This implies that designed catalytically active SCPNs were compatible with substrates of varying hydrophobicity. An intriguing question to be answered is if and how substrate hydrophobicity affects the catalytic activity of SCPNs and this is extensively studied in Chapter 6.





**Figure 5.7** Conversion vs. time for (a) **P1@Ru**, (b) **P2@Ru**, (c) **P3@Ru**, (d) **P4@Ru**, (e) **P5@Ru**. (Ru/cyclohexanone/HCOONa) = 0.001/0.2/0.5 M H<sub>2</sub>O (40 °C) (18 mg mL<sup>-1</sup> polymer). Three catalysis experiments were averaged in each graph.

**Table 5.3** Results of the transfer hydrogenations of substituted cyclohexanones using **P3@Ru** as the catalysts

Entry	Substrate	Reaction time (h) <sup>a</sup>	Conversion (%)	TOF (h <sup>-1</sup> ) <sup>b</sup>
1		40	98	3.9
2 <sup>c</sup>		40	93	4.2
3 <sup>c</sup>		40	80	3.6
4 <sup>c</sup>		40	90	4.1

<sup>a</sup>  $C_{\text{polymer}} = 18 \text{ mg/mL}$  in  $\text{H}_2\text{O}$  at  $40 \text{ }^\circ\text{C}$ . Reaction conditions:  $\text{Ru/cyclohexanone/HCOONa}$ :  $0.001/0.2/0.5 \text{ M}$ . <sup>b</sup>  $\text{TOF} = \text{The amount of products (mol)}/(\text{The amount of the catalyst active sites (mol)} \times \text{Time(h)})$ . <sup>c</sup> *Cis:trans* ratio was not determined for the products.

### 5.5 Conclusions

In this chapter, a versatile way for the preparation of catalytically active SCPNs was introduced. A set of segmented copolymer ligands with a varying BTAMA content was obtained from RAFT polymerization. Post-loading of ruthenium into the copolymers resulted in catalytically active SCPNs.

To understand the non-covalent, directional role of BTA units in the catalytic efficiency of SCPNs, the transfer hydrogenation of ketones in water was evaluated. The results showed that since the micro environment of the Ru catalyst is already tightly structured by metal-ligand coordination bonds, the structural elements of the remaining pocket is not decisive for catalytic performance as long as a hydrophobic pocket is maintained. Thus, in this particular system BTA stacking does not improve the catalytic activity or SCNP formation. Additionally, it was observed that immobilized Ru(II) by pendant SDP units is more efficient than “free” Ru(II) catalyst due to the efficient isolation of catalytic sites *via* single chain folding.

We expect that gaining a better insight into the essentials of a functioning hydrophobic cavity is a step forward to design compartmentalized systems with enzyme-like activity. For example, in addition to high efficiency in water, enzyme selectivity<sup>49</sup> is another very desirable feature to achieve with synthetic analogues. Finally, it is important to expand the function repertoire of SCPNs, so that tandem reactions as a result of the cooperative action of two or more catalytic cycles can be performed by utilizing SCPNs with different functions in one pot.

## 5.6 Experimental

### 5.6.1 Materials

Polymerizations, catalyst loadings and catalysis experiments were carried out by the syringe technique under dry argon in baked glass tubes equipped with a three-way stopcock. Oligo(ethylene glycol) methyl ether methacrylate (*o*EGMA:  $M_n \approx 475$ ) and lauryl methacrylate (LMA: Aldrich, purity >96%) were of commercial source (Aldrich), purified by an inhibitor removal column (Aldrich) and degassed by reduced pressure before use. The phosphine ligand monomer (diphenylphosphinostyrene: SDP), kindly supplied by Hokko Chemical (purity >99.9%), was degassed by reduced pressure before use. Azobisisobutyronitrile (AIBN) was recrystallized from methanol. 4-Cyano-4-methyl-5-(phenylthio)-5-thioxopentanoic acid was kindly provided by SyMO-Chem (Eindhoven, the Netherlands). Dioxane, dichloromethane, pentane and ethanol (Wako Chemicals, anhydrous; purity > 99%) were bubbled with dry nitrogen before use. 1,2,3,4-Tetrahydronaphthalene (tetralin; internal standard for  $^1\text{H-NMR}$  analysis) was dried over calcium chloride, distilled twice from calcium hydride and bubbled with dry nitrogen before use.  $\text{RuCl}_2(\text{PPh}_3)_3$  (Aldrich, 97%) was used as received and handled in a glove box under a moisture- and oxygen-free argon atmosphere ( $\text{H}_2\text{O} < 1 \text{ ppm}$ ,  $\text{O}_2 < 1 \text{ ppm}$ ). Toluene (passed through purification columns; Solvent Dispensing System; Glass Contour) and hexane were bubbled with dry nitrogen for more than 15 min immediately before use. Sodium formate (Aldrich; purity > 98%) was used as received. Cyclohexanone, 4-methylcyclohexanone, 4-ethylcyclohexanone, 4-propylcyclohexanone (Aldrich, purity >99%) and  $\text{H}_2\text{O}$  (Wako; distilled) were of commercial source and bubbled with dry nitrogen for more than 15 min immediately before use. Nile Red was obtained from Sigma-Aldrich. **P5** was kindly provided by Tim Paffen. The synthesis of chiral BTAMA was performed as described in Chapter 2, based on a statistical Schotten-Baumann reaction of benzene-1,3,5-tricarboxylic acyl chloride with 11-aminoundecanol (obtained from 11-bromoundecanol in a Gabriel synthesis) and (*S*)-3,7-dimethyloctylamine. This latter amine was found to have an enantiomeric excess (*ee*) of 98.4%. BTA alcohol was isolated from the resulting reaction mixture with column chromatography and reacted in a second reaction with methacryloyl chloride to form BTAMA.

### 5.6.2 Characterization

The molecular weight  $M_n$  and  $D$  ratios of the polymers were measured by SEC in DMF containing 10 mM LiBr at 40 °C (flow rate = 1 mL/min) on three linear-type polystyrene gel columns (Shodex KF-805L; exclusion limit =  $4 \times 10^6$ , pore size = 5000 Å, 0.8 cm i.d. x 30 cm) that were connected to a Jasco PU-2080 precision pump, a Jasco RI-2031 refractive index detector, and a Jasco UV-2075 UV-vis detector set at 270 nm. The columns were calibrated against 10 standard PMMA samples (Polymer Laboratories;  $M_n = 1680\text{-}1,200,000$ ,  $D = 1.06\text{-}1.22$ ) as well as MMA monomer. The absolute weight-averaged molecular weight ( $M_w$ ) of polymers was determined by multi-angle laser light scattering (MALLS) in DMF containing 10 mM LiBr on a Dawn E instrument (Wyatt Technology: Ga-As laser;  $\lambda = 690 \text{ nm}$ ; scattering angle covered from 20° to 153°), in conjunction with the following SEC system: three linear-type polystyrene gel columns (shodex KF-805L; exclusion limit =  $4 \times 10^6$ ; pore size = 5000 Å; particle size = 10  $\mu\text{m}$ ; 0.8 cm i.d. x 30 cm) connected to a Jasco PU-2080 precision pump, a Jasco RI-1530 refractive index detector, and a Jasco UV-1570 UV/vis detector set at 270 nm. The refractive index increment

(dn/dc) was directly measured in DMF at 40 °C by the on-line RI-1530 refractive index detector. Fluorescence data were recorded on a Varian Cary Eclipse fluorescence spectrometer.

<sup>1</sup>H-NMR and <sup>31</sup>P-NMR spectra were recorded at room temperature by a JEOL JNM-ECA500 spectrometer (operating at 500 MHz (<sup>1</sup>H) and 202 MHz (<sup>31</sup>P)) or on a Varian Mercury Vx 400 MHz and/or a Varian 400MR 400 MHz (operating at 400 MHz (<sup>1</sup>H)). Proton chemical shifts are reported in ppm downfield from tetramethylsilane (TMS). Diethylphosphite (C<sub>2</sub>H<sub>5</sub>O)<sub>2</sub>P(O)H (12 ppm) was used as a standard for <sup>31</sup>P-NMR.

Ultraviolet-visible (UV/Vis) and circular dichroism (CD) measurements were performed on a Jasco J-815 spectropolarimeter where the sensitivity, time constant and scan rate were chosen appropriately (sensitivity: standard; response: 2 sec; band width: 1 nm; data pitch: 0.1 nm; scanning speed: 20 nm/min). Corresponding temperature-dependent measurements (data pitch: 0.1 °C) were performed with a PFD-425S/15 Peltier-type temperature controller with a temperature range of 263-383 K and adjustable temperature slope. In all cases a temperature slope of 1 K/min was used. In all experiments the linear dichroism was also measured and in all cases no linear dichroism was observed. Separate UV/Vis spectra were obtained from a Perkin-Elmer UV/Vis spectrometer Lambda 40 (optical path length = 0.5 cm). The core-bound Ru(II) content was determined by inductively coupled plasma atomic emission spectroscopy (ICP-AES: CIROS<sup>CCD</sup>; SPECTRO).

Dynamic light scattering measurements were performed on a Malvern μV Zetasizer equipped with a 830 nm laser. Samples were prepared by first dissolving the polymer in MilliQ quality water and then sonicating for 2 hours in a Cole Parmer 8891 sonification bath. Immediately after the sonification, a 0.2 μm PVDF-filter (Whatman) was first washed by filtering MilliQ quality water through and then the polymer solution was filtered in a fluorescence cell, that is washed with filtered MilliQ quality water, with a path length of 10x2 mm and chamber volume of 100 μL. Prepared DLS solutions were measured immediately.

### 5.6.3 Synthesis

#### 5.6.3.1 General Procedure for polymerizations

CTA (12 mg, 0.043 mmol) and, for BTAMA containing copolymers, BTAMA (125 mg, 0.172 mmol (**P1**); 50 mg, 0.344 mmol (**P4**); 250 mg, 0.344 mmol (**P2**)) were placed in a 20 mL glass tube. Dioxane (6.5 mL) was added into the tube and the solution was stirred. *o*EGMA (1.7 mL, 3.75 mmol), for LMA containing polymers, LMA (0.12 mL, 0.42 mmol (**P3**, **P4**), 0.06 mL, 0.21 mmol (**P1**)), AIBN (4.2 mg, 0.026 mmol) and tetralin (0.1 mL) were added sequentially under dry argon at room temperature where the total volume of the polymerization mixture was 8.7 mL. Immediately after mixing, a small portion of the mixture was taken as a blank sample (t = 0) and the polymerization mixture was placed in an oil bath at 70 °C. For SDP containing polymers, SDP (0.35 mL of 730.839 mM in toluene, 0.256 mmol) was added under dry argon to the polymerization mixture after methacrylates reached around 30% conversion by <sup>1</sup>H NMR (1 h). Immediately after the addition of SDP monomer, the temperature was increased to 80 °C. The reaction was terminated after 8 h by cooling the mixture to room temperature (conv. *o*EGMA ≈ 90%; <sup>1</sup>H NMR). The monomer conversion was determined from the concentration of residual monomer measured by <sup>1</sup>H-NMR with tetralin as an internal standard. The quenched reaction solutions were evaporated under vacuum and subsequently dissolved in DCM (1.5 mL) (**P3**, **P4**)

or for BTAMA containing polymers in MeOH/DCM (1/1, v/v, total 1.5 mL) (**P1**, **P2**), and precipitated into cold hexane (11 mL) 3 times, evaporated to dryness and subsequently dried overnight under vacuum at room temperature.

*oEGMA/BTAMA/LMA/SDP copolymer (P1)*

$^1\text{H-NMR}$  ( $\text{CD}_2\text{Cl}_2$ ):  $\delta$  (ppm) = 8.40-8.29 (s, Ar-H: BTAMA), 7.83-7.77 (s, broad, NHCO), 7.62-7.31 (s, broad, Ar-H: SDP=O), 7.31-6.82 (s, broad, Ar-H: SDP), 4.13-3.89 (m,  $\text{CO}_2\text{CH}_2\text{CH}_2$ : *oEGMA*), 3.89-3.66 (m,  $\text{CO}_2\text{CH}_2\text{CH}_2$ : BTAMA, LMA), 3.66-3.43 (s, broad,  $\text{OC}_2\text{H}_4\text{O}$ ), 3.37-3.22 (s, broad, - $\text{OCH}_3$ ), 2.00-1.48 (m,  $\text{CH}_2$  backbone), 1.38-0.70 (m, broad,  $\text{CCH}_3$  backbone, BTAMA and LMA pendants). SEC:  $M_n = 28.3$  kDa,  $D = 1.37$ .

*oEGMA/BTAMA/SDP copolymer (P2)*

$^1\text{H-NMR}$  ( $\text{CD}_2\text{Cl}_2$ ):  $\delta$  (ppm) = 8.40-8.29 (s, Ar-H: BTAMA), 7.83-7.77 (s, broad, NHCO), 7.62-7.31 (s, broad, Ar-H: SDP=O), 7.31-6.82 (s, broad, Ar-H: SDP), 4.13-3.89 (m,  $\text{CO}_2\text{CH}_2\text{CH}_2$ : *oEGMA*), 3.89-3.66 (m,  $\text{CO}_2\text{CH}_2\text{CH}_2$ : BTAMA), 3.66-3.43 (s, broad,  $\text{OC}_2\text{H}_4\text{O}$ ), 3.37-3.22 (s, broad, - $\text{OCH}_3$ ), 2.00-1.48 (m,  $\text{CH}_2$  backbone), 1.38-0.70 (m, broad,  $\text{CCH}_3$  backbone, BTAMA pendant). SEC:  $M_n = 30.3$  kDa,  $D = 1.38$ .

*oEGMA/LMA/SDP copolymer (P3)*

$^1\text{H-NMR}$  ( $\text{CD}_2\text{Cl}_2$ ):  $\delta$  (ppm) = 7.62-7.31 (s, broad, Ar-H: SDP=O), 7.31-6.82 (s, broad, Ar-H: SDP), 4.01 (m,  $\text{OCH}_2\text{CH}_3$ ), 4.13-3.89 (m,  $\text{CO}_2\text{CH}_2\text{CH}_2$ : *oEGMA*), 3.89-3.66 (m,  $\text{CO}_2\text{CH}_2\text{CH}_2$ : LMA), 3.66-3.43 (s, broad,  $\text{OC}_2\text{H}_4\text{O}$ ), 3.37-3.22 (s, broad, - $\text{OCH}_3$ ), 2.00-1.45 (m,  $\text{CH}_2$  backbone), 1.35-0.70 (m, broad,  $\text{CCH}_3$  backbone, LMA pendant). SEC:  $M_n = 30.1$  kDa,  $D = 1.36$ .

*oEGMA/LMA copolymer (P4)*

$^1\text{H-NMR}$  ( $\text{CD}_2\text{Cl}_2$ ):  $\delta$  (ppm) = 4.13-3.89 (m,  $\text{CO}_2\text{CH}_2\text{CH}_2$ : *oEGMA*), 3.89-3.66 (m,  $\text{CO}_2\text{CH}_2\text{CH}_2$ : LMA), 3.66-3.43 (s, broad,  $\text{OC}_2\text{H}_4\text{O}$ ), 3.37-3.22 (s, broad, - $\text{OCH}_3$ ), 2.00-1.45 (m,  $\text{CH}_2$  backbone), 1.45-0.70 (m, broad,  $\text{CCH}_3$  backbone, LMA pendant). SEC:  $M_n = 30.2$  kDa,  $D = 1.23$ .

### 5.6.3.2 General procedure for ruthenium catalyst loading

First, polymer and  $\text{RuCl}_2(\text{PPh}_3)_3$  were solubilized in toluene- $d_8$  under argon, in separate tubes. Then, the Ru(II) solution was transferred *via* the syringe technique into the tube containing 1 mL polymer solution (2 mM in toluene- $d_8$ ) where the ratio was thus 2.5 equivalents of Ru(II) per polymer chain. The resulting mixture was stirred under argon at 80 °C for 12 h, and coordination of Ru(II) to the polymer SDP units was followed by  $^{31}\text{P-NMR}$  and  $^1\text{H-NMR}$ . The polymer solution was concentrated *in vacuo* and precipitated into hexane under argon to remove triphenylphosphine liberated from Ru(II) catalyst. Then, the product was dried *in vacuo* at RT and the Ru(II) amount per polymer gram was analyzed *via* ICP-AES: 53  $\mu\text{mol Ru/g}$  for **P1**, 52  $\mu\text{mol Ru/g}$  for **P2**, 54  $\mu\text{mol Ru/g}$  for **P3**, 43  $\mu\text{mol Ru/g}$  for **P4** and 48  $\mu\text{mol Ru/g}$  for **P5**.

### 5.6.3.3 General procedure for transfer hydrogenations in water

In a 10 mL glass tube, Ru(II)-bearing polymer (Ru = 0.001 mmol, polymer = 0.0004 mmol) and HCOONa (0.452 mmol, 30 mg) was placed and H<sub>2</sub>O (1 mL) was added at 25 °C under argon. The solution was stirred at 80 °C for 5 min and a color change from brown to yellow was observed as an indication of Ru(II)H<sub>2</sub> formation. After cooling, cyclohexanone (0.2 mmol, 0.020 mL) was immediately added into the solution ( $[Ru]/[cyclohexanone] = 1/200$ ), and the mixture was placed in an oil bath.

## 5.7 References

- (1) G. J. ten Brink, I. W. C. E. Arends, R. A. Sheldon *Science* **2000**, 287, 1636.
- (2) K. H. Shaughnessy *Chem. Rev.* **2009**, 109, 643.
- (3) Z. Dong, Q. Luo, J. Liu *Chem. Soc. Rev.* **2012**, 41, 7890.
- (4) M. Dürrenberger, T. Heinisch, Y. M. Wilson, T. Rossel, E. Nogueira, L. Knörr, A. Mutschler, K. Kersten, M. J. Zimbron, J. Pierron, T. Schirmer, T. R. Ward *Angew. Chem. Int. Ed.* **2011**, 50, 3026.
- (5) J. Collot, J. Gradinaru, N. Humbert, M. Skander, A. Zocchi, T. R. Ward *J. Am. Chem. Soc.* **2003**, 125, 9030.
- (6) M. T. Reetz, M. Rentzsch, A. Pletsch, M. Maywald, P. Maiwald, J. J. -P. Peyralans, A. Maichele, Y. Fu, N. Jiao, F. Hollmann, R. Mondière, A. Taglieber *Tetrahedron* **2007**, 63, 6404.
- (7) A. J. Boersma, J. E. Klijn, B. L. Feringa, G. Roelfes *J. Am. Chem. Soc.* **2008**, 130, 11783.
- (8) B. M. Rossbach, K. Leopold, R. Weberskirch *Angew. Chem.* **2006**, 118, 1331.
- (9) B. M. Rossbach, K. Leopold, R. Weberskirch *Angew. Chem. Int. Ed.* **2006**, 45, 1309.
- (10) I. Okhupkin; E. Makhaeva; A. Khokhlov, in *Conformation-Dependent Design of Sequences in Copolymers I* (Ed. A. R. Khokhlov), Springer, Berlin Heidelberg, **2006**, 145, pp 177.
- (11) A. W. Bosman, R. Vestberg, A. Heumann, J. M. J. Fréchet, C. J. Hawker *J. Am. Chem. Soc.* **2003**, 125, 715.
- (12) T. Terashima, M. Kamigaito, K. Y. Baek, T. Ando, M. Sawamoto *J. Am. Chem. Soc.* **2003**, 125, 5288.
- (13) T. Terashima, M. Ouchi, T. Ando, M. Sawamoto *J. Polym. Sci. Part A: Polym. Chem.* **2010**, 48, 373.
- (14) B. Helms, S. J. Guillaudeu, Y. Xie, M. McMurdo, C. J. Hawker, J. M. J. Fréchet *Angew. Chem. Int. Ed.* **2005**, 44, 6384.
- (15) Y. Chi, S. T. Scroggins, J. M. J. Fréchet *J. Am. Chem. Soc.* **2008**, 130, 6322.
- (16) K. T. Kim, J. J. L. M. Cornelissen, R. J. M. Nolte, J. C. M. van Hest *Adv. Mater.* **2009**, 21, 2787.
- (17) T.-H. Ku, M.-P. Chien, M. P. Thompson, R. S. Sinkovits, N. H. Olson, T. S. Baker, N. C. Gianneschi *J. Am. Chem. Soc.* **2011**, 133, 8392.
- (18) A. D. Ievins, X. Wang, A. O. Moughton, J. Skey, R. K. O'Reilly *Macromolecules* **2008**, 41, 2998.
- (19) A. C. Evans, A. Lu, C. Ondeck, D. A. Longbottom, R. K. O'Reilly *Macromolecules* **2010**, 43, 6374.
- (20) P. Cotanda, A. Lu, J. P. Patterson, N. Petzetakis, R. K. O'Reilly *Macromolecules* **2012**, 45, 2377.

- (21) S. Striegler, J. D. Barnett, N. A. Dunaway *ACS Catal.* **2012**, *2*, 50.
- (22) Z. Chen, Z. Hua, J. Wang, Y. Guan, M. Zhao, Y. Li *Appl. Catal. A* **2007**, *328*, 252.
- (23) G. Wulff, B.-O. Chong, U. Kolb *Angew. Chem. Int. Ed.* **2006**, *45*, 2955.
- (24) A. W. Bosman, H. M. Janssen, E. W. Meijer *Chem. Rev.* **1999**, *99*, 1665.
- (25) S. M. Grayson, J. M. J. Fréchet *Chem. Rev.* **2001**, *101*, 3819.
- (26) B. Helms, J. M. J. Fréchet, *Adv. Synth. Catal.* **2006**, *348*, 1125.
- (27) B. Helms, E. W. Meijer *Science* **2006**, *313*, 929.
- (28) J. Yu, T. V. RajanBabu, J. R. Parquette *J. Am. Chem. Soc.* **2008**, *130*, 7845.
- (29) A. Sanchez-Sanchez, A. A. J. Colmenero, J. A. Pomposo *ACS Macro Lett.* **2014**, *3*, 439.
- (30) J. Willenbacher, O. Altintas, V. Trouillet, N. Knöfel, M. J. Monteiro, P. W. Roesky, C. Barner-Kowollik *Polym. Chem.* **2015**, *6*, 4358.
- (31) S. Mavila, I. Rozenberg, N. G. Lemcoff *Chem. Sci.* **2014**, *5*, 4196.
- (32) M. A. J. Gillissen, T. Terashima, E. W. Meijer, A. R. A. Palmans, I. K. Voets *Macromolecules* **2013**, *46*, 4120.
- (33) E. A. Appel, J. Dyson, J. del Barrio, Z. Walsh, O. A. Scherman *Angew. Chem. Int. Ed.* **2012**, *51*, 4185.
- (34) T. Terashima, T. Mes, T. F. A. De Greef, M. A. J. Gillissen, P. Besenius, A. R. A. Palmans, E. W. Meijer *J. Am. Chem. Soc.* **2011**, *133*, 4742.
- (35) A. Sanchez-Sanchez, I. Pérez-Baena, J. Pomposo *Molecules* **2013**, *18*, 3339.
- (36) E. Huerta, P. J. M. Stals, E. W. Meijer, A. R. A. Palmans *Angew. Chem. Int. Ed.* **2013**, *52*, 2906.
- (37) R. Rarikowitz, R. Marcus, J. Pellon *J. Polym. Sci. Part A: Polym. Chem.* **1964**, *2*, 1241.
- (38) A. F. Cardozo, E. Manoury, C. Julcour, J-F. Blanco, H. Delmas, F. Gayeta, R. Poli *Dalton Trans.* **2013**, *42*, 9148.
- (39) A. F. Cardozo, E. Manoury, C. Julcour, J-F. Blanco, H. Delmas, F. Gayet, R. Poli *ChemCatChem* **2013**, *5*, 1161.
- (40) T. Mes, R. van der Weegen, A. R. A. Palmans, E. W. Meijer *Angew. Chem. Int. Ed.* **2011**, *50*, 5085.
- (41) M. M. J. Smulders, I. A. W. Filot, J. M. A. Leenders, P. van der Schoot, A. R. A. Palmans, A. P. H. J. Schenning, E. W. Meijer *J. Am. Chem. Soc.* **2010**, *132*, 611.
- (42) M. M. J. Smulders, M. M. L. Nieuwenhuizen, M. Grossman, I. A. W. Filot, C. C. Lee, T. F. A. de Greef, A. P. H. J. Schenning, A. R. A. Palmans, E. W. Meijer *Macromolecules* **2011**, *44*, 6581.
- (43) P. J. M. Stals, J. C. Everts, R. de Bruijn, I. A. W. Filot, M. M. J. Smulders, R. Martin-Rapun, E. A. Pidko, T. F. A. de Greef, A. R. A. Palmans, E. W. Meijer *Chem. Eur. J.* **2010**, *16*, 810.
- (44) Y. Nakano, T. Hirose, P. J. M. Stals, E. W. Meijer, A. R. A. Palmans *Chem. Sci.* **2012**, *3*, 148.
- (45) C. M. A. Leenders, L. Albertazzi, T. Mes, M. M. E. Koenigs, A. R. A. Palmans, E. W. Meijer *Chem. Commun.* **2013**, *49*, 1963.
- (46) C. B. Minkenberg, L. Florusse, R. Eelkema, G. J. M. Koper, J. H. van Esch *J. Am. Chem. Soc.* **2009**, *131*, 11274.
- (47) C. B. Minkenberg, F. Li, P. van Rijn, L. Florusse, J. Boekhoven, M. C. A. Stuart, G. J. M. Koper, R. Eelkema, J. H. van Esch *Angew. Chem. Int. Ed.* **2011**, *50*, 3421.

- (48) N. Madhavan, C. W. Jones, M. Weck *Acc. Chem. Res.* **2008**, *41*, 1153.  
(49) M. Garcia-Viloca, J. Gao, M. Karplus, D. G. Truhlar *Science* **2004**, *303*, 186.





# Chapter 6

## *Single chain polymeric nanoparticles as selective hydrophobic reaction spaces in water*

**Abstract:** *Herein, a Ru(II)-based catalyst trapped within an amphiphilic, folded polymer is employed for the oxidation of secondary alcohols to their corresponding ketones using tert-butyl hydroperoxide (tBuOOH) as the oxidant. Under the applied catalytic conditions, the polymer catalyst forms a compartmentalized structure with a hydrophobic interior. We selected secondary alcohols that differ in hydrophobicity, reactivity, and steric hindrance as substrates, with the aim to elucidate how this affects the rate and the end conversion of the oxidation reaction. Our investigations show that the Ru(II)-based catalyst is very efficient for oxidation reactions in water. Moreover, high selectivity toward the more hydrophobic substrate is observed, which originates from the hydrophobic interior of the compartmentalized catalyst system. This hydrophobic selectivity is also observed in the reverse reaction, the transfer hydrogenation. Finally, the applicability of these compartmentalized systems was explored for cascade catalytic reactions, i.e. reactions in which the product of the first step is the substrate for the next. The compatibility of a one-pot aldol condensation followed by an oxidation sequence was investigated as an example. A mixture of L-proline and Ru(II) bearing amphiphilic polymers was inactive in the aldol reaction, most probably due to the deactivating effect of Ru ligation on the L-proline units. In contrast, L-proline functionalized polymer remained active in the aldol step of the cascade sequence in the presence of a 2,2,6,6-tetramethylpiperidinoxyl (TEMPO) functionalized amphiphilic polymer as the oxidation catalyst. This revealed the importance of a metal-free approach for future studies on cascade systems wherein L-proline bearing single-chain polymeric nanoparticles are applied.*

*Part of this work has been published:*

M. Artar, E. R. J. Souren, T. Terashima, E. W. Meijer, A. R. A. Palmans *ACS Macro Lett.* **2015**, *4*, 1099.

## 6.1 Introduction

The design of systems that perform catalysis in a highly selective manner has attracted considerable attention, not only out of academic interest, but also owing to their potential in industrial applications.<sup>1-4</sup> Enzymes achieve selective and efficient catalysis *via* a combination of hydrophilic/hydrophobic domains, in combination with size, shape and charge recognition mechanisms at the active sites.<sup>5-7</sup> In search for synthetic approaches to achieve enzyme-like selectivity and activity in catalytic conversions, hydrophobic effects such as in cross-linked nanoparticles,<sup>8</sup> micellar structures,<sup>9-11</sup> hydrogels,<sup>12-14</sup> star polymers,<sup>15</sup> and polymersomes,<sup>16</sup> as well as hydrophobic reagents,<sup>17</sup> and size effects,<sup>18</sup> have been explored. In addition to these, single chain technology,<sup>19</sup> the transformation of an individual polymer chain into a folded/collapsed nanoparticle, has been evaluated to create active and selective catalysis in organic media<sup>20</sup> and in water.<sup>21</sup> The advantage of this approach is the easy access to compartmentalized, well-defined, unimolecular nanoreactors of nanometer-size, affording homogenous catalysis solutions. Notably, the supramolecular folding of polymer chains into single chain polymeric nanoparticles (SCPNS), in which a dynamic and adaptive reaction compartment is created, has resulted in efficient catalysis in water. In contrast to the rather dense and kinetically frozen hydrophobic compartments usually applied, these dynamic SCPNS possess a compact yet responsive structure.<sup>20,22</sup> The activity results from the formation of a hydrophobic interior *via* either benzene-1,3,5-tricarboxamide (BTA) self-assembly, resulting in a chiral, structured inner compartment, and/or by diphenylphosphine styrene (SDP) complexation with Ru(II), respectively.<sup>21</sup> This results in the shielding of the catalyst from the aqueous environment. The SCPN approach is an attractive alternative for preparing compartmentalized, water-soluble, nanometer-sized particles with a hydrophobic interior, providing reaction spaces for efficient aldol reactions and, as discussed in Chapter 5, transfer hydrogenations.

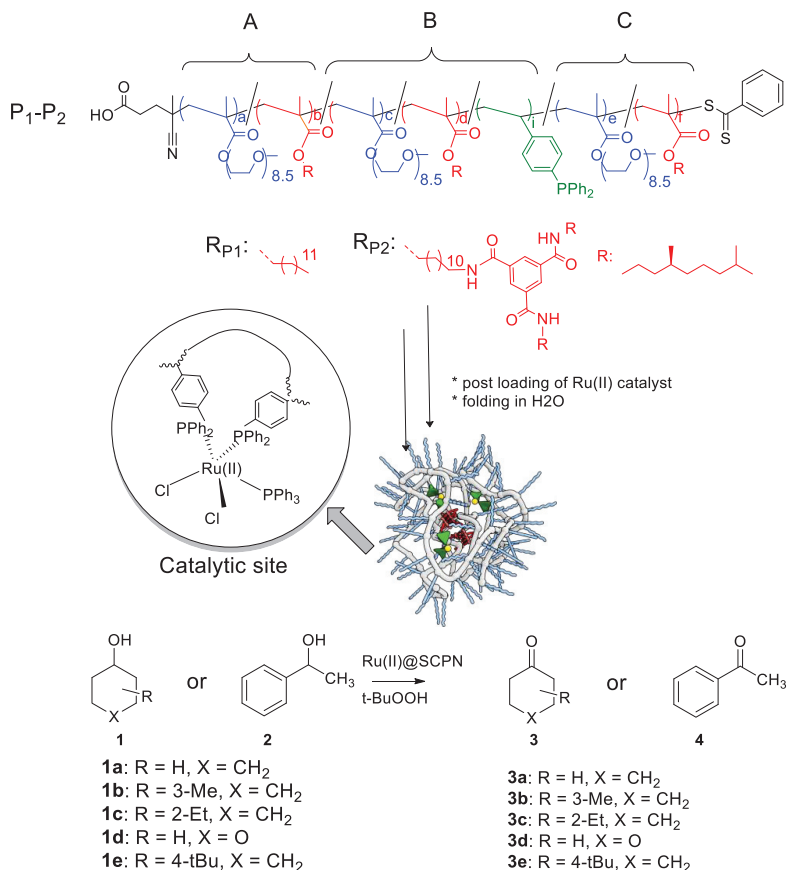
Herein, we employ the amphiphilic polymers, used in Chapter 5 in the transfer hydrogenation of ketones, that fold around a Ru(II) catalyst to create a selective environment around an intrinsically non-selective active center.<sup>21a,c</sup> It is important to achieve the folding of one single polymer chain into one SCPN, because this permits access to well-defined hydrophobic reaction spaces in which hydrophobic substrates can accumulate and catalysts that normally only function in organic media can still operate. We select lauryl-based polymer **P1** that forms a compartmentalized structure due to hydrophobic interactions<sup>23</sup> and BTA-based polymer **P2** that folds as a result of hydrophobic interactions in combination with directional hydrogen-bonding interactions (Scheme 6.1).<sup>21a</sup>

By applying Ru(II)@SCPNS in the presence of the oxidant *tert*-butyl hydroperoxide (*t*BuOOH), a uniquely active and remarkably selective catalyst is formed for oxidation reactions in water. Here, the results of the oxidation in water, at room temperature, of a set of cyclic, secondary alcohols that differ in hydrophobicity, reactivity and steric hindrance around the alcohol function is shown. In addition, the potential of SCPNS as a general concept for compartmentalized nano-reactors for selective catalysis is highlighted.

## 6.2 SCPN catalyzed oxidations

### 6.2.1 Polymer design and synthesis

Methacrylate-based amphiphilic terpolymers **P1** and **P2** (Scheme 6.1) with a degree of polymerization (*DP*) of 150 were prepared by RAFT polymerization of oligo(ethylene glycol) methyl ether methacrylate (*o*EGMA), ligand diphosphinostyrene (SDP) and hydrophobic lauryl methacrylate (LMA) or chiral (*S*) benzene-1,3,5-tricarboxamide-based methacrylate (BTAMA), respectively, following procedures outlined in Chapter 5 (Table 6.1).<sup>21c</sup> SEC traces of **P1** and **P2** (relative to PEO standards) showed unimodal peaks (Figure 6.1), and molecular weights around 14 kDa with molar mass distributions (*M*) below 1.4 (Table 6.1). To procure a catalytically active polymer, **P1** and **P2** were loaded with RuCl<sub>2</sub>(PPh<sub>3</sub>)<sub>2</sub> (Ru(II)), using a post-encapsulation approach to create catalytic centers, as applied in Chapter 5.<sup>21c</sup> The exchange of the phosphines of Ru(II)(PPh<sub>3</sub>)<sub>2</sub>Cl<sub>2</sub> with those of the phosphines attached to the polymer backbone was monitored by <sup>31</sup>P-NMR, as demonstrated in Chapter 5 in detail, which revealed a quantitative immobilization of the Ru-catalyst on the polymer. Thus, **P1** and **P2** comprised 2-3 Ru per polymer chain.



**Scheme 6.1** Design of catalytically active SCPNs for the oxidation of alcohols in water, and chemical structures of the substrates and products

**Table 6.1** Characterization of **P1** and **P2**

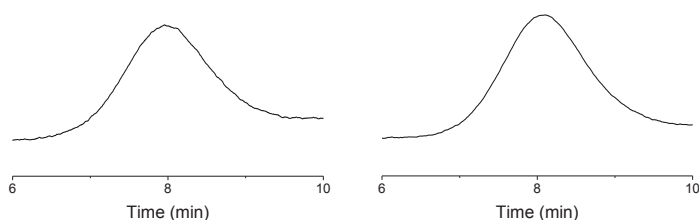
Polymer composition	DP <sub>0</sub> <sup>a</sup> (g/h/i)	M <sub>n</sub> <sup>b</sup> (kDa)	DP <sub>calc</sub> <sup>c</sup> (g/h/i)	M <sub>n,calc</sub> <sup>d</sup> (kDa)	Đ <sup>b</sup>
P1 (LMA/oEGMA/SDP)	14/128/8	13.8	14/110/8	58	1.4
P2 (BTAMA/oEGMA/SDP)	14/128/8	14.5	10/110/8	62	1.4

<sup>a</sup> Degree of polymerization (DP<sub>0</sub>): g = for LMA polymer : [LMA]<sub>0</sub>/[CTA]<sub>0</sub> for BTAMA polymer: [BTAMA]<sub>0</sub>/[CTA]<sub>0</sub>; h = [oEGMA]<sub>0</sub>/[CTA]<sub>0</sub>; i = [SDP]<sub>0</sub>/[CTA]<sub>0</sub>;

<sup>b</sup> Analyzed by SEC in DMF (10 mM LiBr) with poly(ethylene glycol) standard; Đ = M<sub>w</sub>/M<sub>n</sub>.

<sup>c</sup> DP<sub>calc</sub>: g = for LMA polymer: [LMA]<sub>0</sub> × conversion / [CTA]<sub>0</sub> for BTAMA polymer: [BTAMA]<sub>0</sub> × conversion / [CTA]<sub>0</sub>; h = [oEGMA]<sub>0</sub> × conversion / [CTA]<sub>0</sub>; i = [SDP]<sub>0</sub> × conversion / [CTA]<sub>0</sub>; Conversion is determined by <sup>1</sup>H-NMR at RT in CDCl<sub>3</sub>.

<sup>d</sup> M<sub>n,calc</sub> = Σ(FW<sub>monomer</sub> × DP<sub>calc</sub>) + FW<sub>CTA</sub>

**Figure 6.1** SEC-GPC traces of **P1** (left) and **P2** (right).

The amphiphilic polymers and their corresponding catalysts were further characterized with dynamic light scattering (DLS) (Figure 6.2) and circular dichroism (CD) for **P2** (Figure 6.3). SEC measurements were not possible after Ru loading because of strong interactions of the polymers with the column. After the formation of the catalyst complex, the single chain character was preserved in both polymers, as revealed by DLS, while CD experiments showed that **P2** comprised a structured, chiral inner compartment as a result of helical BTA stacking.<sup>21</sup> The sign and the magnitude of the CD effect accords with earlier observations.<sup>21</sup> Moreover, the pseudo-crosslinking of the middle segment *via* the complexation of Ru(II) and the SDP ligands does not alter the magnitude of the Cotton effect (Figure 6.3), indicating that Ru(II)-SDP complexes do not significantly affect BTA aggregation and as a result, these two forces act in an orthogonal way similar to the observations in Chapter 5.

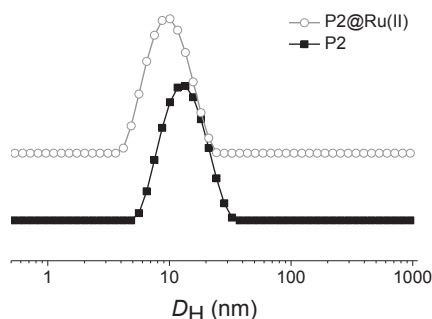


**Figure 6.2.** DLS intensity distribution for BTAMA containing polymer **P2** before loading and **P2@Ru(II)** after catalyst loading.

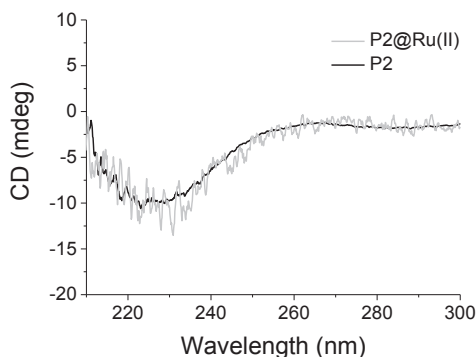


**Figure 6.3.** CD spectra in  $H_2O$  of **P2** and **P2@Ru(II)** wavelength scan at  $40\text{ }^\circ\text{C}$  ( $[BTA]=25\text{ }\mu\text{M}$ )

### 6.2.2 Oxidation reactions

The catalytic activity of the **P1@Ru(II)** catalyst, lacking the structuring BTA units, was evaluated for the oxidation of cyclohexanol (**1a**) to cyclohexanone (**3a**). The reaction was performed in the presence of *t*BuOOH, a highly efficient oxidant at room temperature compared to other oxygen sources.<sup>24</sup> Samples were taken during the course of the reactions, quenched with sodium metabisulfite and directly analyzed with GC-MS (Figure 6.4). The conversion versus time plot showed a fast reaction and after 12 min the conversion levels off at 93% (Figure 6.4, right). The turnover frequency (TOF, mol substrate reacted per mol catalyst per hour) was  $171\text{ h}^{-1}$  (Table 6.2, entry 1). The GC trace showed that no side products are formed during the oxidation reaction. In addition, the color of the catalysis mixture changed from yellow/orange to dark purple after addition of the *t*BuOOH (Figure 6.6a). This was due to the change in oxidation state of the ruthenium from Ru(II) to Ru(IV). Moreover, the mixture remained homogeneous and kept its purple color throughout the reaction, indicating that the catalyst remained active. Polymer **P2**,

comprising a structured, chiral inner compartment, showed a similar result as **P1** (Table 6.2, entry 2).

Control reactions were performed in which either **P1@Ru(II)** or Ru were not added to the reaction mixture. In these cases, no conversion was observed (Table 6.2, entries 3-7). The oxidation of 1-phenylethanol (**2**), a highly reactive and broadly studied substrate, to acetophenone (**4**) was also evaluated using **P1@Ru(II)**. The oxidation of **2** was faster compared to that of **1a**, and complete conversion was reached in 4 min (Table 6.2, entry 8).

The oxidations of both cyclohexanol (**1a**, Table 6.2, entry 1) and 1-phenyl ethanol (**2**) proceeded very fast and to high conversions, 93 and > 99%, respectively. The lack of full conversion for cyclohexanol was intriguing and we anticipated, based on previous literature results.<sup>11,12</sup> that this could be related to a different log *P* value, a well-known quantity to assess the relative hydrophobicities/hydrophilicities of organic compounds. To test this, we investigated a more hydrophilic derivative, 4-tetrahydropyranol (**1d**). Interestingly, a final conversion of 54% was obtained after 15 min, corresponding to a TOF of 86 h<sup>-1</sup> (Table 6.2, entry 9). This increase in hydrophilicity of the substrate resulted in a decrease of both the rate (TOF) and the final conversion of the substrate.<sup>27</sup> On the other hand, more hydrophobic 3-methylcyclohexanol (**1b**) and 2-ethylcyclohexanol (**1c**) were converted to > 99% conversion within 15 min, corresponding to a TOF of 184 and 480 h<sup>-1</sup>, respectively (Table 6.2, entries 10,11; Figure 6.5).

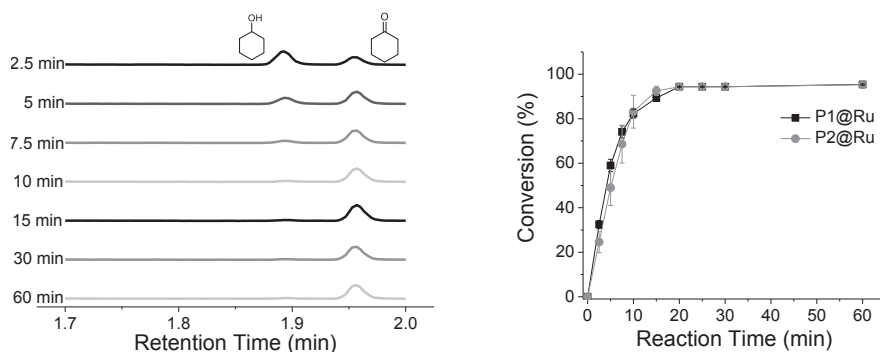


**Figure 6.4** GC spectra of the crude, quenched reaction mixture taken at different times for determining the conversion of cyclohexanol to cyclohexanone (left); Conversion of **1a** as a function of time using **P1@Ru(II)** or **P2@Ru(II)**. Results of three catalysis experiments were averaged for each data point (right). Conditions: Ru/cyclohexanol/*t*-BuOOH = 0.001/0.04/0.2 M in H<sub>2</sub>O at room temperature; *C*<sub>polymer</sub> = 18 mg mL<sup>-1</sup>.

Alcohols **1b** and **1c** were also evaluated with **P2@Ru(II)** that has a partially chiral hydrophobic inner space in order to examine if any enantioselectivity was involved in the catalysis. No enantioselectivity was observed in the oxidation of **1b** and **1c** as evidenced by the similar intensities of the GC traces for stereoisomers of both ketones **3b** and **3c** (Figure 6.5). The lack of enantioselectivity in SCPN@Ru(II) catalyzed oxidations is in line with the report of Terashima *et al* on the transfer hydrogenation of acetophenone.<sup>21a</sup> This is most probably because

the chiral BTA stacks were not close enough to catalytic centers to relay chiral information to achieve a preference for one stereoisomer.

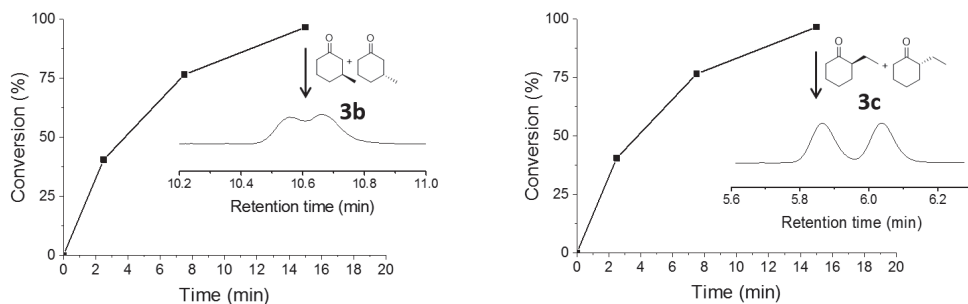


**Figure 6.5.** Conversion profiles of **1b** (left) and **1c** (right) as a function of time with GC (chiral column) spectra of the crude, quenched reaction mixture using **P2@Ru(II)** as catalyst. Conditions: **Ru/1b** or **1c**/**BuOOH** = 0.001/0.04/0.2 M in  $\text{H}_2\text{O}$  at room temperature;  $c_{\text{polymer}} = 18 \text{ mg mL}^{-1}$ .

### 6.3 Competition experiments

#### 6.3.1 Oxidation reactions

The results shown in Table 6.2, higher TOF and higher conversions for more hydrophobic substrates, suggest that there is a hydrophobic selectivity of the SCPN@Ru(II) system. Therefore, we performed a competition experiment by applying a 1:1:1 mixture of three substrates, 4-*tert*-butylcyclohexanol (**1e**), **1d** and **1a**.<sup>28</sup> The log *P* values of these substrates differ significantly (Table 6.2). To assess that the chemical reactivity of the alcohols is similar, the competition experiment of the three substrates was also performed in acetone, using  $\text{Ru(II)(PPh}_3)_2\text{Cl}_2$  as the catalyst. Also, **P1@Ru(II)** was used in acetone in which the hydrophilic/hydrophobic phase separation that creates the driving force for selective accumulation of the substrates, is absent. Finally, the influence of a structured inner compartment on the reaction rates was assessed by comparing **P1@Ru(II)** with **P2@Ru(II)**.

In acetone, all three substrates were converted at the same rate, reaching a final conversion of 25% for  $\text{Ru(II)(PPh}_3)_3\text{Cl}_2$  (Table 6.2, entry 12) and 28-30% for **P1@Ru(II)** (Table 6.2, entry 13). Thus, the chemical reactivity of the three substrates is identical, and selectivity is absent in the absence of a hydrophobic effect. The low end conversion is due to the applied conditions that are identical to the catalysis in water in the presence of SCPN@Ru(II). Previously, a higher end conversion (82%) was reported for the oxidation of cyclohexanol, but, for higher catalyst and oxidant concentrations.<sup>24</sup> In contrast, both the rate and the final conversion of the three substrates differ significantly when **P1@Ru(II)** is used as catalyst in water (Figure 6.6b). Furthermore, **1e** showed the fastest reaction rate while **1d** showed the slowest reaction rate. In addition, the conversion profiles for the three substrates were very similar for both catalysts, **P1@Ru(II)** and **P2@Ru(II)** (Table 6.2, entry 14,15). It is important to note that the oxidations of mixtures **1a/1d** (93%/50%) (Table 6.2, entry 16) and **1a/1e** (60%/>99%) (Table 6.2, entry 17) showed similar rates and almost identical end conversions compared with the oxidation of the mixture of



**1a/1d/1e** mixture. This implies that substrates are converted simultaneously rather than sequentially. In addition, the catalyst remained active, despite the incomplete conversions of **1a** and **1d** as confirmed by a control reaction (Table 6.2, entry 18). Plotting the TOF as a function of the log *P* of the three substrates **1a**, **1d**, and **1e** reveals a remarkable correlation between their log *P* values and their reaction rate in water, which is absent in acetone (Figure 6.6c). This suggests that the hydrophobicity of the substrates plays a crucial role in the rate of the oxidation, and that there is selectivity of the compartmentalized catalyst for more apolar substrates.

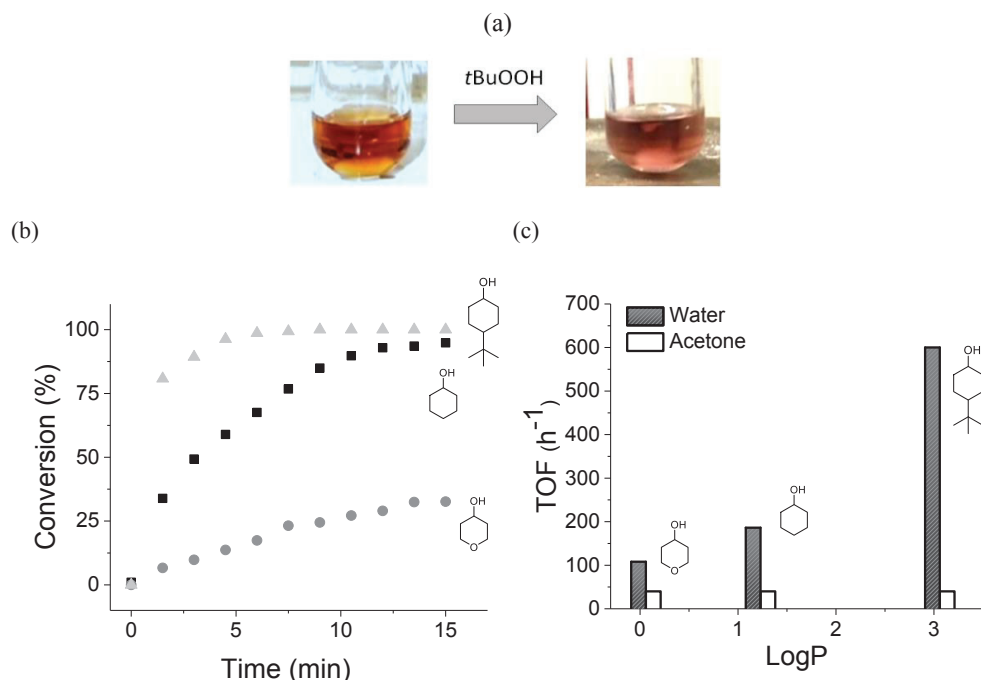


**Figure 6.6** (a) Catalysis mixture before and after the oxidant addition. (b) Conversion as a function of time of alcohols in the oxidation using **PI**@Ru(II) as the catalyst in a competition experiment in water. (c) TOF vs. log *P* comparison in competition experiment using **PI**@Ru(II) in water (filled blocks) and Ru(II)Cl<sub>2</sub>(PPh<sub>3</sub>)<sub>3</sub> without **PI** in acetone (empty blocks). Reaction conditions: Ru/**1a/1d/1e**/*t*-BuOOH = 0.001/0.0133/0.0133/0.0133/0.2 M (17 mg/mL **PI**).

**Table 6.2** Oxidation of secondary alcohols in water with a SCPN system and Ru(II)-based catalyst <sup>a,j</sup>

Entry	Substrate	Polymer	Ru/substrate/oxidant(m M)	Conversion (%) (t (min)) <sup>b</sup>	TOF <sup>l</sup> (h <sup>-1</sup> )	log P <sup>e,f</sup>
1		P1	1/40/200	93 (13)	171	
2		P2	1/40/200	93 (13)	171	
3		P1	1/40/----	0 (60)	0	
4	1a	P1	---/40/200	0 (60)	0	1.23 <sup>e</sup>
5		P1	-/40/-	0 (60)	0	
6		-	-/40/200	0 (60)	0	
7		-	1/40/200	nd <sup>d</sup> (60)	nd <sup>d</sup>	
8	2	P1	1/40/200	>99 (4)	600	1.42 <sup>e</sup>
9	1d	P1	1/40/200	50 (14)	86	0.06 <sup>f</sup>
10	1b	P2	1/40/200	>99 <sup>c</sup> (13)	184	1.59 <sup>f</sup>
11	1c	P2	1/40/200	>99 <sup>c</sup> (5)	480	2.33 <sup>f</sup>
	1a			25(60)	40	1.23 <sup>e</sup>
12	1d	-	1/40 <sup>g</sup> /200	25(60)	40	0.06 <sup>f</sup>
	1e			25(60)	40	3.06 <sup>e, g, h</sup>
	1a			28(60)	45	1.23 <sup>e</sup>
13 <sup>m</sup>	1d	P2	1/40 <sup>g</sup> /200	30(60)	48	0.06 <sup>f</sup>
	1e			28(60)	45	3.06 <sup>e, g, h</sup>
	1a			70 (4), 93 (12) <sup>i</sup>	186	1.23 <sup>e</sup>
14	1d	P1	1/40 <sup>g</sup> /200	20 (4), 54 (12) <sup>i</sup>	108	0.06 <sup>f</sup>
	1e			>99 (4) <sup>i</sup>	600	3.06 <sup>e, g, h</sup>
	1a			67 (4), (94) (12) <sup>g</sup>	166	1.23 <sup>e</sup>
15	1d	P2	1/40 <sup>e</sup> /200	23 (4), 48 (12) <sup>g</sup>	97	0.06 <sup>f</sup>
	1e			>99 (4) <sup>g</sup>	600	3.06 <sup>e, g, h</sup>
	1a			93 (12) <sup>g</sup>	166 <sup>g</sup>	1.23 <sup>e</sup>
16	1d	P1	1/40 <sup>e</sup> /200	50 (12) <sup>g</sup>	97 <sup>g</sup>	0.06 <sup>d</sup>
	1e			>99 (12) <sup>g</sup>	166 <sup>g</sup>	3.06 <sup>e, g, h</sup>
17	1d	P1	1/40 <sup>e</sup> /200	60 (12) <sup>g</sup>	97 <sup>g</sup>	1.23 <sup>e</sup>
	1d			40 (18) <sup>g</sup>		0.06 <sup>f</sup>
18	1a	P1	1/40+40 <sup>k</sup> /200	40 (30) <sup>g</sup>	97 <sup>g</sup>	1.23 <sup>e</sup>

<sup>a</sup> Reactions in entries 1–5, 8–11 and 14–17 were performed with a polymer concentration of 18 mg mL<sup>-1</sup> at room temperature in water; <sup>b</sup> the conversion was determined using GC; <sup>c</sup> no enantioselectivity was observed in the oxidation (Figure 5); <sup>d</sup> nd = not determined, due to insolubility of RuCl<sub>2</sub>(PPh<sub>3</sub>)<sub>3</sub> in H<sub>2</sub>O; <sup>e</sup> experimentally determined log P values<sup>24</sup>; <sup>f</sup> calculated log P values by Molinspiration software<sup>25</sup>; <sup>g</sup> molar ratio **1a:1d:1e** = 1:1:1; <sup>h</sup> the log P values for the cis and trans products were averaged; <sup>i</sup> final conversions; <sup>j</sup> the reaction of entry 12 was performed in the presence of RuCl<sub>2</sub>(PPh<sub>3</sub>)<sub>3</sub> (without polymer) at RT in acetone; <sup>k</sup> **1a** was added after the maximum conversion of **1d(1a:1d (1:1))**; <sup>l</sup> TOF (h<sup>-1</sup>) = [Mol<sub>substrate</sub> × (Final conversion/100)] / [Mol<sub>catalyst</sub> / (t<sub>min</sub>/60)]. <sup>m</sup> The reaction in entry 13 was performed with a polymer concentration of 18 mg mL<sup>-1</sup> at room temperature in acetone.

### 6.3.2 Transfer hydrogenations reactions

To assess the reaction scope of the selectivity for more hydrophobic substrates of the compartmentalized catalysts, a 1:1:1 mixture of the ketones **3d**, **3a** and **3e** was evaluated in the reverse reaction, in the transfer hydrogenation (Table 6.3) to secondary alcohols **1a**, **1d** and **1e**. Gratifyingly, this reaction showed an almost identical selectivity towards the more hydrophobic ketone (conversion **3d/3a/3e** = 30%/70%/>99%, Table 6.3). This indicates that the origin of selectivity is the presence of a hydrophobic reaction space. In addition, this demonstrates the wider applicability of the designed hydrophobic pocket for selective catalysis in aqueous environments.

**Table 6.3.** Results of the transfer hydrogenation of secondary ketones in water<sup>a</sup>

Entries	Substrate	Polymer	Ru/substrate/HCOONa (mM)	Conversion <sup>b</sup> (%) (t (h))	TOF (h <sup>-1</sup> )	log P <sup>c,d</sup>
1	<b>3a</b>	P1	1/40 <sup>e</sup> /200	70 (25) <sup>g</sup>	166	1.23 <sup>c</sup>
	<b>3d</b>			30 (25) <sup>g</sup>	97	0.06 <sup>d</sup>
2	<b>3a</b>	P1	1/40 <sup>e</sup> /200	70 (25) <sup>g</sup>	166	1.23 <sup>c</sup>
	<b>3d</b>			30 (25) <sup>g</sup>	97	0.06 <sup>d</sup>
	<b>3e</b>			>99 (25) <sup>g</sup>	533	3.06 <sup>c,f</sup>

<sup>a</sup> Reactions were performed with a polymer concentration of 18 mg/mL at room temperature in water; <sup>b</sup> the conversion was determined using GC; <sup>c</sup> experimental log P values; <sup>d</sup> Computational log P values determined by online Molinspiration software; <sup>e</sup> **1a:1d** (1:1), **1d:1e** (1:1); <sup>f</sup> a log P of 3.06 is used as being the average of 3.02 (for *cis*) and 3.09 (for *trans*) since **1e** is a mixture *cis* and *trans*; <sup>g</sup> final conversions.

### 6.3.3 The origin of the observed selectivity

Although our SCPN@Ru(II) system in water is slower than recently reported highly active, cationic, water-soluble Ru-complexes,<sup>29</sup> it is much faster and more efficient than the original, non-immobilized RuCl<sub>2</sub>(PPh<sub>3</sub>)<sub>3</sub> catalyst.<sup>30</sup> In addition, our system is highly selective for hydrophobic substrates. Figure 6.6b shows that both the *rate* of the oxidation reaction as well as the *end conversion* correlate well with the partitioning ratio of the substrates between the hydrophobic compartment created by the SCPN and water. Catalytic systems showing differences in reaction rate and end conversion have been reported before. For example, Escuder and coworkers employed *L*-proline-based catalytically active hydrogels, which catalyze the aldol reaction of 4-nitrobenzaldehyde with ketones varying in polarity (log P).<sup>12</sup> An increasing log P of the ketone gave higher yields and higher reaction rates, which was attributed to the hydrophobic structure of the hydrogel; the more hydrophobic ketones were in closer proximity to the catalyst and the aldehyde, which results in a higher stability of the transition state. Moreover, Neumann and coworkers used polyoxometalate-based hydrogels for the oxidation of 2-alkanols to 2-alkanones.<sup>13</sup> A high selectivity was observed for the more hydrophobic substrates in competition reactions with less hydrophobic substrates, which was termed “lipophiloselectivity”. The highest lipophiloselectivity value (defined as TON<sub>high log P alcohol</sub>/TON<sub>low log P alcohol</sub> in which TON is the turnover number) of 2.6 was found in the oxidation

of 2-tetradecanol ( $\log P = 6.11^{31}$ ) with 2-pentanol ( $\log P = 1.25^{31}$ ), two substrates that differ significantly in hydrophobicity.

In our system, we ascribe the enhancement in the reaction rate of the more hydrophobic substrates to the concentrator effect, which gives rise to an increased local concentration of substrates around confined catalytic centers in water.<sup>17,32</sup> The substrates partition between water and the hydrophobic pocket provided by the SCPNs, which results in an enhanced rate for the more hydrophobic substrates, owing to their relatively higher local concentration. The differences in end conversion between substrates varying in  $\log P$  suggest that equilibrium is reached, despite the presence of an excess of oxidant and a catalyst that remains active. Although the catalysis mixture appears homogeneous, our system is thought to comprise a heterogeneous micro-structure providing several, distinctly different phases,<sup>33</sup> which hampers a quantitative determination of the different species in the different micro-environments. In addition, the dispersity of the SCPNs gives rise to the formation of the reaction spaces with different sizes and active sites in different types of local environments. These, in combination with *i*) a complex composite of noncovalent interactions governing the traffic of reactants, active complexes and products among these phases,<sup>34</sup> and *ii*) the distribution/competition of the oxidant *t*BuOOH and its more hydrophilic byproduct *t*BuOH, make it very difficult to predict the end conversion of the different substrates.<sup>34</sup> Nevertheless, we observe lipophiloselectivities of up to 5 in our competition experiments.<sup>35</sup> This high value for chemically almost identical substrates is attributed to the flexible, sterically unconstrained structure of the catalysis environment created within the SCPNs.

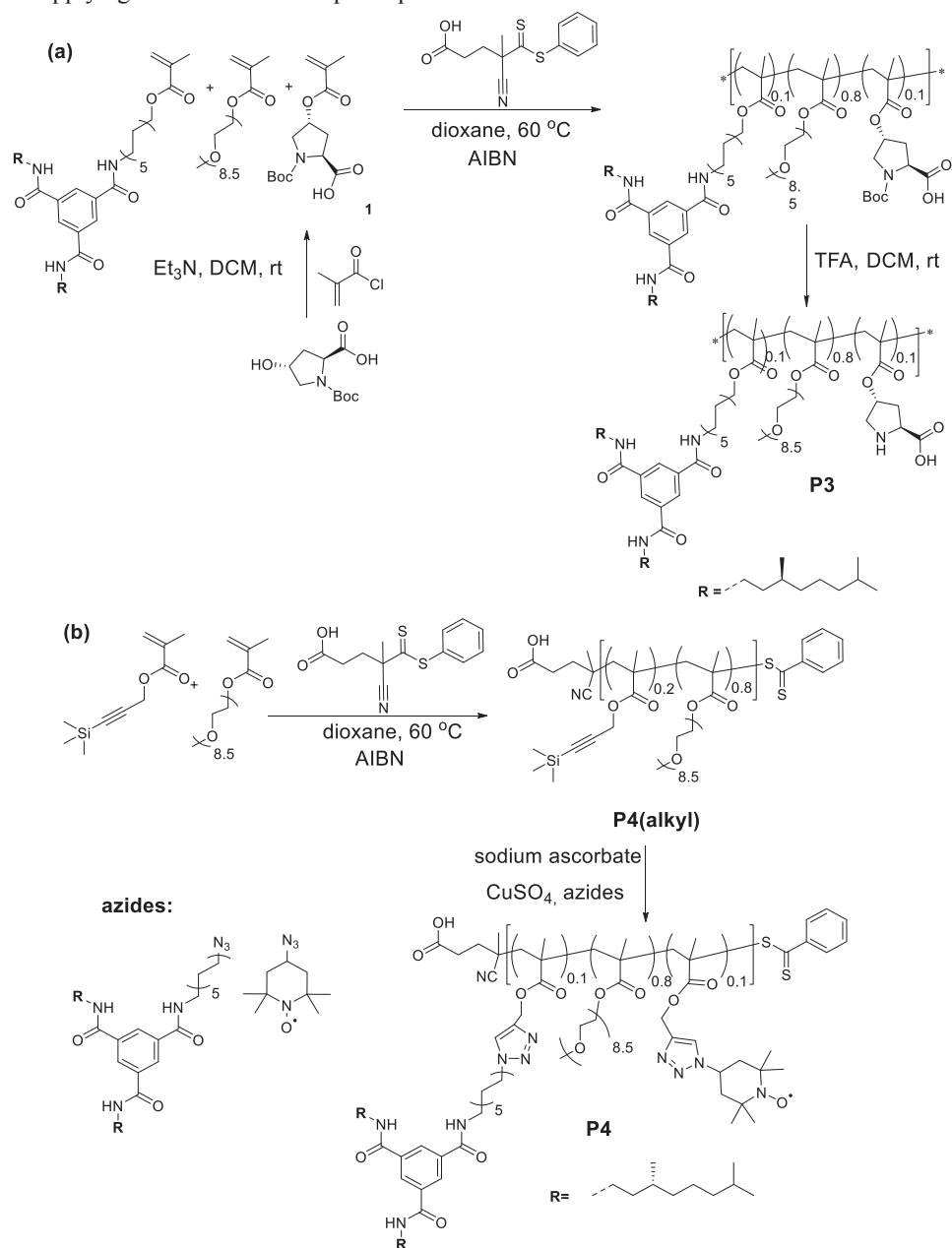
Remarkably, there were no significant differences between catalysts based on **P1** and **P2** in the competition reactions, although the latter has a more hydrophobic, structured inner compartment.<sup>21c</sup> Also, no stereoselectivity was observed in the oxidation reactions when using **P2**. However, the presence of lauryl or BTA groups is required for catalytic activity of SCPN@Ru(II) (Table 6.2). Apparently, the strong Ru(II) complexation to the SDP units in combination with a hydrophobic collapse suffices to effectively shield the Ru center from the aqueous environment. At the same time, the distance between the catalytic centers and the helical BTA aggregates seems to be too large to affect the (stereo)selectivity of the reactions.

#### 6.4 Towards SCPN catalyzed cascade reactions in water

Performing multiple reaction steps in one pot is a convenient way of synthesizing complex molecules that are both of scientific and commercial interest in order to save material, time and labor by avoiding intermediate purification steps, allowing in-situ conversion of otherwise unstable reactants.<sup>36</sup> However, incompatibility of catalytic sites with different functions is an issue that makes designing cascade sequences very challenging. The required isolation of otherwise incompatible natural and/or synthetic active sites has been so far achieved *via* their spatially controlled immobilization in crosslinked nanoparticles,<sup>37,38</sup> resins,<sup>39,40</sup> layer-by-layer microcapsules,<sup>41,42</sup> biohybrid macromolecules<sup>43,44</sup> and polymerzomes.<sup>45</sup>

SCPns provide hydrophobic nano-compartments *via* a controlled folding which induces shielding of active sites for organic reactions to occur in aqueous environment.<sup>21,22</sup> Besides, they enable efficient diffusion of the reactants, reagents and products throughout the system owing to

their dynamic character. Therefore, the SCPN approach serves as a good candidate for performing one pot, multi-step reaction sequences in water. Here we introduce the preliminary experiments on applying SCPNs in multi-step one-pot reactions.



**Scheme 6.2** (a) Synthesis of *L*-proline methacrylate and **P3** (RAFT polymerization: (oEGMA 80%/BTAMA 10%/LProMA 10%)/CTA 250:1, dioxane, 60 °C, 48 h). (b) Synthesis of **P4** (RAFT polymerization: (oEGMA 80%/BTAMA 10%/L-ProMA 10%)/CTA 250:1, dioxane, 60 °C, 48 h).

As a first attempt, we selected L-proline@SCPN (**P3**) catalyzed aldol condensation of cyclohexanone (**3a**) with 4-nitrobenzaldehyde (**4**) as first step, and Ru@SCPN (**P1**) catalyzed oxidation (*t*BuOOH as oxidant to be added after the completion of aldol reaction) of the aldol product as second step of the cascade sequence (Figure 6.7).<sup>21b</sup>

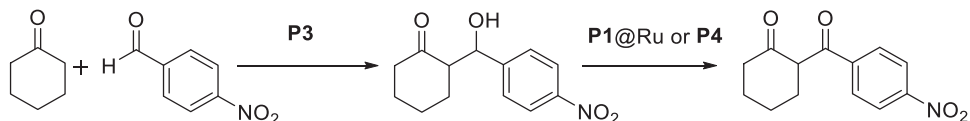


Figure 6.7 Proposed reaction sequence.

Previously, Huerta and Stals *et al.* explored L-proline@SCPN catalyzed aqueous aldol reactions in detail.<sup>21b</sup> **P3** was prepared according to the report of Huerta and Stals *et al.* via copolymerization of L-Pro methacrylate, BTAMA and *o*EGMA using the RAFT technique in the presence of AIBN as initiator and 4-cyano-4-methyl-5-(phenylthio)-5-thioxopentanoic acid as chain transfer agent with a feed ratio of (*o*EGMA 80% / BTAMA 10% / L-prolineMA 10%) (Scheme 6.2).<sup>21b</sup> L-Proline methacrylate was prepared by a simple reaction of Boc-protected *trans*-hydroxy- L-proline with methacryloyl chloride according to the same report (Scheme 6.2). After a subsequent deprotection of *t*-Boc on the polymer pendant L-proline units, **P3** was obtained with a  $M_{n,NMR}$  of 56 kDa and  $D$  of 1.12 (SEC, DMF+LiBr) with matching incorporation ratios (10% L-proline, 10% BTAMA, 80% *o*EGMA). **P3** showed a negative Cotton effect of -15 mdeg (50  $\mu$ M in water) at 223 nm, indicating helical aggregates with a preferred left-handed (*M*) helical sense, and an intensity and shape similar to BTAMA/*o*EGMA-based copolymers that lack the L-proline unit, this implies that L-proline does not interfere with the stacking behavior of polymer pendant BTA units. Moreover, DLS experiments in water showed a  $D_H$  around 11 nm at RT also correlating with our previous studies.<sup>18,20-22</sup> Ru@**P1** was prepared as explained in detail in Chapter 5.

The catalysis mixture was prepared by separately dissolving Ru@**P1** and **P3** in water, mixing them and then adding **3a** and **5** to this mixture to give 3/1/500/50 mM of (L-proline/Ru/**3a/5**) and 36 mg/mL (18 mg Ru@**P1** and 18 mg **P3**) polymer mixture in water. Reactions were carried out stirring in water (1 mL) at room temperature. Conversion of the aldehyde into aldol product was followed *via* <sup>1</sup>H-NMR.

In the first set of control reactions, we planned to add *t*BuOOH to the catalysis mixture after observing completion of aldol reaction for simplicity. However, as evidenced by the dramatic decrease in the conversion (Table 6.4, entry 2) in comparison with the conversion of the catalysis mixture without Ru@**P1** (Table 6.4, entry 1), it appears that the activity of L-proline was inhibited in the presence of Ru@**P1**. It is likely that free Ru(II) complexes with proline. This is in line with literature examples stating that L-proline is a good ligand for ruthenium species owing to the lone pairs of -N-H.<sup>46-48</sup> A 5 fold lower Ru@**P1** amount did not help to avoid L-proline inhibition (Table 6.4, entry 3).

**Table 6.4** Results of the **P3**, **P3 (+P1)** and **P3 (+P4)** catalyzed aldol reactions in water<sup>a</sup>

Entry	Substrate	Polymer	L-proline/Ru/3a/5 (mM)	Conversion <sup>b</sup> (%) (t (h))
1	3a+5	<b>P3</b> (18 mg/mL)	3/-/500/50	96 (36)
2	3a+5	<b>P3+P1@Ru</b> (18 + 18 mg/mL)	3/1/500/50	10 (72)
3	3a+5	<b>P3+P1@Ru</b> (18 + 3.6 mg/mL)	3/0.2/500/50	10 (72)
<b>L-proline /TEMPO/3a/5 (mM)</b>				
4	3a+5	<b>P3</b> (18 mg/mL)	3/-/500/50	50 (36)
5	3a+5	<b>P3+P4</b> (18 + 18 mg/mL)	3/3/500/50	50 (36)

<sup>a</sup> Reactions were performed at room temperature in water.

<sup>b</sup> The conversion of **5** (determined using <sup>1</sup>H-NMR).

DLS experiments were performed on the **P3** (36 mg/mL), Ru@**P1** (36 mg/mL) and **P3+Ru@P1** (36 mg/mL, 1/1:**P1/P3**) mixtures in water. **P3** and Ru@**P1** showed a predominantly single chain character as shown before (Ru@**P1**: 10 nm, **P3**: 14 nm, Figure 6.8a, b).<sup>21,22</sup> However, for **P3+Ru@P1** solution showed a small ( $D_H$ : 24 nm) and relatively larger set of particles ( $D_H$ : 150 nm Figure 6.8c). This larger aggregate size could be explained with the possible interaction between L-proline and the polymer attached Ru(II) which creates an additional driving force for multiple chains to cluster together, which in turn may result in the deactivation of the L-proline units.

Another well-known catalyst employed in the oxidations of alcohols is 2,2,6,6-tetramethylpiperidinoxyl (TEMPO) that was discovered by Lebedev and Kazarnowskii in early 60's.<sup>49,50</sup> TEMPO, together with triazine derivatives such as trichloroisocyanuric acid (TCCA), is known to be a very mild, easy and efficient approach for the general oxidation of carbinols into the corresponding carbonyl compounds. As suggested by mechanistic studies, the reaction with a catalytic amount of TCCA forms the active form 'N-oxoammonium ion' that oxidizes the alcohol forming the hydroxylamine that is regenerated back to the N-oxoammonium ion to close the cycle.<sup>51,52</sup> As a second attempt we employed a metal-free TEMPO incorporated SCPN (**P4**,  $DP_{NMR} = 267$ ,  $M_{n,SEC} = 24.6$  kDa,  $D = 1.90$  (SEC in DMF relative to pEO standards)),<sup>51</sup> kindly provided by Dr. Patrick Stals, as an oxidation catalyst in the presence of TCCA.

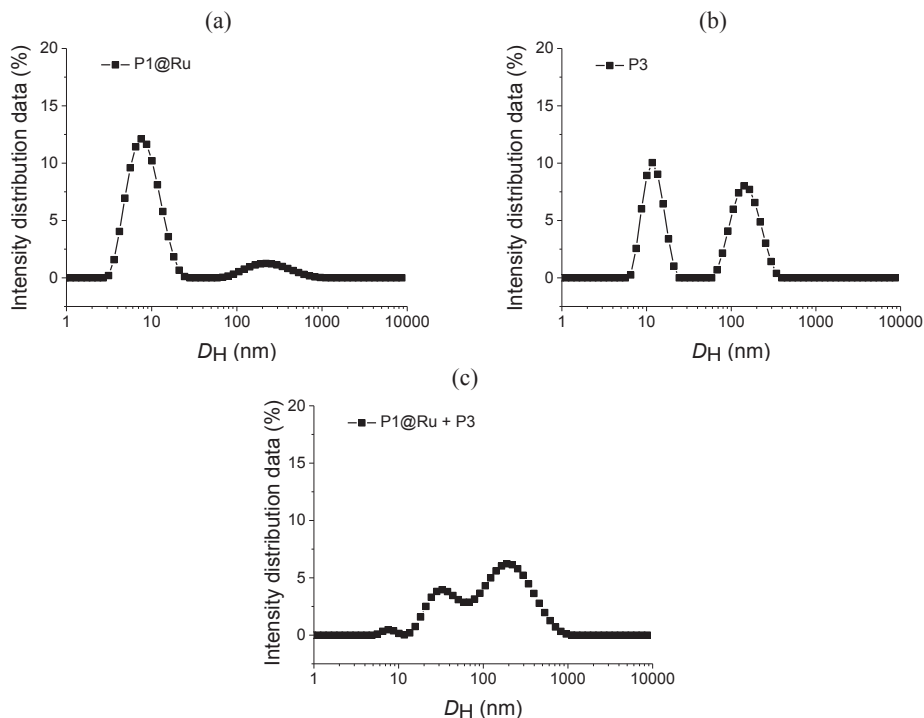


**Figure 6.8** DLS intensity distribution of (a) **P1@Ru** (36 mg/mL), (b) **P3** (36 mg/mL) and (c) **P1@Ru + P3** (36 mg/mL, **P1@Ru/P3**: 1/1) mixtures in water at RT.

**P4** was first tested in the oxidation of **1a** as a model compound in water and complete conversion of **1a** to **3a** was observed in 50 mins (TEMPO/**1a**/TCCA= 0.001/0.04/0.2 M (17 mg/mL **P4**). Next, aldol reaction in the presence of **P3** and **P4** was tested. The catalysis mixture was prepared by separately dissolving **P4** and **P3** in water, mixing them and then adding **3a** and **5** to this mixture to give 3/3/500/50 mM of (L-proline /TEMPO/**3a/5**) and 36 mg/mL polymer mixture in water (18 mg **P4** and 18 mg **P3**). Reactions were carried out by stirring in water (1 mL) at room temperature. Conversion of aldehyde into aldol product was followed *via*  $^1\text{H-NMR}$ . TCCA was planned to be added into the catalysis mixture after the completion of aldol reaction for simplicity of the initial test reactions. The conversion of **5** into the aldol product (Table 6.4, entry 5) was not affected by the presence of **P4** (Table 6.4, entry 4). This result reveals the potential of TEMPO@SCPN/L-proline @SCPN system as a promising couple for cascade catalysis. This promising result is now subject to further experiments.

### 6.5 Conclusions

To conclude, we employed amphiphilic polymers that fold into SCPNs and hereby create a hydrophobic environment around a Ru(II) catalytic center in order to carry out selective catalysis with an intrinsically non-selective active center. The hydrophobic reaction space results in a high local concentration of substrates around the catalytic sites. Moreover, the system shows high selectivity towards hydrophobic substrates, both in oxidation as well as in reduction reactions.



The SCPN structure allows for efficient conversion of even the most water soluble substrates, yet providing a significant selectivity (**1d/1a/1e** = 20%/70%/>99%) for chemically almost identical substrates. As a result, compartmentalized, amphiphilic nanoreactors provide efficient reaction spaces to achieve selectivity, based on hydrophobic effects.

Finally, an attempt was made towards performing cascade reactions with SCPNs. Aldol condensation followed by oxidation was envisioned as the cascade system, therefore firstly, a mixture of proline functionalized **P3** and Ru loaded **P1@Ru** was applied to catalyze a two-step cascade. The shielding of the active sites *via* SCPN collapse was shown to be not efficient enough to prevent Ru from penetrating L-Pro containing particles, causing the poisoning of the L-proline catalyst and resulting in deactivation. However, TEMPO functionalized **P3** and **P1@Ru** mixture was shown to be compatible and active in the aldol reaction, most probably due to the absence of metals in the system as deactivating species. Thus, we have shown the compatibility of the TEMPO@SCPN/ L-proline@SCPN system for aldol reactions, which is the first step of the envisioned aldol/oxidation sequence for future studies.

## **6.6 Experimental**

### **6.6.1 Materials**

All solvents were purchased from Biosolve, cyclohexanol was purchased from Jansen Chemica. *tert*-butylhydroperoxide, 4-*tert*-butylcyclohexanol, tetrahydro-4-pyranol and sodium metabisulfite were purchased from Aldrich. Poly(ethylene glycol) methyl ether methacrylate (*o*EGMA:  $M_n \approx 475$ ) and lauryl methacrylate (LMA: Aldrich, purity >96%) were of commercial source (Aldrich), purified by an inhibitor removal column (Aldrich) and degassed by reduced pressure before use. The phosphine ligand monomer (diphenylphosphinostyrene: SDP), kindly supplied by Hokko Chemical (purity >99.9%), was degassed by reduced pressure before use. Azobisisobutyronitrile (AIBN) was recrystallized from methanol. 4-Cyano-4-methyl-5-(phenylthio)-5-thioxopentanoic acid was kindly provided by SyMO-Chem (Eindhoven, the Netherlands).  $\text{RuCl}_2(\text{PPh}_3)_3$  (Aldrich, 97%) was used as received and handled in a glove box under a moisture- and oxygen-free argon atmosphere ( $\text{H}_2\text{O} < 1 \text{ ppm}$ ,  $\text{O}_2 < 1 \text{ ppm}$ ). Toluene (passed through purification columns; Solvent Dispensing System; Glass Contour) and hexane were bubbled with dry nitrogen for more than 15 min immediately before use. Sodium formate and 1-phenyl ethanol (Aldrich; purity > 98%) were used as received. Cyclohexanone, 4-methylcyclohexanone, 4-ethylcyclohexanone and 4-propylcyclohexanone (Aldrich, purity >99%) were bubbled with dry nitrogen for more than 15 min immediately before use. Polymerizations, catalyst loadings and catalysis experiments were carried out by the syringe technique under dry argon in baked glass tubes equipped with a three-way stopcock. The synthesis of chiral BTAMA was performed as described in Chapter 2, starting from (*S*)-citronellol with an enantiomeric excess (*ee*) of 98.4%.<sup>60</sup>

### **6.6.2 Instrumentation**

DMF-SEC measurements were carried out in PL-GPC-50 plus from Polymer Laboratories (Agilent Technologies) with refractive index detector working in DMF containing 10 mM LiBr at 50 °C at a constant flow rate of 1 mL/min on a Shodex GPC-KD-804 column (exclusion limit = 400000 Da.; 0.8 cm i.d. × 300 mL) which was calibrated with polyethyleneoxide (PEO) samples with a range from 282 - 77350 Da (Polymer Laboratories - Agilent Technologies).

$^1\text{H-NMR}$  and  $^{31}\text{P-NMR}$  spectra were recorded on a Varian Mercury Vx 400 MHz and/or a Varian 400MR 400 MHz. Proton chemical shifts are reported in ppm down from tetramethylsilane (TMS).

Circular dichroism (CD) measurements were performed on a Jasco J-815 spectropolarimeter where the sensitivity, time constant and scan rate were chosen appropriately (sensitivity: standard; response: 2 s; band width: 1 nm; data pitch: 0.1 nm; scanning speed: 20 nm/min). Corresponding temperature-dependent measurements (data pitch: 0.1 K) were performed with a PFD-425S/15 Peltier-type temperature controller with a temperature range of 263–383 K and adjustable temperature slope, in all cases temperature slope of 1 K/min was used. In all experiments the linear dichroism was also measured and in all cases no linear dichroism was observed.

Dynamic light scattering measurements were performed on a Malvern mV Zetasizer equipped with an 830 nm laser. Samples were prepared dissolving 18 mg/mL of polymer **P2** in MilliQ quality water and sonicating for 2 hours, filtering the solution through a 0.2 mm PVDF-filter (Whatman) in a fluorescence cell, that is washed with filtered MilliQ quality water, with a path length of 1 cm.

Ether/chloroform samples were measured on a Shimadzu GC-2010 gas chromatograph connected to a Shimadzu GCMS-QP2010Plus gas chromatograph mass spectrometer using a Phenomenex Zebron ZB-5MS column (length 30 m, internal diameter 0.25 mm, film thickness 0.25  $\mu\text{m}$ , serial number: 123635) using the following method: injector temperature: 250  $^\circ\text{C}$ , oven temperature start: 90  $^\circ\text{C}$ , isothermal: 1 min, oven temperature set 150 $^\circ\text{C}$ , ramp 10 $^\circ\text{C}/\text{min}$ , oven temperature set 320 $^\circ\text{C}$ , ramp 40 $^\circ\text{C}/\text{min}$ . Total time: 11.25 min, gas flow: 20 mL/min

Water/methanol samples were measured on a Perkin Elmer Autosystem gas chromatograph with an FID detector using a phenomenex zebron ZB-FFAP column (length: 30 m, I.D.: 0.25 mm, film thickness: 0.25  $\mu\text{m}$ , serial no.: 168147) using the following method: injector temperature: 300  $^\circ\text{C}$ , oven temperature start: 125  $^\circ\text{C}$ , isothermal: 1min, oven temperature set 250  $^\circ\text{C}$ , ramp 40  $^\circ\text{C}/\text{min}$ , isothermal: 1min. Carrier gas pressure: 30 psi

### 6.6.3 Synthesis

**P1** and **P2** were synthesized according to procedures described in Chapter 5. Also, Ru@SCPN is prepared as discussed in Chapter 5. The synthesis of **P4** is discussed elsewhere.<sup>53</sup>

*N-tert-Butyloxycarbonyl-O-methacryloyl-trans-4-hydroxy-L-proline (L-ProMA)*:

*N-tert-Butyloxycarbonyl-trans-hydroxy-L-proline* (1g, 4.24 mmol) was placed in a round bottom flask under argon and suspended in 10 mL of dry DCM. The mixture was stirred for a few minutes and triethylamine (1.6 mL, 11.86 mmol) was added. The flask was placed in an ice bath and stirred until a clear solution was obtained. Finally, methacryloyl chloride (900  $\mu\text{L}$ , 9.32 mmol) was added and the mixture was stirred overnight at room temperature. The reaction was quenched with 1M HCl (20 mL). The aqueous layer was extracted twice with chloroform (2 x 20 mL) and the combined organic layers were washed with brine and dried over sodium sulfate. The solvent was removed *in vacuo* and the crude compound was purified by flash chromatography in silica gel using dichloromethane/MeOH with a gradient from 0 to 10% as mobile phase affording 700 mg (60 %) of the product as colorless oil. The product showed the same spectroscopic properties reported as before. <sup>21b</sup>  $^1\text{H-NMR}$  ( $\text{CDCl}_3$ ):  $\delta$  = 6.10 (s, 1H, =CH), 5.61 (s, 1H, =CH), 5.33 (s, 1H, -

HCOR), 4.45 (t,  $J = 7.9$  Hz, 1H, -HCOOH), 3.83 - 3.58 (m, 2H, -CH<sub>2</sub>-), 2.61 - 2.23 (m, 2H, -CH<sub>2</sub>-), 1.94 (s, 3H, CH<sub>3</sub>), 1.48 (s, 6H, 2 x CH<sub>3</sub>), 1.44 (s, 3H, CH<sub>3</sub>).

*o*EGMA/LMA/SDP copolymer (**P1**):

The polymer showed similar spectroscopic data as discussed in Chapter 5.  $M_{n,NMR} = 58.0$  kDa,  $M_{n,SEC} = 13.8$  kDa,  $D = 1.4$ .

*o*EGMA/BTAMA/SDP copolymer (**P2**):

The polymer showed similar spectroscopic data as discussed in Chapter 5.  $M_{n,NMR} = 62.0$  kDa,  $M_{n,SEC} = 14.5$  kDa,  $D = 1.4$ .

*o*EGMA/BTAMA/L-proline copolymer (**P3**):

Prepared following the same general procedure as described by Huerta *et al.*<sup>21b</sup> using *o*EGMA (0.8600 g, 1.811 mmol), BTAMA (0.1546 g, 0.2130 mmol), L-ProMA (0.033 g, 0.1119 mmol), 4-cyano-4-methyl-5-(phenylthio)-5-thioxopentanoic acid (1/244 eq., 2.432 mg, 8.716  $\mu$ mol) and AIBN (20% to RAFT-CTA, 0.280 mg, 1.704  $\mu$ mol) dissolved in 4 mL dry dioxane. The polymerization proceeded for 48 h, and was quenched at 91 % conversion.  $M_{n,SEC} = 14.5$  kDa,  $D = 1.1$ ,  $M_{n,NMR} = 56.0$  kDa. <sup>1</sup>H-NMR (CDCl<sub>3</sub>):  $\delta = 8.44$  (bs, Ar-H: BTAMA), 7.37 (b, NH), 7.19 (b, NH), 5.22 (bs, O-CH L-Pro), 4.08 (b, CO<sub>2</sub>-CH<sub>2</sub>), 3.65 (b, CH<sub>2</sub>-O-CH<sub>2</sub>), 3.55 (bt, CO<sub>2</sub>-CH<sub>2</sub>-CH<sub>2</sub>-O), 3.46 (b, NH-CH<sub>2</sub>), 3.36 (bs, O-CH<sub>3</sub>), 2.14-0.67 (m, aliphatic: CH, CH<sub>2</sub>, CH<sub>3</sub>).

*o*EGMA/BTAMA/TEMPO copolymer (**P4**):<sup>53</sup>

**P4-alkyl** precursor:  $M_{n,NMR} = 107$  kDa,  $DP = 255$ .  $M_{n,SEC} = 24.6$  kDa,  $D = 1.90$  (SEC in DMF with 10 mM LiBr).

**P4**:  $M_{n,SEC} = 30.7$  kDa,  $D = 2.80$  (SEC in DMF with 10 mM LiBr). An  $R_H$  of 19 nm was observed in water *via* DLS (1 mg/mL).

### 6.6.4 Catalysis procedures

In a glass tube charged with polymer (18 mg, 0.313  $\mu$ mol) loaded with ruthenium(II) (0.1  $\mu$ mol) in 1 mL water under argon at room temperature, substrate was added (for cyclohexanol (0.04 mmol), for 1-phenylethanol (0.04 mmol)) after degassing by bubbling Ar for at least 15 minutes. After all the substrate was dissolved, *tert*-butylhydroperoxide (80% in water, 24  $\mu$ l, 0.2 mmol) was added drop wise to the mixture. 0.1 mL samples were taken *via* the syringe technique and quenched by adding the sample to a vial. For experiments without tetrahydro-4-pyranol, inside the sample vial there was a 5 fold diethylether and sodium sulfite (3 mg) after which the sample directly was mixed rigorously. GC-MS samples were prepared by diluting 0.1 mL from the diethyl layer with 0.9 mL chloroform. For the experiments containing tetrahydro-4-pyranol, there was Na<sub>2</sub>S<sub>2</sub>O<sub>5</sub> (3 mg) in the sample vial. After addition of the sample, the sample was heavily mixed and diluted with 0.9 mL methanol. After filtration over a 45  $\mu$ m filter, the conversion was determined using GC. All catalysis experiments were done in triplicate.

## 6.7 References

- (1) P. B. Weisz, W. O. Haag, P. G. Rodewald *Science* **1979**, *5*, 57.
- (2) M. Dusselier, P. Van Wouwe, A. Dewaele, P. A. Jacobs, B. F. Sels *Science* **2015**, *3*, 78.
- (3) R. Noyori *Angew. Chem. Int. Ed.* **2002**, *41*, 2008.
- (4) G. J. ten Brink, I. W. C. E. Arends, R. A. Sheldon *Science* **2000**, *287*, 1636.
- (5) A. Warshel *Proc. Natl. Acad. Sci. USA* **1978**, *75*, 5250.
- (6) A. Warshel *Angew. Chem. Int. Ed.* **2014**, *53*, 10020.
- (7) M. Garcia-Viloca, J. Gao, M. Karplus, D. G. Truhlar *Science* **2004**, *303*, 186.
- (8) Y. Liu, Y. Wang, Y. Wang, J. Lu, V. Piñón, M. Weck *J. Am. Chem. Soc.* **2011**, *133*, 14260.
- (9) G. Hamasaka, T. Muto, Y. Uozumi *Angew. Chem., Int. Ed.* **2011**, *50*, 4876.
- (10) Z. Ge, D. Xie, D. Chen, X. Jiang, Y. Zhang, H. Liu, S. Liu *Macromolecules* **2007**, *40*, 3538.
- (11) P. Cotanda, R. K. O'Reilly *Chem. Commun.* **2012**, *48*, 10280.
- (12) C. Berdugo, J. F. Miravet, B. Escuder *Chem. Commun.* **2013**, *49*, 10608.
- (13) A. Haimov, R. Neumann *J. Am. Chem. Soc.* **2006**, *128*, 15697.
- (14) B. L. Moore, D. Moatsou, A. Lu, R. K. O'Reilly *Polym. Chem.* **2014**, *5*, 3487.
- (15) T. Terashima, M. Ouchi, T. Ando, M. Sawamoto *J. Polym. Sci. Part Polym. Chem.* **2011**, *49*, 1061.
- (16) M. C. M. van Oers, K. E. A. Loai, F. P. J. T. Rutjes, J. C. M. van Hest, *Chem. Commun.* **2014**, *50*, 4040.
- (17) M. R. Biscoe, R. Breslow *J. Am. Chem. Soc.* **2005**, *127*, 10812.
- (18) B. Helms, J. M. J. Fréchet *Adv. Synth. Catal.* **2006**, *348*, 1125.
- (19) (a) O. Altintas, C. Barner-Kowollik *Macromol. Rapid Commun.* **2012**, *33*, 958. (b) C. K. Lyon, A. A. M. Prasher, B. T. Hanlon, C. A. Tuten, P. G. Tooley, E. B. Berda *Polym. Chem.* **2015**, *6*, 181. (c) M. Gonzalez-Burgos, A. Latorre-Sanchez, J. A. Pomposo *Chem. Soc. Rev.* **2015**, *44*, 6122.
- (20) (a) I. Perez-Baena, F. Barroso-Bujans, U. Gasser, A. Arbe, A. J. Moreno, J. Colmenero, J. A. Pomposo *ACS Macro Lett.* **2013**, *2*, 775. (b) S. Mavila, I. Rozenberg, N. G. Lemcoff *Chem. Sci.* **2014**, *5*, 4196. (c) A. Sanchez-Sanchez, A. Arbe, J. Colmenero, J. A. Pomposo *ACS Macro Lett.* **2014**, *3*, 439. (d) J. Willenbacher, O. Altintas, V. Trouillet, N. Knöfel, M. J. Monteiro, P. W. Roesky, C. Barner-Kowollik *Polym. Chem.* **2015**, *6*, 4358.
- (21) (a) T. Terashima, T. Mes, T. F. A. de Greef, M. A. J. Gillissen, P. Besenius, A. R. A. Palmans, E. W. Meijer *J. Am. Chem. Soc.* **2011**, *133*, 4742. (b) E. Huerta, P. J. M. Stals, E. W. Meijer, A. R. A. Palmans *Angew. Chem. Int. Ed.* **2013**, *52*, 2906. (c) M. Artar, T. Terashima, M. Sawamoto, E. W. Meijer, A. R. A. Palmans *J. Polym. Sci., Part A: Polym. Chem.* **2014**, *52*, 12.
- (22) (a) M. A. J. Gillissen, T. Terashima, E. W. Meijer, A. R. A. Palmans, I. K. Voets *Macromolecules* **2013**, *46*, 4120. (b) P. J. M. Stals, M. A. J. Gillissen, T. F. E. Paffen, T. F. A. de Greef, P. Lindner, E. W. Meijer, A. R. A. Palmans, I. K. Voets *Macromolecules* **2014**, *47*, 2947. (c) M. Artar, E. Huerta, E. W. Meijer, A. R. A. Palmans, in *Sequence-Controlled Polymers: Synthesis, Self-Assembly, and Properties*; American Chemical Society: **2014**; Vol. 1170, p 313.
- (23) T. Terashima, T. Sugita, K. Fukae, M. Sawamoto *Macromolecules* **2014**, *47*, 589.
- (24) Y. Tsuji, T. Ohta, T. Ido, H. Minbu, Y. J. Watanabe *Organomet. Chem.* **1984**, *270*, 333.
- (25) J. J. Sangster *Phys. Chem. Ref. Data* **1989**, *18*, 1111.

- (26) <http://www.molinspiration.com>, last accessed on 16-01-2016.
- (27) To assure activity of the catalytic system, which is prone to be deactivated by atmospheric O<sub>2</sub>, and to test if any substrate and/or product inhibition is present in the case of **1d** oxidation, **1a** (40 mM) was added to a typical catalysis mixture of **1d** (SCPN@Ru/substrate/oxidant: 1/40/200 mM) as it reached the maximum conversion around 40 % in 18 mins and **1a** was oxidized with 40% conversion (Table 6.2, entry 17). This shows that the system is active, not inhibited and the low end conversion is due to poor partition of the water soluble **1d** in the hydrophobic reaction space.
- (28) Alcohol **1e** is water-insoluble, but in the presence of the more hydrophilic substrates becomes soluble in the water environment.
- (29) C. Aliende, M. F. Pérez-Manrique, A. Jaloń, B. R. Manzano, A. M. Rodríguez, G. Espino *Organometallics* **2012**, *31*, 6106.
- (30) S. I. Murahashi, T. Naota *Synthesis* **1993**, 433.
- (31) S. H. Yalkowsky, S. C. Valvani *J. Pharm. Sci.* **1980**, *69*, 912.
- (32) B. C. Helms, O. Liang, C. J. Hawker, J. M. J. Fréchet *Macromolecules* **2005**, *38*, 5411.
- (33) B.-Ti. Chen, K. V. Bukhryakov, R. Sougrat, V. O. Rodionov *ACS Catal.* **2015**, *5*, 1313.
- (34) J. B. F. N. Engberts *Pure & Appl. Chem.* **1992**, *64*, 1653.
- (35) We observed lipophiloselectivities of 1.4 (Final conversion<sub>1e</sub> (log *P* = 3.06) / Final conversion<sub>1a</sub> (log *P* = 1.23)) and 5 (Final conversion<sub>1e</sub> (log *P* = 3.06) / Final conversion<sub>1d</sub> (log *P* = -0.06)).
- (36) K. C. Nicolaou, J. S. Chen *Chem. Soc. Rev.* **2009**, *38*, 2993.
- (37) B. Helms, S. J. Guillaudeu, Y. Xie, M. McMurdo, C. J. Hawker, J. M. J. Fréchet *Angew. Chem. Int. Ed.* **2005**, *44*, 6384.
- (38) Y. Chi, S. T. Scroggins, J. M. J. Fréchet *J. Am. Chem. Soc.* **2008**, *130*, 6322.
- (39) K. Akagawa, S. Sakamoto, K. Kudo *Tetrahedron Lett.* **2007**, *48*, 985.
- (40) K. Akagawa, S. Takigawa, E. Mano, K. Kudo *Tetrahedron Lett.* **2011**, *52*, 770.
- (41) O. Kreft, M. Prevor, H. Mohwald, G. B. Sukhorukov *Angew. Chem. Int. Ed.* **2007**, *46*, 5605.
- (42) L. Zhang, J. F. Shi, Z. Y. Jiang, S. Z. Qiao, J. A. Li, Wang, R.J. Meng, Y. Y. Zhu, Y. Zheng *Green Chem.* **2011**, *13*, 300.
- (43) G. Delaittre, I. C. Reynout, J. J. L. M. Cornelissen, R. J. M. Nolte *Chem. Eur. J.* **2009**, *15*, 12600.
- (44) A. Grotzky, E. Altamura, J. Adamcik, P. Carrara, P. Stano, F. Mavelli, T. Nauser, R. Mezzenga, A. D. Schluter, P. Walde *Langmuir* **2013**, *29*, 10831.
- (45) R. J. R. W. Peters, M. Marguet, S. Marais, M. W. Fraaije, J. C. M. van Hest, S. Lecommandoux *Angew. Chem. Int. Ed.* **2014**, *53*, 146.
- (46) A. Rathgeb, A. Böhm, M. S. Novak, A. Gavriluta, O. Dömötör, J. B. Tommasino, É. A. Enyedy, S. Shova, S. Meier, M. A. Jakupec, D. Luneau, V. B. Arion *Inorg. Chem.* **2014**, *53*, 2718.
- (47) X. C. Cambeiro, M. A. Pericás *Adv. Synth. Catal.* **2011**, *353*, 113.
- (48) V. F. Kuznetsov, G. P. A. Yap, H. Alper *Organometallics* **2001**, *20*, 1300.
- (49) O. L. Lebelev, S. N. Kazarnovskii *Zhur. Obshch. Khim.* **1960**, 1631.
- (50) M. Shibuya, Y. Osada, Y. Sasano, M. Tomizawa, Y. Iwabuchi *J. Am. Chem. Soc.* **2011**, *133*, 6497.
- (51) L. De Luca, G. Giacomelli, S. Masala, A. Porcheddu *J. Org. Chem.* **2003**, *68*, 4999.

---

(52) L. De Luca, G. Giacomelli, S. Masala, A. Porcheddu *Org. Lett.* **2001**, *3*, 19.

(53) P. J. M. Stals, C-Y. Cheng, L. van Beek, A. C. Wauters, A. R. A. Palmans, S. Han, E. W. Meijer, *Chem. Sci.* **2016**, *7*, 2011.

(54) It should be noted that the decrease in the efficiency of **P3** is due to the hydrolysis of the pendant L-proline units of **P3** in time as was physically confirmed by the color change of the polymer from colorless to slightly reddish which is known as a sign of the reaction of hydrolysis product of L-proline with an aromatic unit, most probably the CTA unit in our case (W. Troll, J. Lindsley *J. Biol. Chem.* **1955**, *215*, 655).



---

## Folding polymer chains *via* orthogonal non-covalent interactions

### *Function through structure*

Merging polymer and supramolecular chemistry allows the preparation of dynamic 3D structures that show adaptive and responsive features. In this thesis, the aim is to develop synthetic routes to achieve complex polymers that fold through orthogonal interactions into defined, dynamic particles, and, to employ these particles as functional, nanometer-sized reactors.

In *Chapter 1*, we introduce the concept of achieving function through structure in synthetic systems by taking nature as a source of inspiration. First, the most important controlled radical polymerization techniques are discussed. Next, approaches to prepare compartmentalized macromolecular systems by controlled radical polymerization techniques and supramolecular chemistry are introduced, with a focus on single chain polymeric nanoparticles (SCPNs) with non-dynamic and dynamic behavior. This has been followed by an overview on the synthesis and characterization of dynamic SCPNs. Finally, catalysis in confined spaces is introduced with an emphasis on dynamic SCPNs as compartmentalized catalysts.

In *Chapter 2*, the effect of the local benzene-1,3,5-tricarboxamide (BTA) concentration on the folding behavior of polymers with pendant BTAs in organic solvents is studied. Hydrophobic methacrylate-based polymers have been prepared with varying molar mass dispersities and BTA distributions, i.e. random, diblock and gradient, by reversible addition fragmentation transfer (RAFT) or atom transfer radical polymerization (ATRP) techniques. The results of circular dichroism (CD) experiments indicate that the distribution and local density of pendant BTAs do affect the folding behavior of the copolymers, whereas molar mass dispersity does not. Moreover, inter-particle interactions are enhanced by increasing the local density of BTAs in one block of the copolymers.

In *Chapter 3*, the level of complexity of folding polymer chains through non-covalent interactions is carried one step further to have better control on the folding process in organic solvents. Therefore, the design and synthesis of an ABC type triblock copolymer that is decorated with complementary motifs, i.e. Hamilton wedge (HW, A block), (BTA, B block) and cyanuric acid (CA, C block) is presented. Orthogonality of the BTA and HW-CA self-assembly is confirmed by <sup>1</sup>H-NMR studies, in combination with CD experiments in dilute solution. Combined scattering techniques and AFM give evidence for the formation of well-defined particles with orthogonally self-assembling domains in MCH. Moreover, the scattering results in MCH and DCE show that the ABC-triblock copolymer design results in a system that is very sensitive to the solvent polarity, which is found to be of crucial importance to balance inter- vs intramolecular self-assembly.

In *Chapter 4*, complex, low and high molecular weight amphiphilic ABA type triblock copolymers with pendant self-assembly motifs are prepared in order to create stimuli-responsive, compartmentalized structures in aqueous media. Amphiphilic ABA type triblock copolymers have been synthesized *via* copper catalyzed ATRP and decorated with BTA and photoprotected 2-ureido-4[1H]-pyrimidinone (phUPy) supramolecular motifs in the B and A blocks, respectively. <sup>1</sup>H-NMR studies in CDCl<sub>3</sub> show that the UPy groups are capable of



dimerization when attached to an amphiphilic polymer backbone. The BTA-based helical stack formation in water, independent of the presence of phUPy or UPy groups, is evidenced *via* CD. UPy dimerization is shown in CHCl<sub>3</sub> *via* <sup>1</sup>H-NMR studies. Moreover, all amphiphilic polymers form compartmentalized structures with a hydrophobic interior in water as shown with Nile Red experiments; fully functionalized UPy-BTA-UPy triblock copolymer appear to form particles with the most hydrophobic environment. Finally, dynamic light scattering (DLS) reveals the formation of well-defined multi-chain aggregates by the functionalized triblock copolymers in water, but also that deprotection of the UPy moieties results in a reduction of the hydrodynamic radius.

In the second part of this thesis, the compartmentalized architectures that are formed *via* the folding of amphiphilic random single chain polymeric nanoparticles have been employed to achieve *function* in water.

In *Chapter 5*, a set of methacrylate based amphiphilic copolymers have been synthesized, loaded with Ru(II), and tested in the transfer hydrogenation of cyclohexanone in order to understand the role of pendant BTA groups for the catalytic activity of SCPNs in water. It is shown that once the micro-environment of the Ru catalyst is tightly structured by metal-ligand coordination bonds, the structural elements of the remaining pocket is not decisive for catalytic performance, as long as a hydrophobic pocket is maintained. Besides, systems in which Ru(II) is immobilized on the polymer pendant SDP units are much more efficient than systems in which “free” Ru(II)Cl<sub>2</sub>(PPh<sub>3</sub>)<sub>3</sub> is added to SCPNs without SDP units. This is likely a result of the more efficient isolation of the catalytic centers when ligands are embedded into the folded single chain.

In *Chapter 6*, the hydrophobic shielding that is formed by SCPNs in water was utilized to create selective hydrophobic reaction spaces. Competition experiments with a mixture of substrates with varying hydrophobicity reveal that a selective, hydrophobic, reaction space is formed by folding polymer chains around an intrinsically non-selective Ru(II) moieties. A significant selectivity has been observed for both oxidation and transfer hydrogenation reactions. Lastly, preliminary experiments have been performed to explore the applicability of these compartmentalized systems for multi-step reactions in one pot.

The results of this PhD study show that controlled folding of polymer chains can be achieved *via* orthogonal supramolecular interactions, and these folded dynamic structures can be applied as highly active and selective reaction spaces for catalysis in water. Although the current state-of-the art in folding synthetic macromolecules into defined structures is still far from the perfection that is achieved in the folding of polypeptides into functional conformations, it is envisioned that there is much to be gained by a further integration of supramolecular chemistry, polymer chemistry, organocatalysis and homogeneous catalysis.

## **Polimer zincirlerinin kovalent olmayan etkileşimlerle katlanması** **Şekilden fonksiyona**

Milyonlarca yıllık evrimin bize armağanı olan enzimler, yaşam için vazgeçilmez olan reaksiyonları çok hızlı, verimli ve seçici bir biçimde su içerisinde gerçekleştirebilmektedir. Vücudumuzdaki yaşamsal aktivitelerin gerçekleştirilmesinin yanı sıra endüstriyel anlamda gıda maddesi, ilaç ve çok çeşitli kimyasalın üretiminde de enzimler kullanılmaktadır. Enzimlerin bu üstün özellikleri, öncelikle doğanın en yetenekli polimer kimyacıları olan ribozomlar tarafından monomer dizilimi ve uzunluğu birebir kontrol edilerek sentezlenmeleri ve katlandıktan sonra aktif merkez etrafında oluşturulan birincil ve ikincil hidrofobik (su sevmeyen) kalkan sayesinde mümkündür. Bilindiği kadarıyla bu enzimlerin kontrollü şekilde katlanmasında, kovalent olmayan, zayıf birden çok etkilesimin bağımsız şekilde etki etmesinin rolü büyüktür.

Polimer kimyası ve süpramoleküler kimya birlikte kullanılarak, enzimleri taklit edebilen, üç boyutlu, adapte olabilen ve dış uyaranlara karşılık verebilen yapılar elde edilebilir. Bu tezin amacı, kompleks, katlanabilen, dinamik, iyi tanımlanmış polimerik yapıların sentezlenme metodlarının geliştirilmesi ve bu nanometre boyutundaki yapıların çeşitli fonksiyonlarda kullanılmasıdır.

*Birinci bölümde*, doğadan ilham alarak nasıl yapı yoluyla fonksiyon elde edileceği konsepti sunuldu. öncelikle, önemli kontrollü radikal polimerizasyon teknikleri tartışıldı. Daha sonra, kontrollü radikal polimerizasyon tekniklerini süpramoleküler kimya ile birlikte kullanarak bölümlenmiş yapılar sentezlemenin yolları, dinamik ve dinamik olmayan tek zincirli polimerik nanopartiküllere vurgu yapılarak sunuldu. Bunu, dinamik tek zincirli polimerik nanopartiküllerin sentezlenmesi ve karakterize edilmesi üzerine genel bir bakış izledi. Ve son olarak, kapalı yapılar içerisinde kataliz, yine dinamik tek zincirli polimerik nanopartiküllerin ağırlıklı olduğu bir biçimde sunuldu.

*İkinci bölümde* ise, polimere bağlı benzene-1,3,5-trikarboksamid (BTA) gruplarının kendiliğinden bir araya gelmesine polimer üzerindeki lokal BTA konsantrasyonunun etkisi tartışıldı. Hidrofobik, metakrilat bazlı polimerler dar ve geniş moleküler ağırlık dağılımları ile düzensiz, ikibloklu ve gradient dizimli olarak, tersinir eklenme-parçalanma zincir transferi (RAFT) ya da atom transfer radikal polimerizasyon (ATRP) tekniği ile sentezlendi. Sirküler dikroizm (CD) deneyleri, moleküler ağırlık dağılımının BTA gruplarının kendiliğinden bir araya gelme davranışına etkisi olmadığını ancak polimer üzerindeki BTA dağılımının kendiliğinden bir araya gelme davranışını kontrol edebildiğini gösterdi.

*Üçüncü bölümde*, kovalent olmayan etkileşimler ile polimer katlanması kontrolü bir üst seviyeye çıkarıldı. Bu sebeple, uc bloklu bir ABC tipi kopolimer RAFT yöntemi ile sentezlenip, Hamilton üçgeni (HW), BTA ve siyanurik asit (CA) grupları ile fonksiyonelleştirildi. BTA sarmal oluşturarak bir araya gelme Özelliği ile HW-CA dimerizasyonunun birbirlerini etkilemeden, birbirlerinden bağımsız bir şekilde gerçekleştiği, <sup>1</sup>H NMR ve CD deneyleri ile gösterildi. Çeşitli saçılım teknikleri ile atomik kuvvet mikroskopisi (AFM) birlikte kullanılarak iyi tanımlanmış nanopartikül oluşumu metilsikloheksan (MCH) çözücüsü içinde gözlemlendi. Buna ek olarak, MCH ve dikloroetan (DCE) içerisinde yapılan saçılım deneyleri, ABC tipi fonksiyonelleşmiş triblok polimerin çözücü polaritesine karşı çok hassas olduğunu, ve bunun partikül içi ve arası etkileşimleri dengelemede çok önemli bir etken olduğu gözlemlendi.

*Dördüncü bölümde* ise, kompleks yüksek ve düşük molekül ağırlığında olan ABA tipi suda çözünür fonksiyonellenmiş triblok kopolimerler, uyarılara tepki verebilen, kapalı yapılar inşa etmek için sentezlendi. Bu polimerler, bakır ile katalizlenmiş ATRP tekniği ile sentezlenip, daha sonra BTA ve uredopirimidinon (UPy) grupları ile fonksiyonelleştirilmiştir. CD spektroskopisi ile BTA gruplarının kendiliğinden sarmalla oluşturma özelliğinin UPy gruplarının varlığından bağımsız olarak gerçekleştiği gözlemlenmiştir. UPy dimerizasyonu kloroform (CHCl<sub>3</sub>) içerisinde <sup>1</sup>H NMR ile gösterilmiştir. Su içerisinde polimerler tarafından hidrofobik, kapalı alanlar oluşturulması Nil Kırmızısı (Nile Red) deneyleri ile gösterilmiş ve hidrofobik alan tamamıyla fonksiyonelleştirilmiş UPy-BTA-UPy polimeri için gözlemlenmiştir. En son olarak, dinamik ışık saçılımı (DLS) deneyleri ile iyi kontrol edilmiş, birden fazla bir polimer zincirinin bir araya gelmesi ile oluşmuş nanopartiküller oluştuğu gözlemlenmiştir ve buna ek olarak UPy gruplarının fotokorunumları kaldırıldığında nanopartikül çapında küçülme gözlemlenmiştir,

Bu tezin ikinci bölümünde, katlanmış polimerlerden meydana gelen nanopartiküllerin oluşturduğu hidrofobik alanların su içerisinde *fonksiyon* elde etmek için kullanılması tartışılmıştır.

*Beşinci bölümde*, bir grup amfifilik polimer sentezlenip, rutenyum(II) ile yüklenip, transfer hidrojenasyon reaksiyonunda test edilerek, BTA gruplarının kendiliğinden sarmal oluşturma özelliğinin nanopartiküllerin kataliz yeteneği üzerindeki etkisi test edilmiştir. BTA gruplarının kendiliğinden sarmal oluşturma özelliğinin, nanopartiküllerin katalizleme özelliğine, rutenyum merkezleri polimer üzerinde bulunan difenilfosfinostiren ligandları tarafından sıkıca çevrelediği sürece bir etkisi olmadığı gözlemlenmiştir. Bu büyük ihtimalle, polimere bağlı ligandlar tarafından çevrelenen rutenyum merkezlerinin daha iyi şekilde izole edilmesine bağlıdır.

*Altıncı bölümde*, tek polimer zincirinin katlanması ile oluşturulan hidrofobik iç alan, seçici şekilde reaksiyon gerçekleştirmek için kullanılmıştır. Esit miktarda ve farklı hidrofobisitelere sahip substratlar üzerinde gerçekleştirilen rekabet deneyleri, özünde seçici olmayan rutenyum(II) merkezlerine, tek zincir katlanması ile elde edilmiş hidrofobik alanların seçicilik özelliği kazandığını göstermiştir. Bu seçicilik, hem transfer hidrojenasyon hem de oksidasyon reaksiyonları için gösterilmiştir. Son olarak, tek zincir katlanması ile oluşturulan farklı fonksiyonlara sahip nanopartiküllerin, ardışık reaksiyonları bir defada katalizlemesini göstermek için ilk deneyler yapılmış ve bu yöntemin kullanılabilirliği gösterilmiştir.

Bu çalışmanın sonuçları, polimer zincirlerinin birbirinden bağımsız etkileşimler yoluyla kontrollü şekilde katlanmasının çeşitli çözücülerde mümkün olduğunu ve bu katlanmış nanopartiküllerin çok aktif ve seçici reaksiyon alanları yaratmak için kullanılabileceğini başarılı bir şekilde göstermiştir. Her ne kadar bu çalışmada gösterilen yapılar, doğal enzimler ile mükemmellik açısından henüz boy ölçümez ise de, polimer kimyası, süpamoleküler kimya, organokataliz ve homojen kataliz alanında yaşanan gelişmelerin bu mükemmeliğe ulaşmada ilerideki çalışmalara yardımcı olacağı düşünülmektedir.

## Het vouwen van polymeer ketens door orthogonale niet-covalente interacties

### *Functie door structuur*

Het combineren van polymeerchemie met supramoleculaire chemie geeft de mogelijkheid om dynamische 3D structuren te maken die adaptief en reagerend gedrag vertonen. Het doel van dit proefschrift is om synthetische routes te ontwikkelen om complexe polymeren te maken die door orthogonale supramoleculaire interacties vouwen tot goed gedefinieerde, dynamische deeltjes, én om deze deeltjes te gebruiken als functionele nano-reactoren.

In *Hoofdstuk 1* werd het concept ‘functie door structuur’ in synthetische systemen geïntroduceerd, waarbij de Natuur als inspiratiebron dient. Als eerste werden de meest belangrijke gecontroleerde radicaal-polymerisatie technieken bediscussieerd. Daarna werden verschillende benaderingen om gecompartmentaliseerde macromoleculaire systemen te maken, via gecontroleerde radicaal-polymerisatie technieken en supramoleculaire chemie, bediscussieerd, met een focus op enkele-keten polymeren nanodeeltjes (SCPNs) met dynamisch of niet-dynamisch gedrag. Hierna werd een overzicht gegeven van de synthetische routes om SCPNs te maken en de methodieken om deze te karakteriseren. Als laatste werd er een introductie over katalyse in beperkte ruimtes gegeven, met een nadruk op het gebruik van dynamische SCPNs als gecompartmentaliseerde katalysatoren.

In *Hoofdstuk 2* werd het effect bestudeerd van de lokale concentratie van benzeen-1,3,5-tricarboxamides (BTAs) op het vouwgedrag van polymeren met daaraan hangend BTAs in organische oplosmiddelen. Hydrofobe, op methacrylaat gebaseerde polymeren zijn gemaakt door middel van een reversibele additie-fragmentatie ketting transfer (RAFT) polymerisatie of een atoom transfer radicaal polymerisatie (ATRP), met een variërende polydispersiteit en een variërende BTA distributie over de polymeerketen. De resultaten van circulair dichroïsme (CD) experimenten aan deze polymeren laten zien dat de distributie en lokale dichtheid van BTAs hangend aan de polymeerketen een duidelijk effect heeft op het vouwgedrag van de copolymeren, maar ook dat de polydispersiteit geen invloed heeft op het vouwgedrag. Bovendien lijken interacties tussen deeltjes verstrekt te worden door de lokale dichtheid van de BTAs in een van de blokken van de copolymeren te verhogen.

In *Hoofdstuk 3* werd de complexiteit van het vouwen van polymeerketens door niet-covalente interacties naar een hoger niveau getild, met als doel om een betere controle over het vouwproces in organische oplosmiddelen te verkrijgen. Derhalve werd in dit hoofdstuk het ontwerp en de synthese van een ABC-type triblok copolymeer gepresenteerd met daaraan complementaire motieven, d.w.z. een Hamilton wig (HW, A blok), BTAs (B blok) en cyaanuurzuur (CA, C blok). De orthogonaliteit van de BTA en de HW-CA zelf-assemblage werd bevestigd door  $^1\text{H-NMR}$  studies, in combinatie met CD experimenten in verdunde oplossingen. Door gebruik te maken van een combinatie van verstrooiingstechnieken en atomaire kracht microscopie (AFM) kon worden aangetoond dat de polymeren goed-gedefinieerde deeltjes vormen met orthogonaal zelf-assemblerende domeinen in methylcyclohexaan (MCH). Daarnaast tonen de verstrooiings- resultaten aan in MCH en dichloorethaan (DCE) aan dat het ontworpen ABC-triblok copolymeer systeem erg gevoelig is voor de polariteit van het oplosmiddel, wat van cruciaal belang is om de zelf-assemblage tussen- én in deeltjes te balanceren.

In *Hoofdstuk 4* werden complexe, amfifiele, ABA-type triblok copolymeren gemaakt met daaraan hangend zelf-assemblerende motieven, om zo stimuli-responsieve, gecompartmentaliseerde structuren in waterige media te verkrijgen. Amfifiele ABA-type triblok copolymeren werden gesynthetiseerd via een koper-gekatalyseerde ATRP en daarna voorzien van BTA moleculen (in het A-blok) én beschermde 2-ureido-4[1H]-pyrimidinon (phUPy, in het B blok). <sup>1</sup>H-NMR studies in CDCl<sub>3</sub> laten zien dat UPy groepen in staat zijn om dimeren te vormen als ze vast zitten aan een amfifiele polymeer-hoofdstructuur, zowel zonder, als in aanwezigheid van BTAs. Door CD spectroscopie werd aangetoond dat de door de BTAs gevormde helische structuren in water gevormd kunnen worden onafhankelijk van de aanwezigheid van phUPy of UPy groepen. Bovendien bleek door middel van Nile-Red experimenten dat alle amfifiele polymeren gecompartmentaliseerde structuren in waterige media vormen, met een hydrofobe binnenkant. De volledig gefunctionaliseerde UPy-BTA-UPy triblok copolymeren bleken de meest hydrofobe binnenkant te hebben. Tenslotte bleek uit dynamische lichtverstrooiing (DLS) metingen dat goed gedefinieerde meerdere-keten aggregaten gevormd werden door de gefunctionaliseerde triblok copolymeren in water, maar ook dat verwijdering van de phUPy beschermgroep resulteerde in een reductie van de hydrodynamische straal van de deeltjes.

In de tweede helft van dit proefschrift werden gecompartmentaliseerde architecturen gebruikt, door middel van het vouwen van een amfifiele, willekeurig gefunctionaliseerde SCPN, om een *functie* te bewerkstelligen in water.

In *Hoofdstuk 5* werd een set op methacrylaat gebaseerde amfifiele copolymeren gesynthetiseerd, vervolgens geladen met Ru(II), en tenslotte getest in een de in the hydrogenatie van cyclohexanon, dit alles om de invloed van BTAs hangend aan een polymeer keten op de katalytische activiteit van SCPNs in water te onderzoeken. Het bleek dat andere structurelementen geen beslissende rol spelen in de katalytische prestatie van de SCPNs, zodra een gestructureerde micro-omgeving rond de Ru katalysator is gevormd, mits een hydrofobe micro-omgeving behouden blijft.

In *Hoofdstuk 6*, werd de hydrofobe afscherming die SCPNs bieden gebruikt om selectieve hydrofobe reactie-omgevingen te creëren. Competitie-experimenten tussen mengsels van substraten met een variërende hydrofobiciteit lieten zien dat een selectieve, hydrofobe reactie ruimte gevormd wordt door het vouwen van polymeerketens rond intrinsiek niet-selectieve Ru(II) katalysatoren. Een significante selectiviteit werd geobserveerd voor zowel oxidatie én hydrogenatie reacties. Tenslotte werden preliminaire experimenten uitgevoerd om vast te stellen of deze gecompartmentaliseerde systemen geschikt zijn voor meerstaps reacties in een pot.

De resultaten van dit promotieonderzoek laten zien dat gecontroleerde vouwing van polymeer ketens bereikt kan worden door orthogonale supramoleculaire interacties en dat deze gevouwen, dynamische structuren gebruikt kunnen worden als zeer actieve én selectieve reactie-omgevingen voor katalyse in water. Alhoewel de huidige stand van de techniek bij het vouwen van synthetische macromoleculen tot gedefinieerde structuren ver weg staat van de perfectie die polypeptiden bereiken bij het vouwen tot functionele confirmaties, valt het te verwachten dat er nog veel te winnen valt bij een verder integratie van supramoleculaire chemie, polymeerchemie, organokatalyse en homogene katalyse.



### Curriculum Vitae

Müge Artar was born on 3<sup>rd</sup> of December 1986 in Ulus, Bartın, Turkey. After finishing high school in 2005 at Davut Fırıncıoğlu Anatolian High School in Bartın, she studied chemistry with a full scholarship at Bilkent University in Ankara, Turkey. In 2008, she was selected as a finalist with her project “My World” in the project competition “Who Has The Campaign To Save The World?”, organized by Bayer, United Nations Environmental Program and World Wildlife Fund within the scope of Bayer Young Environmental Envoy Program among the university students in Turkey. In 2010, she started her master studies within the group of dr. Dönüş Tuncel (Bilkent University, Ankara, Turkey) on the synthesis of water soluble fluorene-based conjugated polymers and CB[n] based rotaxanes in collaboration with dr. Oren Scherman. Within this collaboration, she visited dr. Oren Scherman’s group (Melville Laboratory, Cambridge University, UK) in 2010. In 2010 Fall semester, she received Bilkent University Department of Chemistry Best Teaching Assistant Prize. In January 2012, Müge started as a PhD-student under supervision of prof. dr. E.W.(Bert) Meijer and dr. A.R.A. Palmans in Macromolecular and Organic Chemistry and the Institute for Complex Molecular Systems, at the Eindhoven University of Technology. During her PhD, she worked for 3 months in the research group of prof. dr. Mitsuo Sawamoto with dr. Takaya Terashima at Kyoto University (Kyoto, Japan) on the synthesis and investigation of the catalytically active Ru(II)-based SCPNs in water. Her PhD work focused on the design and synthesis of polymeric structures that can fold *via* orthogonal non-covalent interactions and understanding their catalytic activities in aqueous media. The most important results of this research are presented in this dissertation.



**List of publications and conference contributions****List of refereed publications**

- (1) "Sequence-Specific Self-Sorting of the Binding Sites of a Ditopic Guest by Cucurbituril Homologues and Subsequent Formation of a Hetero[4]pseudorotaxane"  
G. Celtek, M. Artar, O. A. Scherman, D. Tuncel *Chem. Eur. J.* **2009**, *15*, 10360.
- (2) "The effect of cucurbit[n]uril on the solubility, morphology, and the photophysical properties of nonionic conjugated polymers in an aqueous medium"  
D. Tuncel, M. Artar, S. B. Hanay *J. Polym. Sci. Part A: Polym. Chem.* **2010**, *48*, 4894.  
(Published as a front cover).
- (3) "Supramolecular Assemblies Constructed by Cucurbituril-Catalyzed Click Reaction"  
D. Tuncel, Ö. Ünal, M. Artar *Israel J. Chem.* **2010**, *51*, 525.
- (4) "The effect of cucurbit[n]uril on the solubility, morphology, and the photophysical properties of nonionic conjugated polymers in an aqueous medium"  
M. Artar, D. Tuncel *Polym. Prepr.* **2010**, *51*, 239.
- (5) "Understanding the catalytic activity of single-chain polymeric nanoparticles in water"  
M. Artar, T. Terashima, M. Sawamoto, E. W. Meijer, A. R. A. Palmans *J. Polym. Sci. Part A: Polym. Chem.* **2013**, *52*, 12. (Published as a front cover)
- (6) "Consequences of Subtle Chiral Effects: From 'Majority-Rules' to 'Minority-Rules'"  
P. J. M. Stals, M. Artar, P. Vendrig, A. R. A. Palmans, E. W. Meijer *Aust. J. Chem.* **2015**, *68*, 622.
- (7) "Single Chain Polymeric Nanoparticles as Selective Hydrophobic Reaction Spaces in Water"  
M. Artar, E. R. J. Souren, T. Terashima, E. W. Meijer, A. R. A. Palmans *ACS Macro Lett.* **2015**, *4*, 1099. (Published as a front cover)
- (8) "Design and Synthesis of Triblock Copolymers for Creating Complex Secondary Structures by Orthogonal Self-Assembly"  
O. Altintas,\* M. Artar,\* A. R. A. Palmans, C. Barner-Kowollik, E. W. Meijer *Macromolecules* **2015**, *48*, 8921. (\*Equal contribution)
- (9) "Dynamic Single Chain Polymeric Nanoparticles: From Structure to Function"  
M. Artar, E. Huerta, A. R. A. Palmans, E. W. Meijer, In: *Sequence-Controlled Polymers: Synthesis, Self-Assembly, and Properties* (Eds.: J.-F. Lutz, T. Y. Meyer, M. Ouchi, M. Sawamoto), American Chemical Society, Washington, D.C., **2014**, Vol. 1170, p 313. (Book Chapter).
- (10) "Catalysis Inside Folded Single Macromolecules"  
M. Artar, A. R. A. Palmans, In: *Catalysis within nanoconfined spaces* (Ed: R. Poli), Springer, Berlin, accepted for publication (Book chapter).

**List of publications in preparation**

- (11) "Exploring the self-assembly of polymer pendant benzene-1,3,5 tricarboxamides"  
M. Artar,\* Y. Ogura,\* P. J. M. Stals, M. J. G. M. Hummelink, A. R. A. Palmans, T. Terashima, M. Sawamoto, E. W. Meijer, in preparation. (\*Equal contribution)
- (12) "Orthogonal self-assembly of water soluble triblock polymers"  
M. Artar, G. ter Huurne, A. R. A. Palmans, E. W. Meijer, in preparation.



## List of Conference contributions

### Lecture

- (1) M. Artar, A. R. A. Palmans, E. W. Meijer, “Consequences of Folding a Single Chain Polymer in Water”, 250th ACS National Meeting & Exposition 2015, Boston, USA (Oral presentation, invited).
- (2) M. Artar, A. R. A. Palmans, E. W. Meijer, “Consequences of Folding a Single Chain Polymer in Water”, Chemistry As Innovating Science (CHAINS) 2014, Veldhoven, The Netherlands (Oral presentation).
- (3) M. Artar, D. Tuncel, “The Effect of Cucurbituril[n]uril on the Morphology, Solubility, and the Photophysical Properties of Conjugated Polymers in an Aqueous Medium”, 3rd EuCheMS Chemistry Congress 30 August 2010, Nürnberg, Germany (Oral presentation).
- (4) M. Artar, D. Tuncel, “The Effect of Cucurbituril[n]uril on the Morphology, Solubility, and the Photophysical Properties of Conjugated Polymers in an Aqueous Medium”, 43rd IUPAC World Polymer Congress MACRO 2010 Chemistry Congress July 2010, Glasgow, UK (Oral presentation.)
- (5) M. Artar, D. Tuncel, “Effects of Cucurbit(n)uril on Dissolution and Light Emitting Properties of Fluorene-Based Non-Ionic Conjugated Polymers”, NanoTR-2010 June 2010 İzmir, Turkey (Oral presentation).

### Poster

- (1) M. Artar, A. R. A. Palmans, E. W. Meijer, “Consequences of Folding a Single Chain Polymer in Water”, Frontiers in Polymer Science 2015, Riva Del Garda, Italy (Poster presentation).
- (2) M. Artar, A. R. A. Palmans, E. W. Meijer, “Understanding the catalytic activity of single-chain polymeric nanoparticles in water”, Dutch Polymer Days (DPD) 2013, Lunteren, The Netherlands (Poster presentation).
- (3) M. Artar, A. R. A. Palmans, E. W. Meijer, “Understanding the catalytic activity of single-chain polymeric nanoparticles in water”, NWO CW, Design & Synthesis, Structure & Reactivity Study group meeting 2012, Lunteren, The Netherlands (Poster presentation).
- (4) M. Artar, A. R. A. Palmans, E. W. Meijer, “Improving the catalytic activity of single-chain polymeric nanoparticles in water”, Belgian-German (Macro) Molecular Meeting 2012, Houffalize, Belgium (Poster presentation + **award**).
- (5) M. Artar, D. Tuncel, “The Cucurbituril[n]uril Based Rotaxanes in Aqueous Medium”, Synthesis, Characterization, and Applications of Nanomaterials (SCAN) 2010, Ankara, Turkey (Poster presentation).